

ANALYTICA CHIMICA ACTA

An international journal devoted to all branches of analytical chemistry

EDITORS

HARRY L. PARDUE (West Lafayette, IN, U.S.A.)

ALAN TOWNSHEND (Hull, Great Britain)

J.T. CLERC (Berne, Switzerland)

WILLEM E. VAN DER LINDEN (Enschede, The Netherlands)

PAUL J. WORSFOLD (Plymouth, Great Britain)

Editorial Advisers

F.C. Adams, Antwerp
M. Aizawa, Yokohama
J.F. Alder, Manchester
C.M.G. van den Berg, Liverpool
A.M. Bond, Bundoora, Vic.
S.D. Brown, Newark, DE
J. Buffle, Geneva
P.R. Cuulet, Lyon
S.R. Crouch, East Lansing, MI
R. Dams, Ghent
L. de Galan, Vlaardingen
M.L. Gross, Lincoln, NE
W. Heineman, Cincinnati, OH
G.M. Hietje, Bloomington, IN
G. Horvai, Budapest
T. Imasaka, Fukuoka
D. Jagner, Gothenburg
G. Johansson, Lund
D.C. Johnson, Ames, IA
A.M.G. Macdonald, Birmingham
D.L. Massart, Brussels
P.C. Meier, Schaffhausen
M.E. Meyerhoff, Ann Arbor, MI

J.N. Miller, Loughborough
H.A. Mottola, Stillwater, OK
M.E. Munk, Tempe, AZ
M. Ot'o, Freiberg
D. Pérez-Bendito, Córdoba
C.F. Poole, Detroit, MI
S.C. Rutan, Richmond, VA
J. Ruzicka, Seattle, WA
A. Sanz-Medel, Oviedo
S. Sasaki, Toyohashi
T. Sawada, Tokyo
K. Schügerl, Hannover
M.R. Smyth, Dublin
M. Thompson, Toronto
G. Tölg, Dortmund
Y. Umezawa, Tokyo
E. Wang, Changchun
J. Wang, Las Cruces, NM
H.W. Werner, Eindhoven
O.S. Wolfbeis, Graz
V.A. Zolotov, Moscow
J. Zupan, Ljubljana

ANALYTICA CHIMICA ACTA

Scope. *Analytica Chimica Acta* publishes original papers, preliminary communications and reviews dealing with every aspect of modern analytical chemistry. Reviews are normally written by invitation of the editors, who welcome suggestions for subjects. Preliminary communications of important urgent work can be printed within four months of submission, if the authors are prepared to forego proofs.

Submission of Papers

Americas

Prof. Harry L. Pardue
Department of Chemistry
1393 BRWN Bldg, Purdue University
West Lafayette, IN 47907-1393
USA
Tel: (+1-317) 494 5320
Fax: (+1-317) 496 1200

Computer Techniques

Prof. J.T. Clerc
Universität Bern
Pharmazeutisches Institut
Baltzerstrasse 5, CH-3012 Bern
Switzerland
Tel: (+41-31) 654171
Fax: (+41-31) 654198

Other Papers

Prof. Alan Townshend
Department of Chemistry
The University
Hull HU6 7RX
Great Britain
Tel: (+44-482) 465027
Fax: (+44-482) 466410

Prof. Willem E. van der Linden
Laboratory for Chemical Analysis
Department of Chemical Technology
Twente University of Technology
P.O. Box 217, 7500 AE Enschede
The Netherlands
Tel: (+31-53) 892629
Fax: (+31-53) 356024

Prof. Paul Worsfold
Dept. of Environmental Sciences
University of Plymouth
Plymouth PL4 8AA
Great Britain
Tel: (+44-752) 233006
Fax: (+44-752) 233009

Submission of an article is understood to imply that the article is original and unpublished and is not being considered for publication elsewhere. *Anal. Chim. Acta* accepts papers in English only. There are no page charges. Manuscripts should conform in layout and style to the papers published in this issue. See inside back cover for "Information for Authors".

Publication. *Analytica Chimica Acta* appears in 14 volumes in 1993. The subscription price for 1993 (Vols. 267-280) is Dfl. 4214.00 plus Dfl. 462.00 (p.p.h.) (total approx. US\$ 2816.75). *Vibrational Spectroscopy* appears in 2 volumes in 1993. The subscription price for *Vibrational Spectroscopy* (Vols. 4 and 5) is Dfl. 700.00 plus Dfl. 66.00 (p.p.h.) (total approx. US\$ 461.50). The price of a combined subscription (*Anal. Chim. Acta* and *Vib. Spectrosc.*) is Dfl. 4592.00 plus Dfl. 528.00 (p.p.h.) (total approx. US\$ 3084.25). All earlier volumes (Vols. 1-266) except Vols. 23 and 28 are available at Dfl. 259.50 (US\$ 156.25), plus Dfl. 18.00 (US\$ 10.75) p.p.h., per volume. The Dutch guilder price is definitive. The U.S. dollar price is subject to exchange-rate fluctuations and is given only as a guide. Subscriptions are accepted on a prepaid basis only, unless different terms have been previously agreed upon.

Our p.p.h. (postage, packing and handling) charge includes surface delivery of all issues, except to subscribers in the U.S.A., Canada, Australia, New Zealand, China, India, Israel, South Africa, Malaysia, Thailand, Singapore, South Korea, Taiwan, Pakistan, Hong Kong, Brazil, Argentina and Mexico, who receive all issues by air delivery (S.A.L.—Surface Air Lifted) at no extra cost. For Japan, air delivery requires 25% additional charge of the normal postage and handling charge; for all other countries airmail and S.A.L. charges are available upon request.

Subscription orders. Subscription orders can be entered only by calendar year and should be sent to: Elsevier Science Publishers B.V., Journals Department, P.O. Box 211, 1000 AE Amsterdam, The Netherlands. Tel: (+31-20) 5803 642, Telex: 18582, Telefax: (+31-20) 5803598, to which requests for sample copies can also be sent. Claims for issues not received should be made within six months of publication of the issues. If not they cannot be honoured free of charge. Readers in the U.S.A. and Canada can contact the following address: Elsevier Science Publishing Co. Inc., Journal Information Center, 655 Avenue of the Americas, New York, NY 10010, U.S.A. Tel: (+1-212) 6333750, Telefax: (+1-212) 6333990, for further information, or a free sample copy of this or any other Elsevier Science Publishers journal.

Advertisements. Advertisement rates are available from the publisher on request.

Detailed "Instructions to Authors" for *Analytica Chimica Acta* was published in Volume 256, No. 2, pp. 373-376. Free reprints of the "Instructions to Authors" of *Analytica Chimica Acta* and *Vibrational Spectroscopy* are available from the Editors or from: Elsevier Science Publishers B.V., P.O. Box 330, 1000 AH Amsterdam, The Netherlands. Telefax: (+31-20) 5862845.

US mailing notice – Analytica Chimica Acta (ISSN 0003-2670) is published biweekly by Elsevier Science Publishers (Molenwerf 1, Postbus 211, 1000 AE Amsterdam). Annual subscription price in the USA US\$ 2816.75 (subject to change), including air speed delivery. Second class postage paid at Jamaica, NY 11431. *USA Postmasters:* Send address changes to *Anal. Chim. Acta*, Publications Expediting, Inc., 200 Meacham Av., Elmont, NY 11003. Airfreight and mailing in the USA by Publication Expediting.

ANALYTICA CHIMICA ACTA

An international journal devoted to all branches of analytical chemistry

(Full texts are incorporated in CJELSEVIER, a file in the Chemical Journals Online database available on STN International; Abstracted, indexed in: Aluminum Abstracts; Anal. Abstr.; Biol. Abstr.; BIOSIS; Chem. Abstr.; Curr. Contents Phys. Chem. Earth Sci.; Engineered Materials Abstracts; Excerpta Medica; Index Med.; Life Sci.; Mass Spectrom. Bull.; Material Business Alerts; Metals Abstracts; Sci. Citation Index)

VOL. 271 NO. 1

CONTENTS

JANUARY 8, 1993

Environmental Analysis

- Seagoing method for the determination of chromium(III) and total chromium in sea water by electron-capture detection gas chromatography
R.K. Mugo and K.J. Orians (Vancouver, Canada) 1
- Sampling of aquatic sediments. Design of a decision-support system and a case study
R. Wehrens, P. Van Hoof, L. Buydens, G. Kateman (Nijmegen, Netherlands), M. Vossen, W.H. Mulder and T. Bakker (Lelystad, Netherlands) 11
- Trace determination of sugar acids (gluconic acid) in sea water by liquid chromatography
S. Nakabayashi, I. Kudo, K. Kuma, K. Matsunaga (Hakodate, Japan) and K. Hasebe (Sapporo, Japan) 25
- Determination of carbon-13 content of sugars of fruit and vegetable juices. A European inter-laboratory comparison
J. Koziat (Creteil, France), A. Rossmann (Freising-Weihenstephan, Germany), G.J. Martin (Nantes, France) and P.R. Ashurst (Kingstone, UK) 31

Enzyme Analysis

- Simultaneous enzymatic and tautomeric reactions of D-fructose in a reactor with immobilized hexokinase
M. Skoog and G. Johansson (Lund, Sweden) 39
- Flow-injection determination of 1,5-anhydroglucitol in serum with an immobilized pyranose oxidase reactor and chemiluminescence detection
N. Kiba, F. Ueda, K. Saegusa, Y. Goto, M. Furusawa and T. Yamane (Kofu, Japan) 47
- On-line organic-phase enzyme detector
J. Wang and Y. Lin (Las Cruces, NM, USA) 53

Chromatography and other Separation Methods

- Improved methodology for subnanogram quantitation of doxorubicin and its 13-hydroxy metabolite in biological fluids by liquid chromatography
D.T. Rossi, B.A. Phillips, J.R. Baldwin and P.K. Narang (Columbus, OH, USA) 59
- Reversed-phase liquid chromatographic determination of doxorubicin after on-line trace enrichment on iron(III)-loaded 8-hydroxyquinoline-bonded silica
E. Van der Vlis, H. Irth, U.R. Tjaden and J. Van der Greef (Leiden, Netherlands) 69
- Measurement of primary amine groups on surface-modified silica and their role in metal binding
I. Taylor and A.G. Howard (Southampton, UK) 77
- Experimental design approach for supercritical fluid extraction
M. Kane, J.R. Dean, S.M. Hitchen (Newcastle upon Tyne, UK), C.J. Dowle (Middlesbrough, UK) and R.L. Tranter (Barnard Castle, UK) 83

Chemometrics

- Accuracy, precision and information of the adaptive Kalman filter in chromatography
Y. Hayashi (Tokyo, Japan) and S.C. Rutan (Richmond, VA, USA) 91
- Deconvolution in one-dimensional chromatography by heuristic evolving latent projections of whole profiles retention time shifted by simplex optimization of cross-correlation between target peaks
M.D. Hämäläinen (Uppsala, Sweden), Y.-z. Liang, O.M. Kvalheim (Bergen, Norway) and R. Andersson (Uppsala, Sweden) 101

(Continued overleaf)

Contents (continued)

| | |
|---|-----|
| Assessment of environmental water with fuzzy cluster analysis and fuzzy recognition G.N. Chen (Fujian, China) | 115 |
| <i>Electroanalytical Chemistry and Sensors</i> | |
| Diamond-like carbon coated microporous polycarbonate as a composite barrier for a glucose enzyme electrode S.P.J. Higson and P.M. Vadgama (Salford, UK) | 125 |
| Chloride-selective electrodes based on mercury organic compounds as neutral carriers M. Rothmaier and W. Simon (Zürich, Switzerland) | 135 |
| Development of a chemically modified electrode based on carbon paste and functionalized silica gel for preconcentration and voltammetric determination of mercury(II) L.M. Aleixo, M. De Fátima B. Souza, O.E.S. Godinho, G. De Oliveira Neto, Y. Gushkem (Campinas, Brazil) and J.C. Moreira (Araraquara, Brazil) | 143 |
| Potentiometric study of azide complexes of copper(II) in aqueous medium J.F. De Andrade and O.M. Guimarães (Ribeirão Preto, Brazil) | 149 |
| <i>Fluorimetry</i> | |
| Optical sensing of glucose using phase-modulation fluorimetry J.R. Lakowicz and B. Maliwal (Baltimore, MD, USA) | 155 |
| Fluorimetry of haemolysis of red blood cells by catalytic reaction of leaked haemoglobin: application to homogeneous fluorescence immunoassay Y. Tatsu, S. Yamamura, H. Yamamoto and S. Yoshikawa (Osaka, Japan) | 165 |
| <i>Atomic Spectrometry</i> | |
| Different sample introduction systems for the simultaneous determination of As, Sb and Se by microwave-induced plasma atomic emission spectrometry E. Bulska, P. Tschöpel, J.A.C. Broekaert and G. Tölg (Dortmund, Germany) | 171 |
| <i>Micelles</i> | |
| Internal viscosity of sodium dodecyl sulfate micelles as a function of the chain length of <i>n</i> -alcohol modifiers D.A. Piasecki and M.J. Wirth (Newark, DE, USA) | 183 |

ANALYTICA CHIMICA ACTA
VOL. 271 (1993)

ANALYTICA CHIMICA ACTA

An international journal devoted to all branches of analytical chemistry
Revue internationale consacrée à tous les domaines de la chimie analytique
Internationale Zeitschrift für alle Gebiete der analytischen Chemie

EDITORS

HARRY L. PARDUE (West Lafayette, IN, U.S.A.)

ALAN TOWNSHEND (Hull, Great Britain)

J.T. CLERC (Berne, Switzerland)

WILLEM E. VAN DER LINDEN (Enschede, The Netherlands)

PAUL J. WORSFOLD (Plymouth, Great Britain)

Editorial Advisers

F.C. Adams, Antwerp
M. Aizawa, Yokohama
J.F. Alder, Manchester
C.M.G. van den Berg, Liverpool
A.M. Bond, Bundoora, Vic.
S.D. Brown, Newark, DE
J. Buffle, Geneva
P.R. Coulet, Lyon
S.R. Crouch, East Lansing, MI
R. Dams, Ghent
L. de Galan, Vlaardingen
M.L. Gross, Lincoln, NE
W. Heineman, Cincinnati, OH
G.M. Hieftje, Bloomington, IN
G. Horvai, Budapest
T. Imasaka, Fukuoka
D. Jagner, Gothenburg
G. Johansson, Lund
D.C. Johnson, Ames, IA
A.M.G. Macdonald, Birmingham
D.L. Massart, Brussels
P.C. Meier, Schaffhausen
M.E. Meyerhoff, Ann Arbor, MI

J.N. Miller, Loughborough
H.A. Mottola, Stillwater, OK
M.E. Munk, Tempe, AZ
M. Otto, Freiberg
D. Pérez-Bendito, Córdoba
C.F. Poole, Detroit, MI
S.C. Rutan, Richmond, VA
J. Ruzicka, Seattle, WA
A. Sanz-Medel, Oviedo
S. Sasaki, Toyohashi
T. Sawada, Tokyo
K. Schügerl, Hannover
M.R. Smyth, Dublin
M. Thompson, Toronto
G. Tölg, Dortmund
Y. Umezawa, Tokyo
E. Wang, Changchun
J. Wang, Las Cruces, NM
H.W. Werner, Eindhoven
O.S. Wolfbeis, Graz
Yu.A. Zolotov, Moscow
J. Zupan, Ljubljana



Anal. Chim. Acta, Vol. 271 (1993)

ELSEVIER, Amsterdam–London–New York–Tokyo

© 1993 ELSEVIER SCIENCE PUBLISHERS B.V. ALL RIGHTS RESERVED

0003-2670/93/\$06.00

No part of this publication may be reproduced, stored in a retrieval system or transmitted in any form or by any means, electronic, mechanical, photocopying, recording or otherwise, without the prior written permission of the publisher, Elsevier Science Publishers B.V., Copyright and Permissions Dept., P.O. Box 521, 1000 AM Amsterdam, The Netherlands.

Upon acceptance of an article by the journal, the author(s) will be asked to transfer copyright of the article to the publisher. The transfer will ensure the widest possible dissemination of information.

Special regulations for readers in the U.S.A.—This journal has been registered with the Copyright Clearance Center, Inc. Consent is given for copying of articles for personal or internal use, or for the personal use of specific clients. This consent is given on the condition that the copier pays through the Center the per-copy fee for copying beyond that permitted by Sections 107 or 108 of the U.S. Copyright Law. The per-copy fee is stated in the code-line at the bottom of the first page of each article. The appropriate fee, together with a copy of the first page of the article, should be forwarded to the Copyright Clearance Center, Inc., 27 Congress Street, Salem, MA 01970, U.S.A. If no code-line appears, broad consent to copy has not been given and permission to copy must be obtained directly from the author(s). All articles published prior to 1980 may be copied for a per-copy fee of US \$2.25, also payable through the Center. This consent does not extend to other kinds of copying, such as for general distribution, resale, advertising and promotion purposes, or for creating new collective works. Special written permission must be obtained from the publisher for such copying.

No responsibility is assumed by the publisher for any injury and/or damage to persons or property as a matter of products liability, negligence or otherwise, or from any use or operation of any methods, products, instructions or ideas contained in the material herein.

Although all advertising material is expected to conform to ethical (medical) standards, inclusion in this publication does not constitute a guarantee or endorsement of the quality or value of such product or of the claims made of it by its manufacturer.

This issue is printed on acid-free paper.

PRINTED IN THE NETHERLANDS

Seagoing method for the determination of chromium(III) and total chromium in sea water by electron-capture detection gas chromatography

Robert K. Mugo and Kristin J. Orians

Departments of Chemistry and Oceanography, University of British Columbia, Vancouver, British Columbia V6T 1Y6 (Canada)

(Received 7th May 1992)

Abstract

A seagoing method for the determination of Cr(III) and total chromium in sea water is presented. The method employs electron-capture detection of the volatile trifluoroacetylacetone derivative of Cr(III) formed via solvent extraction with toluene; total chromium is determined as Cr(III) after reduction. Detection limits at sea are 0.062 and 0.255 nM for Cr(III) and total chromium, respectively. Accuracy for total chromium was verified by the analysis of standard reference materials from the National Research Council of Canada. The procedure has a precision of 1.3% at 4.7 nM total chromium, and has been applied to stored samples in the laboratory in addition to its use at sea.

Keywords: Gas chromatography; Chromium; Electron-capture detection; Sea water; Solvent extraction; Waters

A variety of factors controls the distribution of trace metals in sea water including the oxidation state of the metal, which can influence input and removal processes in the ocean. Chromium exists in sea water in two different oxidation states, Cr(III) and Cr(VI). The marine geochemistry of chromium is not very well understood, partly because the two chromium oxidation states are characterized by different chemical behaviour and are difficult to analyze accurately without inter-conversion during sample processing. Thermodynamic calculations predict that in oxygenated natural waters chromium should exist almost exclusively as Cr(VI) with the predicted species being chromate, CrO_4^{2-} , and Cr(III) existing as the aquahydroxy species, $\text{Cr}(\text{OH})_2^+(\text{H}_2\text{O})_4$ [1]. However, the ratio of Cr(III) to Cr(VI) in natural waters has been found to vary from 0.02 to 0.99 [2]. It was suggested that this variation and con-

tradiction with theory might be due to the in situ precipitation of chromate only, with strontium or barium sulphate [3]. Cranston and Murray [4], however, have pointed out that speciation changes during sample handling, which vary depending on the technique used to determine the chromium species, might be responsible for these discrepancies.

The oxidation of Cr(III) to Cr(VI) in natural waters is known to be slow, with a reported half-life of several weeks [5]. Early and Cannon [6] have attributed this to the kinetic inertness of aquated Cr(III) species. Various workers (cf. Johnson and Xyla [7]) have investigated the role of various manganese oxides as possible oxidants and have found that these phases are faster oxidants for Cr(III) than is O_2 . Oxygen alone leads to oxidation half-lives of almost two years. The increased rate observed in natural waters, therefore, suggests that manganese oxides, or possibly other mineral oxides, are likely to play an important role in the environmental oxidation of Cr(III). Other factors which may influence the rate of

Correspondence to: R.K. Mugo, Departments of Chemistry and Oceanography, University of British Columbia, 2036 Main Mall, Vancouver, British Columbia V6T 1Y6 (Canada).

oxidation of Cr(III) to Cr(VI) were investigated by Pettine et al. [8], using H_2O_2 in NaCl and the major sea salts at pH 8 and 25°C. They also looked at the effect of aging the Cr(III) solutions before oxidation. An increase in the borate concentration was found to increase the oxidation rate while aging decreased the rate.

A method that allows the determination of both chromium species as quickly as possible after sample collection, has great potential in allowing the factors controlling the marine geochemistry of this element to be studied. Currently most methods for the determination of trace metals in sea water involve an initial sample collection step, followed by preservation or at times by some preliminary sample preparation step (e.g. preconcentration) on board ship. The bulk of the sample-handling procedure plus the analysis, however, are still carried out in a shore-based laboratory sometimes long after the initial sample collection step. As pointed out by Measures and Edmond [9], the ability to do shipboard determinations also offers the important advantage of contamination control which is critical for accurate trace metal determinations. In cases where the element of interest can exist in more than one oxidation state, as does chromium, and where oxidation state interconversion can occur relatively easily during handling or storage, the importance of doing determinations at sea cannot be overemphasized.

Electron-capture detection gas chromatography (GC-ECD) of metal chelates has been applied to the determination of metals in various matrices and has shown advantages over other methods in terms of sensitivity [10] and a reduction in the sample preparation procedure [9]. The compact size, general insensitivity to motion and vibrations on board ships, and the relatively low cost of the instrument make it ideal for use at sea. The electron-capture detector is highly sensitive to fluorinated metal chelates provided they are volatile enough to be chromatographed. The initial problems associated with the gas chromatography of metal chelates had mainly to do with finding suitable ligands [11]. The ligand used in this study, 1,1,1-trifluoroacetylacetone (HTFA), has been employed in studies dealing with the

determination of chromium in various matrices. Chromium was measured in biological samples [10,12] and in lunar samples [13]. Its application to natural waters include the determination in sea water of beryllium [9] and aluminium [14]. Its use for the determination of chromium in natural waters has been confined to total chromium in stored samples often with long reaction times and considerably higher sample volume requirements [15,16]; none of the methods has been adapted for use at sea.

This study was therefore aimed at the development of an accurate and rapid GC shipboard technique for the determination of Cr(III) and total chromium in sea water, which would allow the analysis of these two chromium species during oceanographic cruises. Such a technique allows collection of data on the distribution of chromium redox species in various oceanographic environments and thus allows for the elucidation of the factors responsible for the marine geochemistry of this element.

EXPERIMENTAL

Materials and reagents

Chelating agent. 1,1,1-Trifluoroacetylacetone (HTFA) (Aldrich, Milwaukee, WI) was purified by distillation at atmospheric pressure in a Perfluoroalkoxy (PFA) still as described by Measures and Edmond [9].

Internal standard. 2,6-Dichlorobiphenyl (Chemical Service, Westchester, PA) was used as obtained without further purification.

Solvent. Toluene (BDH, ACS or Omnisolve grade) was purified by distillation 2–3 times through a 4 ft. × 1.5 in. glass still. The distillate was monitored for extraneous peaks by injection into the gas chromatograph. The redistilled toluene was spiked with the internal standard at a concentration of approximately 100 ng ml⁻¹. Acetone (BDH, ACS grade) was used untreated for rinsing the PFA reaction bottles and the separatory funnel during the extraction procedure.

Buffer. Doubly quartz-distilled acetic acid (Seastar Chemicals, Sidney, BC) diluted with

deionized water to give approximately 10% CH_3COOH and 1 M NaAc–HAc were used for pH adjustments. A solution of 1 M NaAc–HAc was prepared from analytical-reagent grade sodium acetate (BDH), which had been recrystallized once to remove trace amounts of chromium and other metal contaminants present. An alternate cleaning procedure for the sodium acetate buffer solution in the same way as the sea-water samples and using the redistilled HTFA ligand to scavenge any chromium present. Both procedures were equally effective in producing NaAc which was clean enough for use in this study. The recrystallization procedure was chosen for all subsequent work as it was less time consuming.

Reducing agent. Sodium sulphite (BDH, ACS grade) solution (1 M), used for the reduction of Cr(VI) to Cr(III), was cleaned via extraction with the redistilled HTFA. This was done by adjusting the pH of the solution to approximately 6 with doubly distilled acetic acid followed by solvent extraction with toluene in a similar manner to the samples (described below). The solution was rinsed several times with the redistilled toluene to ensure that all the HTFA had been removed.

Water. Deionized water was obtained from a Barnstead Nanopure Series 630 deionization system.

Chromium standards. Certified atomic absorption standards for Cr(III) and Cr(VI) (Aldrich, Milwaukee, WI) were used to prepare appropriate extraction standards. Solutions of $1000 \mu\text{g ml}^{-1}$ Cr(III) in 1 wt.% HCl and $1000 \mu\text{g ml}^{-1}$ Cr(VI), as an ammonium dichromate solution in water, were diluted with deionized water to appropriate concentration ranges for use in this study. The optimization procedures for both the gas chromatographic and the solvent extraction steps were monitored on the basis of chromium recoveries obtained by the analysis of chromium trifluoroacetylacetonate $[\text{Cr}(\text{TFA})_3]$ synthesized as described by Fay and Piper [17].

Apparatus

A Hewlett-Packard 5890 Series II gas chromatograph equipped with a 555.0 MBq ^{63}Ni electron-capture detector was used in this study. The

GC-ECD apparatus was run in the split mode with a split ratio of approximately 10:1. A J&W Scientific DB 210 15 m \times 0.25 mm o.d. capillary column with a 0.5- μm film thickness was used. The carrier gas, ultra high purity (UHP)-grade nitrogen, was purified further by passing it through a molecular-sieve trap and a hydrocarbon trap. The detector makeup gas, UHP-grade nitrogen, was purified via a heated carrier gas trap and an indicating oxygen trap. Data handling from the GC runs was performed on an on-line Hewlett-Packard personal computer equipped with HP-Chemstation 3365 software.

pH measurements were performed using an Orion SA 520 pH meter equipped with a 91-02 general-purpose combination electrode. Shaking was accomplished with a Burrell Model 75 wrist action shaker. A Samsung MW2570UC home microwave oven was employed to speed up the chromium extractions. A make-shift PFA separatory funnel for the extractions was constructed as described by Measures and Edmond for aluminium [14].

Sea-water samples

Chromium determinations in the laboratory were conducted on two kinds of stored sea-water samples: (i) samples that had been acidified after collection and (ii) sea-water samples that had been frozen immediately after collection without acidification.

Sea-water samples from the central North Atlantic, near Bermuda, were collected using 5-l Niskin bottles (General Oceanics) mounted on a stainless steel hydrowire, by E.A Boyle and colleagues from the Massachusetts Institute of Technology. The samples were filtered then acidified to $\text{pH } 2 \pm 0.1$ and stored in acid-leached polyethylene bottles. Under these conditions all the chromium is reduced to Cr(III) within 24 h [18], and only total chromium can be determined after adjusting the sample pH to the extraction pH (6.0 ± 0.2) with the NaAc–HAc buffer.

Sea-water samples that had been frozen immediately after collection were collected in the Northeast Pacific Ocean (approximately 30 km off Nootka Sound, 49°N, 127°W) using 30-l Go-Flo bottles (General Oceanics) mounted on a Kevlar[®]

line. The samples were filtered then stored in acid-cleaned polyethylene bottles and frozen immediately on board ship. Analyses of Cr(III) and total chromium were subsequently performed on these samples in the laboratory.

Chromium determinations at sea during an oceanographic cruise were performed on sea-water samples collected using either 10- or 30-l Go-Flo bottles mounted on a Kevlar® line.

Processing

Sample processing in the laboratory took place in a filtered-air environment within a laminar flow bench in an effort to reduce possible contamination from the surroundings. The extractions were carried out in PFA bottles. Before their first use, these 60-ml bottles and the PFA separatory funnel were leached in 4 M hydrochloric acid at 60°C for three days followed by a dilute doubly distilled HNO₃ (approximately 1%) leach for about a week. During usual laboratory runs the PFA reaction bottles and separatory funnel were cleaned between extractions by rinsing three times with approximately 5–10 ml acetone.

A portable high-efficiency particle air (HEPA) filter cabinet was used at sea to reduce possible contamination from the ship environment.

General procedure

Chromium(III). Sea-water samples (15 ml) for Cr(III) determination are measured accurately into the reaction bottles using an adjustable 10-ml Eppendorf pipet. The pH is adjusted from the natural sea water pH of 7.5–8.3 to the extraction pH of 6.0 ± 0.2 with 20 μ l 10% quartz-distilled CH₃COOH, 100 μ l of the purified ligand are then added, followed by the addition of 1 ml toluene. The bottles are shaken manually for 5 s to ensure mixing of the various reagents, then placed in the microwave and heated four at a time for 3 min. To reduce pressure build-up inside the bottles during microwave heating, bottles are partially deflated by squeezing the walls prior to capping, allowing room for expansion. The bottles are removed from the microwave and shaken for 5 s and then returned for another 3

min at the same power level. At the end of this period the sample temperatures are 65–70°C.

During cooling, samples are shaken for 10 min on the mechanical wrist action shaker, fully cooled to room temperature, then carefully transferred to the PFA make-shift separatory funnel where the aqueous layer is separated and discarded. The organic layer is shaken for 10 s with 1 ml of deionized water to help preventing the formation of emulsions from calcium and magnesium hydroxides which can occur when NaOH is added in the next step. The layers are allowed to separate and the organic layer is then shaken for 20 s with 1 ml of 1 M NaOH. This washing step with base is critical as it destroys the excess ligand which would oversaturate the detector if not removed. After separation the organic layer is rinsed two times with a total of 2 ml of deionized water to remove traces of NaOH. The extract is then transferred to a clean glass vial with a PFA-lined cap (once chelate formation is complete and the excess ligand has been removed, the organic extracts are virtually immune from any chromium contamination; contact with glassware is therefore not a problem at this stage). The extracted sample is ready for injection into the gas chromatograph at this stage or it can be stored at room conditions for 1–2 days. For long-term storage, the extracts are stored in the freezer at –15°C and are stable for several weeks. Cr(III) standards are treated in the same manner.

Total chromium. The reaction between the ligand, 1,1,1-trifluoroacetylacetone, and chromium is specific for Cr(III); for total chromium determination it is necessary to convert Cr(VI) to the reduced state before chelation can occur. For samples stored frozen and unacidified, 20 μ l of

TABLE 1

Gas chromatographic conditions for the analysis of chromium as Cr(TFA)₃

| | |
|--------------------------------|--------------------------|
| Injection port temperature | 200°C |
| Oven temperature | 130°C |
| Detector temperature | 350°C |
| Column head pressure | 15 psi |
| Hydrogen carrier gas flow-rate | 2.6 ml min ⁻¹ |
| Nitrogen makeup gas flow-rate | 49 ml min ⁻¹ |

the 10% CH_3COOH and 200 μl of the 1 M sodium sulphite reducing agent are added to 15 ml of thawed sample. In samples which have been stored acidified at pH 2, Cr(VI) is reduced within 24 h and thus no reducing agent is added. These samples are brought to the extraction pH by the addition of 2 ml (for each 15 ml of sample) of the 1 M NaAc–HAc buffer. In both cases the samples are then treated in a similar manner as described for the Cr(III) samples above.

RESULTS AND DISCUSSION

Optimization

Gas chromatography. The GC conditions were selected to ensure the highest possible sensitivity of the electron-capture detector for the $\text{Cr}(\text{TFA})_3$ chelate, as well as good resolution and reasonable retention times for the peaks of interest. Table 1 shows the optimized parameters used for all quantitative work. A typical chromatogram is shown in Fig. 1. Chromium elutes as two peaks for the *trans* and *cis* isomers of the $\text{Cr}(\text{TFA})_3$ chelate. Quantitative determinations were per-

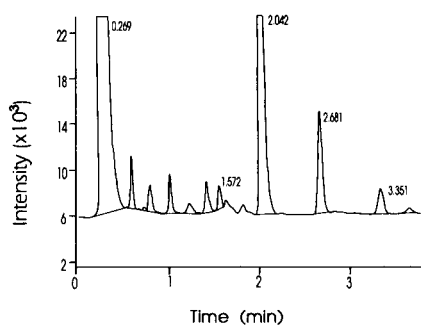


Fig. 1. Typical chromatogram of a chromium determination in sea water. $\text{Cr}(\text{TFA})_3$ elutes as two well resolved peaks with retention times of 2.681 and 3.351 min. The peak with the shorter retention time is assigned to the *trans* isomer (less polar and therefore less interaction with the polar stationary phase). The internal standard, 2,6-dichlorobiphenyl, has a retention time of 2.042 min; the peak with retention time 1.572 min corresponds to the $\text{Al}(\text{TFA})_3$ chelate formed from the reaction of the element in sea water with the ligand (identified by comparison with the results of analysis of the pure chelate); other peaks are not yet identified. GC conditions as in text.

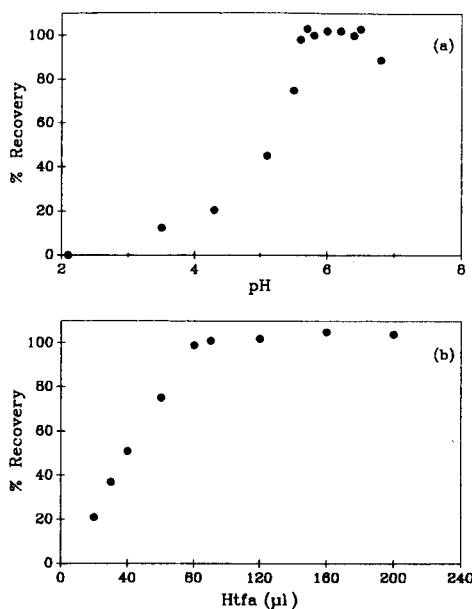


Fig. 2. Total chromium recovery as a function of (a) pH and (b) ligand volume. Samples were 15 ml of sea water, spiked with chromium and allowed to equilibrate for several days. Each point is the mean of two replicate analyses. All other conditions are as in the general procedure.

formed by summing up the areas of the two peaks.

Extraction conditions. The chromium complexation and solvent extraction procedure was optimized with respect to the pH, the ligand concentration, and the temperature/reaction time.

The highest recovery of chromium was achieved at pH range 5.6–6.5 (Fig. 2a). In general use the samples were adjusted to $\text{pH } 6.0 \pm 0.2$.

The extraction of chromium is dependent on the amount of ligand added. At constant pH, reaction time and temperature, the extraction efficiency increased with ligand volume in the range 20–80 μl but was independent of ligand volume at higher levels (Fig. 2b). Hamm et al. [19] observed that in solutions containing the hexa-aqua Cr(III) ion and organic acid anions, the reaction rate and the pH effect were independent of the nature of the anion present or its concentration so long as an excess was maintained, due to the slow chromium complexation kinetics. A volume of 100 μl of the pure ligand was used for all extractions in this study, and this was suffi-

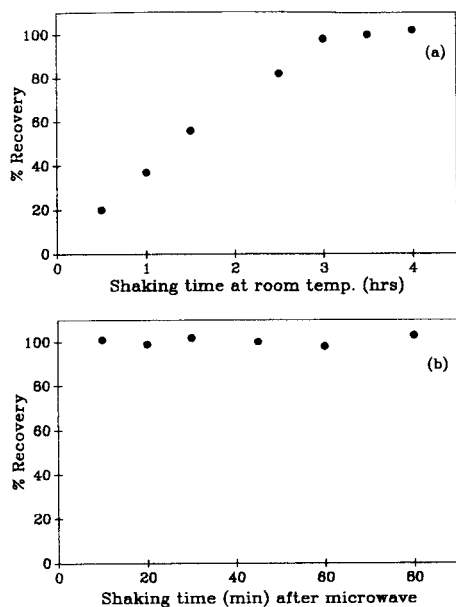


Fig. 3. Total chromium recovery as a function of (a) shaking time at room temperature and (b) shaking time after microwave irradiation. Samples were 15 ml of sea water, spiked with chromium and allowed to equilibrate for several days. Each point is the mean of two replicate analyses. All other conditions are as in the text.

cient for recovery of all the chromium in a 15-ml sample plus any added spikes during the optimization procedure.

The complexation kinetics of Cr(III) with HTFA are very slow at room conditions. Initial attempts to obtain quantitative extraction of chromium by reaction with the ligand at room conditions showed that at least 3–4 h shaking time were required. Figure 3a shows the percentage extraction efficiency of chromium as a function of shaking time at room temperature. Lovett and Lee [15] have reported a room temperature shaking time of at least 2 h for chromium concentrations below $10 \mu\text{g ml}^{-1}$ with the ligand in great excess (0.164 M in benzene) in order to obtain maximum chromium extraction. Measures [20] estimates 87% chromium recovery using 15 ml sea-water samples after shaking at room temperature for 2 h using 100 μl of HTFA.

In order to reduce the reaction time needed for quantitative extraction of chromium, it was necessary to increase the temperature of the re-

action mixture. A microwave oven was chosen for this purpose and resulted in excellent recoveries of chromium being obtained ($100 \pm 4\%$) in a short time. Moreover, the reaction time and the power level could be controlled precisely thus allowing for good reproducibility. As can be seen in Fig. 3b, chromium recovery was quantitative after the microwave procedure followed by 10 min or less of shaking the sample on the wrist action shaker.

Analytical figures of merit

The precision of the technique was evaluated by performing replicate total chromium analyses on a stored acidified sea-water sample. Six replicate analyses gave a relative standard deviation of 1.3% at 4.7 nM.

Absolute recovery studies of both Cr(III) and Cr(VI) spikes added to sea water were performed by spiking known amounts of the two chromium species into sea-water samples and then subjecting the samples to the full extraction procedure after allowing equilibration for 2–3 days. Two replicates for each sample were analyzed and as shown in Table 2, excellent recoveries of both species were achieved.

The excellent recovery of both chromium species shows that reduction of Cr(VI) to Cr(III) and the extraction procedure are both quantitative. Without reduction, however, Cr(VI)-spiked sea-water samples (stored frozen) show no detectable increase in signal. This verifies that

TABLE 2

Recovery of chromium spikes from sea-water samples^a

| Initial total chromium (nM) | Spike chromium added (nM) | Chromium species added | Total chromium recovered ^b (nM) | Recovery (%) |
|-----------------------------|---------------------------|------------------------|--|--------------|
| 4.70 ± 0.08 | 2.15 | Cr(III) | 6.62 ± 0.19 | 97 |
| 4.70 ± 0.08 | 4.31 | Cr(III) | 8.99 ± 0.04 | 100 |
| 4.70 ± 0.08 | 3.85 | Cr(VI) | 8.62 ± 0.21 | 101 |
| 4.70 ± 0.08 | 7.69 | Cr(VI) | 12.3 ± 0.03 | 99 |

^a Samples were 15-ml aliquots of sea water collected at 49°N 127°W in the North Pacific Ocean (see text for details).

^b Mean of two replicates.

chromium reduction during sample handling is insignificant.

The accuracy of the technique was assessed by the analysis of chromium in trace metal sea-water reference standards from the National Research Council of Canada. Two reference sea-water samples, the Nearshore Seawater Reference Material (CASS-2) and the Open Ocean Seawater Reference Material (NASS-3) were analyzed for total dissolved chromium using the technique developed in this study. The results are shown in Table 3.

The good agreement between the certified values for the reference materials and the values obtained by this technique to the samples provide proof for the accuracy of the method.

The limit of detection was estimated by the replicate analysis at sea for Cr(III) and total dissolved chromium in deionized water ($n = 6$ in each case) using the procedure developed here. Detection limits ($3s$) for Cr(III) and total chromium of 0.062 and 0.255 nM, respectively, were obtained.

Determinations at sea

Shipboard determination of Cr(III) and total chromium in the North Pacific were performed on board the C.S.S. "Endeavour" at two stations, P20 (Station "Papa", 50°00'N, 145°00'W) and P26 (49°34'N, 138°40'W) in October 1991. Cr(III) and total chromium analysis was completed for each station within 8 h after collection. Figure 4a and b shows the chromium concentration versus depth profiles at the two stations.

Analysis of filtered and unfiltered sea-water samples for chromium was carried out. Samples were filtered using 0.4- μ m Nucleopore polycarbonate membrane filters, in an acid-cleaned fil-

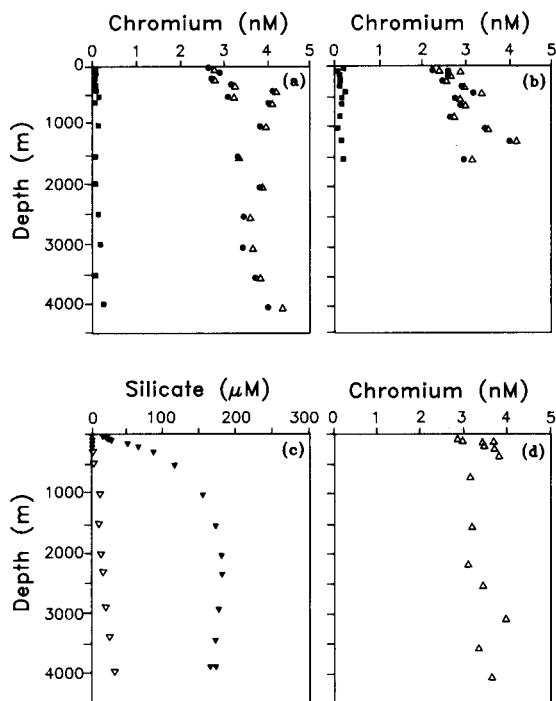


Fig. 4. Concentrations versus depth profiles. (■) Cr(III), (●) Cr(VI) and (Δ) total chromium concentrations at (a) Station P26 ("PAPA", 50°00'N, 145°00'W,) and (b) Station P20 (49°34'N, 138°40'W). Determinations were performed on board the C.S.S. "Endeavour". (c): (▼) Dissolved silicate, given for comparison, at station P26 (50°00'N, 145°00'W, same as "PAPA" [21]) and (▽) in the central north Atlantic Ocean (26°20'N, 33°40'W). (d): (Δ) Total chromium in the central north Atlantic Ocean (26°20'N, 33°40'W), from stored acidified samples.

tration unit hooked up to a vacuum pump. Filtration had no effect on the chromium content of the samples indicating that either particulate chromium concentration in the samples was negligible, undetectable by this technique, or that the particles were so small that they passed through the filters.

Chromium depth distribution

Shipboard determination of chromium at the two stations revealed that the Cr(III) concentration at both stations was very low and was generally at or below the detection limit of 0.06 nM. Total chromium, on the other hand, was considerably higher at 2.3–4.3 nM. These results agree with the prediction from theoretical calculations,

TABLE 3

Accuracy of chromium determination on sea-water samples

| Sea-water sample | Chromium (nM) | |
|------------------|--------------------|---------------|
| | Found ^a | Certified |
| CASS-2 | 2.331 ± 0.068 | 2.327 ± 0.308 |
| NASS-3 | 3.333 ± 0.011 | 3.365 ± 0.192 |

^a Mean of 7 replicates.

Cr(VI) was the dominant chromium species at these stations ($\geq 95\%$ of total chromium). The profiles show a slight surface depletion with a modest increase at depth, suggesting that chromium may be a nutrient-type (bio-intermediate) element.

It has been suggested [5,18] that the depth distribution of total chromium in both the Atlantic and Pacific Ocean is similar to that of silicate in these ocean basins, and that chromium, like silicate, might be involved in a deep regeneration cycle. Figure 4c shows the silicate distribution at Station "Papa" [21] obtained in 1987. Whereas silicate is nearly depleted in the upper waters, total chromium still has a significant surface concentration. Moreover, the slight increase in the concentration of chromium with depth does not in any way match the increase in silicate concentrations with depth. Analysis of stored sea-water samples from the central North Atlantic for total chromium (Fig. 4d) has not produced profiles similar to those of silica (Fig. 4c) either. The claim that chromium has a sea-water distribution similar to that of silica remains largely unsubstantiated.

The explanation for the increase in total chromium with depth is still unclear, as the mechanism of uptake of chromate (CrO_4^{2-}) by opal, CaCO_3 or organic matter has not been well established. Mayer and Schick [22] in their study of the removal of Cr(VI) from estuarine waters by model and natural substrates reported a removal dependence on sediment concentrations and salinity. They suggested a possible reductive adsorption mechanism. Naturally occurring levels of phosphate and silicate showed negligible effects on chromate removal.

The solubility control of Cr(III) in natural waters is not very well understood. Three candidates for this role have been suggested, and include $\text{Cr}(\text{OH})_3$ (s), chromite (FeCr_2O_4) and the mixed hydroxide ($\text{Cr}_x\text{Fe}_{1-x}$) $(\text{OH})_3$ (s) [5,8]. In addition Cr(III) is reported to bind strongly to particles and organic material [23,24], which may be responsible for the low dissolved concentrations observed. The role of organic ligands in Cr(III) speciation and the formation of polynuclear species are not well understood.

The frozen samples collected off Nootka Sound yielded values for Cr(III) which were higher (0.71–1.17 nM) than those found in open-ocean samples analyzed at sea, but still in agreement with other reported values [4,5]. This may be due to artifacts resulting from freezing and storage or to a coastal versus open-ocean effect.

Conclusion

The method described in this paper not only allows for the rapid and accurate determination of Cr(III) and total chromium in sea water in the laboratory but, more importantly, allows their determination at sea. Preliminary results obtained at sea indicate Cr(III)/Cr(VI) ratios between 0.02 and 0.05, which are at the low end of the range reported in the literature (0.02–0.99 [2]). Further investigations are clearly needed to provide a complete understanding of the geochemical cycle of this element. In particular, the use of natural laboratories such as anoxic and seasonally anoxic basins to monitor $\text{Cr}(\text{III}) \rightleftharpoons \text{Cr}(\text{VI})$ interconversion as a result of changes in oxygen concentrations, coupled with kinetic and speciation studies in the laboratory will be important. Additional work on the concentration and distribution of the two chromium species in hydrothermal solutions and buoyant plumes is also planned. It is hoped that these studies will help us elucidate the factors responsible for the marine geochemistry of chromium.

The authors are grateful to E.A. Boyle and colleagues at Massachusetts Institute of Technology (MIT) for the central North Atlantic samples, and to R.D. Bellegay and the Institute of Ocean Sciences (IOS), Sidney, BC, for providing ship-time on the C.S.S. "Endeavour". We also thank C.I. Measures (University of Hawaii) for helpful discussions and suggestions throughout the course of this project.

REFERENCES

- 1 H. Elderfield, *Earth Planet. Sci. Lett.*, 9 (1970) 10.
- 2 T.M. Florence and G.E. Batley, *CRC Crit. Rev. Anal. Chem.*, 9 (1980) 219.

- 3 G. Arrhenius and E. Bonatti, *Prog. Oceanogr.*, 3 (1965) 7.
- 4 R.E. Cranston and J.W. Murray, *Anal. Chim. Acta*, 99 (1978) 275.
- 5 J.W. Murray, B. Spell and B. Paul, in C.S. Wong, E.A. Boyle, K.W. Bruland, J.D. Burton and E.D. Goldberg (Eds.), *Trace Metals in Seawater*, Plenum Press, New York, 1983, pp. 643–669.
- 6 J.E. Earley and R.D. Cannon, *Trans. Metal Chem.*, 1 (1965) 34.
- 7 C.A. Johnson and A.G. Xyla, *Geochim. Cosmochim. Acta*, 55 (1991) 2861.
- 8 M. Pettine, F.J. Millero and T. La Noce, *Mar. Chem.*, 34 (1991) 29.
- 9 C.I. Measures and J.M. Edmond, *Anal. Chem.*, 58 (1986) 2065.
- 10 J. Savory, P. Mushak, F.W. Sundermann, E.M. Esters and N.O. Rozel, *Anal. Chem.*, 42 (1970) 294.
- 11 R.W. Moshier and R.E. Sievers, *Gas Chromatography of Metal Chelates*, Pergamon, Oxford, 1965.
- 12 G.H. Booth, Jr. and W.J. Darby, *Anal. Chem.*, 43 (1971) 831.
- 13 T.L. Isenhour, N.M. Frew and J.J. Leary, *Anal. Chem.*, 44 (1972) 665.
- 14 C.I. Measures and J.M. Edmond, *Anal. Chem.*, 61 (1989) 544.
- 15 R.J. Lovett and G.F. Lee, *Environ. Sci. Technol.*, 10 (1976) 69.
- 16 K.W.M. Siu, M.E. Bednas and S.S. Berman, *Anal. Chem.*, 55 (1983) 473.
- 17 R.C. Fay and T.S. Piper, *J. Am. Chem. Soc.*, 85 (1963) 500.
- 18 J.A. Campbell and P.A. Yeats, *Earth Planet. Sci. Lett.*, 53 (1981) 427.
- 19 R.E. Hamm, R.L. Johnson, R.H. Perkins and R.E. Davis, *J. Am. Chem. Soc.*, 80 (1959) 4469.
- 20 C.I. Measures, personal communications, 1991.
- 21 J.H. Martin, R.M. Gordon, S. Fitzwater and W.W. Broenkow, *Deep-Sea Research*, 36 (1989) 649.
- 22 L.M. Mayer and L.L. Schnick, *Environ. Sci. Technol.*, 15 (1981) 1482.
- 23 S. Osaki, T. Osaki, M. Setoyama and Y. Takashima, *J. Chromatogr.*, 257 (1983) 180.
- 24 G.S. Douglas, G.L. Mills and J.G. Quinn, *Mar. Chem.*, 19 (1986) 161.

Sampling of aquatic sediments. Design of a decision-support system and a case study

R. Wehrens, P. van Hoof, L. Buydens and G. Kateman

Laboratory for Analytical Chemistry, Catholic University of Nijmegen, Toernooiveld 1, 6525 ED Nijmegen (Netherlands)

M. Vossen, W.H. Mulder and T. Bakker

RIZA, P.O. Box 17, 8200 AA Lelystad (Netherlands)

(Received 1st June 1992; revised manuscript received 14th September 1992)

Abstract

The structure of a knowledge-based decision-support system for the sampling of aquatic sediments in lakes is discussed. The system is in the implementation stage and will advise on a sampling strategy that reveals as much as possible of the pollution level of the underwater soil, based on geomorphic information and analytical results for previous samples (if available). Constraints such as the desired precision and maximum sampling costs are taken into account. A case study on Ketelmeer lake (Netherlands) illustrates the techniques and heuristics that will be used in the decision-support system.

Keywords: Decision-support system; Sampling; Sediments; Waters

In each water system, there is a close relationship between the quality of (the suspended matter in) the surface water and the quality of the surface layers in the sediments underneath. As a consequence of water pollution in the past, the sediments in many industrialized countries are polluted in many places. Because of the close relationship between the quality of sediments and the quality of surface water, contaminated sediments can form a long-duration source of diffuse environmental pollution even when water pollution has been drastically reduced.

The potential risks for the environment have been the motivation in The Netherlands for the start of a water-bed cleaning programme in order to reduce the risks where needed. The programme is intended to reach a sediment quality

such that there are only negligible risks to the functioning of balanced aquatic ecosystems. In addition to the direct risks of contaminated sediments there are also problems of coping with contaminated dredging spoil. To describe the potential risks of water-bed pollution and in order to give practical directives for coping with contaminated dredging spoil, five categories of pollution have been defined in The Netherlands [1] (see Table 1).

In order to obtain an overview of the pollution of water-beds, a research programme throughout The Netherlands has been started. The aim is to categorize all water-beds in one of the above five categories. The category in which a sediment is classified depends on the number of compounds exceeding the standards (quality limits) that are defined for compounds most commonly present. Polluting compounds that are taken into account are heavy metals and organic micropollutants such as polycyclic aromatic hydrocarbons (PAHs),

Correspondence to: R. Wehrens, Laboratory of Analytical Chemistry, Catholic University of Nijmegen, Toernooiveld 1, 6525 ED Nijmegen (Netherlands).

polychlorinated biphenyls (PCBs) and pesticides. Consequences such as water-bed cleaning or storage of contaminated dredging spoil in storage depots depend on the classification of the sediment or spoil.

One of the first problems in starting the research programme is the question of where to take the samples. Whereas a lot of work has been done on the sampling of surface waters, sampling of aquatic sediments has been neglected. Further, as the sampling is performed by different water authorities such as the water boards, it is of great importance that one uniform sampling strategy is followed in the different water districts, otherwise the results would not always be intercomparable.

This sampling problem has given rise to start the development of a knowledge-based decision-support system, BIAS (a Dutch acronym for sampling of aquatic sediments). In the last few years, more and more knowledge-based systems have been used in environmental applications [2]. Some systems for sampling strategies have also been developed [3], although they concerned sampling strategies for dry soil, whereas BIAS is meant to provide consistent sampling strategies for water-beds. A first restriction was made to strategies for great lakes. The heuristics and statistical operations used in the expert system are validated using a number of test cases. From these, missing

knowledge may be extracted and existing knowledge may be refined.

Geomorphic information on the water system to be investigated and analytical results for previous measurements, if available, are included in the advice-forming model. General heuristics and statistically calculated parameters are then used to provide the optimum sampling strategy. Constraints such as the costs of sampling and the desired reliability should also be taken into account: the ideal sampling scheme of taking as many samples as possible is not, of course, feasible in practice.

In this paper, the structure of the knowledge-based system is discussed and an outline of the techniques used in the analysis of previous sampling data are given. Results of a case study on the Ketelmeer, a lake in The Netherlands, are discussed. Heuristics and plausible generalizations derived from this case study with respect to sampling strategies are presented. Finally, conclusions and directions for further research are given.

SETTING UP SAMPLING STRATEGIES WITH BIAS

Sampling strategies are used to minimize the amount of samples while still guaranteeing a specified accuracy [4]. To be able to choose the

TABLE 1

Classification of sediments according to level of pollution

| Class | Standard | Consequences for water-bed cleaning policy | Consequences policy on dredging spoils |
|-------|------------------------|--|---|
| 4 | Warning value | Research into necessity for cleaning urgent because of risk to public health and environment | Processing under controlled conditions which become stricter the more the quality of the dredging spoils exceeds the test value |
| 3 | | | |
| 2 | Test value | Research into need for cleaning not urgent | Use and dispersal in the water possible under certain conditions |
| 1 | Quality objective 2000 | | |
| 0 | Target values | No cleaning | Use and dispersal in the environment possible. Waterbed quality may not deteriorate |
| | | | No restrictions on use and dispersal in environment |

most profitable trade-off value in the case of sampling of sediments, one must have a good idea of the geomorphic properties of the water system and the relationships between them and diffusion patterns of the sediments. For the compounds that are of interest here, different distribution patterns may be encountered because of different adsorption on sediment material. Knowledge about the sources of pollution is also very important in this respect. Analytical results for previous samplings will also be very helpful in devising a relevant sampling strategy, as they can provide a model for the spatial correlation in the soil. A knowledge-based system that advises on a sampling strategy for aquatic sediments should be able to combine these different types of knowledge and should contain both statistical and heuristic knowledge. In BIAS, this is achieved by a division into modules each with a distinct task. The structure of BIAS is given in Fig. 1.

Module 1. Input and data validation

In Module 1 the characteristics of the water system are given by the user. These include, amongst others, shape and depth of the water system, soil types, direction and strength of the

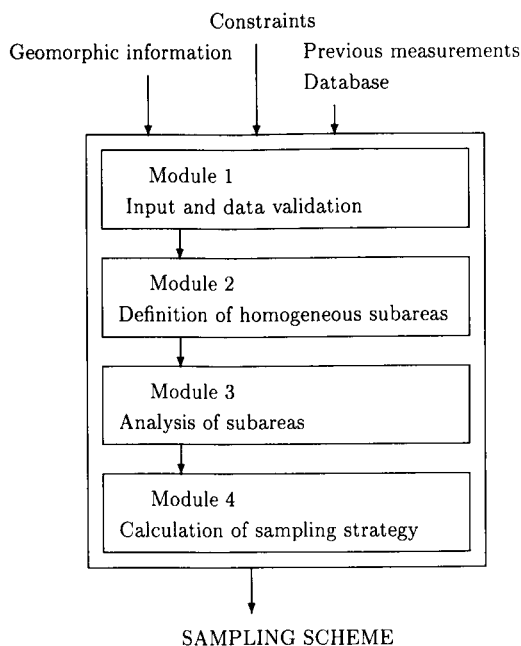


Fig. 1. The structure of BIAS.

current, prevailing direction and strength of the wind, sources of pollution, inlet(s) and outlet(s) of the water system, shipping routes, harbours and special items such as dredging areas. If available, data on previous samplings can be read from a database. These data are validated first to rule out typing and other errors. If all data are validated, control is passed to Module 2.

Module 2. Definition of homogeneous subareas

In Module 2 the water system is divided into more or less homogeneous subareas. These areas then are treated separately. The rationale behind this subdivision is that for each subarea a separate sampling strategy may be feasible; in calm, deep waters where little resuspension takes place only small deviations from the area mean will be expected, and in many cases only a few samples will suffice. In shallow waters with a strong current, many more samples will have to be analysed to obtain a good overview of the local situation.

The division into subareas is based on a set of parameters that influence the pollution level of an underwater soil. They can be divided into the following:

- climatological conditions—wind, prevailing direction and strength;
- hydrological conditions—depth, and direction and speed of the current;
- geomorphological conditions—soil type;
- human activities—shipping, harbours, dredging, sources of pollution.

If results of previous samplings are available, a cluster analysis is done to see whether the clustering of the samples fits the predefined areas. If agreement is found, this means an extra affirmation that the division into subareas was done on relevant grounds. If no agreement is found, the data should be examined more carefully. In some instances, missing knowledge can be detected in this way, e.g., a sample location may be influenced by a parameter that has been overlooked in the input phase. Outliers may also be detected in this way.

Module 3. Analysis of subareas

If results of previous samplings are available, they are analysed here to estimate pollution lev-

els at unsampled locations. The assumption is that locations that are spatially close to each other tend to have similar soil characteristics. Two techniques can be used here: a two-dimensional interpolation technique often used in mining, called kriging [5,6], and a one-dimensional technique, stemming from time series analysis and using autocorrelation [7,8]. Because all spatial correlations can be taken into account in the two-dimensional plane, kriging will give better predictions. Autocorrelation methods, on the other hand, do not require as many data as kriging techniques and are therefore applicable in (frequently occurring) cases where relatively few data are available.

Both methods require a set of conditions to be fulfilled to produce useful predictions. First, the variance of the variable to be estimated depends only on the lag vector between the two locations. Often this condition is replaced by an even stronger one in which only the length of the lag is taken into account and the direction is neglected. This, however, will yield incorrect results in many instances as different correlations will exist in different directions. Second, the variable is stationary, i.e., no drift is present. Effectively, this means that the a priori expectation for all locations in the area is equal. In practice, additional knowledge about the area will often make this assumption false. The subareas obtained in the previous module are meant to satisfy these conditions. In general, it is very difficult to determine whether this is the case. The most popular method to validate the method is cross-validation, where values at sampled locations are predicted using the other locations. However, good predictions still are no guarantee that the conditions are satisfied.

Kriging and related methods. Kriging can be seen an optimum unbiased interpolation method; based on known values in sampled locations, values at other locations are predicted. A measure indicating the amount of correlation between two locations separated τ times a lag distance h apart is the semivariance γ_τ . The semivariance for a lag τ is given by

$$2\gamma_\tau = E\{[z(x) - z(x + \tau h)]^2\} \quad (1)$$

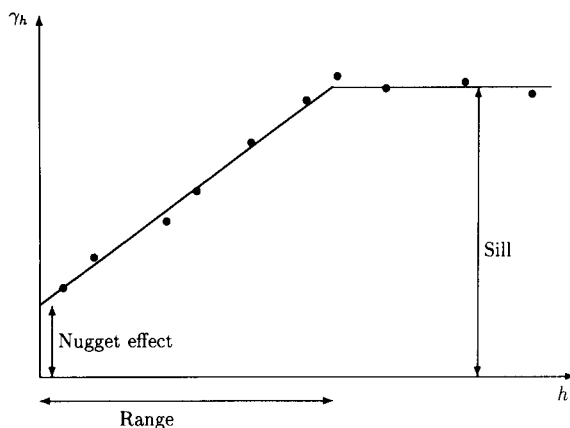


Fig. 2. Idealized example of a semivariogram. In this instance a linear model is chosen to represent the data (see text).

and can be estimated by the equation

$$\hat{\gamma}_\tau = \frac{1}{2n(\tau)} \sum_{i=1}^{n(\tau)} [z(x_i) - z(x_i + \tau h)]^2 \quad (2)$$

where $z(x_i)$ and $z(x_i + \tau h)$ are the values of the variable of interest, x , at location i and a location τ lags away, respectively (in kriging and related topics, variables are termed regionalized, indicating that the variables are a non-random sample from one realization of a random function; this is different from the usual idea of multiple realizations of a random variable but for the present purposes, this difference can be ignored). The number of pairs $[z(x_i), z(x_i + \tau h)]$ is given by $n(\tau)$. The semivariogram, in which semivariances are plotted against the lag number (see Fig. 2), is modelled by fitting a simple function through the data points. Linear, exponential and spherical models are often used. At lag zero, the semivariance is 0. In many instances a discontinuity is present called the nugget effect. This indicates that there is significant variance over distances smaller than the lag distance. At large distances, the semivariance is equal to the variable variance and reaches a ceiling, called the sill. These parameters, and the range where the semivariance increases with the lag, are indicated in Fig. 2.

The value of a variable x at an unsampled location is derived from a linear combination of nearby points. Kriging attempts to minimize the

prediction error. This can be achieved by solving the following matrix equation:

$$\begin{pmatrix} \gamma(h_{1,1}) & \cdots & \gamma(h_{1,n}) & 1 \\ \vdots & & \vdots & \vdots \\ \gamma(h_{1,n}) & \cdots & \gamma(h_{n,n}) & 1 \\ 1 & \cdots & 1 & 0 \end{pmatrix} \begin{pmatrix} W_1 \\ \vdots \\ W_n \\ \lambda \end{pmatrix} = \begin{pmatrix} \gamma(h_{1,p}) \\ \vdots \\ \gamma(h_{n,p}) \\ 1 \end{pmatrix} \quad (3)$$

or the equivalent form

$$\mathbf{A} \cdot \mathbf{w} = \mathbf{b} \quad (4)$$

where $h_{i,j}$ is the distance between the sampled locations i and j , $\gamma(h_{i,j})$ is the semivariance between locations i and j , $\gamma(h_{i,p})$ is the semivariance between the sampled location i and the unsampled location p , obtained from the semi-variogram, W_i is the weight given to location i in the prediction of location p and λ is the La-

grange multiplier. The solution for the unknown vector \mathbf{w} is simple:

$$\mathbf{w} = \mathbf{A}^{-1} \cdot \mathbf{b} \quad (5)$$

This gives for an estimate on location p the value

$$\hat{x}_p = \mathbf{w} \cdot \mathbf{x} \quad (6)$$

with prediction error variance

$$s_\epsilon^2 = \mathbf{w} \cdot \mathbf{b} \quad (7)$$

The weights obtained in this way are optimum in the sense that the predictor is unbiased and has a minimum prediction error variance. The predictor is also exact, which means that the value at a sampled location is predicted exactly and with zero error. Contour maps may be drawn that provide a global view of the situation.

Several other types of kriging exist. In universal kriging [9,10], a polynomial trend is permitted. In co-kriging [11,12], the value of the variable of interest in an unsampled location is determined not only by interpolation from sampled locations, but also by measurements of correlated variables. Disjunctive kriging [13–15] is a variant in which

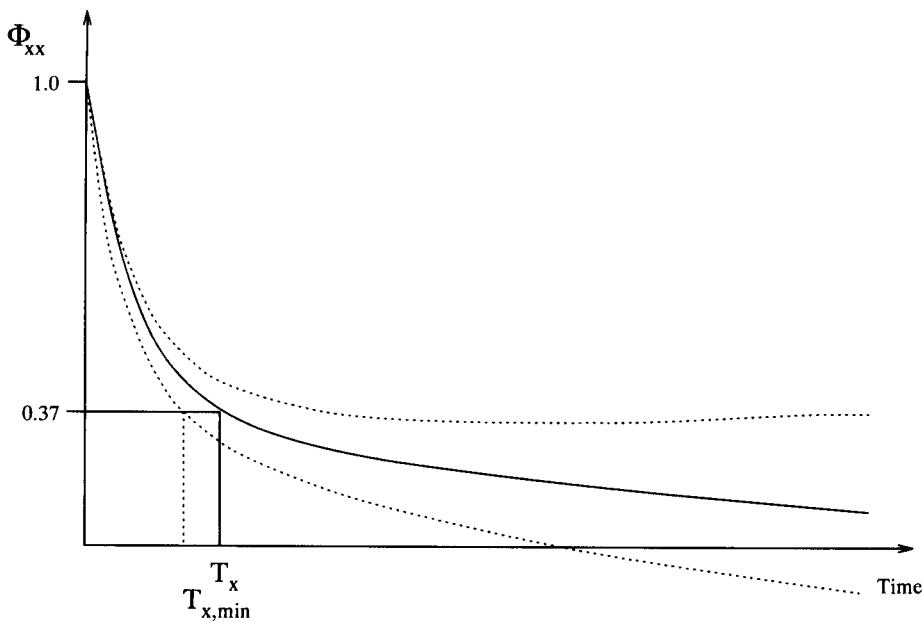


Fig. 3. Example of an autocorrelogram.

the conditional probability that a soil value exceeds a predefined threshold can be calculated and plotted.

Autocorrelation methods. Autocorrelation techniques stem from time series analysis. They are based on the assumption that the value of a measurement can be related to the value of previous measurements. Time can also be replaced with distance, and then the assumption is that the value of a variable at a specific location is related to values at nearby locations. The methods are inherently one-dimensional.

In autocorrelation techniques, autocovariance is used rather than semivariance to express the similarity between two measurements τ times a lag distance h apart:

$$\begin{aligned} \text{cov}(x, x + \tau h) \\ = E\{[z(x) - \mu][z(x + \tau h) - \mu]\} \end{aligned} \quad (8)$$

where μ is the process mean value. If only a few measurements are available, the autocovariance can be estimated by

$$\begin{aligned} \widehat{\text{cov}}(x, x + \tau h) = \frac{1}{n - \tau - 1} \sum_{i=1}^{n-\tau} [z(x_i) - \mu] \\ \times [z(x_i + \tau h) - \mu] \end{aligned} \quad (9)$$

where n is the total number of measurements. The (dimensionless) autocorrelation then is defined by

$$\Phi_{x,x}(\tau) = \text{cov}(x, x + \tau h) / s_x^2 \quad (10)$$

where s_x^2 denotes the variance of x . In an autocorrelogram the autocorrelation is plotted against τ . In many instances, linear first-order models are found to be satisfactory. They give an exponentially decreasing curve such as that depicted in

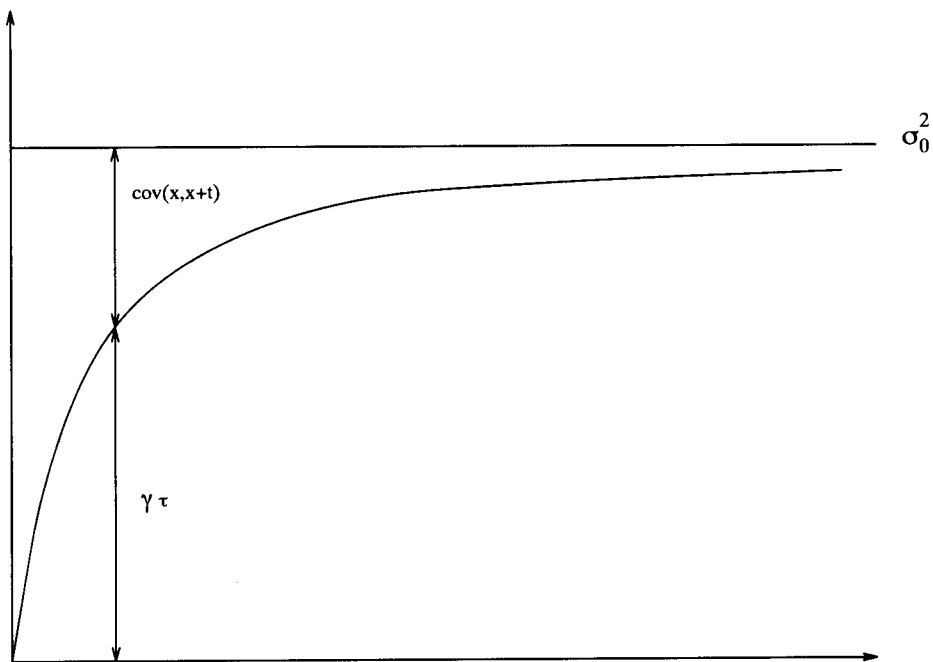


Fig. 4. Relationship between autocovariance $\text{cov}(x, x + \tau)$, semivariance γ , and process variance σ_0^2 .

Fig. 3. The variance of such an autocorrelation function can be estimated by

$$\hat{s}^2[\Phi_{x,x}(\tau)] = \frac{1}{N-\tau} \left[\frac{(1 + e^{-2/T_x})(1 - e^{-2\tau/T_x})}{1 - e^{-2/T_x}} - 2\tau e^{-2\tau/T_x} \right] \quad (11)$$

where T_x and τ are given in lag units. From this function, the upper and lower confidence limits for the autocorrelation function can be calculated. These are depicted in Fig. 3 as dotted lines.

The distance at which the value of the autocorrelation has decreased with a factor of e^{-1} is called the correlation distance T_x . If the autocorrelation at this distance differs significantly from zero, the correlation distance can be seen as a measure of the maximum distance at which a parameter still shows significant autocorrelation (if autocorrelation is used in time series analysis, the parameter T_x is called the time constant). A large correlation distance indicates that the value of a certain parameter does not change much with distance. Whereas in many instances it is not possible to calculate an upper confidence limit for T_x because the upper border diverges from the exponential curve, it is possible to calculate a minimum value $T_{x,\min}$. This is the value where the lower confidence limit has decreased with a factor of e^{-1} .

In practice, the correlation distance may be calculated in a direction parallel as well as perpendicular to the current. If the two are equal, the system is isotropic; in most instances, however, anisotropic systems will be found.

The autocorrelation equations are very closely related to the semivariance equations. If the variable is stationary (i.e., the expected value of the variance is equal in the whole area), the semivariance for a distance h is equal to the difference between the variance σ_0^2 and the spatial autocovariance σ_n^2 for the same distance (see Fig. 4). If the variable is also standardized to have a mean of zero and a variance of 1.0, the semivariogram is a mirror image of the autocorrelation function.

Comparison of autocorrelation methods and kriging. From the above, some conclusions can be

drawn. Both methods require the same assumptions to be valid, with the added condition in autocorrelation techniques that the process variance, s_x^2 , exists. Kriging is the preferred method if many data are available and a reliable semivariogram can be set up. The interpolations take full advantage of the information in the semivariogram, and prediction variances can be plotted. Also sampling strategies can readily be obtained (see below). In cases where only a few data points are sampled, however, often no semivariogram can be calculated. It has been estimated that at least 100 data points, depending on the size and structure of the sampling area, are necessary in order to perform an accurate geostatistical analysis. This value may be different with aquatic sediments, and future research should clarify this point. Until then, the user will have to decide whether the number of data points is sufficient to provide a semivariogram or not. In the latter instance, autocorrelation techniques may provide a more reliable estimate. The upper and lower limits on the autocorrelogram provide useful information on the representativity and reliability of the samples. Although autocorrelation techniques are in most instances inappropriate for stratified objects such as soil and rock [16], they can be used here because of the dynamic nature of the sedimentation process. Another advantage of autocorrelation techniques is that typical values for correlation distances in different water systems can be tabulated and used as a first estimate in case the development of a sampling strategy has to start from scratch.

Module 4. Calculation of a sampling strategy

Several sampling strategies are possible, depending on the aim of the investigation: a strategy to obtain a global view of concentrations of (polluting) compounds with a predetermined reliability; a strategy to obtain an idea of concentrations of (polluting) compounds, as reliable as possible, given the allowed costs; a strategy that does not focus on exact concentrations of (polluting) compounds but more on classifications of soil in pollution classes with a given reliability; a strategy used for monitoring. Each strategy has its own requirements. For both autocorrelation

techniques and kriging and related techniques, such sampling strategies may be set up.

Sampling strategies and kriging. If kriging techniques are applied to develop sampling strategies, several situations may occur [17]. In the simplest case the semivariogram is known. It is then possible to calculate the prediction variances of several sampling set-ups irrespective of the values that will be found. A triangular grid has been shown to yield optimum results, but a cubic grid is in most instances almost as good and easier to achieve. If only additional samples are needed, their location can be derived from the kriged contour map of the prediction variances [18]. If, for instance, only one location has to be added to a set of sampled locations, this can best be done at the place where the prediction variance is largest. In this way, the overall standard deviation is minimized.

If no variogram has been determined previously, a sampling strategy should aim to optimize the sample locations with respect to variogram estimation [19,20]. For this, the sampling locations should be chosen in such a way that all lags contain an approximately equal number of pairs. In general, a nested sampling design is chosen. Whereas many samples are needed to obtain a reliable variogram, for a reliable interpolation given a good variogram many fewer samples will suffice.

In the frequently occurring situations where different variables are correlated, co-kriging methods may be used [11]. In such a case the costs of analysis of different compounds may be taken into account, and cheap analyses may be performed much more often than expensive ones. In this way, it is possible to obtain reliable estimates at much lower cost. Finally, disjunctive kriging may be used to determine what pollution classes are present in the water system, and if the uncertainty of the presence of a certain class is too high additional samples may be taken.

Sampling strategies and autocorrelation techniques. Autocorrelation techniques have been used earlier to predict an optimum sampling frequency for the surveillance of surface water quality [21], and also other applications have been reported [22]. Previously, equations have been

derived to calculate the prediction variance, σ_{est}^2 , as a function of the number of samplings n , the process variance σ_0^2 and the size and spacing of the samples [8]. If the sample size is very small compared with the size of the area, the following equation holds:

$$\frac{\sigma_{\text{est}}^2}{\sigma_0^2} = \frac{1}{n} \left[1 + \frac{2e^{-a}}{1 - e^{-a}} - \frac{2e^{-a}(1 - e^{-p})}{n(1 - e^{-a})^2} \right] - \frac{2}{np} \left(2n - \frac{1 - e^{-p}}{1 - e^{-a}} + \frac{1 - e^{-p}}{1 - e^{-a}} \right) + \frac{2}{p^2} (p - 1 + e^{-p}) \quad (12)$$

where a is the distance between two adjacent samples and p is the length of the sampled area, both divided by the correlation distance. This equation has to be solved iteratively to obtain the distance between adjacent samples in the area in which the correlation distance holds. Autocorrelations obtained in different directions must be used to determine the distances between samples in the grid. Again, if the autocorrelogram has been determined with sufficient reliability, the number of samples needed for a reliable prediction is much smaller than the number of samples needed to set up a good autocorrelogram. In this respect the same situation as in the kriging case is encountered.

Constraints on sampling strategies. Any proposed sampling scheme should be reasonable with respect to constraints such as the number of analyses and the total costs associated with sampling. If the sampling strategy proposed to obtain a required reliability cannot be performed with the means available, a new scheme will have to be set up. Either the reliability will be lower, if the cost constraint is satisfied, or the sampling operation will be more expensive. In both instances, the system may be consulted again with different input values for the constraints. The use of correlation between different compounds may be a very important tool to diminish the costs of sampling: either using a few compounds as guiding parameters or using co-kriging or related methods will decrease the number of samplings of the associated costs.

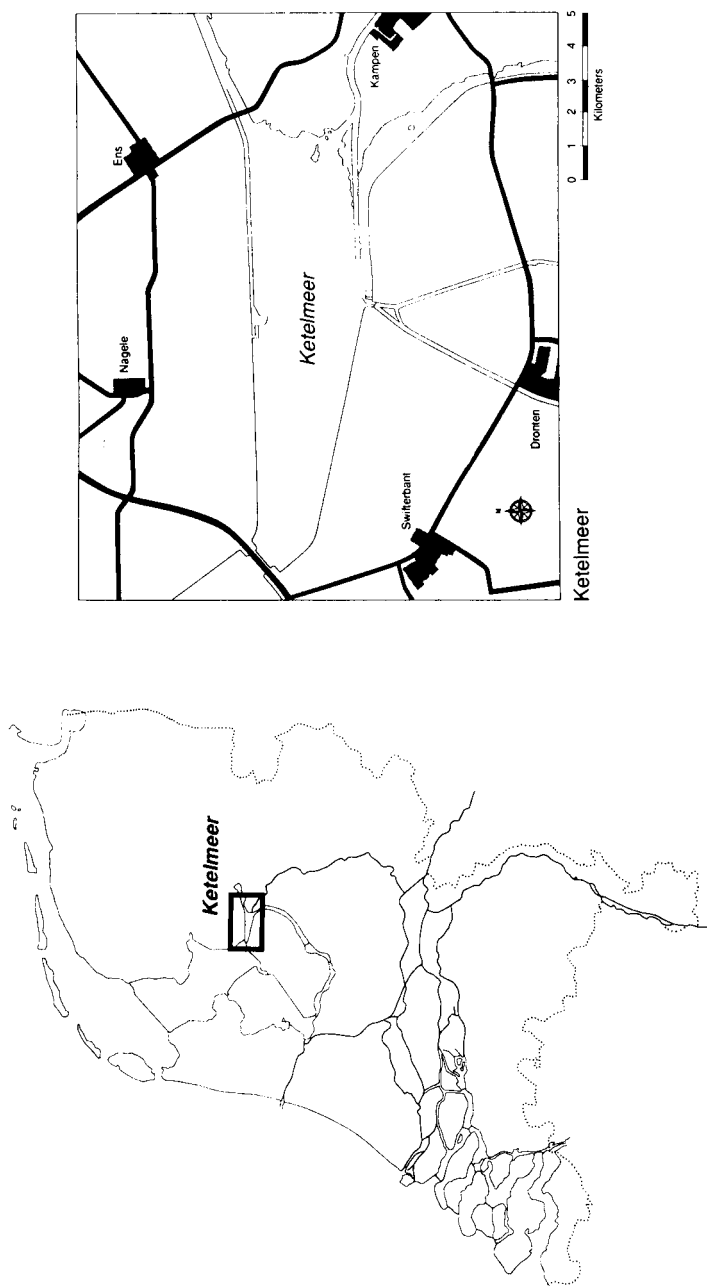


Fig. 5. The Ketelmeer.

THE KETELMEER

The Ketelmeer is a lake 12 km long and 4 km wide, in central Netherlands (Fig. 5). It is shallow, most areas being 2–3 m deep. In the very shallow (< 1 m) part in the east of the lake, the sediment consists of sand; in the other parts the sand is covered with more loam-like sediment. The river IJssel debouches into the south-east corner of the lake and water flows out from the north-east side. There is some shipping and two small harbours can be found on the north and south coasts. The prevailing direction of the wind is south-west. In the following sections, the Ketelmeer will be treated as an example of how a sampling strategy is set up in BIAS. The sections follow the general structure of BIAS: input and data validation, definition of homogeneous subareas, analysis of subareas and calculation of the required sampling strategy.

Validation of previous sampling data of the Ketelmeer

As the Ketelmeer has long been polluted, a relatively large amount of sampling has already taken place [23]. A data set of sampled locations was selected on the following criteria. All locations should be sampled to obtain at least 80% of the top layer. The top 10–20 cm are easily disrupted, even in calm and sheltered areas. Moreover, the degree of pollution of sediment has changed considerably with time, and comparable periods of time should be represented in the samples. Care was taken not to include locations where more than just the top layer was sampled, because the underlying sand will be much cleaner and the samples would not be intercomparable. The depth at the sampled locations should not have changed much since the sample was taken. If significant suspension or erosion has taken place since then, the sample is not representative for the current situation. Local human activities should be taken into account. If, e.g., a harbour is present near one of the sampled locations, or dredging has taken place, again these samples are not representative for the area. Further, most human activities constitute a direct source of pollution and should be considered if samples

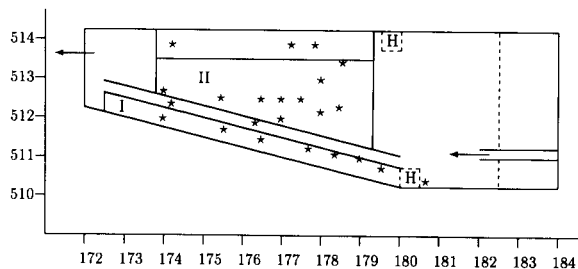


Fig. 6. Schematic drawing of the Ketelmeer. The numbers on the axes are the distances in kilometres to a reference point in Paris, France. Inlet and outlet are indicated by arrows. Harbours are indicated by H. Each point indicates a sampling location. Subareas are drawn and indicated with roman numerals.

have to be taken in an area where much activity takes place.

Definition of homogeneous subareas in the Ketelmeer

At all sampled locations included in the analysis, the same soil type should be present, because different sediment compositions will show different degrees of pollution. Because of the availability of the data, heavy loam [12–25% clay (particles smaller than $2\mu\text{m}$)] was selected. This caused the analysis to concentrate on the central and western part of the lake. In the sandy part in the east, not enough samples were taken for a reliable analysis. Overall, 23 of the locations that satisfied the conditions in module 1 were in the heavy loam area. These are drawn in Fig. 6. The heavy loam part was subdivided into a part sheltered from the wind along the southern dike (area I in Fig. 6 containing seven sampling locations), a central part, exposed to the wind (area II, containing ten locations), a shipping route (the narrow area above area I) and a region containing sand-pits in the western part (left of area II).

A cluster analysis using Euclidean distance confirmed the above subdivision. Further, an area along the northern dike (north of area II) was defined because cluster analysis showed that the samples in this area were not correlated with the other samples in area II, probably because the distances between them were too large. Two sampling locations fell in the shipping route where,

because of dredging, no reliable estimates could be made. One location was very near a harbour and was also excluded. Some locations were considered to be outliers, such as the middle sampling location in area I. Eventually, areas I and II, containing seventeen sampling locations, were used in the following analysis, and sampling strategies for these areas were set up. If sampling strategies have to be set up in areas where no samples have been taken, it must be done on heuristic grounds.

Analysis of subareas of the Ketelmeer

As the Ketelmeer is essentially oblong-shaped, the current plays an important role in the sedimentation process. As the data were scarce, no relevant models could be fitted through the semi-variograms and kriging techniques could not be applied. Therefore, autocorrelation techniques were used. For each of the subareas I and II in Fig. 6 the autocorrelograms for all compounds to be analysed for are calculated. Because over 90% of the pollution comes from the river IJssel, autocorrelograms are drawn using one dimension, the distance to the mouth of the river. This dimension is more or less equal to the direction of the current. Perpendicular to the chosen direction, too few samples were taken to obtain an autocorrelogram.

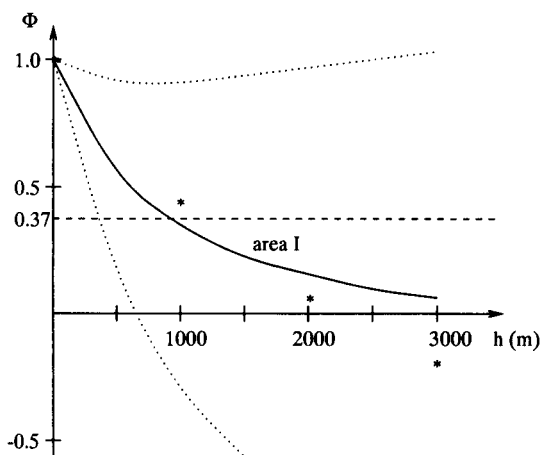


Fig. 7. Autocorrelogram for fluoranthene in the sheltered area I of the Ketelmeer.

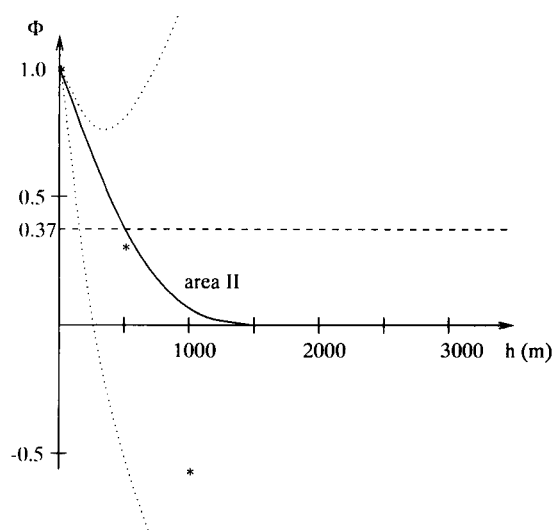


Fig. 8. Autocorrelogram for fluoranthene in the central area II of the Ketelmeer.

The autocorrelograms for fluoranthene in the two areas are depicted in Figs. 7 and 8. Correlation distances are calculated by fitting exponential curves to the data points. Correlation distances are given in Table 2. The values indicated are class means, i.e., the value for the heavy metals is the mean of the value found for Cu, Cd, Cr, Hg, Ni, Pb and Zn. As can be seen, the correlation distance in area I is much larger than that found in area II. This means that in area I the amounts of fluoranthene in the soil change more slowly on going from one place to another than in area II. Also, the minimum correlation distance in area I is much larger than that in area II. This is what would be expected, as the influence of the wind in the sheltered part is much less than the influence in the central part, where currents can easily be induced.

The 95% confidence limits are shown. It is clear that the resulting autocorrelograms are not very reliable. The reason for this is that the correlation distances found are smaller than or equal to the lag distance. In some instances in area II, no correlation distance could be calculated at all. The only way to improve the precision of the functions is to use more sampled locations to set up the autocorrelation functions. At present, there is no reason to doubt the valid-

TABLE 2

Correlation distances in the Ketelmeer^a

| Substance class | T_x (area I) | $T_{x,min}$ (area I) | T_x (area II) | $T_{x,min}$ (area II) |
|-----------------|-------------------|-------------------------|--------------------|--------------------------|
| Heavy metals | 530 | 250 | 390 | 140 |
| PCBs | 460 | 210 | 250 | 110 |
| PAHs | 800 | 320 | 180 | 80 |

^a Distances are given in metres. Areas I and II refer to Fig. 6. The lag distance in area I is 1000 m and in area II 500 m. For three compounds in the PAH class, two compounds in the PCB class and one heavy metal (Cd), no autocorrelation function could be set up in area II because the autocorrelation at the first lag was already less than zero. The figures given are based on the other compounds in the classes.

ity of the first-order linear model, as all data points lie well within the confidence limits.

Calculation of a sampling strategy for the Ketelmeer

Although far from being optimum, the above results reveal a lot of information that can be used to set up a sampling scheme. Because the correlation distances that have been found are in the same order of magnitude as the sampling distances, the resulting autocorrelograms are not very reliable. Therefore, additional sampling should in the first place aim to improve the reliability of the autocorrelograms, which means that extra samples have to be taken at smaller distances from each other. At least three lags should lie within the correlation distance. If one considers the values for the heavy metals, which are determined with the greatest accuracy, this criterion would yield a distance between adjacent samples of 200–250 m for area I and 100–150 m for area II. As these values are estimated from the correlation distances in the direction of the current, they are valid in that direction only. As a first approximation, the same values may be used in the perpendicular direction. It is not necessary to sample the complete (sub)area with the same frequency: as soon as there are enough data points to set up a reliable autocorrelogram, the sampling frequency may be decreased to obtain the required precision (cf., Eqn. 12).

For example, if it is assumed that the above correlation distances are correct and if it is wanted

that the reliability, expressed as the estimation variance divided by the process variance, should have a value of 0.1, then it can be calculated that for area I (length 7 km, mean correlation distance 600 m) one row of five samples is enough. Similarly, for area II (length 6 km, average width 2 km, mean correlation distance 260 m) a grid with spacings of 1000 m in the direction of the current and 500 m in a perpendicular direction suffices. Here, the correlation distance found in the direction of the current is also used in the perpendicular direction (Eqn. 12 also contains the length of the area sampled, and therefore the spacings in the two perpendicular directions are not equal). It is clear that sampling where a reliable autocorrelogram is known is much cheaper than sampling to obtain the autocorrelogram; for the latter objective, in this instance more than seven times as many samples are needed in both areas.

Extrapolations to other parts of the lake will have to be made, based on heuristics. This will provide a complete sampling scheme for the lake. If the costs for this sampling scheme violate the constraints concerning budgets, a lower reliability must be specified, or some subareas will have to be treated separately, with a smaller sampling frequency.

General results obtained in the Ketelmeer case study

For the Ketelmeer, it has been shown that autocorrelation methods can be useful in devising sampling strategies for aquatic sediments. Despite the small number of data points, useful information has been obtained to guide further sampling in the area. The correlation distance determined from previous samplings or geomorphic information can be used to fulfil two objectives simultaneously: to devise a sampling scheme that permits a more precise estimation of the correlation distance, and a sampling scheme that yields a subsequent interpolation to unsampled locations of a specified accuracy. For the first goal, two perpendicular rows of samples may be taken over a distance of four times the correlation distance, with a spacing of one quarter of the correlation distance. This yields a total of sixteen samples. In smaller subareas (such as area I in

the Ketelmeer), fewer samples or one row of samples may suffice. The second goal is achieved by calculating the distances between samples in a rectangular grid that will provide an interpolation with a desired accuracy. In general, the number of samples needed to satisfy the second goal is much smaller than that required to satisfy the first.

The results of the Ketelmeer study, notably the correlation distances and sampling schemes derived from them, may also be extrapolated to other water systems, where depth, current and other parameters are comparable. What parameters exactly are of influence is still a subject of investigation. In cases where different conditions are met, results will be different. For instance, the influence of the wind that was clearly present in the Ketelmeer will be much smaller with deep (> 5 m) waters. There, sedimentation will proceed much more calmly, and larger correlation distances will be expected there. In the Ketelmeer, it proved to be necessary to analyse only those samples which constituted a large portion of the top layer. Correlation values obtained from locations where only small portions of the top layer were sampled showed large scatterings because of continuous whirlings of the top sediment. In deeper waters, this will not be so much of a problem. In the Ketelmeer, good correlations were found between the concentrations of the different compounds of interest. It may be expected that this is generally the case when all pollution stems from the same source. In such a situation, some of the compounds may serve as guiding parameters for others that are perhaps difficult to measure or for which expensive methods are necessary.

Conclusion

The importance of consistent and reliable sampling strategies for underwater soils cannot be overestimated. The amount of money that can be saved and the amount of extra information that can be obtained using sensible sampling schemes are considerable. In this paper, an approach has been presented that aids the water managers of the separate districts in The Netherlands in setting up such strategies. A case study, the

Ketelmeer, has been used to test the validity of the approach and to test the knowledge for a practical situation. The knowledge that is acquired in this way will be implemented in a knowledge-based system, BIAS. More test cases will follow, thus enabling the system to be tested on a wide variety of lakes. This is necessary in order to be able to set up heuristics that can help in the advice-forming module when no previous sampling data are available. Although some heuristics have already been established, the list is far from being complete yet. In the near future, new test cases will be tackled and extra samplings on test cases already analysed will be performed.

The authors thank H.J. Winkels and H.C. Klavers for valuable comments and discussions. This research was carried out with financial support from the Dutch Ministry of Transport and Public Works.

REFERENCES

- 1 Water in The Netherlands: a Time for Action, Ministry of Transport and Public Works, The Hague, 1991.
- 2 J.M. Hushon (Ed.), Expert Systems for Environmental Applications (ACS Symposium Series, No. 431), American Chemical Society, Washington, DC, 1990.
- 3 R.A. Olivero and D.W. Bottrell, in J.M. Hushon (Ed.), Expert Systems for Environmental Applications (ACS Symposium Series, No. 431), American Chemical Society, Washington, DC, 1990, pp. 69–81.
- 4 G. Kateman and F.W. Pijpers, Quality Control in Analytical Chemistry, Wiley-Interscience, New York, 1981.
- 5 A.G. Journel and Ch. Huijbrechts, Mining Geostatistics, Academic Press, London, 1978.
- 6 D.E. Myers, Chemometr. Intell. Lab. Syst., 11 (1991) 209.
- 7 G.E.P. Box and G.M. Jenkins, Time Series Analysis, Holden-Day, San Francisco, 1976.
- 8 P.J.W.M. Müskens and G. Kateman. Anal. Chim. Acta, 103 (1978) 1.
- 9 A. Stein and L.C.A. Corsten, Biometrics, 47 (1991) 575.
- 10 R. Webster and T.M. Burgess, J. Soil. Sci., 31 (1980) 505.
- 11 A.B. McBratney and R. Webster, J. Soil. Sci., 34 (1983) 137.
- 12 D.E. Myers, Math. Geol., 14 (1982) 249.
- 13 R. Webster and M.A. Oliver, J. Soil. Sci., 40 (1989) 497.
- 14 S.R. Yates, A.W. Warrick and D.E. Myers, Water Resour. Res., 22 (1986) 615.
- 15 S.R. Yates, A.W. Warrick and D.E. Myers, Water Resour. Res., 22 (1986) 623.

- 16 G. Kateman, *Top. Curr. Chem.*, 141 (1987) 43.
- 17 T.M. Burgess, R. Webster and A.B. McBratney, *J. Soil. Sci.*, 31 (1981) 643.
- 18 H.J. Di, B.B. Trangmar and R.A. Kemp, *Soil Sci. Soc. Am. J.*, 53 (1989) 1163.
- 19 D. Russo and W.A. Jury, *Soil Sci. Soc. Am. J.*, 52 (1988) 1228.
- 20 A.W. Warrick and D.E. Myers, *Water Resour. Res.*, 23 (1987) 496.
- 21 P.J.W.M. Müskens, *Anal. Chim. Acta*, 103 (1978) 445.
- 22 J. Einax, B. Machelett, S. Geiss and K. Danzer, *Fresenius' Z. Anal. Chem.*, 342 (1992) 267.
- 23 H.J. Winkels and A. van Diem, *The Makeup and Quality of the Ketelmeer Soil. Technical Report, Ministry of Transport and Public Work, The Hague, 1991, Flevovericht 325 (in Dutch).*

Trace determination of sugar acids (gluconic acid) in sea water by liquid chromatography

Shigeto Nakabayashi, Isao Kudo, Kenshi Kuma and Katsuhiko Matsunaga
Department of Chemistry, Faculty of Fisheries, Hokkaido University, Hakodate 041 (Japan)

Kiyoshi Hasebe

Department of Chemistry, Faculty of Science, Hokkaido University, Sapporo 060 (Japan)

(Received 28th April 1992; revised manuscript received 10th August 1992)

Abstract

A liquid chromatographic (LC) method with fluorescence detection was developed with sufficient sensitivity to determine organic acids in sea water and sediments. Sugar acids, except for uronic and α -keto acids, have not previously been measured in sea water because of their low concentrations. After desalting with a column, gluconic acid was esterified with 9-anthryldiazomethane. The reaction mixture containing the gluconic acid derivative was directly chromatographed by LC using an octadecylsilane reversed-phase column and fluorescence detection. The peak areas were linearly related to gluconic acid concentration. The detection limit was less than 10 nM. The reproducibility and recovery were 8% at 200 nM gluconic acid and 99.8%, respectively.

Keywords: Fluorimetry; Liquid chromatography; Gluconic acid; Sea water; Sugar acids; Waters

In previous studies [1,2], Fe(II) was found in surface sea water during spring blooms and the presence of Fe(II) may meet an iron demand for phytoplankton growth. It was proposed that Fe(II) is produced by photochemical reactions with Fe(III) and organic substances under sunlight. Moreover, laboratory experiments showed that the important organic substances that reduce Fe(III) to Fe(II) are sugar acids such as gluconic, glucaric and glucuronic acid [2]. Among these sugar acids, gluconic acid is especially biochemically important as it is an intermediate of glucose metabolism [3] and may be present in sea water. For this reason it is important to know the amount

of sugar acids present in sea water which can contribute to the reduction of iron.

However, except for uronic acids [4,5] and α -keto acids [6], these sugar acids have never been measured in sea water. Liquid chromatographic (LC) methods usually employ ultraviolet or refractive index detectors with low sensitivities (usually $> 1 \text{ mmol l}^{-1}$) and also necessitate pre-concentration by liquid-liquid extraction or an ion-exchange separation prior to LC analysis. If possible, additional separation procedures should be avoided, primarily to minimize possible contamination where nanomolar concentrations of sugars are involved. The method proposed here is simple and by using a fluorescence detector the detection limit of sugar acids has been lowered.

In order to prepare fluorescent derivatives, the samples are treated with 9-anthryldiazomethane

Correspondence to: K. Matsunaga, Department of Chemistry, Faculty of Fisheries, Hokkaido University, Hakodate 041 (Japan).

(ADAM), which is a prelabelling reagent for fatty acids, reacting with the carboxyl group (COOH). The esters produced with ADAM and carboxyl radical emit fluorescence [7]. Gluconic acid contains a carboxyl group, and a method for the determination of gluconic acid by LC was investigated in this study.

EXPERIMENTAL

Apparatus

The LC system consisted of a Shimadzu (Kyoto) LC-6A chromatograph with an SCL-6B system controller, FCV-3AL low-pressure rationing valves, SIL-9A automatic sampler, RF-535 fluorescence detector and a C-R3A data processor. Chromatographic separation was carried out on a 250 × 4.6 mm i.d. column (Tosoh; TSKgel ODS-80Tm, octadecylsilane reversed-phase type).

Separation of sugar acids from sea water was accomplished on a 300 × 8 mm i.d. column (Ultron PS-80H, strong acidic cation-exchange resin type; Chromato Packing Centre, Kyoto) with an SPD-6AV UV-visible spectrophotometric detector (Shimadzu).

Reagents and materials

9-Anthryldiazomethane (ADAM) was purchased from Funakoshi Chemical Industry (Tokyo). The reagent was prepared by dissolving 6.3 mg of ADAM in 1 ml of acetone. Although it has been reported that this solution was stable for about 1 week at -20°C [8], it was prepared just prior to use. Chromatographic-grade organic solvents were obtained from Kanto Chemical (Tokyo) and sugar acids from Sigma (St. Louis, MO). Stock standard solutions (10 mM) were prepared in distilled water and stored at 4°C . All standards were stable and lower concentration standard solutions were prepared by diluting the stock standard solutions with distilled water (pH 4.6, adjusted with HClO_4) just prior to use.

Procedure

A sea-water sample was filtered through a precleaned 0.45- μm Millipore membrane filter. Before the addition of ADAM to the sea-water

sample, the sugar acids were separated from the sea water to avoid salt interference. For this separation, the pH of the filtrate was adjusted to 4–5 with HClO_4 and a 200- μl aliquot of the filtrate was injected into an Ultron PS-80H column and eluted with distilled water (pH 4.6, adjusted with HClO_4) at a constant flow-rate of 0.5 ml min^{-1} at 50°C . A volume of 2 ml of eluate was collected between 11 and 15 min after injection.

The derivatization of the sugar acid fraction with ADAM was carried out as follows. A 25- μl volume of methanol and 25 μl of ADAM solution were added to 25 μl of the eluate. After allowing the solution to stand for 60 min at room temperature in the dark, it was filtered (0.45 μm) with nitrogen pressure. A 10- or 20- μl aliquot of the filtrate was injected into the LC column (TSKgel ODS-80TM) and eluted with methanol–water (1 + 1, v/v) at a constant flow-rate of 1.0 ml min^{-1} at 50°C . The fluorescence of the ADAM ester was measured at 412 nm, with excitation at 365 nm. The concentration was calculated using a data processor.

The compounds of interest were eluted from the TSKgel ODS-80Tm column within 25 min with the aqueous methanol. However, some strongly retained substances were not eluted. Therefore, it was necessary to perform the following exchange to elute these compounds before the next sample injection: methanol–water (1 + 1, v/v) for 25 min, acetone–water (7 + 3, v/v) for 35 min, then methanol–water (1 + 1, v/v) for 30 min to equilibrate the analytical column with the starting mobile phase. One analytical cycle was completed with 90 min. These exchanges of mobile phases were controlled by an SCL-6B system controller and FCV-3AL low-pressure rationing valves.

RESULTS AND DISCUSSION

Separation of sugar acids from sea water

Figure 1 shows a chromatogram of 1 mM gluconic acid in sea water. A 200- μl volume of 1 mM gluconic acid was injected into the column, eluted with distilled water (pH 4.6) and detected spec-

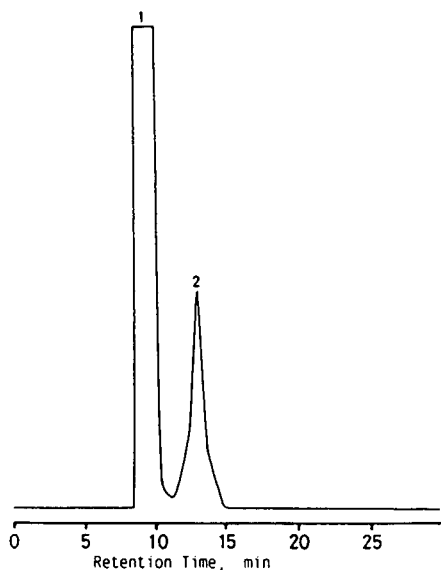


Fig. 1. Chromatogram of 1 mM gluconic acid in sea water. Volume injected, 200 μ l. Peaks 1 and 2 are inhibitors and gluconic acid, respectively.

trophotometrically at 210 nm. The pH of the mobile phase was adjusted to 4.6 with HClO_4 , as ADAM reacts with sugar acids (carboxyl group) within the pH range 4–5. Gluconic acid was eluted at a retention time of 13 min, resulting in its complete separation from salts.

Figure 2 shows the recovery of gluconic acid in each eluate fraction. Each eluate fraction was collected during every 0.25-min period. Approximately 100% gluconic acid was recovered in the fractions of retention time from 11.75 to 14.25 min. Hence, for collection of sugar acids from sea-water samples eluates were collected in the interval from 11 to 15 min.

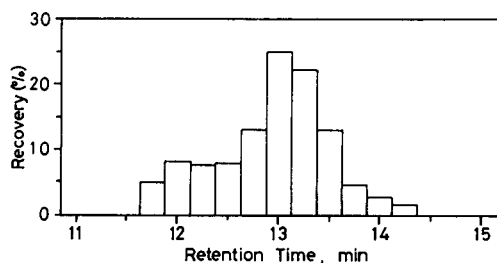


Fig. 2. Recovery of gluconic acid in each eluate fraction. Each eluate fraction was collected during every 0.25-min period.

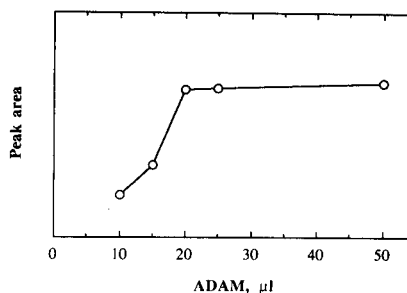


Fig. 3. Effect of the addition of ADAM solution on gluconic acid peak area. Reaction time, 1 h at room temperature in the dark (pH 4.6).

Effect of addition of ADAM

The study was carried out with 1 μ M gluconic acid. The conditions for the reaction with ADAM were basically referred those in a previous method for oxalic acid [8]. The conditions for sugar acid derivatization were optimised. Figure 3 shows the effect of the addition of ADAM solution on the gluconic acid peak area (area/ μ mol gluconic acid). The peak area of gluconic acid was constant when $> 20 \mu$ l of ADAM were added. Thus, 25 μ l of ADAM were sufficient to react with gluconic acid in methanol.

Effect of pH on reaction of sugar acid with ADAM

The pH of the reaction mixture was varied from 2.5 to 7.8 by addition of HClO_4 or NaOH . With a 1-h reaction time at room temperature in the dark, the gluconic acid ester response diminished below pH 4 and above pH 5 (Fig. 4). These effects may be due to decomposition of ADAM at low pH and to the lack of reaction between

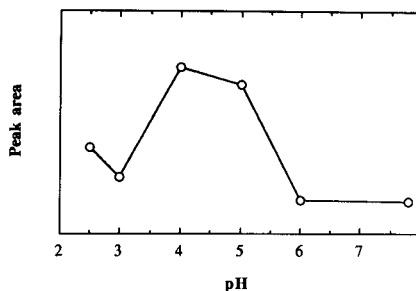


Fig. 4. Effect of pH on reaction of gluconic acid with ADAM. Reaction time, 1 h at room temperature in the dark.

ADAM and COO^- at higher pH. Based on these results, the pH adopted was between 4 and 5.

Reaction time of sugar acid with ADAM

The reaction time of gluconic acid with ADAM was varied from 5 min to 16 h prior to chromatography. The reaction in methanol was completed within 60 min and the reaction mixture was stable for 12 h at room temperature (Fig. 5). This result is similar to that observed for the reaction of ADAM with oxalic acid, which was faster in methanol than in a low-polarity solvent such as ethyl acetate [8].

LC profile

A chromatogram of sugar acid esters [gluconic (1), glucaric (2) and glucuronic acid (3)] is shown in Fig. 6. Gluconic acid ester was eluted at 19.0 min under these conditions and glucaric acid and

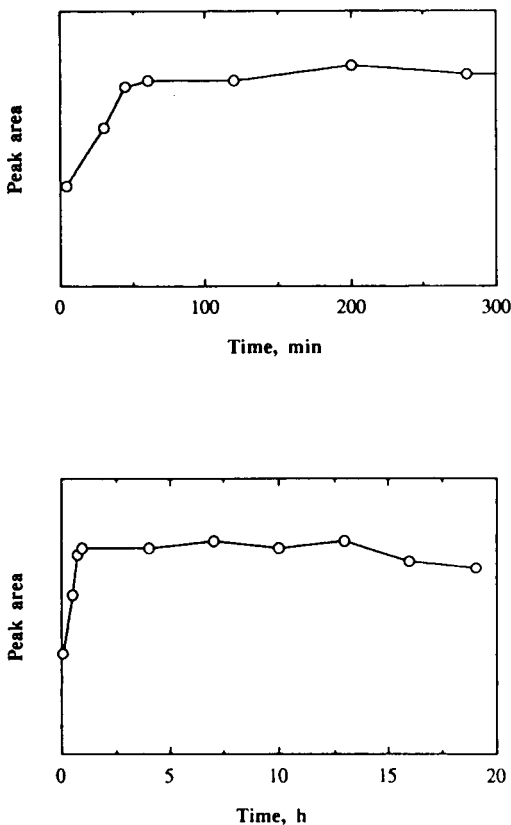


Fig. 5. Effect of reaction time of gluconic acid with ADAM at pH 4.6 and stability of the ester.

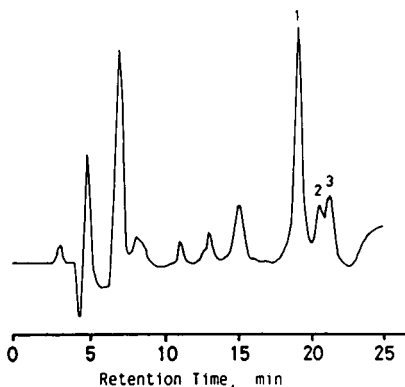


Fig. 6. Chromatogram of sugar acid standards. Peaks 1, 2 and 3 are gluconic, glucaric and glucuronic acid, respectively.

glucuronic acid appeared at 20.5 and 21.2 min, respectively. Hence gluconic acid was separated from glucaric and glucuronic acids. The other isomeric carboxylic acids were well separated from gluconic acid.

Calibration

A calibration graph was plotted of peak area, computed by the data processor, against the concentration of gluconic acid in sea water using standard additions. The relationship between peak area and concentration was linear in the range 0–1.0 μM with the regression equation A (peak area) = $7.5 \times 10^3 + 2.57 \times 10^5 C$ (μM). The correlation coefficient was 0.994 ($n = 6$). The detection limit of gluconic acid ester with fluorescence detection was < 10 nM based on the minimum area of the integrator. The blank was esti-

TABLE 1

Recovery of gluconic acid added to sea water (100 nM)

| Amount found (nM) | |
|----------------------------------|---------------------------------|
| Original sample (A) ^a | After addition (B) ^a |
| 181 | 270 |
| 198 | 299 |
| 194 | 267 |
| 164 | 284 |
| 171 | 263 |
| 172 | 296 |
| Mean: 180.0 ± 13.6 | Mean: 279.8 ± 15.4 |

^a $B - A = 99.8 \pm 20.5$ nM; recovery = 99.8%.

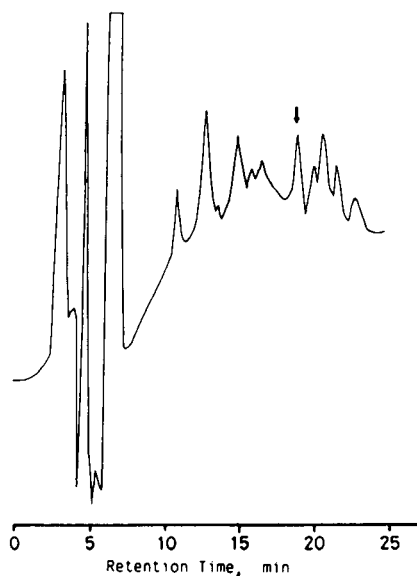


Fig. 7. Typical chromatogram of a derivatized sea-water sample. Volume injected 20 μ l.

mated to be 30 nM using sea water subjected to UV irradiation for 6 h to destroy organic substances.

The reproducibility and recovery were 8% at 200 nM gluconic acid and 99.8%, respectively as shown in Table 1.

Measurement of dissolved gluconic acid in sea water

Dissolved gluconic acid was measured in surface sea-water samples during a phytoplankton bloom at Funka Bay, Japan. Figure 7 shows an example of a chromatogram obtained for a sea-

water sample that contained 850 nM of gluconic acid.

In conclusion, a method for the determination of sugar acids in sea water has been established and the presence of dissolved gluconic acid in sea water during a spring bloom was confirmed. The occurrence of gluconic acid in sea water may be significant, as it may catalyse the photoreduction of Fe(III) to Fe(II). This method may be also applicable to the measurement of other carboxylic compounds in natural waters. The distribution of sugar acids and the relationship with Fe(II) in sea water during a spring bloom will be reported in detail elsewhere.

The authors thank M. Koide of Scripps Institution of Oceanography for helpful comments on the manuscript.

REFERENCES

- 1 S. Nakabayashi, I. Kudo, K. Kuma, K. Toya and K. Matsunaga, *Bull. Jpn. Soc. Fish. Oceanogr.*, 53 (1989) 128.
- 2 K. Kuma, S. Nakabayashi, Y. Suzuki, I. Kudo and K. Matsunaga, *Mar. Chem.*, 37 (1992) 15.
- 3 A.L. Lehninger, *Biochemistry*, Worth, New York, 1979, p. 1104.
- 4 K. Mopper, *Mar. Chem.*, 5 (1977) 585.
- 5 K. Mopper and K. Larsson, *Geochim. Cosmochim. Acta*, 42 (1978) 153.
- 6 D.J. Kieber and K. Mopper, *Anal. Chim. Acta*, 183 (1986) 129.
- 7 N. Nimura and T. Kinoshita, *Anal. Lett.*, 13 (1980) 191.
- 8 S. Imaoka, T. Funae, T. Sugimoto, N. Hayahara and M. Maekawa, *Anal. Biochem.*, 128 (1983) 459.

Determination of carbon-13 content of sugars of fruit and vegetable juices

A European inter-laboratory comparison

J. Koziat

Pernod–Ricard Research Centre, 120 Avenue du Maréchal Foch, F-94015 Creteil (France)

A. Rossmann

Lehrstuhl für Allgemeine Chemie und Biochemie, T.U.M., D(W)-8050 Freising-Weihenstephan (Germany)

G.J. Martin

Laboratoire de RMN et Réactivité Chimique, URA–CNRS 472, 2 Rue de la Houssinière, 44072 Nantes Cedex (France)

P.R. Ashurst

Dr. P.R. Ashurst & Associates, Unit 5, Gooses Foot Estate, Kingstone, Hereford HR2 9HY (UK)

(Received 28th May 1992; revised manuscript received 30th July 1992)

Abstract

An inter-laboratory comparison, organized by a working group of the technical committee for the analysis of fruit and vegetable juices of the European Commission of Standardization (CEN/TC 174), was carried out between fifteen laboratories in seven European countries on the determination of the carbon-13 content of sugars of fruit juices. Each laboratory received two randomly selected samples, each of 250 ml, of orange and pineapple juice and two samples, each of 50 g, of sucrose from beet and cane sources. The determination of carbon-13 in sugars of fruit juices was evaluated using the same experimental protocol but under different conditions (operator, spectrometer, period of time). The results obtained for this method were considered to be acceptable by specialists in the field of isotopic analysis: the repeatability (r) and reproducibility (R) obtained in the ring test were 0.3‰ and 0.7‰, respectively, according to the ISO Standard 5725–1986.

Keywords: Mass spectrometry; Carbon-13; Collaborative studies; Fruit juices; Sugars; Vegetable juices

This comparison was organised within the framework of CEN/TC 174, which is a technical committee for the analysis of fruit and vegetable juices of the European Committee for Standardization [1], which was formed in November 1988 by the CEN Technical Board (CEN/BT). The objectives of the CEN/TC 174 Technical Com-

mittee are to draw up a system of reference analytical methods to attest the quality of fruit juices and to improve measurements within participating countries to avoid difficulties in the trade of fruit juices arising from the use of different analytical methods. The reference system will include standardization of the methods of analysis recommended. It should be emphasized that the purpose of this work was not to determine the natural dispersion of the $^{13}\text{C}/^{12}\text{C}$ ratio in the

Correspondence to: J. Koziat, Pernod–Ricard Research Centre, 120 Avenue du Maréchal Foch, F-94015 Creteil (France).

whole populations of fruit juices or sugars, which has been studied elsewhere [2–4], but to check the repeatability and the reproducibility of the method.

Methods of analysis reviewed by the technical committee can be classified in one of three categories: so-called classical analysis (for which consensus should be easy to obtain); more sophisticated methods of analysis which are widely used in Europe, e.g., liquid chromatography (LC) and atomic absorption spectrometry (AAS); and prospective methods which are in use (but not widely) or are likely to be introduced in order to improve the control of the purity of fruit juices (isotopic analysis, determination of the polyphenols of the methoxylated flavonoids, etc). All methods have to be subjected to a ring test.

The $^{13}\text{C}/^{12}\text{C}$ isotope ratio is a useful parameter for distinguishing products (carbohydrates, metabolites) extracted from plants having a Calvin or a Hatch–Slack metabolism [5]. In food sciences, the $^{13}\text{C}/^{12}\text{C}$ ratio is a good probe for detecting the addition of cane sugar or maize

glucose syrup to honeys and orange and apple juices, for example.

Determination of the carbon-13 content in sugars of fruit juices is in the third category and the present method involves the determination of the stable carbon isotope ratio ($^{13}\text{C}/^{12}\text{C}$) of sugars in fruit juices by use of isotope ratio mass spectrometry (IRMS).

The corresponding method and the ring test, described here, were drawn up and organized by a working group, “Isotopes Working Group 1” (WG 1), appointed by CEN/TC 174 [6] for this purpose.

EXPERIMENTAL

Nature of the samples

Fifteen laboratories in seven European countries, listed alphabetically in Table 1, agreed to collaborate in this comparison of the analysis of the carbon-13 content in the sugars of fruit juices.

TABLE 1

List of the participants in the inter-laboratory comparison ^a

| No. | Name | Organization | Location | Country |
|-----|-------------------------------|---|-----------------------------|-------------|
| 1 | S. Brookes | Europa Scientific | Crewe | UK |
| 2 | H. Casabianca | Centre National de la Recherche Scientifique | Solaize | France |
| 3 | J. Fairchild/ A. Robertson | Atomic Energy Authority/Campden Food and Drink Research Association | Harwell Chipping Campden | UK |
| 4 | A. Filly | Laboratoire d'Hydrologie et de Géochimie Isotopique de l'Université Paris Sud | Orsay | France |
| 5 | P. Johnson | Bureau of Stable Isotope Analysis | Brentford | UK |
| 6 | J. Koziet | Pernod–Ricard Research Centre | Creteil | France |
| 7 | B. McGaw | Rowett Res. Services | Aberdeen | UK |
| 8 | N. Naulet | Université de Nantes | Nantes | France |
| 9 | F. Pichlmayer | Österreichisches Forschungszentrum | Seibersdorf | Austria |
| 10 | J. Van der Plicht | State University | Groningen | Netherlands |
| 11 | F. Reniero | Istituto Agrario Provinciale | San Michele | Italy |
| 12 | A. Rossmann | Technical University | Munich | Germany |
| 13 | A.L. Thelin | Nestlé | Lausanne | Switzerland |
| 14 | C. Tisse | Délégation Générale de la Concurrence, de la Consommation et de la Répression des Fraudes | Marseille | France |
| 15 | P. Trimborn | Neuherberg/Institut für Hydrologie | Neuherberg | Germany |

^a Protocol of ring test requires that published results cannot be identified to specific participants. For this reason the identification numbers of laboratories listed in Tables 1 and 2 do not coincide with those in Tables 3–6 where the numbers are co-incident.

One hundred cans each containing 250 ml of a homogeneous orange juice and 100 cans each containing 250 ml of a homogeneous pineapple juice were prepared, as were two batches each of 1000 g of homogeneous sucrose of beet and cane origin.

Each participant received two cans of each juice, randomly selected, and a sample of 50 g of each sucrose. A mineral oil reference standard (NBS 22), provided by the International Atomic Energy Agency (IAEA), was also circulated to all participants as a secondary standard of carbon-13 measurements. The participating laboratories were asked to make three determinations on the contents of one can of each juice (the second being retained for any problems), on each sample of the two sugars and on NBS 22 standard. The method described here was recommended and the participants (Table 1) were only asked to indicate any differences from the proposed procedure (Table 2).

Preparation of samples

All reagents used were of analytical-reagent grade. Calcium hydroxide (powdered) and 95–97% sulphuric acid were used.

Purification and separation of sugars. The insoluble constituents of a sample of ca. 50 ml of natural or reconstituted fruit juice were eliminated by centrifugation (10 min at 1400 g). Soluble substances remaining in the supernatant liquid after centrifugation were purified by addition of 2 g of powdered calcium hydroxide to the solution whilst stirring it well (using, e.g., a magnetic stirrer) and heating on a water-bath at 90°C for 3 min.

Organic acids, amino acids and other compounds were precipitated during that stage of the procedure. The precipitate was separated by centrifugation of the hot solution (3 min at 1400 g) and the clear supernatant liquid was decanted and acidified with 1 M sulphuric acid to give pH \approx 5 when colour of the solution changed. This

TABLE 2

Procedures used by each participant

| Participant | Treatment of sample | CO ₂ preparation | Mass spectrometer |
|-------------|---|--|------------------------------|
| 1 | No isolation of sugars | On-line combustion, GC separation | Europa Tracer, direct inlet |
| 2 | According to protocol | Microanalyser on-line | Finnigan Delta S |
| 3 | According to protocol | Manual combustion | VG 602, dual inlet |
| 4 | According to protocol | Manual combustion | VG 602 C, dual inlet |
| 5 | According to protocol | On-line combustion, trapping box system | VG SIRA II, dual inlet |
| 6 | According to protocol | Manual combustion | Finnigan Delta S, dual inlet |
| 7 | According to protocol | [11] | VG SIRA 12, dual inlet |
| 8 | (a) According to protocol | (a) Microanalyser, Carlo Erba 1500 (on-line) | Finnigan Delta E, dual inlet |
| | (b) Evaporation instead of lyophilization | (b) Manual combustion | |
| 9 | According to protocol | On-line combustion, trapping box system | Finnigan MAT 251, dual inlet |
| 10 | According to protocol | Manual combustion | VG SIRA 9, dual inlet |
| 11 | Evaporation instead of lyophilization | On-line combustion, trapping box system | VG SIRA II, dual inlet |
| 12 | According to protocol | Manual combustion | VG MM 903/602, dual inlet |
| 13 | According to protocol | On-line combustion, trapping box system | Finnigan MAT 251, dual inlet |
| 14 | According to protocol | Microanalyser VG ISOPREP 13 | VG 602 E, dual inlet |
| 15 | According to protocol | On-line combustion, trapping box system | Finnigan Delta S, dual inlet |

solution contained mainly sugars, calcium sulphate and some colorants as minor ingredients. Residual calcium sulphate was then partially removed by storage of the solution in a refrigerator at about 4°C overnight and decanting the supernatant liquid. After freeze-drying, the substance was homogenized to a fine powder and stored in a glass vial with an air-tight plastic cap.

Combustion of sugars. Samples were combusted in a circulating oxygen gas stream or in an elemental analyser [7,8]. Suitable microcombustion systems are commercially available. It is essential to effect complete conversion of organic carbon into carbon dioxide by a method that avoids any isotopic fractionation and allows the collection of the gas as a whole. A liquid nitrogen trap is usually employed to collect the carbon dioxide.

Mass spectrometric measurements

Apparatus. $^{13}\text{C}/^{12}\text{C}$ isotopic ratios in the carbon dioxide obtained from combustion of the sugars were determined with the aid of an isotope ratio mass spectrometer. The instrument had the ability to determine the ^{13}C content at natural abundance with a precision of 0.05‰ or better (one measuring cycle with ten integration periods).

TABLE 3

Experimental data for orange juice sugar ($\delta^{13}\text{C}$ ‰ PDB)

| Laboratory ^a | Mean | S.D. | No. of replicates |
|-------------------------|--------|--------|-------------------|
| 1 | -24.73 | 0.0506 | 10 |
| 2 | -24.17 | 0.1484 | 3 |
| 3 | -24.46 | 0.1188 | 12 |
| 4 | -24.91 | 0.1446 | 9 |
| 5 | -24.46 | 0.0602 | 20 |
| 6 | -24.64 | 0.1050 | 3 |
| 7 | -24.43 | 0.0733 | 12 |
| 8 | -24.67 | 0.0385 | 8 |
| 9 | -24.42 | 0.0216 | 6 |
| 10 | -24.56 | 0.0263 | 4 |
| 11 | -24.99 | 0.2040 | 6 |
| 12 | -24.51 | 0.0058 | 3 |
| 13 | -24.64 | 0.0499 | 4 |
| 14 | -24.57 | 0.0729 | 5 |
| 15 | -25.16 | 0.1102 | 3 |

^a The laboratories are not referenced with the same numbers as in Tables 1 and 2.

TABLE 4

Experimental results for pineapple juice sugar ($\delta^{13}\text{C}$ ‰ PDB)

| Laboratory ^a | Mean | S.D. | No. of replicates |
|-------------------------|--------|--------|-------------------|
| 1 | -12.34 | 0.0379 | 10 |
| 2 | -12.05 | 0.2532 | 3 |
| 3 | -11.89 | 0.0701 | 12 |
| 4 | -11.85 | 0.1768 | 9 |
| 5 | -12.23 | 0.2720 | 17 |
| 6 | -12.36 | 0.0115 | 3 |
| 7 | -12.15 | 0.0799 | 12 |
| 8 | -12.31 | 0.0741 | 8 |
| 9 | -12.05 | 0.0314 | 6 |
| 10 | -12.29 | 0.1344 | 2 |
| 11 | -12.37 | 0.0950 | 6 |
| 12 | -12.03 | 0.0153 | 3 |
| 13 | -11.71 | 0.0707 | 4 |
| 14 | -12.29 | 0.0661 | 5 |
| 15 | -12.56 | 0.1877 | 3 |

^a The laboratories are not referenced with the same numbers as in Tables 1 and 2.

Isotopic ratio mass spectrometers generally have a triple collector. In CO_2 analysis, the ionic currents are simultaneously registered as mass numbers 44, 45 and 46. The ratio for the isotopic species $^{13}\text{CO}_2/^{12}\text{CO}_2$ is then determined from the corresponding intensities. Mass spectrometers should be additionally equipped with a dual inlet system for alternately measuring the unknown sample and a standard. This method of measurement offers the highest degree of accuracy for the determination of variations of the isotopic content in the range of the natural abundance. However by using an on-line system with gas chromatographic separation of the combustion products, but without a dual inlet facility, correct results can still be obtained if a secondary standard is used.

Expression of results. In addition to the commonly used mass isotopic abundance (in % of atoms), the so-called delta value (δ) is also used as an alternative system of units for indicating isotope content. Delta values are used exclusively for indicating variations (of the third decimal place) in the natural isotopic abundance.

The $\delta^{13}\text{C}$ value is generally expressed as the relative difference per thousand between the ^{13}C and ^{12}C ratios of a sample in relation to a stan-

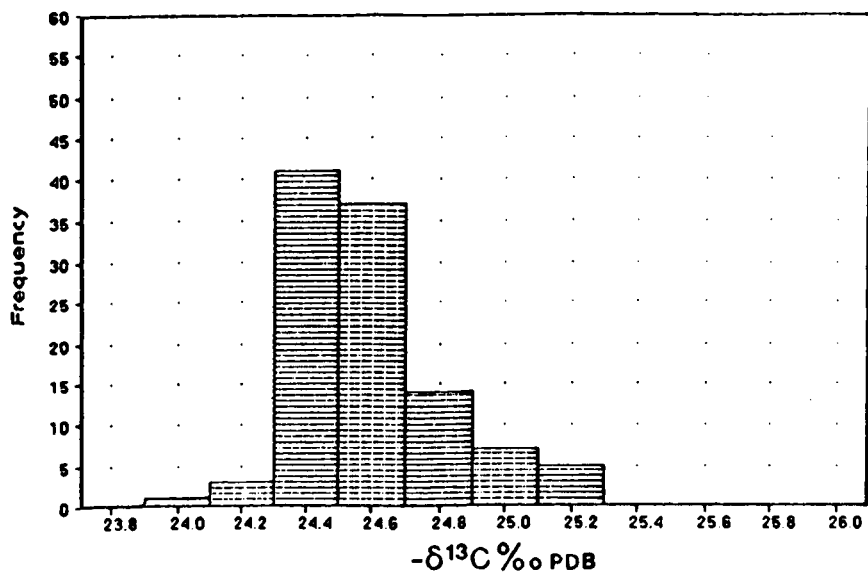


Fig. 1. Determination of the relative carbon-13 content of orange juice sugar expressed as $\delta^{13}\text{C} \text{ ‰ PDB}$. Histogram of the total individual data. Mean value: $-24.5 \pm 0.25 \text{ ‰ PDB}$.

dard, Pee Dee Belemnite from South Carolina in America (the PDB standard). This is a fossil calcium carbonate with an isotopic ratio ($^{13}\text{C}/^{12}\text{C}$)_{PDB} ≈ 0.0112372 [9] for the emitted CO_2 . This value is the reference point of the common inter-

national PDB scale for $\delta^{13}\text{C}$ values:

$$\delta^{13}\text{C}(\text{‰})\text{PDB} = \frac{([\text{C}^{13}]/[\text{C}^{12}])_{\text{sample}} - ([\text{C}^{13}]/[\text{C}^{12}])_{\text{PDB}}}{([\text{C}^{13}]/[\text{C}^{12}])_{\text{PDB}}} \times 1000$$

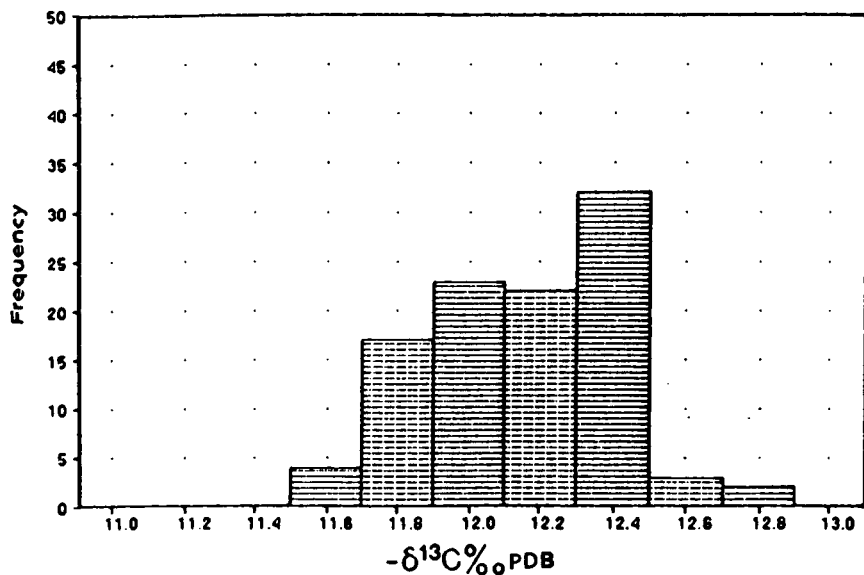


Fig. 2. Determination of the relative carbon-13 content of pineapple juice sugar expressed as $\delta^{13}\text{C} \text{ ‰ PDB}$. Histogram of the total individual data. Mean value: $-12.1 \pm 0.3 \text{ ‰ PDB}$.

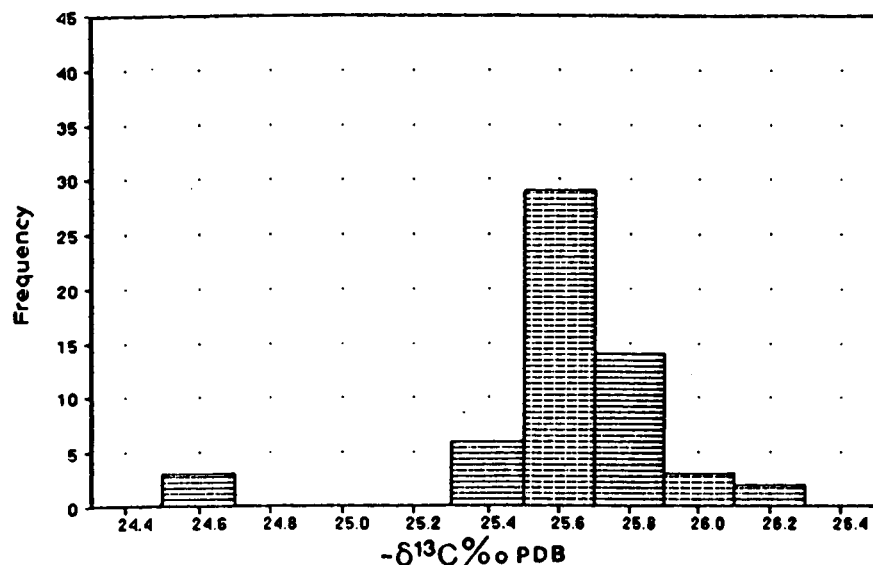


Fig. 3. Determination of the relative carbon-13 content of beet sugar expressed as $\delta^{13}\text{C}$ ‰ PDB. Histogram of the total individual data. Mean value: -25.5 ± 0.17 ‰ PDB. The low value (-24.6 ‰) may be considered as an outlier, not on a statistical basis but for experimental reasons, as the working standard was accidentally spoiled.

A suitable secondary standard for routine use in this method is NBS 22 (obtained from IAEA, Vienna), which has a value of -29.73 ‰ relative to PDB [10].

RESULTS

The results of the evaluation are given in Tables 3–6 and illustrated by a series of histograms (Figs. 1–4).

TABLE 5

Experimental data for beet sugar ($\delta^{13}\text{C}$ ‰ PDB)

| Laboratory ^a | Mean | S.D. | No. of replicates |
|-------------------------|--------|--------|-------------------|
| 1 | -25.52 | 0.0313 | 5 |
| 2 | -24.56 | 0.1097 | 3 |
| 3 | -25.62 | 0.0619 | 6 |
| 4 | -26.05 | 0.1323 | 3 |
| 5 | -25.40 | 0.0499 | 4 |
| 6 | -25.73 | 0.0458 | 3 |
| 7 | -25.68 | 0.0676 | 8 |
| 8 | -25.52 | 0.0289 | 3 |
| 9 | -25.64 | 0.0265 | 3 |
| 10 | -25.72 | 0.0000 | 1 |
| 11 | -25.78 | 0.0493 | 3 |
| 12 | -25.70 | 0.0208 | 3 |
| 13 | -25.67 | 0.0556 | 4 |
| 14 | -25.66 | 0.0567 | 5 |
| 15 | -26.02 | 0.0321 | 3 |

^a The laboratories are not referenced with the same numbers as in Tables 1 and 2.

TABLE 6

Experimental data for cane sugar ($\delta^{13}\text{C}$ ‰ PDB)

| Laboratory ^a | Mean | S.D. | No. of replicates |
|-------------------------|--------|--------|-------------------|
| 1 | -11.26 | 0.0507 | 5 |
| 2 | -11.45 | 0.0577 | 3 |
| 3 | -11.07 | 0.1019 | 6 |
| 4 | -11.48 | 0.2363 | 3 |
| 5 | -11.02 | 0.0603 | 3 |
| 6 | -11.51 | 0.0115 | 3 |
| 7 | -11.27 | 0.0936 | 8 |
| 8 | -11.16 | 0.0800 | 3 |
| 9 | -11.19 | 0.0252 | 3 |
| 10 | -11.34 | 0.0000 | 1 |
| 11 | -11.10 | 0.0889 | 3 |
| 12 | -11.37 | 0.0231 | 3 |
| 13 | -10.76 | 0.2220 | 4 |
| 14 | -11.18 | 0.0513 | 5 |
| 15 | -11.30 | 0.0603 | 3 |

^a The laboratories are not referenced with the same numbers as in Tables 1 and 2.

International standard NBS 22 was chosen as the secondary reference for calibration of this method. The mean value of the carbon-13 content of this standard determined by the participants under the ring test conditions was $\delta^{13}\text{C} = -29.8 \pm 0.2\text{‰}$ PDB (in agreement with the IAEA value, $\delta^{13}\text{C} = -29.73\text{‰} \pm 0.09$ PDB). The results of the ring test were standardized against this value.

Differences in the preparation of the samples and in the isotope ratio mass spectrometers used were tested statistically and found to have no significant influence on the results (Table 2).

Repeatability and reproducibility

The different steps of the analysis (sugar isolation, combustion, separation of CO_2 , IRMS determination) were expected to be performed in triplicate. However, some laboratories produced more than three results and, in order to avoid any bias in selecting arbitrarily three data out of a larger set, the inter-laboratory test was calculated on the whole population of experimental results (Tables 3–6).

The standard deviations of repeatability and reproducibility are calculated in agreement with the ISO Standard 5725–1986 [12].

The repeatability r is the value below which the absolute difference between two individual measurements carried out under the experimental conditions (operator, spectrometer) and during a short period of time should lie with a 95% probability. In the present case, it is demonstrated that the average repeatability, calculated from the mean of the repeatability variance obtained in measuring four different sugars, is not greater than 0.3‰ (standard deviation of repeatability $S_r = 0.10\text{‰}$).

The reproducibility R may be understood in terms of the closeness of agreement between individual results obtained with the same method but under different conditions (operators, spectrometers, laboratories, periods of time). Then, it may be expected that, at the 95% confidence level, the absolute difference between two individual results would be below 0.7‰ (standard deviation of reproducibility $S_r = 0.25\text{‰}$). Examination of Figs. 1–4 shows that this condition is obeyed.

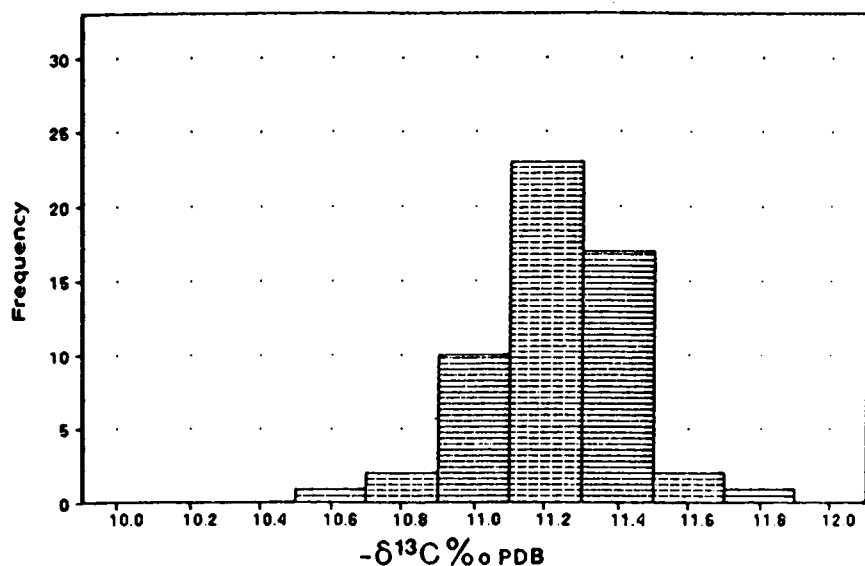


Fig. 4. Determination of the relative carbon-13 content of cane sugar expressed as $\delta^{13}\text{C} \text{‰ PDB}$. Histogram of the total individual data. Mean value: $-11.2 \pm 0.23\text{‰}$ PDB.

Conclusion

The main objective of this inter-laboratory comparison was to identify analytical difficulties and the feasibility of this type of analysis in fruit quality control as performed routinely by different laboratories working in the field of isotopic determination. Despite slight differences in sample preparation in this collaborative study, the repeatability and reproducibility obtained for the method described in this ring test were acceptable. The working group considered that this method gave satisfactory results for the determination of the carbon-13 content in sugars of fruit juices and the introduction of this technique in the area of fruit juice quality control will improve control of authenticity.

This method has been submitted to CEN/TC 174 for approval.

REFERENCES

- 1 Document N35 of CEN/TC 174, Technical Committee on Fruit and Vegetable Juices—Methods of Analysis, of the European Committee for Standardization, Association Française de Normalisation, Paris-La Défense, 1991.
- 2 J. Bricout and J. Koziat, *J. Agric. Food Chem.*, 35 (1987) 758.
- 3 L.W. Doner, H.O. Ajie, L.S.L. Sternberg, J.M. Milbarn, M.J. De Niro and K.B. Hicks, *J. Agric. Food Chem.*, 35 (1987) 610.
- 4 G.J. Martin, D. Danho and C. Vallet, *J. Sci. Food Agric.*, 56 (1991) 419.
- 5 M. O'Leary, *Bioscience*, 38 (1988) 328.
- 6 Document N2 of CEN/TC 174, Technical Committee on Fruit and Vegetable Juices—Methods of Analysis, of the European Committee for Standardization, Association Française de Normalisation, Paris-La Défense, 1989.
- 7 J. Bricout and J. Koziat, *Ann. Falsif. Expert. Chim.*, 69 (1976) 845.
- 8 F.-J. Winkler and H.-L. Schmidt, *Z. Lebensm.-Unters.-Forsch.*, 171 (1980) 85.
- 9 H. Craig, *Geochim. Cosmochim. Acta*, 12 (1957) 133.
- 10 G. Hut, Consultants' Group Meeting on Stable Isotope Reference Samples for Geochemical and Hydrological Investigations, IAEA, Vienna, 16–18 September 1985, IAEA Report, April 1987.
- 11 B. McGaw, E. Milne and G.J. Duncan, *Biomed. Mass Spectrom.*, 16 (1988) 269.
- 12 Document ISO 5725-1986, International Organisation for Standardisation, Geneva, 1986.

Simultaneous enzymatic and tautomeric reactions of D-fructose in a reactor with immobilized hexokinase

Mikael Skoog and Gillis Johansson

University of Lund, Department of Analytical Chemistry, P.O. Box 124, S-221 00 Lund (Sweden)

(Received 8th July 1992; revised manuscript received 11th August 1992)

Abstract

The combined effect of tautomerization and enzymatic conversion on the phosphorylation of D-fructose by hexokinase has been studied. A computer model has been developed to describe the simultaneous enzymatic and tautomerization reactions in small immobilized enzyme reactors. The tautomer composition of fructose was calculated from available rate constants, taking into account α -fructofuranose, β -fructofuranose, β -fructopyranose, and the open-chain keto form. The conversion to fructose-6-phosphate predicted by the model was compared with conversions determined experimentally in a flow-injection system. An iteration procedure permitted the determination of the enzymatic rate constant as well as the rate constants for ring opening and ring closing of the β -fructopyranose anomer, which were 0.038 and 4.29 s^{-1} , respectively. Each tautomer and tautomer combination was tested as possible candidates for the enzymatic phosphorylation. The only alternatives consistent with experimental data were reaction with β -fructofuranose alone or in combination with the α -form. From structural arguments the β -form is more likely to be the substrate, as shown in the literature. The slow ring-opening of β -fructopyranose complicates fructose determinations using rapid, tautomer-selective enzymatic methods.

Keywords: Flow injection; D-Fructose; Hexokinase; Immobilized enzymes; Phosphorylation

The rate of a chemical reaction in a packed-bed enzyme reactor is jointly determined by the rates of the enzymatic reaction and mass transfer. Explicit expressions describing the catalytic efficiency of a reactor have been derived [1] for substrate concentrations well below K_M , the Michaelis constant. In such cases, the enzymatic conversion can be approximated by a pseudo-first order reaction and the mass transfer can be calculated by the usual methods of chemical engineering. The numerical expressions are more complex if the backward reaction has to be taken into account [2], than if a unidirectional reaction model is sufficient [3].

Enzymatic conversions of monosaccharides are frequently complicated by the complex intrinsic chemistry of these compounds. Some monosaccharides (e.g. glucose) show predominantly α - β interconversions in aqueous solutions. They are said to exhibit simple mutarotation and the process is more specifically denoted as anomerization [4]. Others, like fructose, undergo tautomerization between furanoid and pyranoid forms along with anomerism. The mutarotation of these monosaccharides is typically biphasic, and is referred to as complex [5–8].

Enzymes in many cases are specific for a single molecular configuration of the substrate and may be completely inactive with other anomers. With the discussion limited to fructose it has thus been argued that hexokinase (E.C. 2.7.1.1) should be specific for β -fructofuranose. An examination of

Correspondence to: G. Johansson, University of Lund, Department of Analytical Chemistry, P.O. Box 124, S-221 00 Lund (Sweden).

the reactivity of the enzyme towards different de-oxy derivatives indicated that the OH-groups in positions C-2, C-3, and C-6 of β -fructo-furanose should bind to the active site and that other tautomers should be inactive [9]. This assumption, to the best of our knowledge, has not been tested experimentally, except preliminary in a previous work by us [10]. The purpose of the present work is to study the applicability of tautomeric models to analytical enzyme reactor systems and to assess the tautomer selectivity of hexokinase.

The rate of mutarotation is usually of little importance in classical analytical methods where a reaction is allowed to proceed to equilibrium before measurements by, for example, spectrophotometry [11]. The usual equilibrium times for fructose determinations are at least 30 min. The residence times in small enzyme reactors, however, are short compared to the mutarotation rates. Thus pseudo-first order kinetics alone, applied to the total fructose concentration, are insufficient to explain the conversion rate of fructose in an immobilized hexokinase reactor [10]. The rate constants for the anomeric equilibria are, however, available [12] and it should be possible to set up a model in which both anomeric and enzymatic conversions are taken into account. Computer simulations have already been used to elucidate the progress of mutarotation in α -galactopyranose and β -arabinofuranose [7,13]. An extended model comprising tautomeric equilibria as well as a tautomer-selective enzymatic reaction is presented in this work.

EXPERIMENTAL

Hexokinase (E.C. 2.7.1.1) from baker's yeast (Type F-300, 300 U glucose mg^{-1} , Sigma, St. Louis) was coupled to controlled pore glass (CPG-10, particle diameter 40–80 μm , pore size 38 nm, Serva, Heidelberg) which had been silanized with 3-aminopropyltriethoxysilane and activated with glutaraldehyde. Hexokinase, 8.1 mg (7.5 mg protein), was dissolved in 1.0 ml phosphate buffer, pH 7.0, containing 0.28 μM Mg^{2+} and 0.28 μM ATP (adenosine triphosphate) and

mixed with 50 mg activated glass. The coupling yield was 80% as determined spectrophotometrically at 280 nm in the supernatant before and after immobilization. The enzyme glass was packed into plexiglas reactors, volume 10 μl , 1.2 mm i.d. and volume 50 μl , 2.0 mm i.d.

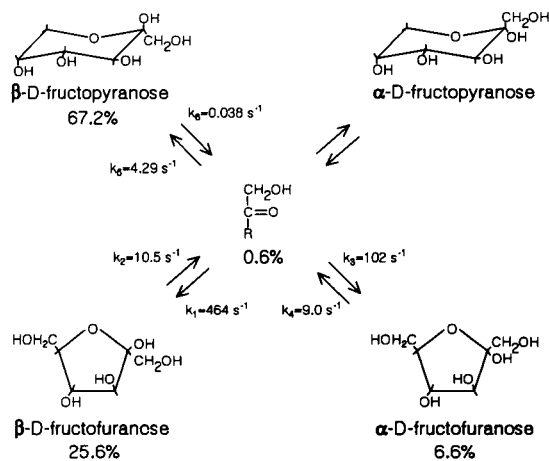
The kinetic properties were studied at 25.0°C in a steady-state flow system. Rate constants are available for pH 8.4 [12] and this pH was therefore used throughout this work. The solution consisted of 0.2 M tris(hydroxymethyl)amino-methane buffer, pH 8.4, containing 2.0 mM ATP, 6.0 mM MgCl_2 , and 0.7 mM NAD^+ (nicotinamide adenine dinucleotide). This buffer was mixed with an equal flow of standard solutions of fructose in pure water, using a peristaltic pump. The actual concentrations in the enzyme reactor will therefore be half of those given above. Fructose standards were prepared from β -D-fructopyranose at least 30 min before use to allow the mutarotational equilibrium at 25.0°C to be established.

Hexokinase phosphorylates fructose to fructose-6-phosphate, which was determined off-line by flow-injection analysis (FIA). Fractions were collected and injected into an FIA system containing an enzyme reactor with coimmobilized glucose phosphate isomerase (EC 5.3.1.9) and glucose-6-phosphate dehydrogenase (EC 1.1.1.49). The first reaction in this reactor is an interconversion to glucose-6-phosphate catalyzed by the isomerase. The next step is a selective oxidation to 6-phosphogluconate with the simultaneous reduction of a stoichiometric amount of NAD^+ to NADH, which is subsequently detected amperometrically at a phenoxazine modified graphite electrode. The preparation of the enzyme reactor as well as the details of the FIA system have been reported elsewhere [10].

RESULTS AND DISCUSSION

Tautomerization equilibria

The tautomerization of fructose is shown in Scheme 1, where the percentages (at pH 8.4 and 25°C) are calculated from Ref. 12 as described later. Two furanose forms and two pyranose forms



Scheme 1.

are assumed to be in equilibrium through the acyclic keto form [8,12,14–17]. α -Fructopyranose is reportedly present at a very low percentage (0.5%), and since no rate constants for its equilibrium with the open-chain form are available it will be neglected in the following. A postulated open-chain hydrate (*gem*-diol) in equilibrium with the acyclic keto form has not been detected by any investigator and will similarly be disregarded here. The rate constants for the remaining equilibria have been determined under alkaline conditions by Goux [12] using ^{13}C NMR spectroscopy, and will form the basis for the calculations made in this paper.

The rates of interconversion can be expressed by the following set of equations

$$d[\beta\text{-f}]/dt = k_1[\text{acycl}] - k_2[\beta\text{-f}] \quad (1)$$

$$d[\alpha\text{-f}]/dt = k_3[\text{acycl}] - k_4[\alpha\text{-f}] \quad (2)$$

$$d[\beta\text{-p}]/dt = k_5[\text{acycl}] - k_6[\beta\text{-p}] \quad (3)$$

$$d[\text{acycl}]/dt = -[(d[\alpha\text{-f}] + d[\beta\text{-f}] + d[\beta\text{-p}])/dt] \quad (4)$$

where f refers to furanose, p to pyranose and acycl to the open-chain molecule. The derivatives will be zero at equilibrium and therefore

$$[\beta\text{-f}]_{\text{eq}} = k_1/k_2[\text{acycl}]_{\text{eq}} \quad (5)$$

$$[\alpha\text{-f}]_{\text{eq}} = k_3/k_4[\text{acycl}]_{\text{eq}} \quad (6)$$

$$[\beta\text{-p}]_{\text{eq}} = k_5/k_6[\text{acycl}]_{\text{eq}} \quad (7)$$

$$[\text{acycl}]_{\text{eq}} = F_{\text{tot}}/(1 + k_1/k_2 + k_3/k_4 + k_5/k_6) \quad (8)$$

where F_{tot} is the total fructose concentration. The anomer concentrations at any time can be expressed as the equilibrium concentration minus the time integral of the changes.

$$[\beta\text{-f}] = [\beta\text{-f}]_{\text{eq}} - \int (k_1[\text{acycl}] - k_2[\beta\text{-f}]) dt \quad (9)$$

The integral can be approximated by a sum which can be used for computer calculations.

$$[\beta\text{-f}] = [\beta\text{-f}]_{\text{eq}} - \sum_{n=0}^N (k_1[\text{acycl}]_n - k_2[\beta\text{-f}]_n) \Delta t \quad (10)$$

where $N\Delta t = t$, the total time. Corresponding equations can be written for the other anomers and all equations have to be solved simultaneously with the enzymatic rate equation.

Enzyme kinetics

The rate of an enzymatic reaction obeying Michaelis–Menten kinetics is

$$dS/dt = (V_{\text{max}}S)/(K_M + S) \quad (11)$$

or, in integrated form

$$\begin{aligned} -\ln(1 - X) &= (V_{\text{max}}t - S_0X)/K_M \\ &\approx |(V_{\text{max}}/K_M)t|_{S_0 \ll K_M} \end{aligned} \quad (12)$$

where S is the substrate concentration at time t , S_0 is the substrate concentration at $t = 0$, and X is the fractional conversion: $X = (S_0 - S)/S_0$; K_M is the Michaelis constant and V_{max} the maximum rate, which is obtained at $S \gg K_M$. The quantities S , S_0 and X relate to the concentration of the enzymatically active anomer. Equation 12 takes a simpler form if $S_0 \ll K_M$, i.e. if pseudo-first order kinetics can be assumed.

An enzyme reactor can be described by a similar equation

$$-\ln(1 - X) = K_{\text{ps}}^{\text{app}}\tau \quad (13)$$

where τ is the mean residence time and $K_{\text{ps}}^{\text{app}}$ is the pseudo-first order apparent rate constant [3]. The mean residence time can be expressed by

$$\tau = \pi R^2 L \epsilon / Q = L / F \quad (14)$$

where Q is the volumetric flow-rate, R the radius, L the length of the reactor, ϵ the total void

fraction and F the linear flow velocity. The kinetics in a reactor will depend on the amount and activity of immobilized enzyme and the affinity for the substrate (V_{\max}/K_M) as well as on the flow-rate dependent mass transfer resistance. The substrate concentration at the surface of a particle will be less than in the bulk because of substrate consumption in the particle. The effect of this external mass transfer can be expressed by

$$1/K_{ps}^{\text{app}} = d^{3/2}/(B \cdot F^{1/2}) + 1/K_{ps} \quad (15)$$

where B is a constant, d the mean particle diameter, and K_{ps} a new rate constant, which is independent of the external mass transfer resistance. K_{ps} includes the particle size dependent effect of internal mass transfer resistance. It is determined experimentally in this work and only one particle size is used. The size of the internal mass transfer resistance is therefore unimportant.

A physical reactor of length L can be treated as a large number of discrete reactor elements, N , each of them having the length l . The fractional conversion will then be

$$X = 1 - \left[\exp(-K_{ps}^{\text{app}} N F^{-1}) \right] \quad (16)$$

This equation has been given a form suitable for iterative operation in a computer. A parameter, X_{tot} , denoting the conversion as a fraction of the total amount of fructose is also computed and used when experimental and calculated reaction rates are compared.

Initial data

There has been considerable uncertainty about the anomeric composition of fructose solutions due to widely different reports in the older literature [8]. The most recent studies by Goux using ^{13}C NMR spectroscopy [12] and Cockman et al. using gas chromatography of the silylated sugars [8] seem to agree quite well when differences in temperature and pH are accounted for. Goux estimates the relative error for the amounts of the cyclic forms to about 5%, whereas the amount of the acyclic form seems to be more uncertain.

The rates for the ring-opening reactions were more accurate than those for the ring-closing reactions [12]. Therefore, we recalculated the

TABLE 1

Rate constants for fructose anomer interconversion at pH 8.4 and 25°C, as depicted in Scheme 1

| Reaction | | Rate constant (s ⁻¹) |
|--|-------|----------------------------------|
| β -Furanose \leftarrow acyclic | k_1 | 464 ^a |
| β -Furanose \rightarrow acyclic | k_2 | 10.5 ^b |
| α -Furanose \leftarrow acyclic | k_3 | 102 ^a |
| α -Furanose \rightarrow acyclic | k_4 | 9.0 ^b |
| β -Pyranose \leftarrow acyclic | k_5 | 4.29 ^c |
| β -Pyranose \rightarrow acyclic | k_6 | 0.038 ^d |

^a Recalculated from equilibrium constants and ring-closing rate constants in Ref. 12. ^b Read from the logarithm of the rate constants vs. $1/T$ diagrams in Ref. 12. ^c Calculated from k_6 and equilibrium constants from Ref. 12. ^d This work.

ring-closing rate constants from the ring-opening constants and the equilibrium data, after correcting the total of the percentages to be 100% when the concentration of the acyclic form was included. This gives a consistent set of data based on the most accurate measurements. The rate constants used in this work are given in Table 1. In our previous communication [10] we used the rate constants as the primary information and obtained a set of less accurate, but consistent equilibrium concentrations from the ratios.

The value of k_6 (see Eqn. 7) has been reported to be of the order of 0.1 s⁻¹ and that of k_5 to be less than 20 s⁻¹ [8]. These values were used as initial guesses in our computer simulations. A fairly good estimate can be obtained from our experimental results as will be shown later.

The residence time (Eqn. 13) is varied by varying the volumetric flow-rate and a value for the constant B in Eqn. 14 is therefore needed. B can be calculated from physical constants and the calculation has been validated for a reactor with the same kind of porous glass as that used in this work [18]. B became 3.9×10^{-5} when the diffusion constant of fructose was taken to be 0.67×10^{-9} m² s⁻¹.

Computer simulations

The Eqns. 10 and 13–16, were solved with a time increment usually of 0.001 s using an initial guess of K_{ps} . The calculated fractional conver-

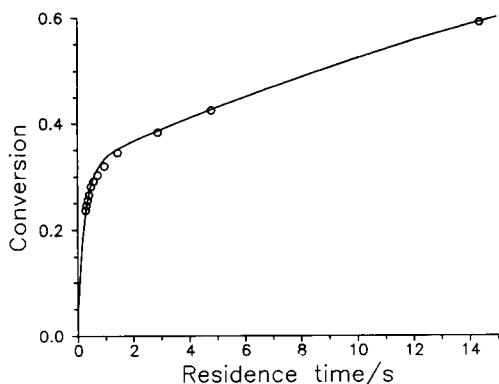


Fig. 1. Fractional conversion of fructose to its phosphorylated form at pH 8.4, 25°C. The solid line is the computed conversion using rate constants given in Table 1. The open circles are experimentally determined conversions.

sion, X_{tot} , was then compared with the experimentally determined conversion. K_{ps} was adjusted stepwise until a sufficiently accurate agreement was obtained. K_{ps} values obtained in this way for the shortest residence times were averaged and used in the rest of the simulations. Then k_6 was adjusted (k_5 was obtained from the new k_6 and the equilibrium concentration given by Goux [12]) until agreement was obtained between experimental and calculated conversions at residence times longer than 2–3 s.

Figure 1 shows the fractions of fructose which have been phosphorylated when the mean residence time is varied by varying the flow-rate. The predictions have been calculated using the rate constants in Table 1. The figure also shows the experimentally determined conversions and it can be seen that the fit is excellent, except at residence times around one second.

Two constants have been adjusted iteratively, namely K_{ps} and k_6 . K_{ps} was 7.48, 7.41, and 7.20 s^{-1} for the first three experimental points and a mean value of 7.37 s^{-1} was used in the rest of the calculation. Similarly, k_6 was determined to be 0.038 s^{-1} . The major uncertainty behind this value is the estimate of the reactor void volume.

The value of K_{ps} is quite insensitive to changes in the value of k_6 and vice versa. Changes in k_6 move the second part of the calculated curve (cf. Fig. 1) up or down without much effect on the slope of the first part. The slope is, however,

altered by changing k_5 and k_6 and keeping the ratio, k_5/k_6 , constant. It is therefore easy to make a good estimate of k_6 using values obtained at residence times > 3 s.

A similar set of data was collected for a 10- μl reactor and the K_{ps} values were 6.83, 7.34, 6.98 and 7.19 s^{-1} with a mean of 7.08 s^{-1} , which agreed well with those from the 50- μl reactor. The enzyme glass was the same, but the linear flow-rates will be five times higher in the big reactor for the same residence time. The agreement indicates that the flow-rate compensation by Eqn. 15 works well; k_6 became 0.028, i.e. 26% smaller than that obtained with the bigger reactor. It is quite difficult to pack a 10- μl reactor (1.2 mm i.d.) in a reproducible way and any variation will show up as a deviation in the void volume and thus affect the calculation of τ . The k_6 value obtained with the 50- μl reactor is considered to be more reliable and is the one reported.

It can be seen from the initial part of Fig. 1 that close to 30% of the fructose reacts quickly, but that the conversion rate then becomes much slower. This is illustrated in more detail in Fig. 2 where it can be seen that all anomers except β -fructopyranose disappear within 2 s. The enzyme reactor is so efficient that β -fructofuranose, which is present at around 25% initially, disappears in less than 1 s. It should have been quite

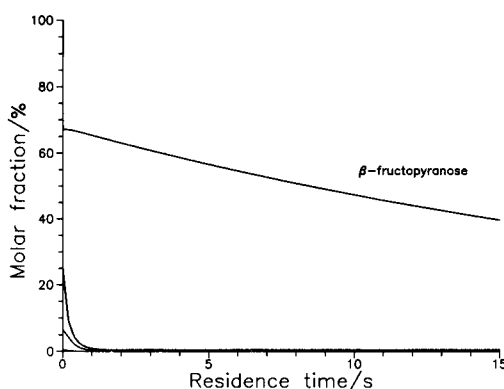


Fig. 2. Molar fractions of the different fructose anomers as a function of residence time in the enzyme reactor. The curves from top to bottom are for β -pyranose, β -furanose, α -furanose and, barely visible, the acyclic form.

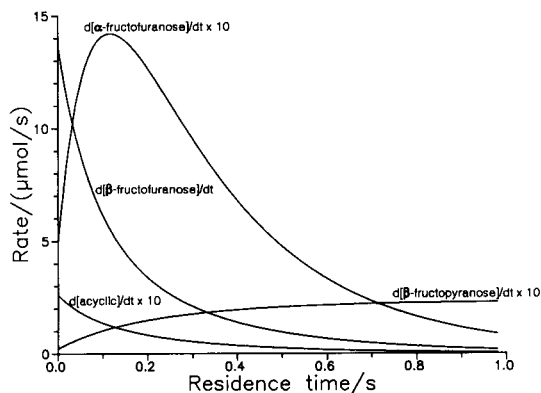


Fig. 3. Reaction rates during the first second of residence in the enzyme reactor.

easy to design an analytical system for complete phosphorylation of all fructose anomers except β -pyranose. The very slow ring opening of this anomer is the sole cause of the analytical complications.

The fast processes in the enzyme reactor are illustrated in Fig. 3. β -furanose is removed by the enzyme and this will increase the rate of ring closing of the acyclic form to β -fructofuranose. As acyclic fructose will pour into the β -form the concentration of acyclic fructose will decrease and this will in turn result in an increasing rate of transfer from the other forms to the acyclic. Depletion of the quickly available reservoirs will later on result in decreasing rates of transfer. The curve will therefore have a maximum, but it is barely visible in the time scale of the diagram. The rate of conversion of α -fructofuranose will increase as the concentration of the acyclic form decreases. Most of the α -form will eventually be consumed and the rate will decrease. The maximum occurs later because of the lower values of the rate constants. The ring-opening rate of the β -fructopyranose then soon reaches an almost constant value.

Anomer selectivity of hexokinase

The possibility that β -fructopyranose reacts enzymatically can be excluded directly on the basis of Fig. 1. If that had been the case there should have been phosphorylation of about 65% within the first few seconds. The possibility that

α -furanose alone is the reacting moiety is directly ruled out by the computer program. It is completely impossible to find a K_{ps} value which gives a conversion high enough to compare with that found experimentally.

The results shown in the figures were obtained with the assumption that β -furanose was the only enzymatically active anomer. An assumption that both the α - and β -anomers react with the enzyme with the same rate will result in an equally good fit between predicted and experimentally found conversions. The K_{ps} values will be somewhat lower, as expected, but k_5 will not be affected at all. It is not possible to distinguish between the two alternatives, mainly because the relative concentration of the α -form is low and its contribution to the conversion will be partly compensated for by fitting K_{ps} in the same time range. So there is no reason to challenge the conclusion reached from structural arguments [9] that β -fructofuranose is the only enzymatically active anomer.

This work was supported by the Swedish Natural Research Council.

REFERENCES

- 1 L.D. Mell and J.T. Maloy, *Anal. Chem.*, 47 (1975) 299.
- 2 H. Huck, A. Schelter-Graf and H.-L. Schmidt, *Bioelectrochem. Bioenerg.*, 13 (1984) 199.
- 3 G. Johansson, L. Ögren and B. Olsson, *Anal. Chim. Acta*, 145 (1983) 71.
- 4 H.S. El Khadem, *Carbohydrate Chemistry. Monosaccharides and Their Oligomers*, Academic Press, San Diego, CA, 1988.
- 5 H.S. Isbell and W. Pigman, *Adv. Carbohydr. Chem. Biochem.*, 23 (1968) 11.
- 6 H.S. Isbell and W. Pigman, *Adv. Carbohydr. Chem. Biochem.*, 24 (1969) 13.
- 7 L. Anderson and J.C. Garver, *Adv. Chem. Ser.*, 117 (1973) 20.
- 8 M. Cockman, D.G. Kubler, A.S. Oswald and L. Wilson, *J. Carbohydr. Chem.*, 6 (1987) 181.
- 9 R.K. Crane, in P.D. Boyer, H. Lardy and K. Myrbäck (Eds.), *The Enzymes*, Vol. 6, 2nd edn., 1962, pp. 60–66.
- 10 M. Skoog, G. Johansson, B. Olsson and R. Appleqvist, *Mikrochim. Acta*, 3 (1988) 131.
- 11 H.U. Bergmeyer (Ed.), *Methods of Enzymatic Analysis*, Verlag Chemie, Weinheim, 1984.

- 12 W.J. Goux, *J. Am. Chem. Soc.*, 107 (1985) 4320.
- 13 P.W. Wertz, J.C. Garver and L. Anderson, *J. Am. Chem. Soc.*, 103 (1981) 3916.
- 14 D. Doddrell and A. Allerhand, *J. Am. Chem. Soc.*, 93 (1971) 2779.
- 15 L. Que and G.R. Gray, *Biochemistry*, 13 (1974) 146.
- 16 S.G. Angyal and G.S. Bethell, *Aust. J. Chem.*, 29 (1976) 1249.
- 17 W. Funcke, C. Vonsonntog and C. Triantaphylides, *Carbohydr. Res.*, 75 (1975) 305.
- 18 B. Olsson and L. Ögren, *Anal. Chim. Acta*, 145 (1983) 101.

Flow-injection determination of 1,5-anhydroglucitol in serum with an immobilized pyranose oxidase reactor and chemiluminescence detection

Nobutoshi Kiba, Fumito Ueda, Kazuya Saegusa, Yuusuke Goto and Motohisa Furusawa

Department of Applied Chemistry and Biotechnology, Faculty of Engineering, Yamanashi University, Kofu 400 (Japan)

Takeshi Yamane

Department of Chemistry, Faculty of Education, Yamanashi University, Kofu 400 (Japan)

(Received 30th June 1992; revised manuscript received 18th August 1992)

Abstract

A flow-injection system with a separation column and an immobilized enzyme reactor is described for the determination of 1,5-anhydro-D-glucitol in serum. Serum samples diluted with water are injected into an anion-exchange column (4 cm × 4 mm i.d.). The eluate is passed through an immobilized pyranose oxidase reactor (5 cm × 4 mm i.d.). The hydrogen peroxide produced is detected chemiluminometrically with a luminol–hexacyanoferrate(III) reaction. The calibration graph is linear over the range 4×10^{-7} – 2×10^{-4} M; the detection limit is 2×10^{-7} M. The sample throughput is 20 h^{-1} with a relative standard deviation of less than 2.5%.

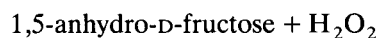
Keywords: Chemiluminescence; Enzymatic methods; Flow injection; Anhydroglucitol; Enzyme reactor; Pyranose oxidase; Serum

1,5-Anhydro-D-glucitol (AG) is a one of main polyols in human serum [1]. A decrease in serum AG in human diabetes mellitus has been found [2–4] and has been proposed as a novel clinical marker of glycaemic control in diabetes mellitus [5].

The best method for the determination of AG is gas chromatography [6,7], but it is unsuitable for the rapid analysis of large numbers of samples. Yabuuchi et al. [8] developed an enzymatic method based on pyranose oxidase and spectrophotometric monitoring, which was applied to

the determination of AG in plasma for the diagnosis of diabetes mellitus. However, the method is time consuming.

Pyranose oxidase (EC 1.1.3.10) (PyOD) oxidizes the hydroxyl group at the C-2 position of the pyranose ring of AG to 1,5-anhydro-D-fructose and hydrogen peroxide in the presence of molecular oxygen:



PyOD also oxidizes hexoses and pentoses having a pyranose ring, such as glucose, galactose and xylose, often at higher rate than AG itself. PyOD has been immobilized on glass beads and used as a reactor for the determination of monosaccharides [9] and glucose [10].

Correspondence to: N. Kiba, Department of Applied Chemistry and Biotechnology, Faculty of Engineering, Yamanashi University, Kofu 400 (Japan).

In this work, immobilized PyOD was used as a column reactor in a flow-injection system for the specific detection of AG in serum. Interference from glucose in the sample was avoided by separation on an anion-exchange column. The H_2O_2 produced in the immobilized PyOD reactor was determined by measuring the chemiluminescence emitted on admixing with luminol and potassium hexacyanoferrate(III). One assay cycle was completed within 3 min.

EXPERIMENTAL

Materials and reagents

PyOD (from *Corioliolus versicolor*, 1150 U ml⁻¹) was obtained from Kyowa Hakko Kogyo (Tokyo). Aminopropyl-CPG (mean pore diameter 59 nm, amount of amine 76 $\mu\text{mol g}^{-1}$, particle size 200–400 mesh) was purchased from CPG (Fairfield, NJ). AG and saccharides were obtained from Sigma (St. Louis, MO). All other reagents were commercially available and were of analytical-reagent grade.

A stock solution of AG (1 mM) was prepared in water and stored in a refrigerator. McIlvaine buffer (pH 4.5) was prepared from 0.1 M sodium hydrogenphosphate and 0.05 M citric acid. Luminol solution [0.7 mM luminol in 0.3 M carbonate buffer (pH 10.5)] was prepared daily. A potassium hexacyanoferrate(III) stock solution (200 mM) was prepared and diluted ten-fold with distilled water before use.

Separation column

TSK gel SAX anion-exchange resin (10 μm , Cl⁻ form) (Tosoh, Tokyo) was packed into a stainless-steel column (4 cm \times 4 mm i.d.) by the slurry-packing method. The packed column was washed with 3 mM NaCl at a flow-rate of 0.5 ml min⁻¹ for 20 min and with water at a flow-rate of 1.0 ml min⁻¹ for 10 min. Then volumes of 50 μl of 1 M NaOH were injected into the column five times at a flow-rate of 1.0 ml min⁻¹.

Immobilized PyOD reactor

Enzyme solution (230 U ml⁻¹) was loaded on a column (10 cm \times 7.8 mm i.d.) of HCA-100S

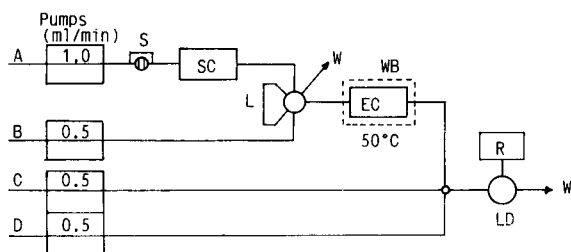


Fig. 1. Schematic diagram of chemiluminometric flow-injection system for the determination of 1,5-anhydro-D-glucitol with immobilized pyranose oxidase reactor. A = water (1.0 ml min⁻¹); B = McIlvaine buffer (pH 4.5, 0.5 ml min⁻¹); C = 20 mM $[\text{Fe}(\text{CN})_6]^{3-}$; D = 0.7 mM luminol in 0.3 M phosphate buffer (pH 10.5); S = sample injector with 50- μl loop; SC = separation column (TSK gel SAX, 10 μm) (4 cm \times 4 mm i.d.); L = loop (1 m \times 0.5 mm i.d.); EC = immobilized enzyme column reactor (5 cm \times 4 mm i.d.); WB = water-bath thermostated at 50°C; LD = luminescence detector; R = recorder; W = waste.

hydroxyapatite (Mitsui Toatsu, Tokyo) equilibrated with 10 mM phosphate buffer (pH 6.8) and the enzyme was eluted with a linear buffer concentration gradient of 10–100 mM phosphate buffer (pH 6.8). The active fractions were combined and used as purified enzyme.

Aminopropyl-CPG was packed into a stainless-steel column (5 cm \times 4 mm i.d.) by the slurry-packing method. Glutaraldehyde solution (2%) in 0.1 M phosphate buffer (pH 7.0) was pumped through the column for 30 min at a flow-rate of 0.3 ml min⁻¹. The column was washed with deaerated water for 15 min at a flow-rate of 0.5 ml min⁻¹. The enzyme solution (ca. 20 ml) was circulated through the activated CPG column at a flow-rate of 0.2 ml min⁻¹ for 3 h at room temperature. PyOD was immobilized with a 65% yield.

Flow system and procedure

A schematic diagram of the flow system is shown in Fig. 1. The system consisted of two LC pumps (Hitachi L-6000) and a reagent delivery pump (Kyowa Seimitsu KHW-52), an injector (Sanuki SV1-6U7) equipped with a 50- μl sample loop, a six-way valve system (Sanuki TVM-6M2) with a loop (1 m \times 0.5 mm i.d.) and a luminometer (Niti-On LF-800) with a flow-through detector cell (270 μl). The samples were injected into the

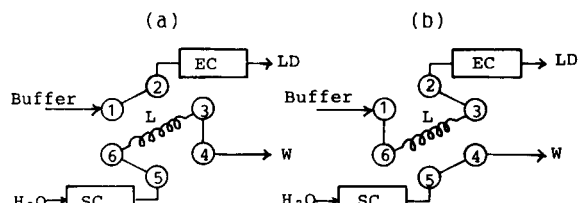


Fig. 2. Flow arrangements for (a) separation position and (b) detection position. SC = separation column; EC = immobilized enzyme reactor; L = loop (1 m × 0.5 mm i.d.); LD = luminescence detector; 1–6 = small openings; W = waste. Buffer, pH 4.5, 0.5 ml min⁻¹; water, 1.0 ml min⁻¹.

separation column at a flow-rate of 1.0 ml min⁻¹. The eluate from the column was passed through the valve system prior to elution through the enzyme reactor.

The arrangement of the flow with the valve and the schematic flow diagram is shown in Fig. 2. In the “separation” position (Fig. 2a), the flow-through part from the separation column (SC) flowed into the loop (L). In this position, buffer (pH 4.5) was pumped through the enzyme reactor (EC). At 45 s after the injection, the rotor of the valve was rotated at an angle of 60° from the separation position and the loop contents were flashed with the buffer (pH 4.5) to the enzyme reactor (EC). The enzyme reactor was kept at 50°C with a thermostated water-bath. The eluate from the enzyme reactor was combined with the luminol solution and potassium hexacyanoferrate(III) solution at a mixer. The total flow-rate was 1.5 ml min⁻¹. In the “detection” position (Fig. 2b), the separation column was washed with water at a flow-rate of 5.0 ml min⁻¹ for 100 s and then at a flow-rate of 1.0 ml min⁻¹ for 35 s. The rotor of the valve was then rotated to the separation position and the next sample was injected into the separation column. One assay cycle was completed within 3 min.

Serum samples (3 μl) were diluted 30-fold with water and then filtered through a membrane filter (Tosoh Airpress-30, cut-off at relative molecular mass 30 000), because serum contains about 100 mM chloride ion and proteins above 3 g l⁻¹ interfered with the chemiluminescent reaction. An aliquot (50 μl) of the filtrate was injected into the system. In order to regenerate the separation

column, 50-μl volumes of 1 M NaOH were injected twice into the system in the separation position, without the rotation of the valve, every 60 samples.

RESULTS AND DISCUSSION

Evaluation of enzyme reactor

The properties of immobilized PyOD were first evaluated without using the separation column. The influence of pH on the enzymatic reaction was studied over the pH range 4.0–6.0. A standard solution of AG (10 μM) was injected into the carrier stream (water) and mixed with 0.1 M McIlvaine buffer at various pH values prior to elution through the enzyme reactor. The total flow-rate through the enzyme reactor was 1.0 ml min⁻¹. The other conditions were identical with those shown in Fig. 1. The optimum pH for the enzymatic reaction was about 4.5. The reactor was placed in a water-bath and the temperature was varied between 20 and 60°C. The reactor exhibited the highest activity at 60°C. At 70°C, the enzyme was deactivated rapidly. The conversion efficiencies to H₂O₂ at 60, 40 and 20°C were 77, 66 and 45%, respectively.

The reactor was used for 8 h (about 200 injections) per day and stored at 4°C in 0.1 M phosphate buffer (pH 7.0) when not in use. The activity remained at 90% of the initial value for 6 weeks. The plot of peak height against concentration was linear from 0.2 to 100 μM. The substrate

TABLE 1
Substrate specificity for immobilized PyOD^a

| Substrate | Relative activity | Substrate | Relative activity |
|-------------|-------------------|--------------|-------------------|
| AG | 100 | L-Xylose | 28 |
| α-D-Glucose | 118 | Melibiose | 87 |
| β-D-Glucose | 118 | Cellibiose | 6 |
| L-Sorbose | 80 | Maltose | 5 |
| D-Galactose | 170 | Raffinose | 13 |
| D-Xylose | 148 | myo-Inositol | 20 |

^a The immobilized PyOD did not oxidize D-mannose, D-fructose, L-fucose, sucrose, lactose, xylytol, sorbitol, mannitol, glycerol, ethylene glycol and ethanol.

specificity for the immobilized PyOD reactor is shown Table 1.

Separation

The separation of a mixture of AG and glucose was effected by anion-exchange chromatography on a TSK gel SAX ($10\ \mu\text{m}$, Cl^- form) column ($4\ \text{cm} \times 4\ \text{mm}$ i.d.) with water as the mobile phase. AG and glucose were hardly retained on the column. In order to change part of the resin into the OH^- form, $50\text{-}\mu\text{l}$ portions of $1\ \text{M}$ NaOH were injected into the column five times. Using the column, the retention times of AG and glucose were $35\ \text{s}$ and $3.3\ \text{min}$, respectively, at a flow-rate of $1.0\ \text{ml}\ \text{min}^{-1}$, with refractive index detection, as shown in Fig. 3. The AG eluted from the column was passed through the loop in the valve system. The rotor of the valve was rotated and the loop contents were ejected into the buffer ($\text{pH}\ 4.5$). As shown in Fig. 4, the flow changeover time after injections was chosen to be $45\ \text{s}$. Immediately after the rotation the separation column was washed with water at a flow-rate of $5.0\ \text{ml}\ \text{min}^{-1}$ for $100\ \text{s}$ because the volume of the mobile phase needed to clear the system was $5.5\ \text{ml}$, as shown in Fig. 3. As chloride

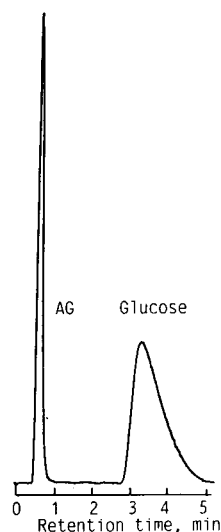


Fig. 3. Chromatogram of mixture of AG ($50\ \text{mg}\ \text{ml}^{-1}$) and glucose ($500\ \text{mg}\ \text{ml}^{-1}$). Mobile phase, water ($1.0\ \text{ml}\ \text{min}^{-1}$); column, TSK gel SAX ($10\ \mu\text{m}$) ($4\ \text{cm} \times 4\ \text{mm}$ i.d.); detection, refractive index (attenuation $\times 8$).

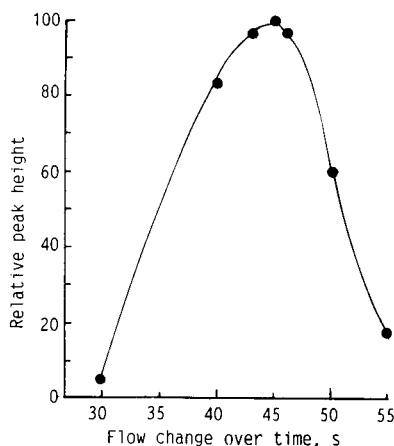


Fig. 4. Effect of flow changeover time after injection.

ion contributed to the decrease in the retention time of glucose, a serum sample that contained about $100\ \text{mM}$ chloride ion was diluted 30-fold with water. When the injection of $50\ \mu\text{l}$ of glucose solution ($1\ \text{mM}$) in $3\ \text{mM}$ NaCl was repeated 100 times, the glucose peak was shifted forward by $1\ \text{min}$. In practical operation, after 60 injections of sample solution the glucose peak was restored to its original position by two injections of $50\ \mu\text{l}$ of $1\ \text{M}$ NaOH.

Linearity of calibration graph

Under the conditions shown in Fig. 1, the peak heights were plotted against the concentration of AG. Four calibration graphs were prepared, covering the ranges $0.4\text{--}4$ ($0.066\text{--}0.66$), $1\text{--}10$ ($0.16\text{--}1.6$), $10\text{--}100$ ($16\text{--}160$) and $20\text{--}200$ ($32\text{--}320\ \text{mg}\ \text{l}^{-1}$). The least-squares calibration equations were $y = 19.98x + 0.04$, where y is peak height and x is AG concentration, with a linear correlation coefficient of $r = 0.997$ (seven data points) for the range $0.4\text{--}4\ \mu\text{M}$ with the luminescence intensity of $4\ \mu\text{M}$ AG being taken as 100 divisions, $y = 19.99x + 0.02$ with $r = 0.998$ (seven data points). For the range $1\text{--}10\ \mu\text{M}$ with the luminescence intensity of $10\ \mu\text{M}$ AG being taken as 100 divisions, $y = 20.00x + 0.02$ with $r = 0.999$ (seven data points) for the range $10\text{--}100\ \mu\text{M}$ with the luminescence intensity of $100\ \mu\text{M}$ AG being taken as 100 divisions and $y = 20.00x + 0.01$ with $r = 0.999$ (seven data points) for the range $20\text{--}200$

μM with the luminescence intensity of $200 \mu\text{M}$ AG being taken as 100 divisions. The relative standard deviation (R.S.D.) for ten injections was 1.9% at $5 \mu\text{M}$ AG. The detection limit (signal-to-noise ratio = 3) was $0.2 \mu\text{M}$ (2 ng in a $50\text{-}\mu\text{l}$ injection).

Precision and reproducibility

Pooled human serum was repeatedly analysed during 10 days. This system gave satisfactorily precise and reproducible results: for serum containing $144 \mu\text{M}$ (23.6 mg l^{-1}) AG, the within-day R.S.D. was 2.0% and day-to-day R.S.D. was 2.4%.

Recovery

A sample of pooled human sera of known AG concentration was supplemented with AG to give final concentrations of $19.2\text{--}25.2 \text{ mg l}^{-1}$. The recoveries were in the range 97–104%.

Comparison

Serum AG results ($n = 20$, range $5.5\text{--}24.7 \text{ mg l}^{-1}$) obtained using this system compared well with results obtained using a batchwise method [8], which employed soluble enzymes and spectrophotometry. The calculated linear regression and correlation coefficient were $y = 1.01x + 0.08$ and $r = 0.9861$, respectively, indicating excellent agreement between the results of the two methods over a wide range of AG concentrations.

Conclusion

It is important to identify subjects at an early stage of diabetes mellitus, because early treatment can prevent complications of the disease. The level of serum AG has been shown to decrease sensitively in patients with diabetes mellitus. The enzymatic method, which employed soluble PyOD, peroxidase and spectrophotometry [8], for the determination of AG is time consuming and is impractical for the routine screening of large populations. Attempts were made to deter-

mine AG in serum using the described flow system, and it proved possible to determine AG in serum with $3 \mu\text{l}$ of serum at a sampling rate of 20 h^{-1} . An immobilized PyOD column reactor forced AG to react with many PyOD molecules in a limited space, ensuring a rapid reaction. When a $5 \text{ cm} \times 4 \text{ mm}$ i.d. column is packed with 150 U of immobilized PyOD, the concentration of PyOD in the column should exceed 230 U ml^{-1} . In a batchwise method [8] using soluble enzyme, PyOD is present in solution at a concentration of only 2 U ml^{-1} . With the higher concentrations of enzyme, the present flow system with an immobilized PyOD reactor can effect rapid analyses.

The chemiluminometric assay for AG described here is at least 100 times more sensitive than the spectrophotometric assay method. It employs a flow system that permits a rapid sample throughput, and gives precise and reproducible results which show an excellent correlation with results obtained by the spectrophotometric assay method.

REFERENCES

- 1 E. Pitkanen, Clin. Chim. Acta, 48 (1973) 159.
- 2 E. Pitkanen, Clin. Chim. Acta, 38 (1972) 221.
- 3 H. Akanuma, K. Ogawa, Y. Lee and Y. Akanuma, J. Biochem., 90 (1981) 157.
- 4 S. Yoshioka, S. Saitoh, T. Fujisawa, A. Fujimori, O. Takatani and M. Funabashi, Clin. Chem., 28 (1982) 1283.
- 5 T. Yamanouchi, S. Minoda, M. Yabuuchi, Y. Akanuma, H. Akanuma, H. Miyashita and I. Akaoka, Diabetes, 38 (1989) 723.
- 6 E. Pitkanen, Scand. J. Clin. Lab. Invest., 42 (1982) 445.
- 7 T. Yamanouchi, H. Akanuma, T. Asano, C. Konishi, I. Akaoka and Y. Akanuma, Diabetes, 36 (1987) 709.
- 8 M. Yabuuchi, M. Masuda, K. Katoh, T. Nakamura and H. Akanuma, Clin. Chem., 35 (1989) 2039.
- 9 L. Olsson, C.F. Mandenius and J. Volc, Anal. Chem., 62 (1990) 2688.
- 10 N. Kiba, F. Ueda, M. Furusawa and T. Yamane, Anal. Chim. Acta, 269 (1992) 187.

On-line organic-phase enzyme detector

Joseph Wang and Yuehe Lin

Department of Chemistry, New Mexico State University, Las Cruces, NM 88003 (USA)

(Received 18th May 1992; revised manuscript received 27th July 1992)

Abstract

The utility of flow carbon-fiber enzyme electrodes for on-line biomonitoring of organic streams is illustrated. The enzymes peroxidase and tyrosinase are immobilized by simple adsorption onto an electrochemically pretreated carbon-fiber surface. The resulting detectors respond very rapidly to dynamic changes in the concentration of organic peroxides and phenolic compounds in flowing chloroform and acetonitrile solutions. The flow-injection operation is characterized with high sample throughputs (60 h^{-1}), good precision (1.1–1.7% R.S.D.) and detection limits of $2\text{--}4 \times 10^{-5} \text{ M}$. The organic-phase enzyme electrode could be combined with various types of analytical flow systems and should allow on-line monitoring of previously inaccessible organic matrices.

Keywords: Enzymatic methods; Flow injection; Carbon-fiber enzyme electrodes; On-line biomonitoring; Peroxidase; Peroxides; Phenolic compounds; Tyrosinase

The ability of enzymes to operate in organic solvents [1–3] offers unique opportunities to the field of biosensors [4]. Organic-phase biocatalytic sensing possesses distinct advantages (over common aqueous operations), including monitoring of hydrophobic substrates, assays of inaccessible sample matrices, enhanced thermostability, simplified immobilization schemes, or prevention of undesirable side reactions. Such opportunities have already been documented in connection with various enzymes [5–9] and tissues [10]. Many industrial and biotechnological processes are thus expected to benefit from the unique features of organic-phase enzyme electrodes. However, despite the growing opportunities for on-line monitoring of many processes, flow detectors based on organic-phase enzyme electrodes have not been developed. Immobilized enzyme reactors were employed for flow-injection analysis of organic media [6].

This paper describes the performance of a cell based on an enzyme micro electrode for ampero-

metric monitoring of flowing organic streams. Analytical flow systems are being increasingly applied for real-time monitoring of various processes or for automated assays of discrete samples. The adaptation of organic-phase biosensors to on-line measurements is thus a logical extension of their scope. The new flow carbon-fiber peroxidase and tyrosinase electrodes are inexpensive and easy to construct, and respond rapidly to dynamic changes in the concentration of peroxides and phenolic species. Although their performance is presented here in terms of flow-injection operation, it could be easily extended to other analytical flow systems. Hence, on-line organic-phase biosensors should be applicable to a large number of analytical problems and should open up new possibilities for flow analysis.

EXPERIMENTAL

Apparatus

Amperometric detection was performed with an EG & G PAR Model 174A polarographic ana-

Correspondence to: J. Wang, Department of Chemistry, New Mexico State University, Las Cruces, NM 88003 (USA).

lyzer, the output of which was displayed on a Houston Omniscrite strip-chart recorder. The flow-injection system consisted of a 50-ml syringe/carrier reservoir, held by the syringe pump (Model 341B, Sage), a Rainin Model 5041 injector (20- μ l loop), interconnecting PTFE tubing and the carbon-fiber based detector.

The detector was fabricated according to the procedure of Huiliang et al. [11]. The Tygon tubing (0.065 in. i.d., 0.195 in. o.d.) was cleaned by soaking it in acetone for 30 min. Subsequently, an injection needle was passed through the wall of the tube (perpendicularly to the flow direction). Three carbon fibers (7 μ m diameter each, Thornell 300 grade WYP-90, Union Carbide) were then inserted into the injection needle, which was subsequently removed from the tubing, leaving the fibers behind. A non-conducting epoxy was then used to seal the holes, while a silver glue was placed on the outer end of the fibers to provide the electrical contact. The Ag/AgCl reference electrode (Model RE-1, BAS) and platinum tube auxiliary electrode were placed in a downstream compartment (Model RC-2, BAS).

The adsorptive immobilization was accomplished by placing 20 μ l of the enzyme solution [containing 1 mg horseradish peroxidase (HRP) or 0.8 mg tyrosinase in phosphate buffer, pH 7.4] within the working-electrode flow compartment. The solution contacted the carbon fiber for 20 min at 4°C. Subsequently, the enzyme solution was removed and the cell was allowed to dry at room temperature.

Reagents

Tyrosinase (EC 1.14.18.1, 2400 U mg⁻¹) and horseradish peroxidase (HRP, EC 1.11.1.7, 90 U mg⁻¹) were received from Sigma. Phenol (Fisher), 2-butanone peroxide, lauroyl peroxide, ferrocene, tetraethylammonium *p*-toluenesulfonate (TEATS), *p*-cresol (Aldrich), acetonitrile (EM Science), and chloroform (Baker) were used as received. The chloroform solution was presaturated with phosphate buffer (0.05 M, pH 7.4) [4], while the acetonitrile solution was mixed with water (95 + 5, v/v). Electrolyte (TEATS) concentrations were 0.1 M (in chloroform) and 0.05 M (in acetonitrile).

Procedure

Flow-injection experiments were performed at room temperature after applying the desired potential (-0.25 or 0.0 V for phenols and peroxides, respectively) and allowing the transient background current to decay. Measurements of peroxide species were performed in the presence of 4×10^{-3} M ferrocene in the carrier and sample solutions.

RESULTS AND DISCUSSION

Two model enzymes, HRP and tyrosinase, known for their effective biocatalytic activity in non-aqueous media, were employed to illustrate the suitability of organic-phase enzyme electrodes for flow analysis. Figures 1 and 2 display typical flow-injection detection peaks for organic peroxides and *p*-cresol, respectively, in chloroform and acetonitrile. The enzyme fiber detector exhibits defined peaks with a rapid increase and decrease of the current (similar to those common in aqueous solutions). The peak half width (8–20 s) allows injection rates of 60–90 samples per hour. Such response is attributed to the immediate proximity of the biocatalytic and sensing sites and to the absence of supporting membranes. The current increases with the substrate concentration, but in a non-linear fashion (expected for enzymatic reactions). The different sensitivities for these compounds are also attributed to the specificity of the enzymes [8,10]. The favorable signal-to-noise characteristics permit convenient quantitation of submillimolar concentrations, with detection limits of 2×10^{-5} M (Fig. 1 and Fig. 2B) and 4×10^{-5} M (Fig. 2A) ($S/N = 3$). These data clearly indicate that the tyrosinase- and HRP-based detectors are very suitable for on-line monitoring of their corresponding substrates in flowing organic streams. The detection of lauroyl peroxide (Fig. 1B) is of particular significance because this hydrophobic peroxide is water insoluble. No response was observed in analogous measurements at the unmodified carbon-fiber electrode (containing no enzyme).

The non-aqueous operation greatly simplifies the enzyme immobilization scheme, as fast ad-

sorptive attachments may be sufficient [4]. During this work we found that the efficiency of such immobilization procedure can be improved significantly via an electrochemical pretreatment of the carbon-fiber substrate (prior to its exposure to the enzyme). Figure 3 compares calibration plots for *p*-cresol (in chloroform) for untreated (a) and treated (b) microelectrodes. The electrochemical pretreatment results in ca. 3-fold enhancement of the flow-injection response. Such improvement is attributed to the dramatic increase in the surface area and to the increased hydrophilic character of the surface. Such changes in the surface have been reported recently for anodic pretreatments of carbon-fiber microelectrodes [12]. Apparently,

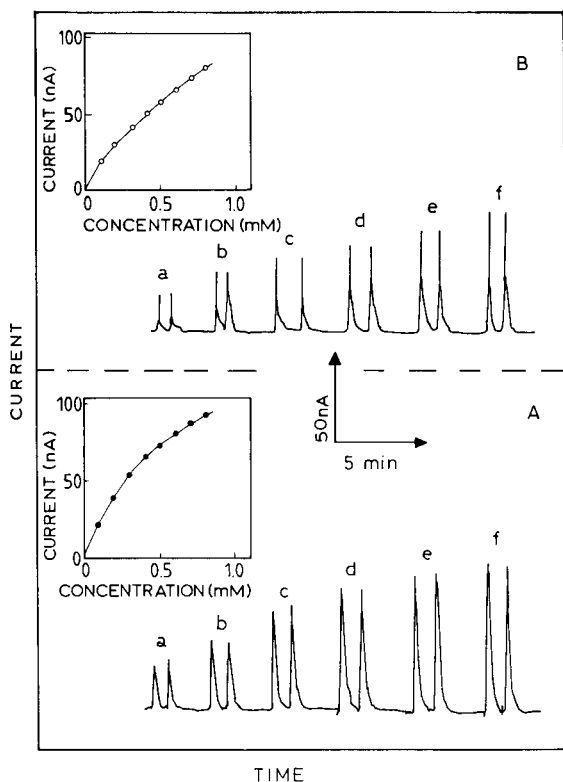


Fig. 1. Flow-injection peaks for chloroform solutions containing increasing levels of (A) 2-butanone peroxide and (B) lauroyl peroxide, $1-6 \times 10^{-4}$ M (a-f). HRP/carbon-fiber detector; carrier/electrolyte, chloroform containing 0.1 M TEATS and 4 mM ferrocene. Operating potential, 0.0 V; flow-rate, 0.7 ml min^{-1} . Also shown (inset) are the resulting calibration plots.

these changes lead to a more stable adsorption of higher enzyme loadings.

The use of a carbon-fiber based detector, with its low current outputs, can be advantageous for minimizing ohmic losses in the flowing organic media. Figure 4 (A and B) compares the amperometric response to phenol in acetonitrile solutions in the presence and absence of added electrolyte. Despite the resistance of the electrolyte-free solution, well-defined and sharp peaks are observed; the peak height is similar to that observed in the electrolyte-containing solution. The ohmic drop problem, however, becomes more severe when non-polar solutions (e.g. chloroform) are employed (Fig. 4D). Such media require the presence of some electrolyte. Batch organic-phase enzymatic assays have also benefited from the minimization of ohmic drops at ultramicroelectrodes [5].

The flow-injection biosensing response in the organic medium is strongly affected by experimental variables, such as the operating potential or solution flow-rate (Fig. 5). The current-potential curve (a) has a sigmoidal shape, characteristic of hydrodynamic voltammograms (HDVs) in aqueous solutions. Such HDV indicates again negligible ohmic distortions. Accordingly, an operating potential of -0.25 V was employed in all subsequent phenol measurements. The amperometric response decreased gradually upon increasing the flow-rate between 0.4 and 2.4 ml min^{-1} (b). Such dependence is attributed primarily to a shorter contact of the sample zone with the enzyme/carbon fiber at high flow-rates. We have found also that the stability of the response is improved at slow flow-rates.

The response of the enzyme electrode in flowing organic media is highly reproducible. Figure 6 illustrates characteristics flow-injection peaks for 20 repetitive injections of chloroform or acetonitrile solutions containing lauroyl peroxide (A), 2-butanone peroxide (B) and *p*-cresol (C). These prolonged (20–25 min) series exhibit a stable response, with relative standard deviations of 1.6, 1.7, and 1.1%, respectively. Such reproducibility is common in analogous assays of aqueous solutions. Another longer operation, involving 36 repetitive injections of a $1 \times 10^{-3} \text{ M}$ *p*-cresol (in

chloroform) solution, every 5 min over a 3-h period, resulted in a very slight (ca. 9%) decrease of the response. The system construction and cost permit easy and fast replacement of the detector (when needed).

In summary, the above results illustrate the suitability of bioelectrodes for amperometric monitoring of flowing organic streams. The en-

zyme electrode responds rapidly to changes in the substrate concentration that characterize flow-injection systems. A multiflow cell arrangement, with a number of enzyme microelectrodes, will allow the determination of a larger number of analytes. Other types of automated flow systems (e.g., process monitors, segmented flow autoanalyzers, liquid chromatographic systems) can bene-

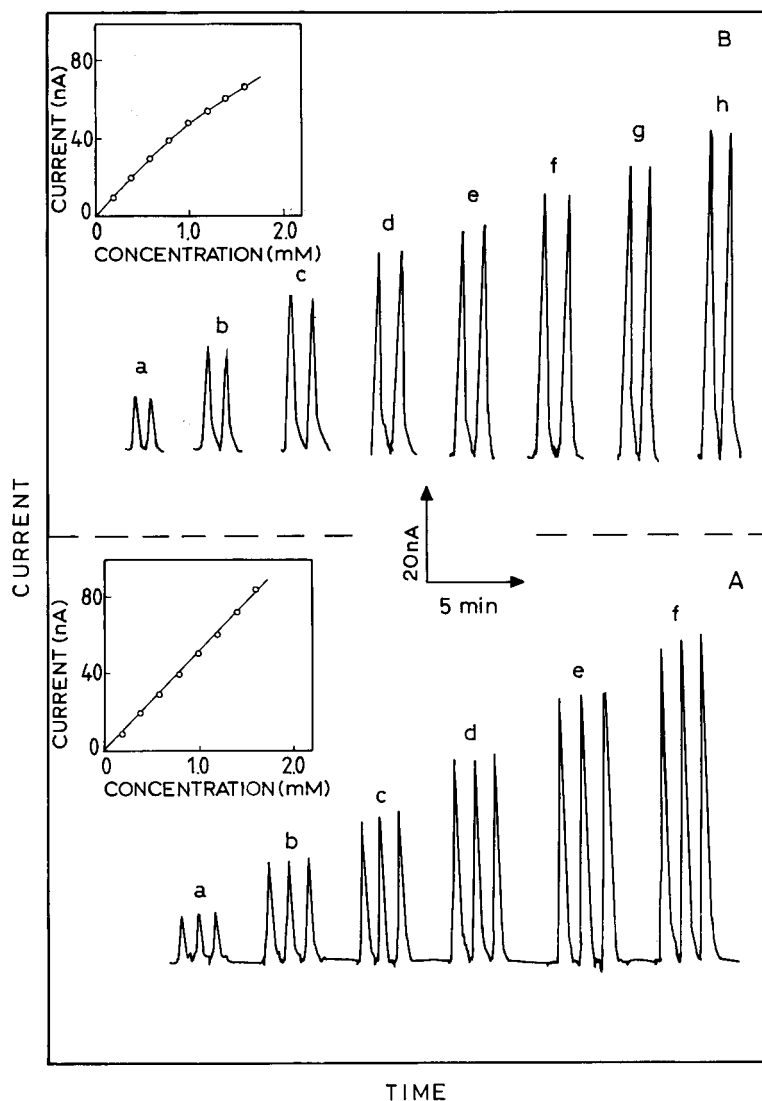


Fig. 2. Flow-injection peaks for (A) acetonitrile solutions containing increasing level of *p*-cresol, $1-6 \times 10^{-4}$ M (a-f) and (B) chloroform solutions containing increasing levels of *p*-cresol $2-12 \times 10^{-4}$ M (a-h). Tyrosinase/carbon-fiber detector; carrier/electrolyte, (A) acetonitrile-water (95 + 5, v/v) containing 0.05 M TEATS; (B) chloroform containing 0.1 M TBATS. Operating potential, -0.25 V; flow-rate, 0.7 ml min^{-1} . Also shown (inset) are the resulting calibration plots.

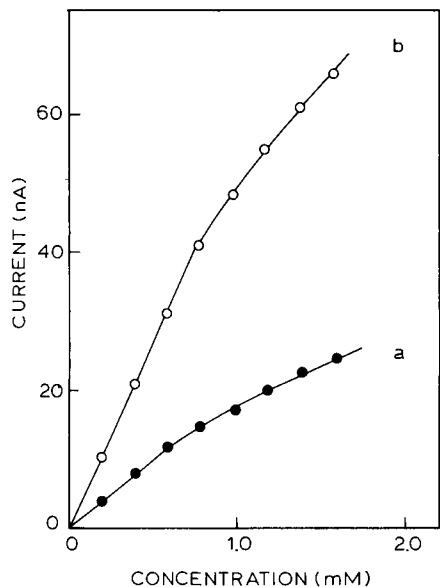


Fig. 3. Calibration plots for *p*-cresol at (a) untreated and (b) treated carbon-fiber microelectrodes. Flow-injection operation as in Fig. 2B (with chloroform containing 0.1 M TBATS as carrier). The electrochemical pretreatment (b) proceeded at +1.80 V for 60 s in the presence of a flowing (0.5 ml min⁻¹) phosphate buffer (0.05 M, pH 7.4) solution.

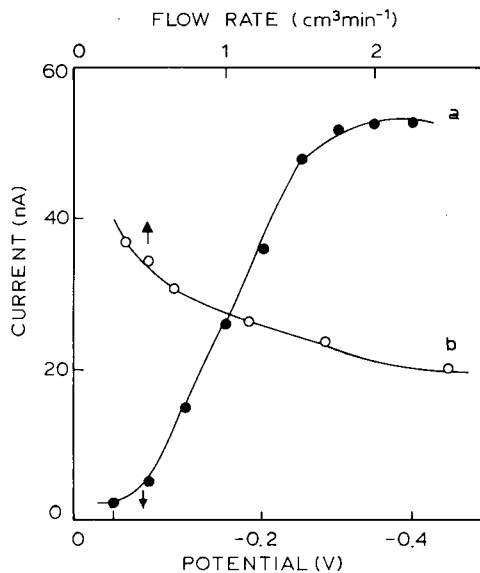


Fig. 5. Dependence of the peak current upon (a) the operating potential and (b) flow-rate. Response to (a) 1×10^{-3} M and (b) 6×10^{-4} M *p*-cresol. Other conditions as in Fig. 2.

fit from the dynamic properties of organic-phase biosensors. Applicability to other solvent systems, different enzymes or substrates and additional

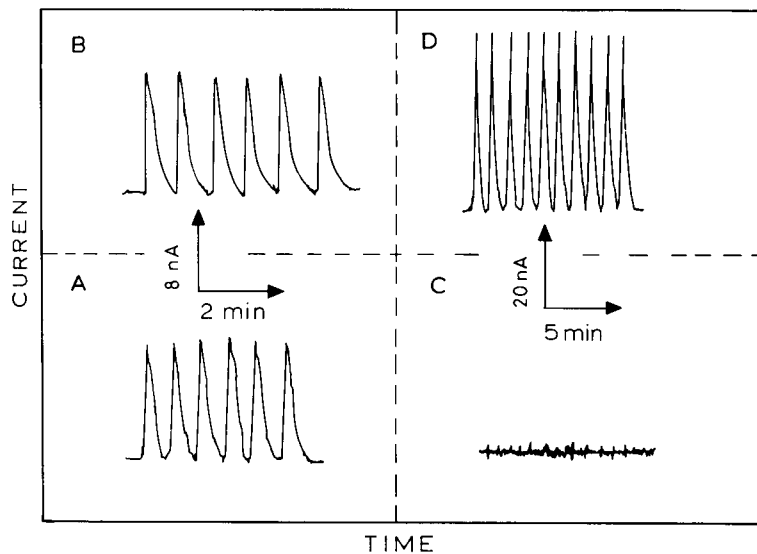


Fig. 4. Flow injection peaks for (A, B) 2×10^{-4} M phenol and (C, D) 1×10^{-3} M *p*-cresol acetonitrile and chloroform solutions, respectively, (A, C) without and (B, D) with added electrolyte. Other conditions as in Fig. 2.

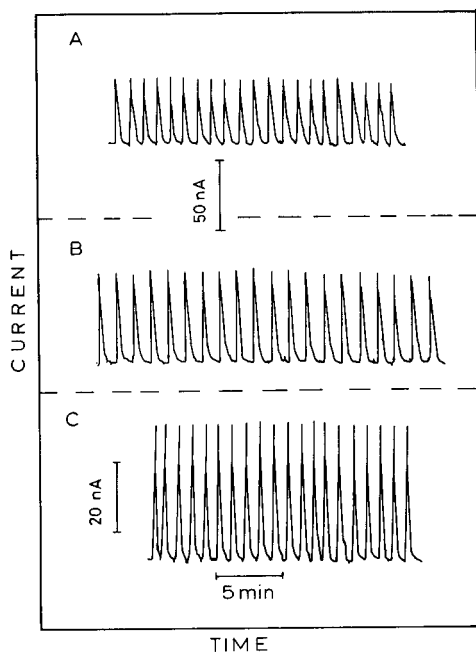


Fig. 6. Detection peaks for repetitive injections of (A) 4×10^{-4} M lauroyl peroxide, (B) 2-butanone peroxide, and (C) *p*-cresol. Conditions (A, B) as in Fig. 1 and (C) as in Fig. 2.

(non-electrochemical) detection schemes can also be envisioned. Hence, organic-phase flow detectors should lead to a wide range of important applications using previously inaccessible matri-

ces. For example, a flow-injection procedure for rapid measurements of phenols in olive oils is currently being developed.

This work was supported in part by the U.S. Environmental Protection Agency (Grant No. CR-817936-010). Mention of trade names does not constitute endorsement by the U.S. EPA.

REFERENCES

- 1 A.M. Klibanov, *CHEMTECH*, 16 (1986) 354.
- 2 P. Aldercreutz and B. Mattiesson, *Biocatalysis*, 1 (1987) 99.
- 3 K.P. Natarajan, *J. Chem. Ed.*, 68 (1991) 13.
- 4 S. Saini, G.F. Hall, M.E. Downs and A.P.F. Turner, *Anal. Chim. Acta*, 249 (1991) 1.
- 5 J. Wang, L.H. Wu and L. Angnes, *Anal. Chem.*, 63 (1991) 2993.
- 6 L. Braco, J. Daros and M. de la Guardia, *Anal. Chem.*, 64 (1992) 129.
- 7 F. Schubert, S. Saini and A. P.F. Turner, *Anal. Chim. Acta*, 245 (1991) 133.
- 8 J. Wang, B. Freiha, N. Naser, E.G. Romero, U. Wollenberger, M. Ozsoz and O. Evans, *Anal. Chim. Acta*, 254 (1991) 81.
- 9 G.F. Hall and A.P.F. Turner, *Anal. Lett.*, 24 (1991) 1375.
- 10 J. Wang, N. Naser, H. Kwon and M. Cho, *Anal. Chim. Acta*, 264 (1992) 7.
- 11 H. Huiliang, C. Hua, D. Jagner and L. Renman, *Anal. Chim. Acta*, 193 (1987) 61.
- 12 G. Swain and T. Kuwana, *Anal. Chem.*, 63 (1991) 517.

Improved methodology for subnanogram quantitation of doxorubicin and its 13-hydroxy metabolite in biological fluids by liquid chromatography

David T. Rossi¹, Barbara A. Phillips, John R. Baldwin and Prem K. Narang

Bioanalytical Research Laboratory, Department of Pharmacokinetics / Dynamics, Adria Laboratories, P.O. Box 16529, Columbus, OH 43216 (USA)

(Received 24th February 1992; revised manuscript received 24th June 1992)

Abstract

Sensitive and specific methodology for quantifying doxorubicin (DOX), a potent antineoplastic drug, and its 13-hydroxy metabolite, doxorubicinol (DOX-OL), in plasma and urine has been developed and validated. The plasma method uses solid-phase extraction for analyte isolation and a narrow-bore (2.0 mm i.d.) column for liquid chromatographic separation with optimized fluorescence detection. The dynamic ranges for both drug and metabolite in plasma are linear from 0.2 to 100 ng ml⁻¹. Drug and metabolite are quantified in unextracted, diluted urine over a 16 to 400 ng ml⁻¹ range. Epirubicin, an epimeric analogue of doxorubicin, is used as an internal standard. Mean extraction efficiencies for drug, metabolite and internal standard from plasma are 88, 86 and 90%, respectively. The instrumental detection limit (signal-to-noise ratio = 3) for doxorubicin or metabolite was 18 pg on column, while the lower limit of quantitation (LLOQ) was 0.3 and 0.6 ng ml⁻¹, respectively for DOX and DOX-OL. The typical intra-day accuracy and imprecision in plasma was < 8% bias and < 9% relative standard deviation (R.S.D.) for DOX at or above 0.3 ng ml⁻¹, and < 15% and < 10% for DOX-OL at or above 0.6 ng ml⁻¹. For the urine method, the average intra-day imprecision was < 7% R.S.D. and the average bias was < 5% for both drug and metabolite over the entire dynamic range. Determinations of these two components in patient samples has verified the robustness and utility of the method.

Keywords: Fluorimetry; Liquid chromatography; Antineoplastic drugs; Biological fluids; Doxorubicin; Plasma; Urine

Doxorubicin (DOX) is a well established and widely accepted antineoplastic agent used in the treatment of many cancer types [1]. The duration of its use, hence its ultimate effectiveness as an anticancer agent, is limited by potentially irreversible, dose-dependent cardiotoxicity. Thus, there is considerable interest in the development

of agents which ameliorate or prevent this toxicity [2]. It is of interest to determine whether the disposition, and thus the therapeutic index of this effective antineoplastic is altered in the presence of such cardioprotectants.

Several recent papers have described sensitive bioanalytical methodologies for DOX. Two of these papers employ liquid-liquid extraction, liquid chromatography (LC) and oxidative electrochemical detection [3,4] and report a best case detection limit (signal-to-noise = 3) of 0.7 ng ml⁻¹. A third paper [5], utilized solid-phase extraction (SPE) and reversed-phase LC with fluorescence detection to achieve a detection limit of

Correspondence to: P.K. Narang, Bioanalytical Research Laboratory, Department of Pharmacokinetics/Dynamics, Adria Laboratories, P.O. Box 16529, Columbus, OH 43216 (USA).

¹ Present address: Parke Davis Pharmaceutical Research Division, Warner-Lambert Company, 2800 Plymouth Road, Ann Arbor, MI 48106-1047 (USA).

0.2 ng ml⁻¹ (108 pg on column). None of these papers, however, report precision estimates at or near the detection limit.

We report here the development of a sensitive, accurate and precise assay procedure permitting quantitation of DOX and its 13-dihydroxy metabolite, doxorubicinol (DOX-OL), in biological fluids. Considerable emphasis has been placed on enhancing sensitivity by optimizing fluorescence spectral parameters and chromatographic conditions, and on characterizing the quantitative performance throughout the dynamic range. We have also compared the performance of standard (4.6 mm i.d.) and narrow-bore (2.0 mm i.d.) LC columns as applied to plasma. This method has been applied to a study assessing DOX disposition in the presence of the cardioprotectant dexrazoxane.

EXPERIMENTAL

Chemicals

Doxorubicin · HCl, doxorubicinol · HCl, and epirubicin · HCl were procured from Farmitalia Carlo Erba (Milan, Italy). All other reagents were analytical grade or better and were used without further purification. Water was purified in-house with a Milli-Q water purification system (Millipore, Bedford, MA). Unless otherwise indicated, all standards and controls were prepared using human plasma or urine.

Apparatus

The SPE columns contained 500 mg of ODS/silica sorbent (p/n 51910, Sep-pak, Waters, Milford, MA). Columns were eluted on a 24-port vacuum manifold system (Burdick and Jackson, Muskegon, MI). The analytical LC columns were Ultrasphere ODS for both plasma (5 μm, 25 cm × 2.0 or 4.6 mm i.d.) and urine (5 μm, 25 cm × 4.6 mm i.d.), and were obtained from Beckman (San Ramon, CA). The guard column was an RP-18 New Guard (Brownlee, Santa Clara, CA). The chromatograph consisted of a pump (Model 400, ABI, Ramsey, NJ), an autosampler (Model 9090, Varian, Walnut Creek, CA) with a 100 μl loop, a fluorescence detector

(Model LS40, Perkin-Elmer, Norwalk, CT) and a data acquisition system (PE-Nelson, Cupertino, CA) with ACCESS*CHROM[®] software. The detector excitation and emission wavelengths were set at 470 nm (grating) and 550 nm (50% transmittance cutoff filter), respectively. The detector time constant was set at 1.0 s. The instrument was configured to send a 1 V signal to the data system.

Unextracted and extracted plasma samples were handled in 4.5-ml polypropylene centrifuge tubes. Small volume (200 μl), silanized glass autosampler vial inserts (p/n 997503 Varian) were used to accommodate reconstituted samples following extraction. Sample dry down was performed with a vortex evaporator (Buchler, Fort Lee, NJ). All anthracycline solutions were prepared with silanized glassware to minimize adsorptive losses. Urine samples were diluted in polypropylene tubes and transferred to silanized, amber glass autosampler vials (p/n 996689 Varian).

Liquid chromatographic conditions

For plasma samples separated on the 2.0 mm column, the mobile phase composition was 75% phosphate buffer (20 mM KH₂PO₄, 0.05% (v/v) triethylamine, adjusted to pH 3.0 with concentrated phosphoric acid) and 25% acetonitrile. The separation was isocratic, with a 0.2 ml min⁻¹ flow-rate and, typically, 100 bars (1450 psi) of back pressure. For urine and comparative plasma samples, a 250 × 4.6 mm column was used, and the acetonitrile content and mobile phase flow-rate were increased to 28% and 0.80 ml min⁻¹, respectively.

Preparation of standards and controls

Plasma. Individual stock standards of DOX and DOX-OL (100 μg ml⁻¹) were prepared by dissolving weighed amounts (as free bases) in 10 mM aqueous phosphoric acid. Working standards containing between 1000 and 2 ng ml⁻¹ each of both DOX and DOX-OL were prepared by volumetric dilution of the stock standard with 10 mM aqueous phosphoric acid. Plasma standards of DOX/DOX-OL were prepared daily by spiking 100-μl aliquots of working standards into aliquots

of blank plasma to produce concentrations of 100, 50, 20, 10, 5, 2, 1, 0.5, 0.3 and 0.2 ng ml⁻¹. Standard curves for both components were run on each of seven days for the 2.0-mm column, and on each of eight days for the 4.6-mm column.

From independent weighings, control samples at 0.30, 0.60, 3.00, 6.00, 30.0 and 60.0 ng ml⁻¹ in both DOX and DOX-OL were prepared in human plasma. The control samples were portioned (3.5 ml) into 4.5-ml polyallomer vials (Perfector Scientific, Atasacadero, CA) and stored at -20°C until assayed. Using the 2.0-mm column, six replicates of the 0.30, 3.00, and 30.0 controls were run on each of three days, while six replicates of the 0.60, 6.00, and 60.0 controls were run on each of four days. For the 4.6-mm column, six replicate controls at both 0.6 and 60 ng ml⁻¹ were run on each of eight days. Controls were always run with a standard curve of each component.

Urine. From a 100 µg ml⁻¹ stock solution, working standards containing between 4000 and 160 ng ml⁻¹ each of DOX and DOX-OL were prepared in 10 mM phosphoric acid. These working standards were appropriately diluted to give, urine standards at 400, 200, 100, 40, 24 and 16 ng ml⁻¹. Three standard curves were run. Aliquots of stock standards were diluted 10-fold with blank urine to produce urine controls at 300 and 30 ng ml⁻¹. The control samples were portioned (3.5 ml) into 4.5-ml polyallomer vials and stored at -20°C until assayed.

Sample preparation procedure

Plasma. To 1.0 ml of a plasma sample in a 4.5-ml polypropylene tube, 50 µl of EPI (500 ng ml⁻¹) was added. For standards, 100 µl of the appropriate DOX/DOX-OL working standard was added to 1.0 ml of blank plasma. The resulting solutions were briefly vortexed (5 s) and loaded onto prewashed (1 × 2 ml of methanol, 1 × 2 ml of water and 1 × 2 ml of 3:1 (v/v) 10 mM potassium phosphate (aq.), pH 8.0–methanol) SPE columns. During sample loading, the manifold vacuum was always below 25 kPa. Following loading, each column was washed with 1 ml of water and 2.5 ml of 3:1 (v/v) water–methanol. The analytes were eluted with 2 ml of 26 mM methanolic phosphoric acid, which was

collected in a polypropylene tube and evaporated to approximately 0.3 ml under vacuum (90 kPa) at 35°C. Appropriate volumes of aqueous 10 mM phosphoric acid were added to samples inadvertently dried below 0.3 ml, but samples were never evaporated to dryness. Solutions were transferred to silanized, glass microvial autosampler inserts and injected (10 or 90 µl) into the chromatographic system.

Urine. Standards, samples and controls were not extracted. In a polypropylene tube, 1 ml of urine (volumetrically prediluted with blank urine) was spiked with 100 µl of EPI solution (1.0 µg ml⁻¹), diluted (2.0 ml of 10 mM phosphoric acid), vortexed (5 s), transferred to a silanized vial and injected (50 µl) into the LC apparatus.

Calculations

Calibration curves of peak-height ratio (DOX or DOX-OL/EPI) versus mass ratio (DOX or DOX-OL/EPI) in the matrix were constructed and used to estimate regression parameters. A weighted (1/concentration) model was employed for both plasma and urine. Using peak-height ratios and regression equation parameters, analyte concentrations in unknown samples were calculated.

RESULTS AND DISCUSSION

Epirubicin (EPI), an epimeric analog of DOX was selected as the internal standard for these methods because it is available in high purity, has extraction and spectral characteristics which closely resemble DOX and has a convenient chromatographic capacity factor (*k'* of 6.9 relative to *k'* of 5.2 for DOX). Idarubicin and daunorubicin were considered as internal standards but had much larger capacity factors (> 10), resulting in long run times. To minimize quantitation error resulting from unanticipated interferences, chromatographic peak-height was used instead of peak area.

Spectral properties of doxorubicin

The ultraviolet absorbance spectrum for DOX in mobile phase has a broad maximum between

468 and 496 nm. This particular band is analytically useful because it gives rise to intense fluorescence and potentially offers greater specificity than more intense maxima at 200, 234 and 250 nm. An emission spectrum ($\lambda_{\text{ex}} = 470$ nm) for DOX in mobile phase showed intense fluorescence above 530 nm. Using the above information as a guide, emission filters with 50% transmittance cutoffs of 530, 550 and 570 nm were evaluated for maximizing sensitivity. The 550-nm filter yielded an 87% greater peak-height than the 570-nm filter, with comparable noise and specificity against a plasma matrix. The 530-nm filter yielded only a 2% greater peak-height than the 550-nm filter, with noticeably poorer specificity. On this basis, the 550-nm filter was chosen. Emission spectra for DOX-OL and EPI in mobile phase are virtually identical to that for DOX.

Chromatographic performance

Capacity factors for DOX-OL, DOX and EPI were 3.7, 5.2 and 6.9, respectively, on the 2.0-mm, and 3.2, 5.4 and 6.8, respectively, on the 4.6-mm column. In all cases, resolution between component peaks (R_s) was 2.7 or greater. Column efficiency, as indicated by the number of theoretical plates (N) was a minimum of 4000 for the 2.0-mm diameter column and a minimum of 9500 for the 4.6-mm column [6].

Representative undiluted plasma and urine blanks showed clean chromatographic windows for DOX and EPI. Although the windows were clean in urine, a small endogenous plasma matrix peak sometimes coeluted with DOX-OL. This peak corresponds to less than 0.05 ng ml^{-1} of DOX-OL and could result in 25% bias at 0.2 ng ml^{-1} and less at higher concentrations. Similar blanks were obtained with several other human plasma sources. A comparison of blank plasma chromatograms, showed a decreased solvent envelope for the 4.6-mm column relative to the 2.0-mm column. In practice, this difference between the blanks affects quantitation very little because analyte peaks are adequately retained and do not compete with the solvent envelope. A comparison of chromatograms for the 0.3 ng ml^{-1} standard on 4.6- and 2.0-mm columns is given in Figs. 1A and B, respectively. For either column,

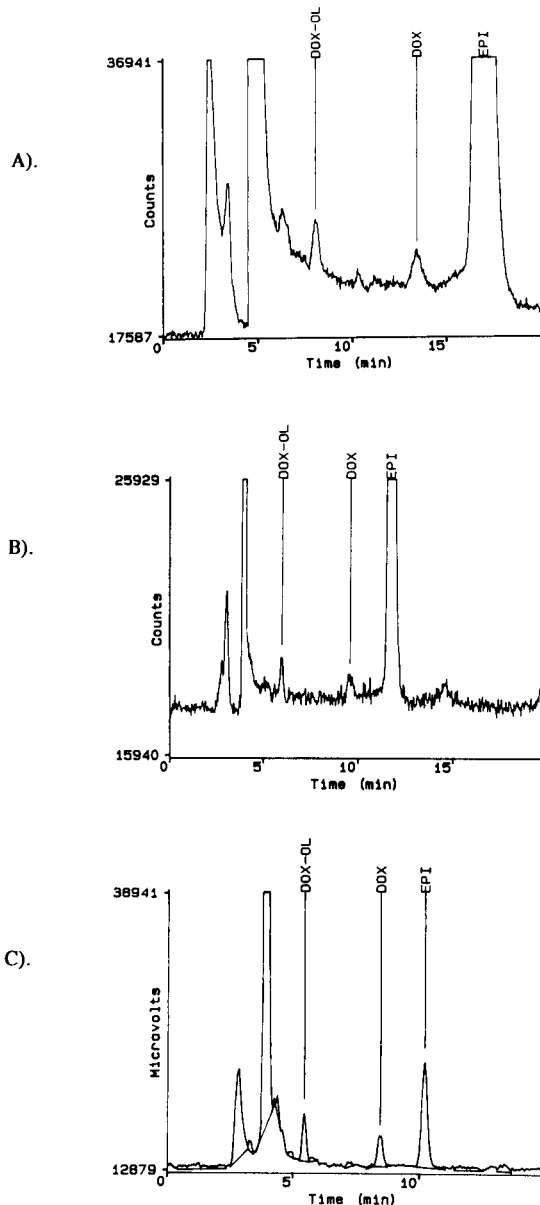


Fig. 1. Chromatograms for standards prepared in (A) plasma (0.3 ng ml^{-1} , 2.0-mm i.d. column), (B) plasma (0.3 ng ml^{-1} , 4.6-mm i.d. column), and (C) urine (16 ng ml^{-1} , 4.6-mm i.d. column).

the peaks are well resolved and readily detectable. Peaks generated on the 4.6-mm column have lower signal-to-noise ($S/N \approx 5$ compared to ≈ 9 for the 2.0-mm column) but are narrower and, therefore, less prone to interference from

unanticipated matrix components. A chromatogram of a 16 ng ml⁻¹ urine standard is given in Fig. 1C.

Chromatograms of plasma samples collected 168 h post-dose (50 mg m⁻²) are presented for comparison in Figs. 2A (4.6-mm) and B (2.0-mm). These chromatograms demonstrate the effectiveness of either column for determining low levels in patient samples. Concentrations of DOX and DOX-OL in the sample depicted in Fig. 2A are approximately 2.5 and 1.2 ng ml⁻¹, respectively, while those in 2B are both approximately 2.5 ng ml⁻¹. In all cases, chromatographic windows are free from interferences. Fig. 2C shows a predose (blank) plasma chromatogram.

Linearity

Plasma. For the 2.0-mm column, back-calculated standard concentrations and weighted regression parameters for seven calibration curves, covering a 500-fold concentration range, demon-

strate excellent linearity for both DOX ($r^2 \geq 0.9964$, bias in back-calculated standards $\leq 7.0\%$) and DOX-OL ($r^2 \geq 0.9969$, bias in back-calculated standards $\leq 10.9\%$). The percent R.S.D. in slopes for DOX and DOX-OL were 3.5% and 11.0%, respectively, indicating good inter-day reproducibility. For the 4.6-mm column, DOX results displayed excellent linearity over 0.3 to 100 ng ml⁻¹, with $r^2 > 0.9987$, and bias in back-calculated concentration of generally $< 4\%$ and always $< 15\%$. Doxorubicinol results over the same range displayed similar results ($r^2 > 0.9986$, bias in back-calculated standards $< 8\%$). Standards at 0.2 ng ml⁻¹ generally produced peaks with $S/N < 3$.

Urine. Back-calculated standard concentrations and regression parameters for three standard urine curves, covering a 25-fold range, demonstrate excellent linearity ($r^2 \geq 0.9988$, average bias in back-calculated standards $\leq 7.5\%$) for both components. The percent R.S.D. in

TABLE 1

Accuracy and precision estimates for DOX plasma controls

| Label concentration of control sample (ng ml ⁻¹) | Day | n | Accuracy | | Precision | | | |
|--|-----|---|-----------------------------------|--------------|--------------------|----------------------------|-----------------------------------|---------------------------------|
| | | | Mean found (ng ml ⁻¹) | Percent bias | Standard deviation | Percent R.S.D. (intra-day) | Pooled percent R.S.D. (inter-day) | Pooled percent bias (inter-day) |
| 0.300 | 1 | 5 | 0.313 | 4.3 | 0.105 | 33.5 | | |
| | 2 | 6 | 0.248 | -17.3 | 0.010 | 4.0 | | |
| | 3 | 6 | 0.290 | -3.3 | 0.023 | 8.1 | 21.6 | -6.0 |
| 0.600 | 4 | 6 | 0.718 | 19.7 | 0.051 | 7.1 | | |
| | 5 | 6 | 0.591 | -1.5 | 0.060 | 10.2 | | |
| | 6 | 6 | 0.630 | 5.0 | 0.037 | 5.9 | | |
| 3.00 | 7 | 6 | 0.588 | -2.0 | 0.014 | 2.3 | 10.4 | 4.7 |
| | 1 | 6 | 2.95 | -1.7 | 0.11 | 3.9 | | |
| | 2 | 6 | 3.12 | 4.0 | 0.21 | 6.7 | | |
| 6.00 | 3 | 6 | 2.77 | -7.6 | 0.33 | 12.0 | 9.0 | -1.8 |
| | 4 | 6 | 6.49 | 8.2 | 0.40 | 6.2 | | |
| | 5 | 5 | 6.12 | 2.0 | 0.50 | 8.2 | | |
| 30.0 | 6 | 6 | 5.87 | -2.2 | 0.54 | 9.3 | | |
| | 7 | 6 | 6.10 | 1.7 | 0.30 | 5.0 | 7.7 | 2.5 |
| | 1 | 6 | 30.2 | 0.7 | 1.6 | 5.3 | | |
| 60.0 | 2 | 6 | 30.3 | 1.0 | 1.1 | 3.6 | | |
| | 3 | 6 | 27.8 | -7.3 | 0.9 | 3.3 | 5.7 | -2.0 |
| | 4 | 6 | 60.0 | 0.1 | 1.9 | 3.2 | | |
| | 5 | 6 | 62.0 | 3.3 | 2.5 | 4.0 | | |
| | 6 | 6 | 59.8 | -0.3 | 2.4 | 4.1 | | |
| | 7 | 5 | 61.8 | 3.0 | 3.3 | 5.3 | 4.2 | 1.5 |

slopes were 1.8% and 5.0% for DOX and DOX-OL, respectively, again indicating excellent inter-day reproducibility.

Precision

Plasma. Precision estimates from replicate DOX and DOX-OL plasma controls on a 2.0-mm column, on each of three or four days, are presented in Tables 1 and 2, respectively. Determination of 6 replicate DOX controls at 0.3, 0.6, 3.0, 6.0, 30.0 and 60.0 ng ml⁻¹ yielded typical intra-day imprecision of < ±10% R.S.D. (Table 1) and inter-day imprecision of ±21.6, 10.4, 9.0, 7.7, 5.7 and 4.2%, respectively. Intra-day imprecision for DOX-OL was also generally < ±10% (Table 2) at the same concentrations, while inter-day imprecisions were ±44.6, 22.3, 6.4, 8.3, 6.0 and 4.8, respectively. A comparison of inter-day precision estimates for 2.0- and 4.6-mm columns at the 0.6 and 60.0 ng ml⁻¹ levels is presented in Table 3.

Urine. Typical intra-day percent R.S.D. (low and high) for DOX controls at 30 and 300 ng ml⁻¹ were < ±4 and < ±3%, while those for DOX-OL were < ±5 and < ±4%, respectively. Inter-day imprecision estimates were ±5.0% and ±3.2% (low and high) for DOX, and ±5.3% and ±3.8% for DOX-OL controls.

Accuracy

Plasma. For the 2.0-mm column, accuracy estimates (expressed as % bias) from replicate plasma controls are presented in Tables 1 and 2 for DOX and DOX-OL, respectively. For DOX, the intra-day bias was typically < 8% and the inter-day bias was < 6.0%. The intra-day bias for DOX-OL was generally < 22% at 0.3 ng ml⁻¹ and < 3.4% at all higher levels. The inter-day bias was -19.3% for the 0.3 ng ml⁻¹ level and < 3.5% for all higher levels. For the 4.6-mm column, percent bias was generally < 15% at the lowest level and < 10% at high levels. Inter-day

TABLE 2

Accuracy and precision estimates for DOX-OL plasma controls

| Label concentration of control sample (ng ml ⁻¹) | Day | n | Accuracy | | Precision | | | |
|--|-----|---|-----------------------------------|--------------|--------------------|----------------------------|-----------------------------------|---------------------------------|
| | | | Mean found (ng ml ⁻¹) | Percent bias | Standard deviation | Percent R.S.D. (intra-day) | Pooled percent R.S.D. (inter-day) | Pooled percent bias (inter-day) |
| 0.300 | 1 | 6 | 0.256 | -14.7 | 0.128 | 50.0 | | |
| | 2 | 6 | 0.187 | -37.8 | 0.133 | 71.2 | | |
| | 3 | 6 | 0.288 | -4.1 | 0.027 | 9.3 | 44.6 | -19.3 |
| 0.600 | 4 | 6 | 0.733 | 22.1 | 0.048 | 6.6 | | |
| | 5 | 6 | 0.688 | 14.6 | 0.035 | 5.0 | | |
| | 6 | 6 | 0.562 | -6.4 | 0.030 | 5.3 | | |
| | 7 | 6 | 0.409 | -31.9 | 0.013 | 3.2 | 22.3 | -1.3 |
| 3.00 | 1 | 6 | 2.99 | -0.4 | 0.10 | 3.5 | | |
| | 2 | 5 | 3.09 | 3.0 | 0.29 | 9.4 | | |
| | 3 | 5 | 3.08 | 2.7 | 0.19 | 6.4 | 6.4 | 1.2 |
| 6.00 | 4 | 6 | 6.30 | 5.0 | 0.62 | 9.8 | | |
| | 5 | 5 | 6.05 | 0.8 | 0.59 | 9.8 | | |
| | 6 | 6 | 5.82 | -3.0 | 0.44 | 7.5 | | |
| | 7 | 6 | 5.97 | -0.5 | 0.35 | 5.8 | 8.3 | 0.7 |
| 30.0 | 1 | 6 | 31.1 | 3.6 | 1.7 | 5.6 | | |
| | 2 | 6 | 32.3 | 7.8 | 1.1 | 3.4 | | |
| | 3 | 5 | 29.2 | -2.8 | 1.2 | 4.0 | 6.0 | 2.9 |
| 60.0 | 4 | 6 | 61.4 | 2.3 | 1.9 | 3.1 | | |
| | 5 | 6 | 65.4 | 9.0 | 2.2 | 3.4 | | |
| | 6 | 6 | 60.7 | 1.1 | 2.6 | 4.3 | | |
| | 7 | 5 | 60.8 | 1.3 | 2.8 | 4.7 | 4.8 | 3.5 |

bias, summarized in Table 3, was nearly equal for the 4.6-mm column and the 2.0-mm column at low and high levels, respectively. These results, interpreted in conjunction with the above imprecision results, show that concentrations obtained using the 4.6-mm column are indistinguishable from those obtained using the 2.0 mm column at the 95% confidence level.

Urine. Typical intra-day bias for DOX was $< \pm 2\%$ at 30.6 ng ml^{-1} and $< \pm 6\%$ at 305.7 ng ml^{-1} . For DOX-OL these values were $< \pm 9\%$ and $< \pm 4\%$, respectively. The inter-day bias was $+1.3$ and $+5.8\%$ for DOX, and -8.7 and -3.6% for DOX-OL low and high controls, respectively. The results demonstrate that these compounds can be accurately quantified in urine at ng ml^{-1} concentrations.

Instrumental lower-limit of detection (ILLD)

The ILLD was established by estimating the smallest amounts of analyte which could be detected in clean solution. Using $90\text{-}\mu\text{l}$ injections and a 2.0-mm i.d. column, 0.200 ng ml^{-1} of either component was readily detectable, with S/N of approximately 3. This corresponds to 18 pg of either component injected on column. By comparison, a 0.2 ng ml^{-1} plasma standard represents 60 pg on column, after extraction and analyte enrichment to ca. $300 \mu\text{l}$. The best previously reported detection limit for DOX by conventional means (no laser induced fluorescence) was 108 pg injected on column [5].

Lower limit of quantitation (LLQ)

With the 2.0-mm column, the LLQ in plasma, as determined by the imprecision of 6 replicate

controls, is 0.3 ng ml^{-1} for DOX (generally $< 10\%$ intra-day R.S.D.). Imprecision at 0.2 ng ml^{-1} increased to 24.9% R.S.D. For DOX-OL, replicate controls showed an imprecision of 28.4, 22.3 and 6.5% R.S.D. at 0.2, 0.3 and 0.6 ng ml^{-1} , respectively, suggesting that an acceptable LLQ is between 0.3 and 0.6 ng ml^{-1} . For DOX, the LLQ was limited by detectability rather than the presence of interferences. For DOX-OL, LLQ was limited in part by a small interference which gave rise to high bias ($> 19\%$) below 0.3 ng ml^{-1} . The LLQ for DOX and DOX-OL using the 4.6-mm column was near 0.6 ng ml^{-1} , based on inter-day imprecision results of 13.4 and 17.3% (Table 3), respectively.

Extraction efficiency

Extraction efficiency experiments show $88.0 \pm 6.1\%$ recovery of DOX from plasma over a broad concentration range. The extraction efficiency for DOX-OL at 5.0 and 50.0 ng ml^{-1} was $> 90 \pm 5.9\%$ but decreased to 73% at 0.50 ng ml^{-1} with decreased precision. This reduced and variable recovery for DOX-OL may explain the decreased precision and accuracy observed at this level. The mean extraction efficiency for EPI at 25 ng ml^{-1} was similar to DOX ($89.5 \pm 2.6\%$).

Parallelism

For six replicate determinations of a 1000 ng ml^{-1} spiked sample, mean percent biases of $+3.8$ and $+4.0\%$ were obtained for DOX and DOX-OL, respectively, when diluted 10-fold with blank plasma, while mean percent biases of $+7.2$ and $+9.3\%$ were obtained when reduced (0.1-ml) volumes of plasma were extracted without prior di-

TABLE 3

Comparison of inter-day precision and accuracy for DOX/DOX-OL plasma control on 2.0 and 4.6 mm columns

| Column | No. of plasma runs included | DOX controls | | | DOX-OL controls | | |
|---------------|-----------------------------|---|--------------------------|------------------------|---|--------------------------|------------------------|
| | | Nominal concentration (ng ml^{-1}) | Inter-day percent R.S.D. | Inter-day percent bias | Nominal concentration (ng ml^{-1}) | Inter-day percent R.S.D. | Inter-day percent bias |
| 2.0-mm column | 7 | 0.600 | 10.4 | +4.7 | 0.600 | 22.3 | +1.3 |
| | | 60.0 | 4.2 | +1.5 | 60.0 | 4.8 | +3.5 |
| 4.6-mm column | 8 | 0.564 | 13.4 | +2.5 | 0.574 | 17.3 | +3.8 |
| | | 56.4 | 7.6 | 0.0 | 57.4 | 6.8 | -3.8 |

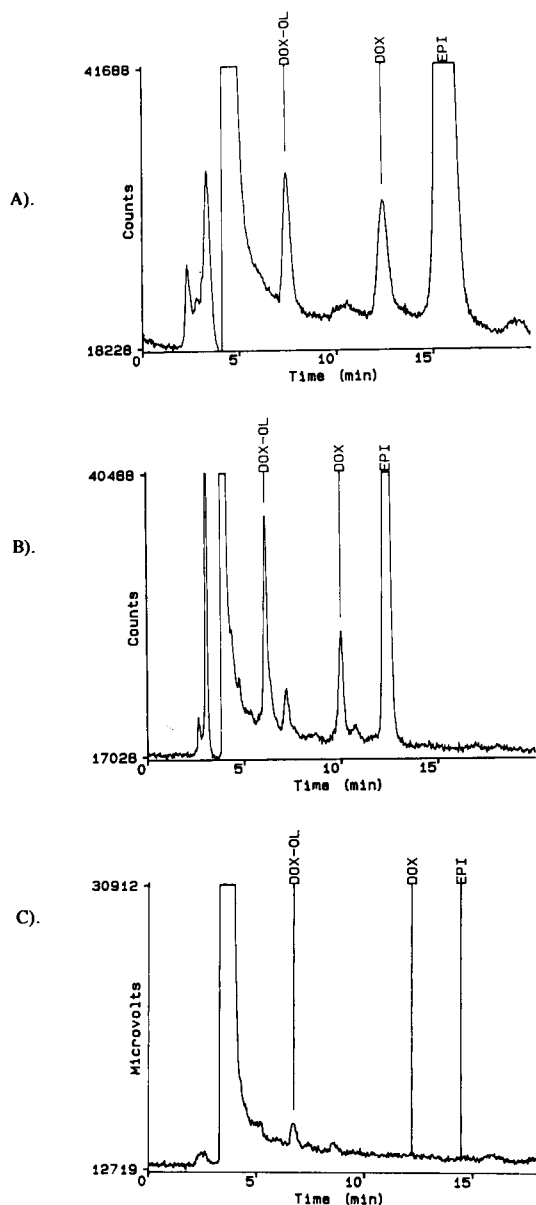


Fig. 2. Chromatograms for plasma samples drawn from human cancer patients intravenously dosed with 50 mg m^{-2} of DOX. Chromatograms are for (A) 168 h post-dose (2.0-mm i.d. column), (B) 168 h post-dose (4.6 mm i.d. column) and (C) 20 min before (2.0-mm i.d. column).

lution. Percent R.S.D. decreased from 7.6 and 7.3% to 4.1 and 4.9% for DOX and DOX-OL, respectively, when blank plasma was used to di-

lute samples. Preliminary experiments involving direct extraction of 0.2-ml aliquots and reduced ($5\text{-}\mu\text{l}$) injection volumes were not successful and were discontinued. Solid-phase extraction studies suggest a mixed mode retention, involving both partitioning and ion-exchange mechanisms. It appears that by adding blank plasma to a sample to give a total volume of 1 ml, the ionic strength is kept constant relative to standards and controls, resulting in comparable recoveries and low bias. We conclude that better accuracy and precision can be achieved by diluting concentrated samples with blank plasma rather than by simply reducing sample volume prior to extraction.

Parallelism experiments for DOX and DOX-OL urine controls yielded average biases of +4.8 and -2.3% , respectively, when diluted between 11- and 201-fold with blank urine. When only water was used as a diluent, the biases were -25.8 and $+23.7\%$, respectively, over the same range of dilution factors, thus indicating that better accuracy can be achieved when blank urine is used as the diluent.

Stability

Solution standards (in aqueous 10 mM phosphoric acid) displayed no decrease in analyte peak height when stored for 3 months at $+5^\circ\text{C}$ in silanized, low actinide glassware.

Plasma. Controls (60 and 0.6 ng ml^{-1} nominal) stored at -20°C showed no loss in DOX concentration after 8 months, and only small losses ($<10\%$) in DOX-OL. Extracted standards were stable for at least 24 h when stored in silanized autosampler vials at ambient conditions. DOX standards displayed an average loss in peak height of 6.1%, while those for DOX-OL lost an average of 10.4%. After 24 h at ambient conditions, decreases in the slope of the calibration curves of -2.8 and -4.6% were observed for DOX and metabolite, respectively.

Plasma controls, assayed in triplicate, displayed 14–20% losses in DOX (60 and 0.6 ng ml^{-1}) when cycled through 3 consecutive freeze-thaw cycles. The decrease in DOX-OL was $<7.5\%$. These experiments suggest that it is desirable (for $<10\%$ loss) to perform no more than 2 freeze-thaw cycles on plasma samples.

Urine. Urine controls (30 and 300 ng ml⁻¹ nominal) stored at -20°C for 8 and 16 weeks displayed no losses, and 10–12% losses in DOX and 35–38% losses in DOX-OL, respectively. These results suggest that under present conditions some degradative losses of DOX and DOX-OL in urine samples could occur at storage times longer than 8 weeks. It could be possible to improve the stability of frozen urine samples by pH adjustment prior to freezing [7]. Urine standards, stored for 24 h under ambient conditions in silanized, amber autosampler vials, displayed average peak-height changes of +0.3 and +1.8% for DOX and DOX-OL, respectively. Slopes of the calibration curves changed by only -2.0 and +0.7%, respectively, thus indicating good stability of prepared samples. Urine controls submitted to 2 freeze-thaw cycles showed between 10 and 18% loss in the concentrations of DOX and DOX-OL.

Specificity

Figures 2A and B are representative chromatograms for plasma samples collected from a human subject dosed intravenously with 50 mg m⁻² of DOX. When compared to a plasma blank (Fig. 2C), these chromatograms show no apparent interferences (other metabolites, etc.) for either

DOX or DOX-OL. Several potential concomitant medications, including cyclophosphamide, methotrexate, 5-fluorouracil and dexrazoxane were undetectable at 1000 ng ml⁻¹.

Drug disposition

Figure 3 shows the plasma disposition profile of DOX and DOX-OL in a human cancer patient following a 10-min intravenous infusion of a single 50 mg m⁻² dose. Drug concentration declined in a multiphasic manner with an apparent terminal half-life of approximately 65 h. The method permitted quantitation of DOX and DOX-OL to at least 192 h, at which time concentrations for both analytes were above 1 ng ml⁻¹.

Conclusions

This work describes the development of sensitive and specific procedures for quantifying DOX and its predominant metabolite, DOX-OL, in plasma and urine. The plasma procedure uses SPE for sample cleanup followed by reversed-phase LC with fluorescence detection. Sensitivity has been enhanced relative to previous work [3–5] by optimization of fluorescence spectral parameters and chromatographic conditions, including the novel use of a 2.0-mm i.d. LC column. The methods have proven to be precise and capable

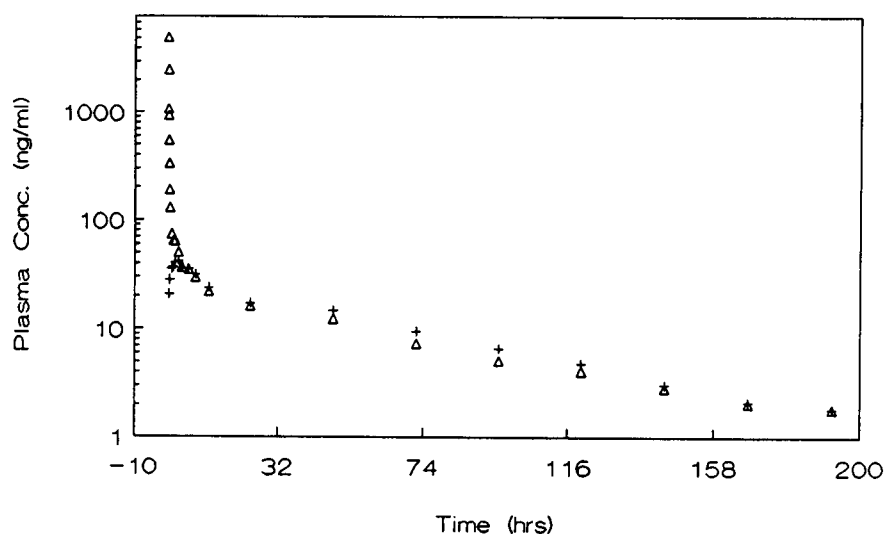


Fig. 3. Representative plasma disposition profile of DOX (Δ) and DOX-OL (+) in a cancer patient following a 50 mg m⁻² dose of DOX given as a 10-min intravenous infusion.

of accurately quantifying the drug over a wide linear range (0.2 to 100 ng ml⁻¹) of concentrations. The detection limit ($S/N = 3$) was estimated at 18 pg of DOX or DOX-OL on a 2.0 mm i.d. column. The lower limit of quantitation in plasma was estimated to be 0.3 ng ml⁻¹ (generally < 10% R.S.D.) for DOX and 0.6 ng ml⁻¹ (5.0% R.S.D.) for DOX-OL. Above these levels, average intra-day imprecision and bias estimates were always below 7.5% and 8.2%, respectively. While the 4.6 mm column was not as effective at the extreme low end of the calibration range (below 0.6 ng ml⁻¹), it appeared to offer modest improvements in selectivity by virtue of decreased peak widths. The drug demonstrated satisfactory stability (< 10% loss) in plasma samples, when stored at -20°C for up to 8 months. Some degradation of metabolite was observed in urine after eight weeks of storage. Prepared samples were stable for at least 24 h when stored at ambient conditions. The utility of the method has been

demonstrated through assay of patient plasma samples, collected up to 192 h after drug administration.

REFERENCES

- 1 R.T. Skeel, Handbook of Cancer Chemotherapy, Little-Brown, Boston, MA, 1987, p. 77.
- 2 J. Speyer, M. Green, E. Dramer, M. Rey, J. Sanger, C. Ward, N. Dublin, V. Ferrans, P. Stecy, A. Zeleniuch-Jacquotte, J. Wernz, F. Feit, W. Slater, R. Blum and F. Muggia, N. Engl. J. Med., 319 (1988) 745.
- 3 C.M. Riley, A.K. Runyan and J. Graham-Pole, Anal. Lett., 20 (1987) 97.
- 4 J. Dubois, M. Hanocq and G. Atassi, Anal. Lett., 20 (1987) 1611.
- 5 C.M. Camaggi, R. Comparsi, E. Stocchi, F. Testoni and F. Pannuti, Cancer Chemother. Pharmacol., 21 (1988) 216.
- 6 L.R. Snyder and J.J. Kirkland, Introduction to Modern Liquid Chromatography, Wiley, New York, 1979, Ch. 2.
- 7 J. Bouma, J.H. Beijnen, A. Bult and W.J.M. Underberg, Pharm. Weekblad Sci. Ed., 8 (1986) 108.

Reversed-phase liquid chromatographic determination of doxorubicin after on-line trace enrichment on iron(III)-loaded 8-hydroxyquinoline-bonded silica

E. van der Vlis, H. Irth, U.R. Tjaden and J. van der Greef

Division of Analytical Chemistry, Center for Bio-Pharmaceutical Sciences, University of Leiden, P.O. Box 9502, 2300 RA Leiden (Netherlands)

(Received 6th June 1992)

Abstract

A selective on-line trace enrichment technique for doxorubicin in plasma based on complex formation between iron(III) and the analyte is described. Fe(III) immobilized on 8-hydroxyquinoline (HQ)-bonded silica was used as a solid support for the enrichment of doxorubicin. Sorption of the analyte on the iron(III)-loaded HQ-silica (FeHQ-silica) was investigated as a function of pH, flow-rate, content of organic modifier and ionic strength. Desorption was based on protonation of doxorubicin and simultaneous removal of Fe(III) from the HQ-silica. Efficient on-line desorption to the C₁₈ analytical column was achieved by injecting a plug of nitric acid solution on to the FeHQ-silica precolumn. Desorption was optimized by determining the recovery of doxorubicin as a function of the acidity and the volume of the nitric acid plug. An example of the determination of doxorubicin in plasma is presented.

Keywords: Liquid chromatography; Doxorubicin; Pharmaceuticals; Preconcentration

Doxorubicin is a widely used anthracycline cytostatic agent that has been successfully applied in the treatment of several types of cancer [1–6]. All anthracycline analogues consist of a tetracyclic aglycone in a glycoside linkage to an aminosugar (Fig. 1). Pharmacokinetic studies demand sensitive analytical techniques for the determination of cytostatic drugs in plasma, including doxorubicin, owing to their severe toxic side effects [4]. Most analytical methods are based on liquid chromatography [7–9], and recently the determination of trace levels of some anthracyclines by capillary electrophoresis in combination with laser-induced fluorescence detection has been described [10]. In order to decrease the detection limits for doxorubicin, trace enrichment

techniques such as solid-phase isolation or liquid–liquid extraction are usually implemented in the sample pretreatment method. Most published methods are off-line methods, which either use solid-phase isolation or liquid–liquid extraction, and on-line sample pretreatment techniques have only rarely been applied [7–9].

Solid phase isolation is usually carried out by using cartridges packed with, for example, C₁₈- or C₈-bonded silica or styrene–divinylbenzene copolymers. The selectivity of these sorbents, however, is often too low for trace level analysis in, e.g., complex biological matrices such as plasma or urine. In this instance more selective sorbents such as metal-loaded phases [11–13] or immobilized antibodies [14,15] may be advantageous.

Doxorubicin and its analogues are well known to form very stable complexes with iron(III). May et al. [16] reported the formation of 1:1, 2:1 and

Correspondence to: H. Irth, Division of Analytical Chemistry, Center for Bio-Pharmaceutical Sciences, University of Leiden, P.O. Box 9502, 2300 RA Leiden (Netherlands).

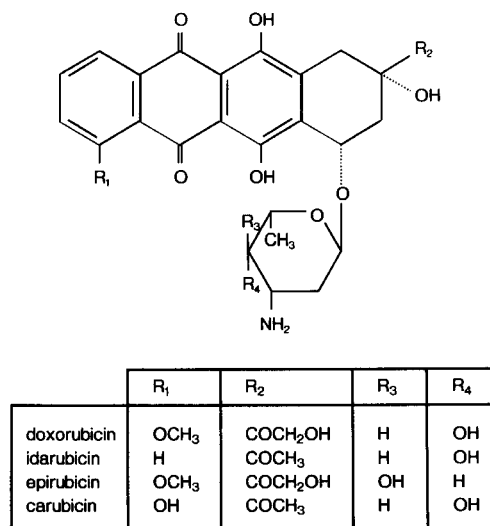


Fig. 1. Structures of doxorubicin and related compounds.

3:1 doxorubicin–Fe(III) complexes with stepwise association constants of 10^{18} , 10^{11} and $10^{4.4}$, respectively. Myers et al. [17] and Beraldo et al. [18] suggested that the 3:1 compound is a six-membered chelate in which Fe(III) is bound to the quinone–hydroxyquinone moiety of doxorubicin. Based on the high association constant of the 1:1 complex, a selective preconcentration system using immobilized Fe(III) was developed for the determination of doxorubicin in plasma. In this paper different parameters that influence the sorption of doxorubicin on immobilized Fe(III) such as the pH value, ionic strength, organic modifier content and flow-rate are discussed. On-line desorption to the reversed-phase HPLC system is carried out by substantially lowering the pH value as described by Lipschitz et al. [13].

EXPERIMENTAL

Chemicals

All salts and acids used were of analytical-reagent grade. All aqueous solutions were prepared using water purified with a Milli-Q system (Millipore).

Acetonitrile (HPLC grade) was obtained from Rathburn (Walkerburn, UK), doxorubicin, idaru-

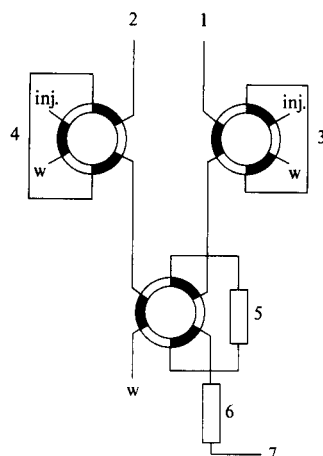


Fig. 2. Schematic diagram of the preconcentration and analytical system. 1 = LC pump; 2 = preconcentration pump; 3 = nitric acid injection loop ($100 \mu\text{l}$); 4 = sample injection loop (3.5 ml); 5 = FeHQ-silica precolumn; 6 = analytical column; 7 = to detector.

bicin and epirubicin from Carlo Erba (Nivelles, Belgium), carubicin from Bristol-Myers (Weesp, Netherlands), 8-hydroxyquinoline- (HQ-) and iminodiacetate-bonded silica from Sigma (Heidelberg), iron(III) nitrate from Aldrich (Steinheim), potassium nitrate, sodium acetate and orthophosphoric acid from Merck (Darmstadt), acetic acid and nitric acid from J.T. Baker (Deventer) and octylamine hydrochloride from Kodak (Rochester, NY).

Solutions of the anthracyclines were prepared freshly before use in water–acetonitrile (70 + 30, v/v) and stored at 4°C in polypropylene tubes or Eppendorf vials. Addition of 30% acetonitrile was sufficient to avoid adsorption of the anthracyclines on the container walls, which had been reported earlier by Tomlinson and Malspeis [19].

Apparatus

A schematic diagram of the preconcentration and analytical system is shown in Fig. 2. The preconcentration system consisted of a Rheodyne (Cotati, CA) Model 5031 low-pressure Teflon rotary valve, a Gilson (Bergen op Zoom, Netherlands) Model 302 HPLC pump, a Rheodyne Model 7125 stainless-steel injector with a 3.5-ml loop and an HQ-silica ($5\text{-}\mu\text{m}$ particle size)

TABLE 1

Procedure for the clean-up and trace enrichment of doxorubicin on FeHQ-silica

| Step | Solvent | Volume (ml) |
|-----------------------------------|---|-------------|
| Loading of HQ-silica with Fe(III) | Fe(NO ₃) ₃ (1 mM) | 4.0 |
| Washing | Water | 2.0 |
| Conditioning | Carrier solution ^a | 3.0 |
| Sample loading | Sample dissolved in carrier solution ^a | 3.5 |
| Washing | Carrier solution ^a | 4.0 |
| | Acetonitrile–water (25 + 75, v/v) | 3.0 |
| Desorption | Nitric acid (1 mM) | 0.1 |

^a Carrier solution: acetonitrile–acetate buffer (pH 6.5, 100 mM) (50 + 50, v/v) containing 1 M potassium nitrate; flow-rate, 1.5 ml min⁻¹.

slurry-packed precolumn (5.0 × 2.0 mm i.d.). The analytical system consisted of a Kratos (Ramsey, NJ) Analytical Spectroflow 400 solvent-delivery system, a Rheodyne Model 7125 stainless-steel injector with a 200-μl loop, a Spherisorb (Phase Separations, Queensferry, UK) ODS-2 analytical column (100 × 4.6 mm i.d., 3-μm particle size), a Perkin-Elmer (Beaconsfield, UK) LS4 spectrofluorimeter and a Kipp & Zonen (Delft) BD 40 recorder. Both systems were linked by a Spark Holland (Emmen) MUST Multiport Stream-switch system.

The preconcentration and on-line desorption procedure is shown in Table 1. The mobile phase for the analytical system was acetonitrile–(0.01 M) phosphoric acid (75 + 25, v/v) containing 0.03% (w/v) octylamine and was pumped at a flow-rate of 1.0 ml min⁻¹. Fluorescence detection was performed at 466 nm excitation wavelength and 600 nm emission wavelength.

In preliminary experiments a Kratos Spectroflow 757 UV detector (254 nm) and an AN-TEC Leyden (Leiden) amperometric electrochemical detector consisting of a CU-04AZ potentiostat and a VT03 conventional detector cell (working potential +800 mV vs. Ag/AgCl reference electrode) were used to investigate their applicability.

Pretreatment of plasma samples

To 1.5 ml of the plasma sample, 3.5 ml of acetonitrile were added and the mixture was vortex mixed for 1 min. After centrifugation for 10 min at 2000 g, 3.5 ml of the supernatant were injected on to the iron(III)-loaded HQ-silica (FeHQ-silica) precolumn and subsequently treated according to the procedure shown in Table 1.

RESULTS AND DISCUSSION

Preconcentration system

Choice of sorbent. Two different stationary phases, iron(III)-loaded 8-hydroxyquinoline (FeHQ)-silica and iminodiacetate (FeIDA)-silica, were investigated with respect to their capability to bind doxorubicin. In the first instance, the non-specific binding of doxorubicin to these supports, e.g., sorption via hydrophobic or electrostatic interactions, was investigated, since this process would greatly reduce the selectivity of the sorption process. For this purpose, breakthrough experiments were carried out at pH 4 and 9 (100 mM acetate buffer) using the metal-free supports. Both HQ-silica and IDA-silica showed very high non-specific binding with breakthrough volumes larger than 10 ml for the sorption of doxorubicin from purely aqueous solutions. With IDA-silica, non-specific sorption could virtually be eliminated by increasing the ionic strength (addition of 1 M KNO₃) of the sorption solution, which indicates that IDA-silica behaves as a cation exchanger binding doxorubicin via the positively charged amino group. An increase in the ionic strength did not eliminate non-specific binding on HQ-silica, which can be explained by a "salting-out" effect thereby increasing the hydrophobic interactions between doxorubicin and HQ-silica. Addition of 50% acetonitrile finally reduced the non-specific sorption on HQ-silica to 4–5% of the amount of doxorubicin sorbed via complexation (see below).

Preliminary breakthrough experiments at pH 4 and 9 revealed that FeHQ-silica exhibits a high affinity for doxorubicin with breakthrough volumes larger than 8 ml for a 5.0 × 2.0 mm i.d.

precolumn containing 6.5 mg of HQ-silica. The amount of Fe(III) sorbed on FeHQ-silica was $133 \pm 13 \text{ mmol g}^{-1}$. Similar breakthrough volumes on FeHQ-silica were obtained for carubicin, epirubicin and idarubicin (for structures, see Fig. 1). FeIDA-silica, however, showed only a weak affinity for these compounds under the same conditions.

The different number of available coordination sites of the immobilized Fe(III) might be a possible explanation for this behaviour. With IDA-silica, Fe(III) probably forms a tridentate 1:1 complex which leaves only three coordination sites for the sorption of the analyte, resulting in the formation of an unsaturated mixed-ligand complex. On HQ-silica, on the other hand, Fe(III) is bound via a bidentate 1:1 complex, and therefore four coordination sites are available for the formation of a saturated, more stable 1:3 mixed-ligand complex. Therefore, all subsequent experiments were carried out using Fe(III)-HQ silica.

Sorption conditions. In order to assess the optimum sorption conditions, the influence of the pH of the acetate buffer, of which the carrier comprised 50%, and flow-rate on the recovery of doxorubicin were investigated. The effect of the pH on the sorption process for FeHQ-silica in the presence of 50% acetonitrile and 1 M KNO_3 is shown in Fig. 3. The highest recovery (> 95%) was obtained in the pH range 6–7. At lower pH protonation of the phenolic hydroxyl group which is involved in complex formation may occur, whereas at higher pH values hydroxo complex formation by Fe(III) might prevent the sorption of doxorubicin.

At $\text{pH} > 3$, Fe(III) forms strong hydroxo complexes which might cause slow ligand-exchange kinetics. The influence of the flow-rate on the sorption of doxorubicin on FeHQ-silica was therefore investigated. All recoveries measured in the range $0.25\text{--}3 \text{ ml min}^{-1}$ were $90 \pm 4\%$, which indicates that the presence of hydroxo complexes is not rate limiting for the binding of doxorubicin to immobilized Fe(III).

On-line desorption. Desorption of doxorubicin from the FeHQ-silica was performed by protonation of the functional groups involved in complexation as described by Lipschitz et al. [13]. In the

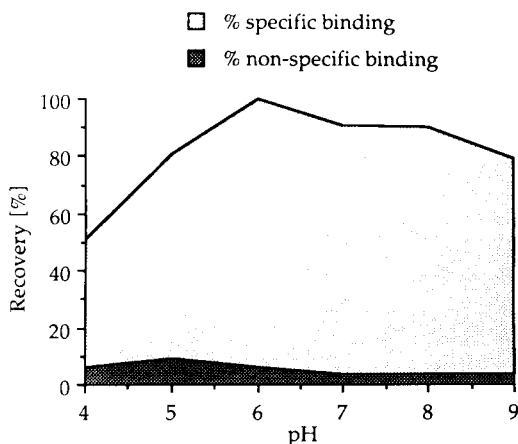


Fig. 3. Recovery of doxorubicin on FeHQ-silica as a function of the carrier pH value (non-specific binding was determined on the metal-free support). Conditions: carrier solution, acetate buffer (100 mM) at different pH; detection, fluorescence (excitation wavelength 466 nm, emission wavelength 600 nm); doxorubicin concentration, 50 ng ml^{-1} ; for other conditions, see Experimental.

first instance, it was investigated whether the LC mobile phase consisting of phosphoric acid (pH 2.2) was capable of efficiently desorbing doxorubicin. It was found that, although desorption occurred, a broad peak was obtained, indicating slow desorption kinetics at this pH. By injecting a plug of nitric acid on to the FeHQ-silica precolumn, the desorption efficiency considerably improved. Figure 4 shows the dependence of the

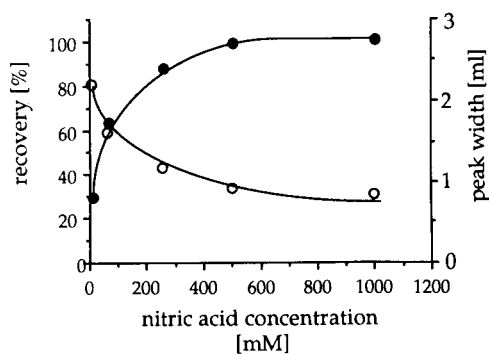


Fig. 4. (○) Peak width and (●) recovery of doxorubicin as a function of the nitric acid concentration used for desorption from FeHQ-silica. Conditions: volume of desorption solution, $200 \mu\text{l}$; detection, fluorescence (excitation wavelength 466 nm; emission wavelength 600 nm); doxorubicin concentration, 50 ng ml^{-1} ; for other conditions, see Experimental.

peak width and recovery on the concentration of nitric acid. The recovery was strongly pH dependent and reached a maximum at a nitric acid concentration of 1.0 M. Higher nitric acid concentrations did not result in a further decrease in the peak width.

In Fig. 5 the recovery is shown as a function of the plug injection volume (injection of 1 M nitric acid). Complete recovery of doxorubicin was obtained at a plug volume of 100 μl . Under these conditions, Fe(III) is also stripped off from the precolumn, and therefore reloading of the HQ-silica prior to the subsequent analysis is required. Compared with desorption using a strongly acidic mobile phase [12], no deterioration of the performance of both the precolumn and the analytical column due to injection of a nitric acid plug was observed. The FeHQ-silica precolumn could be used for at least 30 injections of deproteinated plasma (see below) before repacking was required.

Detection

Three different detection modes, UV, electrochemical and fluorescence, were tested for their compatibility with the desorption procedure (see Fig. 6). With UV detection (Fig. 6A) a large peak

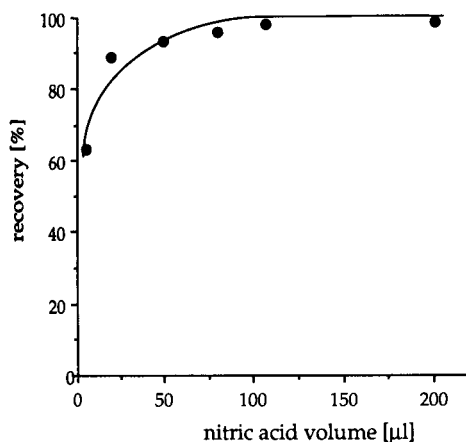


Fig. 5. Recovery of doxorubicin after desorption from FeHQ-silica as a function of the nitric acid plug injection volume. Conditions: desorption solution, 1 M nitric acid; detection, fluorescence (excitation wavelength 466 nm; emission wavelength 600 nm); doxorubicin concentration, 50 ng ml⁻¹; for other conditions, see Experimental.

eluting with the dead volume was obtained, which is derived from Fe³⁺ eluted from the HQ-silica precolumn during the desorption step. Another restriction on the applicability of UV detection to anthracycline drugs is its relatively low sensitivity. Fe³⁺ was not detected at all by electrochemical and fluorescence detection, thus allowing a more sensitive detection of doxorubicin. Although in principle with electrochemical detection the most favourable signal-to-noise ratio can be obtained, the momentary drop in pH owing to the nitric acid plug injection caused a considerable baseline shift (Fig. 6B), whereas fluorescence detection (Fig. 6C) provided a stable baseline at the highest possible detector sensitivity setting.

With the present method using fluorescence detection, a detection limit (signal-to-noise ratio 3:1, sample volume 3.5 ml) of 0.5 ng ml⁻¹ was obtained. The repeatability ($n = 5$) was 5% at a concentration level of 14 ng ml⁻¹ and the method was linear over three orders of magnitude ($r = 0.998$, 2–2000 ng ml⁻¹).

Determination of doxorubicin in plasma

The applicability of the method was demonstrated in the determination of doxorubicin in plasma. For this purpose plasma was spiked at a concentration of 50 ng ml⁻¹. The plasma samples (1.5 ml) (blank and spiked) were deproteinized by vortex mixing with acetonitrile (plasma-to-acetonitrile ratio = 3:7). After centrifugation, an aliquot of 3.5 ml of the supernatant was injected on to the FeHQ-silica precolumn. On-line desorption, separation and detection were performed as described under Experimental. The chromatograms in Fig. 7 for blank (Fig. 7A) and spiked (Fig. 7B) plasma demonstrate that no endogenous plasma components interfere in the determination of doxorubicin after deproteination and on-line preconcentration on FeHQ-silica. The recovery of doxorubicin was 35 \pm 5% (50 ng ml⁻¹, $n = 4$). This low recovery can be attributed to the inclusion of the analyte in the precipitate after deproteination with acetonitrile owing to plasma-protein binding [10]. The present method can be used for the determination of doxorubicin analogues such as carubicin, epirubicin or idarubicin without modification.

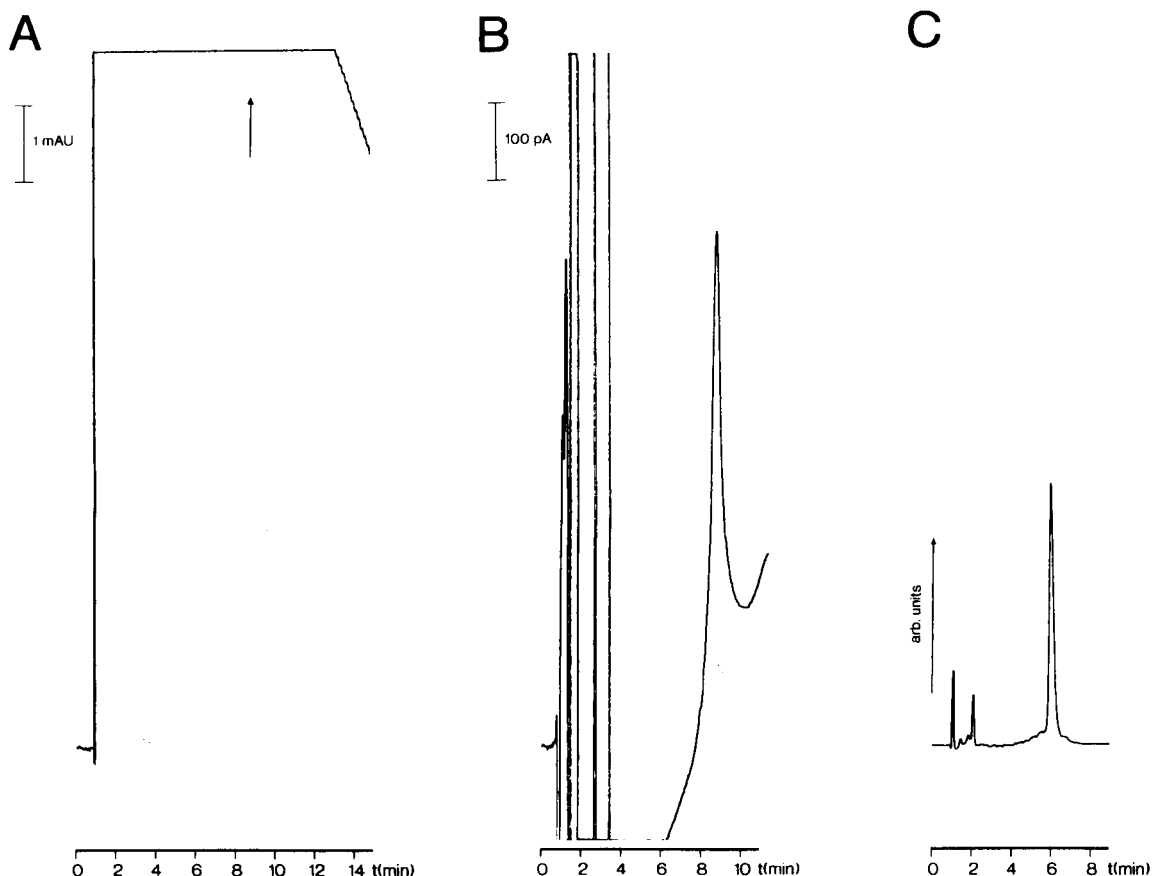


Fig. 6. Comparison of different detection techniques in combination with on-line desorption from FeHQ-silica. (A) UV detection. Conditions: detection wavelength, 254 nm; doxorubicin concentration, $1 \mu\text{g ml}^{-1}$; for other conditions, see Experimental. The retention time of doxorubicin is indicated by an arrow. (B) Electrochemical detection. Conditions: LC mobile phase, acetonitrile-acetate buffer (pH 4.3, 200 mM) (77 + 23, v/v) containing 0.1 mM EDTA and 0.03% (w/v) octylamine; doxorubicin concentration, 100 ng ml^{-1} ; for other conditions, see Experimental. (C) Fluorescence detection. Conditions: excitation wavelength, 466 nm; emission wavelength, 600 nm; doxorubicin concentration, 14 ng ml^{-1} ; for other conditions, see Experimental.

Conclusions

An iron(III)-loaded 8-hydroxyquinoline stationary phase is a selective sorbent for phenolic hydroxyl group-containing ligands such as anthracyclines. Sorption of analytes to the immobilized Fe(III) ions is based on the pH-dependent formation of strong complexes. Desorption proceeds simply via protonation of the phenolic hydroxyl group of the analyte that is involved in the mixed-ligand complex. Only a small volume of strong acid is needed for this purpose.

Because of the high affinity of the analyte for Fe(III) it is possible to preconcentrate large sam-

ple volumes. After coupling the preconcentration system to the analytical system by means of a valve-switching system, the system can easily be automated. Off-line sample pretreatment is limited to a deproteination step prior to analysis. This method might be extended to other phenolic hydroxyl group-containing compounds which form sufficiently strong complexes with iron(III) [20]. For non-fluorescent compounds, desorption to a non-selective precolumn, e.g., packed with C_8 - or C_{18} -bonded silica, may eliminate interferences due to Fe^{3+} desorption without decreasing the selectivity of the overall method. Removal of the

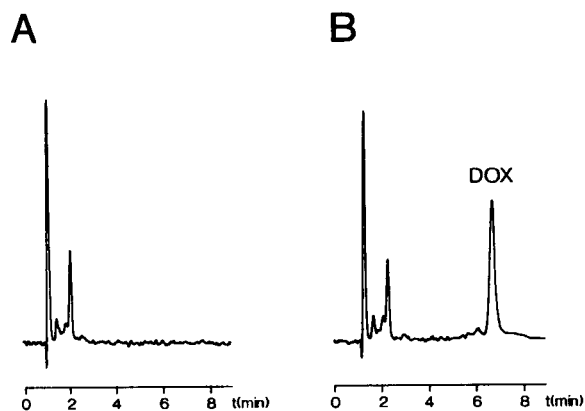


Fig. 7. Determination of doxorubicin in plasma after deproteination and trace enrichment on FeHQ-silica. (A) Blank plasma; (B) plasma spiked with 50 ng ml⁻¹ doxorubicin. For conditions, see Experimental.

desorbed Fe³⁺ ions can also be achieved by using a precolumn ion-exchange technique.

REFERENCES

- G. Bonadonna, R. Zucali, S. Monfardini, M. De Lena and C. Uslenghi, *Cancer*, 36 (1975) 252.
- E.P. Cortes, J.F. Holland, J.J. Wang and O. Glidewell, *Cancer Chemother. Rep., Part 3*, 6 (1975) 305.
- H.M. Pinedo and Y. Kenis, *Cancer Treat. Rev.*, 4 (1977) 67.
- R.C. Young, R.F. Ozols and C.E. Myers, *N. Engl. J. Med.*, 305 (1981) 139.
- D.C. Tormey, *Cancer Chemother. Rep., Part 3*, 6 (1975) 319.
- U.R. Tjaden and E.A. de Bruijn, *J. Chromatogr.*, 531 (1990) 235.
- J. de Jong, P.A. Maesson, A. Akkerdaas, S.F. Cheung, H.M. Pinedo and W.J.F. van der Vijgh, *J. Chromatogr.*, 529 (1990) 359.
- P. Maessen, H.M. Pinedo, K. Mross and W.J.F. van der Vijgh, *J. Chromatogr.*, 424 (1988) 103.
- C.A. Riley, W.R. Crom and W.A. Evans, *Ther. Drug Monit.*, 7 (1985) 455.
- N.J. Reinhoud, U.R. Tjaden, H. Irth and J. van der Greef, *J. Chromatogr.*, 574 (1992) 327.
- M.W.F. Nielen, H.E. van Ingen, A.J. Valk, R.W. Frei and U.A.Th. Brinkman, *J. Liq. Chromatogr.*, 10 (1987) 617.
- M. Bagnoud and W. Haerdi, *Int. J. Environ. Anal. Chem.*, 38 (1990) 97.
- C. Lipschitz, H. Irth, G.J. de Jong, U.A.Th. Brinkman and R.W. Frei, *J. Chromatogr.*, 471 (1989) 321.
- A. Farjam, G.J. de Jong, R.W. Frei, U.A.Th. Brinkman, W. Haasnoot, A.R.M. Hamers, R. Schilt and F.A. Huf, *J. Chromatogr.*, 452 (1988) 419.
- B. Johansson, *J. Chromatogr.*, 381 (1986) 107–113.
- P.M. May, G.K. Williams and V.R. Williams, *Eur. J. Cancer*, 16 (1980) 1275.
- C.E. Myers, L. Gianni, C.B. Simone, R. Klecker and R. Greene, *Biochemistry*, 21 (1982) 1707.
- H. Beraldo, A. Granier-Suillerot, L. Tosi and F. Lavelle, *Biochemistry*, 24 (1985) 284.
- E. Tomlinson and L. Malspeis, *J. Pharm. Sci.*, 71 (1982) 1121.
- G.J. Shahwan and J.R. Jezorek, *J. Chromatogr.*, 256 (1983) 39–48.

Measurement of primary amine groups on surface-modified silica and their role in metal binding

I. Taylor and A.G. Howard

Department of Chemistry, University of Southampton, Southampton, Hampshire (UK)

(Received 22nd June 1992; revised manuscript received 12th August 1992)

Abstract

The characterization of a chelating silica, modified by coupling ethylenediamine to a surface-linked epoxide, was carried out using an improved ninhydrin-based procedure for the measurement of primary amines, and elemental analysis. Whilst the primary amine content of model monoamines was accurately assessed, for diamines in which the amine groups were separated by 2, 3 or 4 carbon atoms, the number of primary amine groups was underestimated.

Chemically modified silicas were prepared by activation of the surface with different loadings of an epoxide modifier, which was in turn coupled to ethylenediamine. Elemental analysis and the ninhydrin reaction were used to assess the involvement of primary amine groups in copper complexation by these modified silicas and the degree of bridging resulting from the modification. Increasing the quantity of epoxide modifier resulted in an increased coverage of epoxide groups on the silica surface, but whilst this increased the quantity of diamine that could be coupled onto the surface, increased diamine bridging occurred. The copper capacity of the silica was linked to the primary amine content of the silica and not to its total nitrogen content. Copper complexation or chelation by the resin is therefore more favoured by the linear modification than by the bridged form.

Keywords: Complexing silica; Elemental analysis; Preconcentration; Primary amines; Trace metals

The chemical modification of the surface of solids has led to increased possibilities in a number of fields. In the laboratory, chemical modifications have been employed in applications as diverse as the deactivation of glass surfaces to reduce losses during storage to the opening up of new approaches to chromatography and trace metal concentration. Amine-modified silicas have found a number of applications; these include the preparation of packings for liquid chromatography, sorbents for affinity chromatography [1] and trace metal preconcentration. Leyden et al. [2–5]

pioneered the analytical application of these materials, developing silicas which were modified with 3-(2-aminoethyl)aminopropyl and 3-aminopropyl groups and their dithiocarbamate derivatives. From the amine-modified surface a number of particularly useful synthetic routes have been developed for the synthesis of more complex functionalized solids. The amine-modified solids can themselves be used as chelating agents or they can be used as an attachment point for further modification. The complexing agent 2,2',4-trihydroxyazobenzene, for example, can be attached to an amine-modified base solid using trichloro-1,3,5-triazine [6] or iminodiacetic acid groups can be synthesised [7]. Several examples of such materials are to be found in the review by Kantipuly et al. [8].

In order to optimise the performance of these

Correspondence to: A.G. Howard, Department of Chemistry, University of Southampton, Southampton, SO9 5NH Hampshire (UK).

¹ Present address: Water Research Centre, P.O. Box 16, Henley Road, Medmenham, Buckinghamshire (UK).

materials and to understand the factors which govern their performance, it is necessary to be able to assess the nature of the surface binding. There are, however, comparatively few simple methods for the quantitative assessment of specific groups which are bound onto a solid surface. The measurement of primary monoamines can be carried out using the ninhydrin colour reaction [9]. This reaction is comparatively rare amongst colorimetric reactions in that it results in the release of the coloured product from the surface into solution. Amine groups coupled to a solid surface can then be quantified using solution colorimetry.

This paper reports improvements in the ninhydrin-based procedure for the measurement of primary amines, investigates the performance of the techniques with polyamines and reports on the application of the techniques in the study of chemically modified silicas.

EXPERIMENTAL

Preparation of modified silica

The chemical modification of the silica surface was carried out using a generalised coupling procedure. The silica was first reacted with 3-glycidoxypropyltrimethoxysilane and the resulting epoxy-modified silica was then linked to the amine under basic conditions.

Silica preparation. Chromatographic-grade flash silica (0.04–0.063 mm particle size) was washed twice with hydrochloric acid (1 + 99, v/v) for 30 min, rinsed twice with distilled water for 15 min and then oven dried at 150°C for 24 h.

Epoxy-functionalized silica. 3-Glycidoxypropyltrimethoxysilane (typically 79 g) was dissolved in 500 ml of toluene in a round-bottomed flask. Whilst the solution was stirred vigorously, 100 g of silica were slowly added and a reflux condenser was fitted. The speed of agitation was then reduced and maintained at a level just sufficient to keep the silica in suspension. The mixture was heated on a boiling-water bath for 6 h, left to cool with constant stirring for a further 8 h and the silica was then rinsed with toluene.

Amine coupling. 1,2-Diaminoethane was redis-

tilled under nitrogen at reduced pressure. An amount of 50 g of epoxy-modified silica was suspended in 100 ml of toluene in a 250-ml round-bottomed flask. Excess diamine (typically 20 ml) was then slowly added, a condenser was fitted to the flask and the mixture was heated at ca. 90°C on a water bath for 2 h. The silica was then filtered from the solution and washed with 50 ml of methanol, 50 ml of hydrochloric acid (1 + 99, v/v) and a further 50 ml of methanol. The silica was then dried overnight at 50°C and stored in airtight glass bottles.

Measurement of primary amines

The procedure which was employed for the measurement of primary amines was an improved version of the procedure described by Shapilov et al. [9].

Procedure. To an accurately weighed portion of modified silica (in this study typically 50–100 mg), were added 5.0 ml of a phosphate buffer (0.1 mol l⁻¹, pH 6.4–6.5) and 1.0 ml of ninhydrin reagent solution [5% (w/v) in ethanol]. The mixture was then heated on a boiling-water bath with periodic shaking for 1 h. After the mixture had cooled to room temperature the supernatant was transferred to a 100-ml volumetric flask. A volume of 10 ml of hot (70°C) distilled water was then added to the silica residue and the mixture was maintained at 70°C for 10 min. The new supernatant was then added to the original extract and the washing step was repeated until no further blue coloration was extracted from the silica. The solution was made up to 100 ml with distilled water. After shaking, the absorbance was measured at 565 nm against a blank solution prepared using unmodified silica according to the above procedure.

Calibration. Calibration was carried out using a solution of 3-aminopropyltriethoxysilane. Aliquots of a 1 mg ml⁻¹ solution of the calibrant were added to 5.00 ml of phosphate buffer and 1.0 ml of ninhydrin solution. After heating the mixture on a boiling-water bath for 1 h it was cooled, transferred to a 100-ml volumetric flask and made up to volume with distilled water. The absorbance was measured at 565 nm against a reagent blank.

Measurement of copper capacity

The chelating capacity of the modified silicas was assessed by equilibration with a strong copper solution and measurement of bound metal.

Procedure. To an accurately weighed portion of silica in an acid-washed 25-ml polycarbonate vial were added 10 ml of a 100 $\mu\text{g Cu ml}^{-1}$ solution in an acetate buffer of pH 5.0. After gently mixing the contents for 1 h, the mixture was centrifuged and the supernatant discarded. The silica was then washed twice with acetate buffer solution of pH 5 (ca. 20 ml) to remove excess unbound metal. An amount of 10 ml of hydrochloric acid (1 mol l^{-1}) was then added to the silica and the mixture was agitated for 1 h. The silica was filtered from the solution and the copper content of the solution was measured by atomic absorption spectrometry.

Measurement of total nitrogen

Total nitrogen was determined using a CHN elemental analyzer employing a manganese dioxide catalyst to ensure complete combustion at 900°C. The instrument was calibrated using bipyridyl-spiked silica.

RESULTS AND DISCUSSION

Analysis of unbound amines

In order to assess the range of applicability of the method, the procedure was first applied to

the measurement of the primary amine groups in a number of model compounds chosen to contain primary, secondary and tertiary amine groups and with a varying carbon chain length between reactive amines (see Table 1).

The method successfully estimated the number of primary amine groups in all the test compounds, except the model diamines in which the amine groups were separated by 2, 3 or 4 carbon atoms, in which the procedure reported only ca. 1 primary amine group. The modified silica employed in this work, however, could only result in either one primary amine group remaining after epoxide binding or none at all. The ninhydrin method was therefore believed to be suitable for assessing the primary amine coverage of the modified silica.

Analysis of bound amines

Reproducibility. Multiple ($n = 6$) analyses of a sample of ethylenediamine-modified silica were carried out to assess the reproducibility of the method. The relative standard deviation of the result was $\pm 4.0\%$.

Characteristics of studied silicas. Four batches of epoxide-modified silica were prepared. In order to produce a range of materials of differing degrees of modification, the quantity of epoxide used in the preparation was altered. The quantity required in each synthesis was judged from a theoretical estimate of the quantity of modifying agent required to completely cover the silica sur-

TABLE 1

Analysis of model amines

| Compound | Predicted primary amine groups | Found primary amine groups |
|--|--------------------------------|----------------------------|
| $\text{CH}_3\text{CH}_2\text{NH}_2$ | 1 | 0.94 |
| $(\text{CH}_3\text{CH}_2)_2\text{NH}$ | 0 | 0.02 |
| $(\text{CH}_3\text{CH}_2)_3\text{N}$ | 0 | 0.08 |
| $\text{CH}_3(\text{CH}_2)_2\text{NH}_2$ | 1 | 1.12 |
| $\text{H}_2\text{N}(\text{CH}_2)_2\text{NH}_2$ | 2 | 0.97 |
| $\text{H}_2\text{N}(\text{CH}_2)_3\text{NH}_2$ | 2 | 1.03 |
| $\text{H}_2\text{N}(\text{CH}_2)_4\text{NH}_2$ | 2 | 1.15 |
| $\text{H}_2\text{N}(\text{CH}_2)_6\text{NH}_2$ | 2 | 1.89 |
| $[\text{H}_2\text{N}(\text{CH}_2)_2]_2\text{NH}$ | 2 | 2.14 |
| $[\text{H}_2\text{N}(\text{CH}_2)_3]_2\text{NH}$ | 2 | 2.03 |
| $\text{H}_2\text{N}(\text{CH}_2)_2\text{NH}(\text{CH}_2)_2\text{NH}(\text{CH}_2)_2\text{NH}_2$ | 2 | 1.87 |
| $[\text{H}_2\text{N}(\text{CH}_2)_2\text{NH}(\text{CH}_2)_2]_2\text{NH}$ | 2 | 1.92 |

face. Each batch of epoxide-modified silica was then reacted with ethylenediamine. The eight modified silicas were then analyzed for their carbon and nitrogen contents (Table 2).

Increasing the quantity of epoxide modifier employed in the synthesis resulted in attainment of the coverage limit at around the theoretical maximum. The addition of ethylenediamine led to a corresponding increase in the nitrogen content of the modified silicas. From elemental analyses alone it was not possible to identify whether this results from 1:1 binding of an amine to an epoxide or whether the diamine bridges two surface-linked epoxides (Fig. 1).

Total nitrogen and primary amine

When a diamine containing two primary amine groups is coupled to a silica surface which has been epoxy modified, coupling can occur via a single epoxide to give a linear primary amine product or through two adjacent epoxides to give a bridging product containing no residual primary amines. The extent of bridging largely depends on the surface epoxide coverage of the silica. In order to assess the binding of ethylenediamine onto the epoxy-modified silica, the silicas were analyzed for both total nitrogen (using an elemental analyzer) and primary amine groups (by the ninhydrin method).

The total nitrogen content of the silica can be predicted from the ninhydrin-derived primary amine measurements by assuming that one pri-

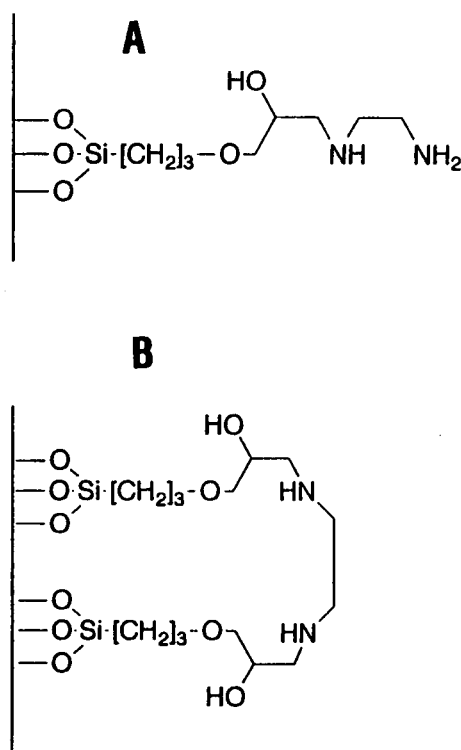


Fig. 1. Two possible modes of coupling of a diamine to a silica surface. (A) Linear form; (B) bridged form.

TABLE 2

Elemental analyses of modified silicas

| Silica | Loading ^a (%) | Carbon (mg g ⁻¹) | Nitrogen (mg g ⁻¹) |
|---------|-----------------------------|---------------------------------|-----------------------------------|
| Epoxide | 10 | 30.2 | |
| | 50 | 60.9 | |
| | 100 | 89.7 | |
| | 200 | 87.3 | |
| Amine | 10 | 36.6 | 8.36 |
| | 50 | 76.6 | 16.9 |
| | 100 | 106 | 22.0 |
| | 200 | 107 | 20.8 |

^a Expressed as the quantity of epoxide used in the synthesis as a percentage of the quantity required for maximum theoretical coverage.

mary amine should be present together with one secondary amine. If, however, the diamine bridges between two surface-linked epoxides, the number of primary amine groups will be reduced and the predicted total nitrogen content of a silica will be lower than the total nitrogen content measured by elemental analysis. The ratio of the determined nitrogen to that which is predicted from the primary amine content is therefore a measure of the extent of bridging. With the experimental silicas (Table 3), the degree of bridging is therefore seen to increase with increasing surface loading.

Copper capacity and primary amine content. By varying the surface coverage at the epoxide-modification stage, samples of amino-modified silica were prepared with varying amine group contents. The analysis of the copper capacity of these silicas, together with the primary amine contents measured by the ninhydrin reaction, permitted a

TABLE 3

A comparison of the total nitrogen content of modified silicas calculated from measurements of primary amine and measurements of total nitrogen by elemental analysis

| Silica (%) | Predicted N from primary amine (mg g ⁻¹) | Determined total N (mg g ⁻¹) | (Determined N)/total (predicted N) |
|-----------------|--|--|------------------------------------|
| 10 ^a | 4.84 | 8.36 | 1.73 |
| 50 | 10.08 | 16.9 | 1.68 |
| 100 | 8.62 | 22.0 | 2.55 |
| 200 | 7.81 | 20.8 | 2.66 |

^a Expressed as the quantity of epoxide used in the synthesis as a percentage of the quantity required for maximum theoretical coverage.

comparison to be made of the two measures of the extent of surface modification (Table 4).

The ratio of one copper to each available primary amine group implies the pre-eminent involvement of the primary amine group in metal binding. As the primary amine group is present only from a single-ended coupling of the diamine, the intrinsic flexibility and steric availability of the two amine groups in this structure favours metal binding. The coordination of only one primary amine to each copper atom would not be expected to occur if the ligand were free in solution, but when bound to a surface the inter-ligand spacing of non-bridged groups may be such that multiple coordination, by primary amines, is not favoured. In addition, the high concentration of copper employed in the capacity assay will drive

TABLE 4

The relationship between bound copper and the primary amine groups present on the surface of a ethylenediamine modified silica

| Silica (%) | Copper capacity (mmol g ⁻¹) | Primary amine (mmol g ⁻¹) | (Copper capacity)/primary amine |
|-----------------|---|---------------------------------------|---------------------------------|
| 10 ^a | 0.130 | 0.173 | 0.75 |
| 50 | 0.332 | 0.360 | 0.92 |
| 100 | 0.301 | 0.308 | 0.98 |
| 200 | 0.283 | 0.278 | 1.02 |

^a Expressed as the quantity of epoxide used in the synthesis as a percentage of the quantity required for maximum theoretical coverage.

the system towards single coordination. Bridged amines, anchored at both ends of the diamine, structurally more rigid and sterically hindered to metal binding, do not therefore appear to be favourable metal-binding sites.

Conclusions

The ninhydrin colour reaction has been shown effectively to estimate the number of free amino groups in a molecule provided that the analysis of polyamines in which the primary amine groups are separated by 2,3 or 4 carbon atom chains is avoided. The method is particularly suitable for the measurement of structures containing a single primary amine group.

Used in combination with conventional elemental analyses, the ninhydrin reaction provides a ready means of assessing the primary amine content of chemically modified silicas. In the studied silicas, increasing the quantity of epoxide modifier resulted in an increased coverage of epoxide groups on the silica surface. This greater density increased the quantity of diamine that could be coupled onto the surface but also resulted in a higher proportion of bridging of the coupled amine between neighbouring epoxides. The copper capacity of the resulting silicas was linked to the primary amine content of the silica and not to its total nitrogen content. Copper complexation or chelation by the resin is therefore more favoured by the linear coupling than by the bridged form. The development of chelating silicas of this type for the preconcentration of trace metals must therefore involve steps to maximize coupling to give a linear-form product whilst minimizing bridging.

This work was supported by a studentship from the Natural Environment Research Council.

REFERENCES

- 1 J.N. Kinkel, B. Anspach, K.K. Unger, R. Wieser and G. Brunner, *J. Chromatogr.*, 297 (1984) 167.
- 2 D.E. Leyden, G.H. Luttrell and T.A. Patterson, *Anal. Chim. Acta*, 8 (1975) 51.
- 3 D.E. Leyden, G.H. Luttrell, W.K. Nonidez and D.B. Werho, *Anal. Chem.*, 48 (1976) 67.

- 4 D.E. Leyden, M.L. Steele and B.B. Jablonski, *Anal. Chim. Acta*, 100 (1978) 545.
- 5 R.S. Field, D.E. Leyden and R.S. Shreedhara-Murthy, *Anal. Chim. Acta*, 186 (1986) 123.
- 6 M.A. Ditzler, L.H. Melendez, T.J. Onofrey and K.A. Mills, *Anal. Chim. Acta*, 228 (1990) 235.
- 7 A. Figueroa, C. Corradini, B. Fiebush and B.L. Karger, *J. Chromatogr.*, 371 (1986) 335.
- 8 C. Kantipuly, S. Katragadda, A. Chow and H.D. Gesser, *Talanta*, 37 (1990) 491.
- 9 O.D. Shapilov, V.G. Kayumov and A.I. Krashenyuk, *J. Anal. Chem. USSR*, 38 (1983) 436.

Experimental design approach for supercritical fluid extraction

M. Kane, J.R. Dean and S.M. Hitchen

Department of Chemical and Life Sciences, University of Northumbria at Newcastle, Ellison Building, Newcastle upon Tyne NE1 8ST (UK)

C.J. Dowle

ICI plc, Wilton Research Centre, P.O. Box 90, Wilton, Middlesbrough, Cleveland TS6 8JE (UK)

R.L. Tranter

Glaxo Manufacturing Services, Harmire Road, Barnard Castle, County Durham DL12 8DT (UK)

(Received 1st June 1992; revised manuscript received 9th July 1992)

Abstract

Experimental design with multilinear regression has been used to examine the relative contribution of the main experimental variables during supercritical fluid extraction. Six steroidal compounds of various solubilities in supercritical CO₂ were considered. The results indicate that the density of the supercritical fluid has the greatest effect on the solubilisation and transfer of steroid from extraction cell to collection device. The minimum number of cell volumes of supercritical CO₂ required for effective extraction was experimentally determined.

Keywords: Carbon dioxide; Extraction; Multilinear regression; Steroids; Supercritical fluid extraction

The status of current analytical instrumentation is such that the reliability and robustness of measurement is not often an issue. However, the analytical chemist must consider problems associated with sample preparation and the interpretation of large amounts of experimental data. This paper examines how the use of supercritical fluid extraction [1,2] for sample preparation and experimental design in data generation can simplify both of these areas.

Supercritical fluid extraction (SFE) is a rela-

tively new technique [3] for sample preparation based on the use of carbon dioxide above its critical temperature, 31.1°C, and critical pressure, 73.8 bar. The high diffusivity of the supercritical carbon dioxide allows for rapid and effective extractions of mainly non-polar solutes [4] without the need for the costly organic solvents frequently used in traditional sample clean-up procedures. The main operating variables in analytical SFE are density, temperature, flow-rate and time of extraction and it is expected that there are interactions between these variables. Experimental design techniques [5,6] may be used both to model and optimise chemical information, where there are many potentially interacting variables, and

Correspondence to: J.R. Dean, Department of Chemical and Life Sciences, University of Northumbria at Newcastle, Ellison Building, Newcastle upon Tyne NE1 8ST (UK).

are proving to be valuable assets to the analytical chemist [7]. Experimental design allows a consideration of the overall number of experiments, the arrangement of the experiments and the possible interaction effects between the variables. A simultaneous experimental design based on multi-linear regression has been used [8] for the optimization of extraction conditions. This has allowed both the prediction of optimal experimental conditions and interaction effects between variables. The combination of these two powerful techniques enables the main operating variables of SFE fully to be investigated.

EXPERIMENTAL

Apparatus

Supercritical extractions were undertaken on a computer driven system, the Hewlett-Packard (Avondale) Model 7680A SFE. The instrument operates as an off-line extraction unit with a solvent washed chromatographic trap as the collection device for all samples [9]. Figure 1 illustrates the main components of the system. All critical parameters are monitored and controlled by the personal computer (PC) software. It should be noted that the variable restrictor device allows for the independent control of both the flow-rate and the back pressure during the extraction. Liquid carbon dioxide is pumped with constant flow by a twin piston reciprocating pump. The low viscosity of carbon dioxide requires that the pump head is cooled to avoid leaks at the pump head.

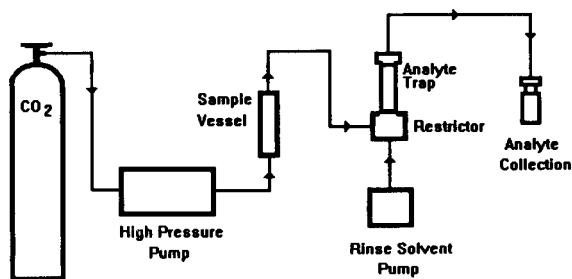


Fig. 1. Block diagram of the HP 7680A extractor.

A second carbon dioxide cylinder provides cryogenic cooling to the system. Sample cells are made of stainless steel with re-usable hand tightened PEEK caps at each end. The cells are available in 1.5- and 7.0-ml volumes. Both cell volumes have been studied in this investigation, although the majority of the results were achieved using the smaller cells. Temperature conditions are maintained accurately at each stage of the extraction by the use of focused cryogenics in conjunction with a series of electrothermal heating blocks. A two minute period of static extraction, where there is no fluid flow, was used at the beginning of each extraction sequence to allow the analyte to be fully solubilised. The mass transfer occurs when the instrument is operating in the dynamic flow mode and this is taken as the time of extraction. After the depressurisation stage, the final rinse step washes an appropriate solvent (methanol in the experiment) throughout the entire solvent line, restrictor and trapping column into 2-ml sample vials contained in a fraction collector. The trap, 7 cm in length and 5 mm i.d., is loosely packed with Hypersil ODS (particle size 30 μm) and has a valid volume of 650 μl . Volatile analyte loss is avoided by cryogenic cooling of the trap.

Analysis of the extracts was performed on a Shimadzu (Tokyo) Model UV-160 double beam UV-visible spectrophotometer using 10-mm silica cells (Thermal Syndicate) for all measurements. Quantitation was achieved by diluting all extracted samples to 10 ml using Technico class B graduated flasks and measuring absorbance against a four point linear calibration graph. None of the compounds studied demonstrated any instability in methanol when monitored over a week.

Reagents

Supercritical fluid grade carbon dioxide (Air Products, Sunderland) of certified purity 99.995% was used for extraction, while industrial grade carbon dioxide was used for cryogenic cooling. All six steroidal compounds (Fig. 2) studied were analytical working standards of certified purity supplied by Glaxo, Barnard Castle. Methanol (BDH, Poole) of AnalaR grade was used throughout the experimentation.

Sample introduction

All steroids were studied as pure compounds thus minimising potential matrix effects. To achieve this each sample was introduced into the extraction cell as a 50- μg pure standard deposited on the internal surface of a glass capillary tube. This was done by measuring a precise 50- μl volume of a 1000 $\mu\text{g ml}^{-1}$ stock solution prepared in methanol onto the glass and allowing the solvent to evaporate. By reducing the complexity of the extraction solubility effects, the mass transfer due to flow-rate and cell geometry can be studied. The interactions of the sample with the matrix and their resulting effect on extraction efficiency cannot be studied by this method of extraction. Spiking onto glass allows the visual confirmation of successful extraction.

Flow-rate

The carbon dioxide is pumped from the cylinder at approximately 53 bar at 15°C. Carbon dioxide is liquid under these conditions and the flow-rate is measured at this stage. Under super-

critical conditions the flow-rate will depend on the density achieved. At high densities (as the supercritical fluid tends towards more liquid-like conditions) the flow-rate through the extraction vessel will remain similar to the liquid pump-rate. Lower densities (as the supercritical fluid tends towards more gas-like conditions) result in greater flow-rate values. All quoted values of flow-rate are the liquid carbon dioxide pump-rate.

Experimental design

If the correct conclusions are to be drawn from an experiment, the various factors which affect the result must be identified and, if possible, controlled [10]. In this case the solubility of the analytes in carbon dioxide has been assumed to depend on a number of experimental factors e.g. density (g ml^{-1}), temperature ($^{\circ}\text{C}$), time of extraction (min) and flow-rate (ml min^{-1}). Any design of the experimentation should involve a consideration of these variables in order to obtain the best solubility parameters and hence the best experimental extraction conditions. Fractional factorial experimental design [5,6] allows for the detection and estimation of any interactions between the experimental factors. Classical univariate optimisation fails to give any information about factor interactions, and as a result can produce unsatisfactory optimum conditions. Factorial design also needs fewer measurements than the classical approach to achieve the same precision, thus reducing the method development time.

As four variables (three considered as quadratics) were considered a large number of possible combinations of experiments could be selected. As the length of each individual experiment can have serious effects on the method development time it was important to reduce the number of experiments to a minimum without serious confounding [11], random or systematic errors being introduced. This was established as 18 experiments (Table 1). The quadratic terms were studied at low, intermediate and high values: temperature was studied at 40, 60 and 80°C; carbon dioxide density at 0.40, 0.65 and 0.80 g ml^{-1} and flow-rate at 2.0, 3.0 and 4.0 ml min^{-1} . However, the time of extraction was considered at only two levels, 2 and 10 min. It should be noted that the

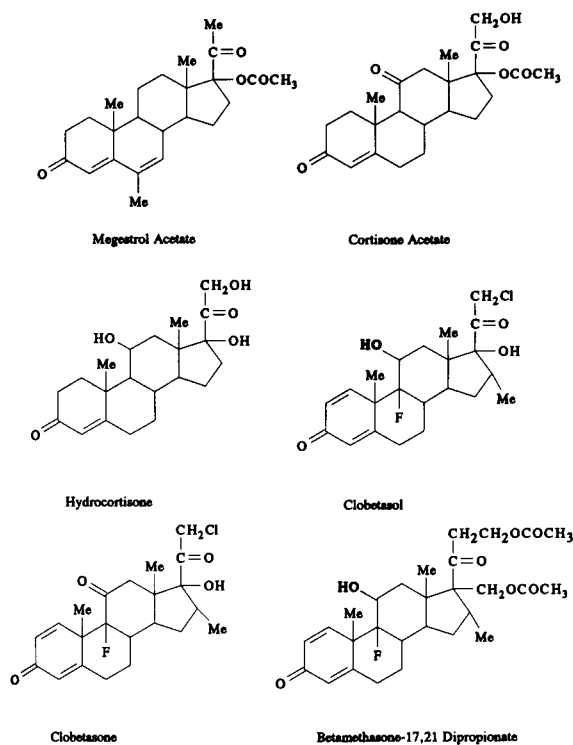


Fig. 2. Structural formulae of the steroidal compounds.

TABLE 1

The experimental design with the UV-visible percentage recoveries observed for the six steroids using 1.5 ml cell volume

| Temperature (°C) | Density (g min ⁻¹) | Time (min) | Flow-rate (ml min ⁻¹) | Steroid (% recovery) ^a | | | | | |
|------------------|--------------------------------|------------|-----------------------------------|-----------------------------------|-------|-------|-------|-------|-------|
| | | | | No. 1 | No. 2 | No. 3 | No. 4 | No. 5 | No. 6 |
| 80 | 0.40 | 2.0 | 2.0 | 93 | 0 | 0 | 13 | 4 | 43 |
| 40 | 0.65 | 2.0 | 2.0 | 98 | 22 | 16 | 26 | 2 | 86 |
| 40 | 0.40 | 10.0 | 2.0 | 91 | 0 | 20 | 12 | 11 | 12 |
| 80 | 0.90 | 2.0 | 2.0 | 99 | 88 | 32 | 109 | 24 | 101 |
| 60 | 0.65 | 10.0 | 2.0 | 103 | 100 | 20 | 5 | 4 | 107 |
| 40 | 0.90 | 10.0 | 2.0 | 78 | 97 | 26 | 108 | 17 | 109 |
| 60 | 0.40 | 2.0 | 3.0 | 22 | 59 | 0 | 4 | 0 | 35 |
| 80 | 0.40 | 10.0 | 3.0 | 44 | 0 | 0 | 20 | 2 | 79 |
| 80 | 0.65 | 2.0 | 4.0 | 95 | 73 | 12 | 43 | 4 | 87 |
| 40 | 0.40 | 2.0 | 4.0 | 6 | 16 | 1 | 10 | 0 | 2 |
| 40 | 0.90 | 2.0 | 4.0 | 99 | 33 | 22 | 64 | 4 | 106 |
| 60 | 0.40 | 10.0 | 4.0 | 0 | 0 | 1 | 5 | 0 | 45 |
| 40 | 0.65 | 10.0 | 4.0 | 102 | 107 | 12 | 18 | 0 | 106 |
| 80 | 0.90 | 10.0 | 4.0 | 95 | 108 | 19 | 123 | 56 | 101 |
| 80 | 0.90 | 10.0 | 2.0 | 103 | 98 | 54 | 99 | 49 | 0 |
| 80 | 0.90 | 2.0 | 3.0 | 99 | 97 | 41 | 108 | 34 | 86 |
| 80 | 0.40 | 2.0 | 4.0 | 0 | 0 | 1 | 5 | 0 | 42 |
| 40 | 0.90 | 2.0 | 2.0 | 98 | 23 | 26 | 51 | 7 | 101 |

^a No. 1 = megestrol acetate; No. 2 = cortisone acetate; No. 3 = clobetasol; No. 4 = clobetasone; No. 5 = hydrocortisone; No. 6 = betamethasone-17,21-dipropionate.

chosen values should be within the working limits of the instrumentation and that extrapolation of the response curves beyond the constraints of the initial design is to be avoided. The experiments were carried out in a randomised order for each steroid to minimise the effect of bias due to, for example, sample carry over.

RESULTS AND DISCUSSION

Six steroids were selected for analysis (Fig. 2). The selection of the steroids was based on a common structural backbone with a range of functional groups. It was determined experimentally that the six steroids had some degree of solubility

TABLE 2

Coefficients of regression and standard error of linear Eqn. 1 for cortisone acetate

| Variable | Descriptor | Beta | Standard error | <i>b</i> | Standard error | <i>t</i> (4) | <i>P</i> level |
|----------|--------------|---------------|----------------|----------------|----------------|---------------|----------------|
| 1 | ν_1 | 2.701 | 1.419 | 6.377 | 3.350 | 1.903 | 0.129 |
| 2 | ν_2 | 3.171 | 1.236 | 618.821 | 241.176 | 2.889 | 0.044 |
| 3 | ν_3 | 0.088 | 0.473 | 0.953 | 5.116 | 0.186 | 0.861 |
| 4 | ν_4 | 4.771 | 1.473 | 225.290 | 69.552 | 3.239 | 0.039 |
| 5 | $\nu_1\nu_1$ | -2.501 | 1.358 | -0.049 | 0.027 | -1.842 | 0.139 |
| 6 | $\nu_1\nu_2$ | 1.001 | 0.392 | 2.260 | 0.885 | 2.555 | 0.063 |
| 7 | $\nu_1\nu_3$ | -1.029 | 0.311 | -0.167 | 0.051 | -3.309 | 0.029 |
| 8 | $\nu_1\nu_4$ | -0.603 | 0.391 | -0.324 | 0.209 | -1.547 | 0.197 |
| 9 | $\nu_2\nu_2$ | -3.512 | 0.964 | -525.04 | 144.152 | -3.642 | 0.022 |
| 10 | $\nu_2\nu_3$ | 1.237 | 0.294 | 17.874 | 4.241 | 4.214 | 0.013 |
| 11 | $\nu_2\nu_4$ | -0.057 | 0.354 | -3.037 | 18.717 | -0.161 | 0.879 |
| 12 | $\nu_3\nu_4$ | 0.006 | 0.297 | 0.021 | 0.987 | 0.021 | 0.984 |
| 13 | $\nu_4\nu_4$ | -4.219 | 1.378 | -33.18 | 10.828 | -3.062 | 0.037 |

in supercritical carbon dioxide, ranging from the totally soluble megestrol acetate and betamethasone-17,21-dipropionate to the very slightly soluble clobetasol and hydrocortisone. Cortisone acetate is used in the following discussion as an example of the optimisation process.

The model assumes that nothing is known about possible interactions, therefore the parametric equation used, Eqn. 1, contains fourteen terms. Each of the terms represents either the variable or its interaction with another variable. The squared terms are quadratics and allow for curvature of the experimental response. The time variable is not considered as a quadratic as the response (percentage extraction) cannot reduce with increasing time.

$$Y = b_0 + b_1v_1 + b_2v_2 + b_3v_3 + b_4v_4 + b_5v_1^2 + b_6v_1v_2 + b_7v_1v_3 + b_8v_1v_4 + b_9v_2^2 + b_{10}v_2v_3 + b_{11}v_2v_4 + b_{12}v_3v_4 + b_{13}v_4^2 \quad (1)$$

where, Y is the response (percent extracted); v_1, v_2, v_3, v_4 are the four main variables: tempera-

ture, density, time, and flow-rate, respectively; $b_1 \dots b_{13}$ are the parametric coefficients; b_0 is the intercept.

Multilinear least squares regression was used to calculate the coefficients, b , in Eqn. 1. Because of the quite large differences between the magnitude of the squares of temperature and density (v_1^2 and v_2^2 in Eqn. 1), the coefficients were calculated also with the data for each variable standardized to its mean of zero and a standard deviation of unity. The coefficients of cortisone acetate are reported in Table 2 as b_n and $Beta_n$ for the un-standardised and standardised variables, respectively. As this data is well behaved there is no difference in the conclusions drawn by the two approaches. A pictorial representation of the coefficients for the standardised data is given in Fig. 3.

Significance is determined by a t -test with a confidence level of 0.05 (95% confidence limit) at 4 degrees of freedom. In Table 2 a coefficient with a probability (P) level of less than 0.05 or a t -test value of greater than 2.78 will be consid-

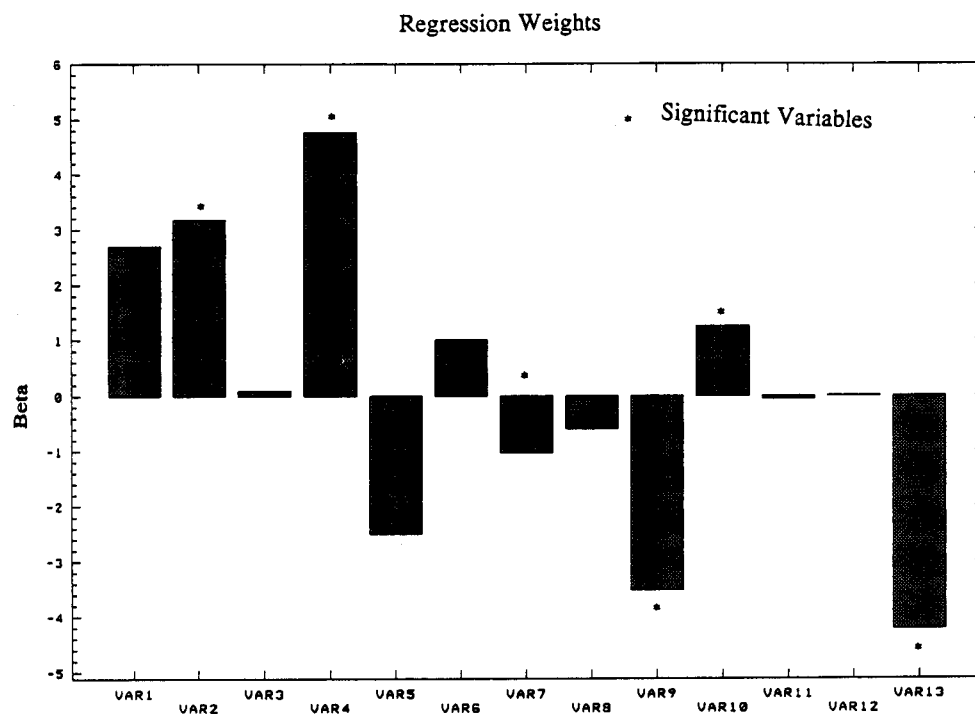


Fig. 3. Standardised regression weights of variables for cortisone acetate. * = Significant variables.

TABLE 3

Significant variable descriptors determined by multilinear regression

| Steroid | Significant variable | | | | | |
|----------------------------------|----------------------|---|---|---|----|----|
| Megestrol acetate | 2 | – | – | 9 | – | 11 |
| Cortisone acetate | 2 | 4 | 7 | 9 | 10 | 13 |
| Clobetasol | – | – | – | – | – | – |
| Clobetasone | 2 | – | – | 9 | – | – |
| Hydrocortisone | – | – | – | – | – | – |
| Betamethasone-17,21-dipropionate | 2 | – | – | 9 | – | – |

ered significant. The significant coefficients are highlighted in **bold** in Table 2. Table 3 is a summary of the significant variables determined for the six steroids by multilinear regression. Two of the steroids (clobetasol and hydrocortisone) show no significant variables and this may be attributed to their low solubility in carbon dioxide. Of the remaining four steroids, the two common terms are the density (variable 2) and the density squared term (variable 9) suggesting that density is the single major factor to affect the extraction of the steroids.

Flow-rate and temperature were also identified as significant for cortisone acetate with interactions involving time. However, it is apparent from the response curves that density is the most significant variable in achieving optimum extraction conditions. Example surfaces of cortisone acetate are given in Figs. 4 and 5 for a 10-min extraction time. These show the optimum extraction conditions are approximately 55°C, 3 ml min⁻¹ and 0.80 g ml⁻¹, and that flow-rate has a greater effect on extraction than the temperature.

The response surfaces of the density and flow-rate based on the model were calculated for the other compounds studied. Clobetasol and hydrocortisone, both of which failed to produce any significant variables (Table 3), succeeded in only showing a straight density gradient with no dependence on flow-rate. Betamethasone-17,21-dipropionate and clobetasone both demonstrated some dependency on the flow-rate at lower densities.

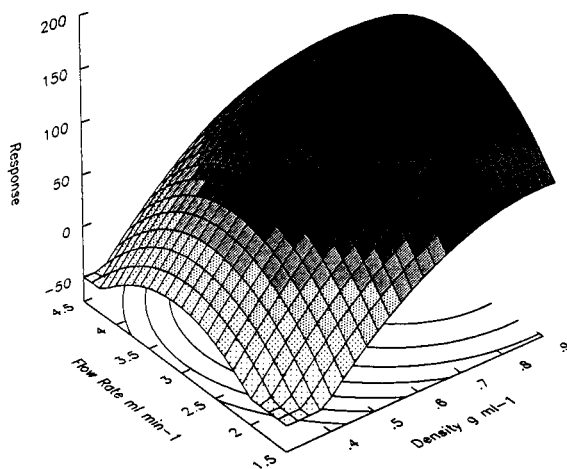


Fig. 4. Response surface for cortisone acetate studying the effect of density and flow-rate on the extraction efficiency at 55°C and 10 min extraction time.

Effects of cell geometry

The effects of cell geometry [12–14] have been studied using the commercially available 1.5-ml and 7.0-ml extraction cells for one steroid under the same conditions. Each cell is constructed of stainless steel and has an internal diameter of 1.0 cm. The 1.5-ml cell has a length of 4.0 cm in contrast to the 7.0-ml cell which has a length of

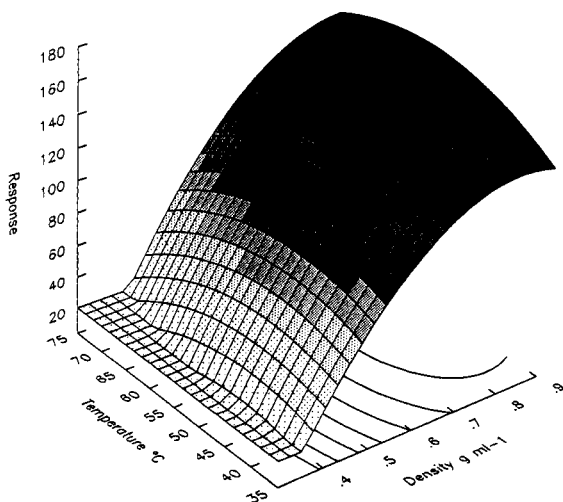


Fig. 5. Response surface for cortisone acetate studying the effects of density and temperature on the extraction efficiency at 3.0 ml min⁻¹ and 10 min extraction time.

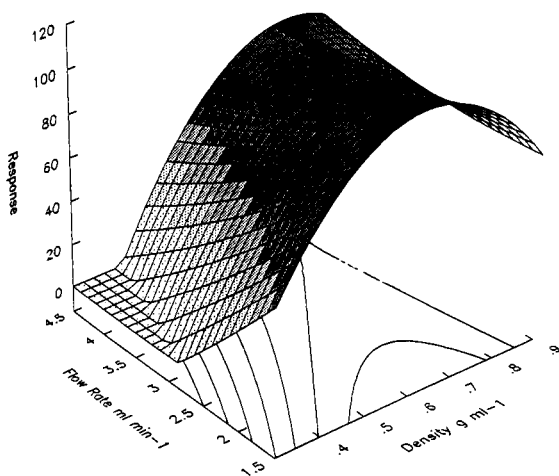


Fig. 6. Response surface for megestrol acetate studying the effects of density and flow-rate on the extraction efficiency using 1.5-ml cell at 55°C and 10 min extraction time.

9.5 cm. The results for megestrol acetate, a steroid totally soluble in carbon dioxide, are shown in Figs. 6 and 7. The response surfaces show the contrasting effects of flow-rate and density when only the volume of the cell is changed. With the 1.5-ml cell there is quite clearly a drop in response with an increasing flow rate at an intermediate density (Fig. 6). At higher densities the drop in response is not as pronounced, although the optimum response region is restricted to low flow

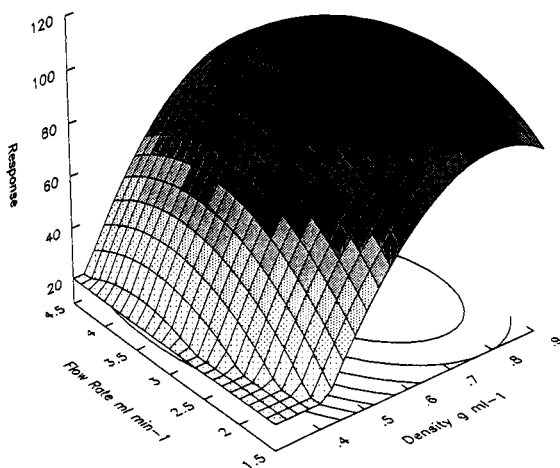


Fig. 7. Response surface for megestrol acetate studying the effects of density and flow-rate on the extraction efficiency using the 7.0-ml Cell at 55°C and 10 min extraction time.

and high density combinations (the darker shaded region). Increasing the flow-rate for the 1.5-ml cell apparently reduces the interaction between the supercritical fluid and the steroid. The 7.0-ml (Fig. 7) cell has the effect of making the flow-rate much less critical to the optimum extraction recovery.

It is probable that the supercritical fluid flow within the sample cell has some effect on the extraction efficiency in SFE. It is thought that turbulent flow is more desirable than laminar flow as the resulting eddies produced within the sample cell will aid diffusion within the sample matrix. The Reynolds number [15] (Eqn. 3)

$$Re = \frac{\rho v d}{\mu} \quad (3)$$

(where ρ = density of carbon dioxide, v = velocity of carbon dioxide flow, d = internal diameter of cell, μ = viscosity of carbon dioxide) was used to investigate the type of flow which exists within the sample cells both of which have the same internal diameter (0.01 m). The calculation is dependent on high density conditions (0.9 g ml^{-1}), a flow-rate of 3 ml min^{-1} and an extraction time of 10 min. The viscosity of carbon dioxide was taken as the liquid value at $1.5 \times 10^{-4} \text{ N s m}^{-2}$. The small amount of mass flow-rate, calculated to be $4.5 \times 10^{-5} \text{ kg s}^{-1}$ at a density of 0.92 g ml^{-1} , and the internal diameter for the sample cells means that the Reynolds number will be considerably lower than the 2000 threshold value for the transition between laminar and turbulent flow, even assuming low (gas-like) viscosity conditions for the carbon dioxide. The calculated values for the Reynolds number varied between 40 and 400 according to the viscosity of carbon dioxide value taken. Thus laminar flow is the most likely type of supercritical fluid flow within the sample cell. This situation may be beneficially altered when the extraction cell is packed with sample where a disruption of the supercritical fluid flow may produce sufficient eddies to create turbulent flow. However, this was not the situation in this experiment as the bulk of the extraction cell was empty. Therefore, changes in supercritical fluid flow were ruled out as a reason for the observed effects when cell size was changed.

TABLE 4

Comparison of cell volumes swept using 1.5-ml and 7.0-ml cell volumes

| Density (g ml ⁻¹) | Cell volume swept (ml) | |
|----------------------------------|------------------------|-------------|
| | 1.5-ml cell | 7.0-ml cell |
| 0.4 | 41 | 7 |
| 0.6 | 19 | 4 |
| 0.9 | 14 | 3 |

One factor which has undoubtedly altered by using different sized cells is the number of cell volumes swept with supercritical carbon dioxide. The number of cell volumes swept can be calculated using Eqn. 4.

Cell volumes swept

$$= \frac{\text{Mass of carbon dioxide (g)}}{\text{Density (g ml}^{-1}) \times \text{cell volume (ml)}} \quad (4)$$

where mass of carbon dioxide = density of liquid carbon dioxide (0.92 g ml⁻¹) × flow-rate (ml min⁻¹) × time of extraction (min). The effect on the mass transfer of the analytes by reducing the number of cell volumes swept is likely to be detrimental to the extraction process. This is supported by the fact that the percentage recoveries for the 7.0-ml cell were lower by approximately 20–40% than those of the 1.5-ml cell quoted in Table 1, under exactly the same conditions. With increasing density of supercritical carbon dioxide the number of cell volumes swept for a given time, will be reduced (Table 4). When the density approaches 0.9 g ml⁻¹ the number of cell volumes swept for the 7.0-ml cell is only sufficient for partial mass transfer to occur. This is shown in Fig. 7 as the decrease in extraction efficiency that occurs at a density of 0.8 to 0.9 g ml⁻¹ and flow-rates of 2–2.5 ml min⁻¹. Increasing the flow-rate will compensate for this effect as the mass of carbon dioxide used is then increased. It is therefore not recommended to extract when the number of cell volumes swept of carbon dioxide is below 4.

Conclusions

It is apparent from the results that density is the major variable for the extraction into supercritical carbon dioxide of the steroid compounds

studied. Although the experimental optimisation can be applied only to each individual compound, the overall trend gives a basis on which to approach unknown steroids. It must be noted that individual sample matrices will affect the relative contributions of the extraction parameters. The minimum number of cell volumes swept for effective extraction has been determined experimentally to be four. Below this there is insufficient contact between the sample and supercritical carbon dioxide. This is particularly important when using cell sizes of different dimensions.

The financial support of ICI plc, Wilton Materials Research Centre and Glaxo Manufacturing Services is gratefully acknowledged, and particularly the cooperation of Dr. W. Campbell (ICI) and Mr. K. Leiper (Glaxo). Finally, we acknowledge the loan of the HP7680A SFE from Hewlett-Packard (UK) Ltd.

REFERENCES

- 1 S.B. Hawthorne, *Anal. Chem.*, 62 (1990) 633.
- 2 R.E. Majors, *Liq. Chromatogr. – Gas Chromatogr.*, 4 (1991) 10.
- 3 M.L. Lee and K.E. Markides, *Analytical Supercritical Fluid Chromatography and Extraction, Chromatography Conferences, Inc., Provo, UT, 1990, Chap. 5.*
- 4 J.W. King, *J. Chromatogr. Sci.*, 27 (1989) 355.
- 5 R.L. Mason, R.F. Gunst and J.L. Hess, *Statistical Design and Analysis of Experiments*, Wiley, Chichester, 1989.
- 6 R.G. Brereton, *Chemometrics Applications of Mathematics and Statistics to Laboratory Systems*, Ellis Horwood, Chichester, 1990.
- 7 P.L. Goldsmith, C.A.E.D. ICI Fibres, Harrogate, 1987, personal communication.
- 8 CSS: *Statistica*, Release 3.0F, Statsoft U.K., Letchworth.
- 9 M. Kane, J.R. Dean, S.M. Hitchen, C.J. Dowle and R.L. Tranter, *Anal. Proc.*, 29 (1992) 31.
- 10 J.C. Miller and J.N. Miller *Statistics for Analytical Chemistry*, Ellis Horwood, Chichester, 1984.
- 11 E.P. Box, W.G. Hunter and J.S. Hunter, *Statistics for Experimenters*, Wiley, New York, 1978.
- 12 K.G. Furton and J. Rein, *Anal. Chim. Acta*, 248 (1991) 263.
- 13 J. Rein, C.M. Cork and K.G. Furton, *J. Chromatogr.*, 545 (1991) 149.
- 14 K.G. Furton, and J. Rein, *Chromatographia*, 31 (1991) 297.
- 15 J.M. Coulson and J.F. Richardson, *Chemical Engineering*, 4th edn., Pergamon Press, Oxford, 1990.

Accuracy, precision and information of the adaptive Kalman filter in chromatography

Yuzuru Hayashi

National Institute of Hygienic Sciences, Kami-Yoga, Setagaya, Tokyo 158 (Japan)

Sarah C. Rutan

Department of Chemistry, Virginia Commonwealth University, Box 2006, Richmond, VA 23284-2006 (USA)

(Received 27th April 1992; revised manuscript received 16th July 1992)

Abstract

The accuracy and precision of the adaptive Kalman filter were examined using computer simulations of chromatographic situations, where a known (target) peak overlaps with an unknown (interferent) peak. The peak overlap, area ratio and noise level in the chromatograms significantly affect the reliability of the concentration estimates obtained from the filter. The accuracy (bias of the estimates) and precision (relative standard deviation, SD) for the known peak have similar tendencies as a function of peak overlap and area ratio. For an area ratio of 1, a noise level of 0.2% of the peak maximum and a peak resolution of 1.0, the bias for the known peak is 0.1% and the SD is 0.042%; if the peak resolution is 1.5, then the bias is 0.004% and the SD is 0.036%. The function of mutual information (FUMI) is shown to represent approximately the reliability (bias and standard deviation) of the concentration estimates obtained from the adaptive Kalman filter.

Keywords: Liquid chromatography; Optimization methods; Accuracy; Kalman filter

The separation of overlapped peaks is essential in every area of separation science, including chromatography and electrophoresis. For example, liquid chromatographic quantification of a small peak adjacent to a large interfering peak requires careful consideration of the degree of peak separation, e.g., an assay of a small impurity of an optical isomer or of a drug degradation product present in only a small amount [1].

The degree of peak separation will strongly influence the reliability of an analytical method [2,3]. There have been several publications concerning the evaluation of the accuracy of analyti-

cal methods in chromatographic situations where the peaks are overlapped [4–7]. Snyder [4] and Foley [5] have studied the errors in peak area measurement by the perpendicular-drop algorithm and in peak height measurements. The size effect and asymmetry effect of overlapped peaks were treated quantitatively. In every instance, the concentration of the smaller peak is overestimated and that of the larger peak is underestimated to a substantial extent, especially as the degree of overlap increases [6,7].

The degree of peak separation plays a critical role in the determination of the precision of the results, especially for Kalman filter-based analyses. This algorithm, originally developed in 1960 for engineering applications [8], allows for the recursive, least-squares estimation of the compo-

Correspondence to: S. Rutan, Department of Chemistry, Virginia Commonwealth University, Box 2006, Richmond, VA 23284-2006 (USA).

nent concentrations from an overlapped response. Previous studies have established that the Kalman filter gives more accurate estimates for peak area than the perpendicular drop algorithm [9]. Adaptive Kalman filters are modified versions of the Kalman filter that offer a mathematical means for predicting the “concentration” of a known peak (modeled peak) when it is interfered with by an unknown peak (unmodeled peak) [10–18].

Ideally, the degree of peak separation should be related mathematically to the analytical parameters of interest, the accuracy and precision of analysis. This is because the goal of typical optimization procedures is to select the most accurate and/or precise analysis. If a mathematical relationship exists, a large number of experiments will not be required to establish the optimum conditions for analysis. Recently, the function of mutual information (FUMI) has been shown to relate theoretically the precision (standard deviation) of the concentration estimates to the peak shape, size, overlap and noise level and has been successfully used as a criterion in the optimization of precision and efficiency in liquid chromatography [3]. FUMI is derived based on information theory and the Kalman filter.

The accuracy and precision of an analysis are not entirely independent in practice [19]. Their theoretical treatments, however, are very different, especially for the Kalman filter. The precision of the regular Kalman filter (not the adaptive filter) can be estimated exactly by FUMI or the error covariance matrix P_k , but the accuracy, as measured by the bias, is assumed to be zero.

The aims of this work were to elucidate the relationship between the accuracy and precision of the adaptive Kalman filter in chromatographic separations and to examine the influence of peak overlap, peak area ratio and white noise on these statistical parameters. Previous work has demonstrated the applicability of an adaptive Kalman filter based on the correlation of the innovations sequence for peak resolution and quantification in analytical chemistry [10–18]. For proper use of the filter, however, the reliability of the estimates obtained should be established theoretically or empirically. A combination of FUMI and the

error variance of the adaptive Kalman filter is shown to be more useful for estimating the reliability of the adaptive Kalman filter for estimating the concentration of the target compound than either of these measures used separately.

THEORY

If the chromatograms are reproducible under the same operating conditions except for the presence of zero mean white noise, the square root of the error covariance matrix P_k is equal to the observed standard deviation (SD) of the regular Kalman filter estimates for the concentration from replicate experiments. In this situation, the Shannon mutual information (FUMI) of the Kalman filter can be related to the error covariance P_k or observed SD:

$$\begin{aligned}\phi_j &= -1/2 \ln(\{P_k\}_{jj}) \\ &= -\ln(\text{SD}_j)\end{aligned}\quad (1)$$

where j denotes peak j in the chromatogram, $\{P_k\}_{jj}$ is the j th diagonal element of P_k and k represents the number of data points that have been filtered. This relationship assumes that the true value for the concentration is one.

In the present example, a one-dimensional Kalman filter [20] is used to estimate the amplitude (concentration), X_j , of the j th chromatographic response, where a model of the chromatographic peak shape is available. This one-dimensional filter is based on the assumption that there are regions of the chromatogram which can be modeled by a single component [20]. FUMI is calculated from the sum of the squared signal intensities h_k^2 of the peak over the region where no interferences exist, divided by the variance of the white noise W_c :

$$\phi_j = \frac{1}{2} \ln \left(\frac{\sum_k h_k^2}{W_c} \right)\quad (2)$$

If a Gaussian peak j of area A_j , width σ_j (standard deviation) and retention time t_j (mean) is separated from all other peaks, then FUMI ψ_j

(> 0) for peak j can be described in terms of the peak parameters A_j and σ_j and the noise level \tilde{a} :

$$\psi_j = 1/2 \ln \left[A_j^2 / (2\pi^{1/2} \sigma_j \tilde{a}) \right] \quad (3)$$

The noise level \tilde{a} is defined to be the product of the variance W_c of the noise in the chromatogram and the sampling interval ΔT of the A/D converter [21]: $\tilde{a} = W_c \Delta T$. If peak j overlaps with adjacent peaks $j-1$ and/or $j+1$, FUMI ϕ_j is reduced by the information loss $\delta\phi_j$ (> 0) caused by the overlap:

$$\phi_j = \psi_j - \delta\phi_j \quad (4)$$

As is evident from Eqns. 3 and 4, FUMI ϕ_j depends on four factors: peak overlap ($\delta\phi_j$), peak area (A_j), peak width (σ_j) and noise (\tilde{a}). The theoretical SD for peak j can be calculated from FUMI as $SD = \exp(-\phi_j)$. One of the most prominent advantages of FUMI is that the information or observed SD can be predicted before the analysis by knowing only the peak shape (A_j and σ_j), the position (t_j), noise level \tilde{a} and the degree of overlap with adjacent peaks.

Although FUMI and the regular, one-dimensional Kalman filter require that the region in the chromatogram where the single component assumption is valid be identified, this information may not always be available. In this event, a modification of the Kalman filter, known as the adaptive filter, can be used to detect deviations from the single component assumption.

Essentially, those regions of the chromatogram where significant interferences are present are identified by the adaptive filter and a low weight is assigned to those points in fitting the data. This is accomplished by averaging the innovations sequence, ν_k , (the on-line residuals) over a preset window size (m) as the filter processes the data. When a region of data is filtered where the data are inconsistent with the model (as determined by the magnitude of the innovations sequence), the variance of the measurements (r_k) is recalculated according to the equation

$$r_k = \sum_{j=1}^m (\nu_{k-j} \nu_{k-j}) - h_k^T P_k h_k \quad (5)$$

where h_k is the measurement function which

describes the shape of the model peak as a function of time, t_k , and m is a smoothing window [10,16]. The weighting of the data points is inversely proportional to r_k , so those regions of the chromatogram with large residuals (ν_k) are given low weights in the fits. This should result in a more accurate estimate for the amplitude of the known peak when interferences are present.

The limits of this approach are reached when significant interferences occur across the entire elution profile of the known component, i.e., cases of severe chromatographic overlap. The studies reported to date on the analytical applications of the adaptive filter have mentioned this limitation. However, the degree of overlap that can be tolerated under various conditions has not been carefully examined. In this work, we evaluated the ability of the adaptive filter to estimate quantitatively target peak magnitudes in the presence of an interfering peak as a function of peak overlap, peak area ratio and noise. In addition, the theoretical error derived from FUMI is not exactly equal to the observed error of the adaptive Kalman filter, as FUMI was originally derived for the regular Kalman filter. In this paper, the relationship between FUMI and the error in the adaptive Kalman filter results is considered.

EXPERIMENTAL

Computer-generated Gaussian peaks were used in this study. The plate number N was assumed to be 10000 and the retention time t_j and width σ_j of the Gaussian peak were calculated using the fundamental chromatographic equation: $N = (t_j/\sigma_j)^2$.

The accuracy (bias) and precision (standard deviation, SD) of the filter estimates for the amplitude of the target peak were calculated by repeated computer simulations. First, the retention times of the known (modeled) and unknown (unmodeled) peaks were fixed as shown in Fig. 1. A filter estimate of the target (known) peak is obtained by adaptive Kalman filtering of the noisy chromatogram. The mean and SD of the estimates for the target peak amplitude were obtained by repeating this process 500 times. Each

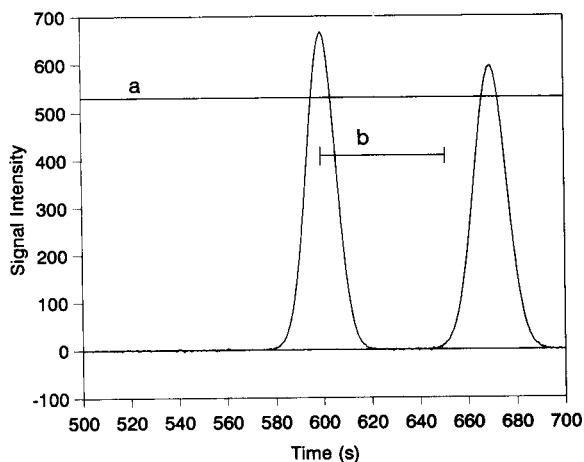


Fig. 1. Two Gaussian peaks with white noise. $N = 10000$. Fig. 2 is illustrated for the target peak in region a and Figs. 3–6 for the target peak in region b.

chromatogram was different only in the pattern of the noise with the noise level \bar{a} held constant. Gaussian-distributed noise was generated using a twelve-point pseudo-random number generator. The above process was repeated for different positions of the target peak. Plots of the mean and SD of the known component concentration versus the position of the target peak were obtained for a specified noise level and peak area ratio.

The unknown peak was fixed at a time of 600 s; the known peak was moved from 700 to 500 s at intervals of 0.5 s (Fig. 2) or from 650 to 600 s at intervals of 0.2 s (Figs. 3–6). The adaptive filtering was performed in the backward direction so that the known peak to be quantified was filtered first (for the second set of the simulations), as the known peak always eluted later than the unknown peak. A single filter pass was used in all instances.

The information FUMI in these studies was calculated from Eqn. 2 and was based on the assumption that the data analysis method is ineffective when the signal from the interfering peak exceeds 0.5% of the intensity of the maximum of the target peak. FUMI for the target peak was calculated from the sum of the squared signal intensities, h_k^2 , as the elution time decreased until the interfering signal first reached the above-mentioned limit. In Figs. 1–4 and 6, the peak areas of the modeled and unmodeled peaks are the same (10000) and the concentration of the target peak is unity. The smoothing window (m) was set at six data points for the adaptive Kalman filter.

According to the FUMI theory, if the noise level \bar{a} is kept constant and if the sampling interval ΔT is decreased, the noise variance W_c in-

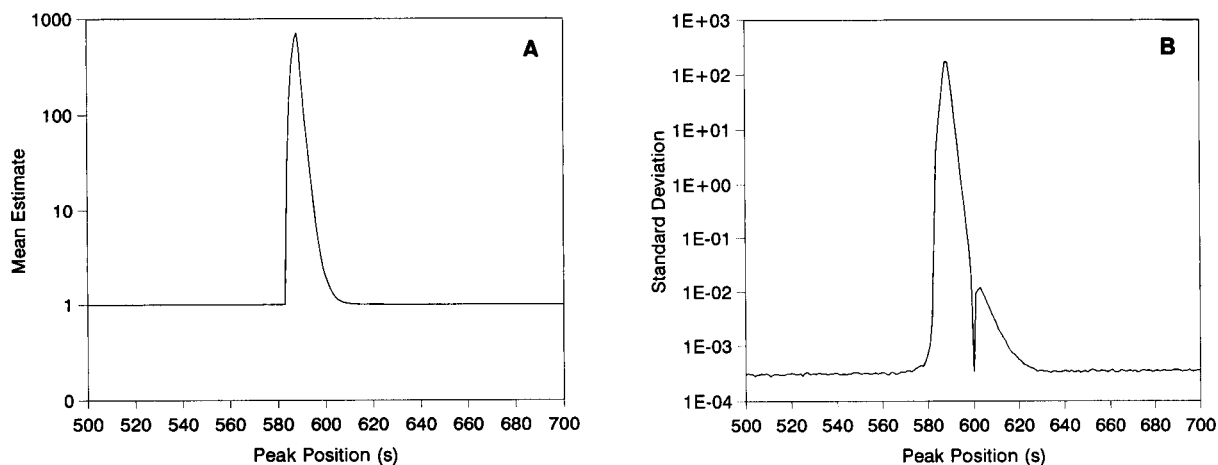


Fig. 2. Influence of peak overlap on the average and standard deviation of the estimates from the adaptive Kalman filter. Abscissa, the position of the target (known) peak (the unknown peak is fixed at $t_j = 600$ s). (A) Average of the filter estimates for the target peak. (B) Standard deviation (SD) of the filtering estimates for the target peak. The areas A_j of the peaks are the same.

creases. Assuming that the sampling interval and integration period are both equal to ΔT , it is impossible to gain more information by simply decreasing the sampling interval ΔT of the A/D converter.

For the Kalman filter results, the values used for W_c and ΔT were 1 and 0.5, respectively; for the calculation of FUMI, values of W_c (= 2.5) and ΔT (= 0.2) were used to give a more precise calculation ($\tilde{a} = 0.5$) (Figs. 2–5). A tenfold larger noise level ($\tilde{a} = 5$) was used for the results in Fig. 6 [$W_c = 10$ and $\Delta T = 0.5$ for Kalman filter results (Figs. 6A and B); $W_c = 25$ and $\Delta T = 0.2$ for FUMI (Fig. 6C)]. The initial conditions for the filter were $X_0 = 0$, $P_0 = 10^6$ and $r_0 = W_c$.

RESULTS

Figure 2 shows that both the bias and standard deviation of the filter estimates for the target peak concentration take maximum values when the target peak elutes at $t_j = 587$ s, where the unmodeled peak is filtered before the modeled peak. This is because the maximum activity of the Kalman filter, represented by the Kalman gain, occurs “before” the maximum of the target peak. When the target peak elutes at $t_j < 600$ s, the unmodeled interferant peak is encountered first by the filter and erroneous estimates result (filtering occurs from 700 to 500 s). The minimum in Fig. 2B at 600 s will be explained below.

The true “concentration” of the target peak in Fig. 2 is unity. If the peaks are completely separated from each other, the SD is about 0.0003 (at t_j values of 640–700 s in Fig. 2). The maximum values for the average concentration (= 863) and the SD (= 177) of Fig. 2 are so large that in practice adaptive filtering when an unknown peak is processed first should be avoided (in Fig. 2, this unfavorable area is from 580 to 600 s). Therefore, the region of practical interest ranges from 600 to 650 s.

The variation of the initial guess for the concentration, X_0 , has been proposed as a means to improve the adaptive filter estimates for the situation where the unmodeled peak was filtered first [10]. In that case, much smaller values for the

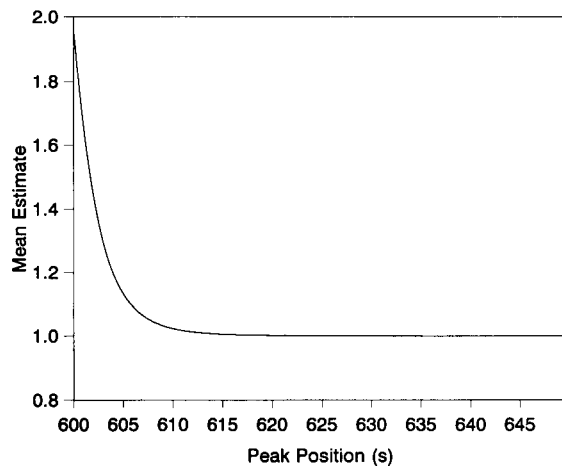


Fig. 3. Dependence of accuracy on peak overlap. Abscissa, the position of the target peak (the unknown peak is fixed at $t_j = 600$ s); ordinate, the average of the filter estimates of the target peak for 500 simulations.

initial error covariance P_0 were used. However, for the present studies, it was found that the estimates from the adaptive filter were insensitive to variations in the initial guess for the concentration, X_0 , as long as the known peak was filtered first.

Figure 3 shows the influence of peak overlap on the accuracy. If the target peak is completely separated from the unknown peak, the average estimate for the target peak is very close to the true concentration (= 1). As the target peak position approaches that of the unknown peak, the average of the estimates begins to exceed the true value. If the two peaks coelute ($t_j = 600$ s), the average Kalman estimate is equal to the sum of the concentrations of the two peaks (= 2).

Figure 4 shows the dependence of the precision on the peak overlap for the same situation as shown in Fig. 3. Curve a represents the observed SD from filtering replicate simulations. As the target peak becomes more severely overlapped with the fixed unknown peak, the observed SD begins to increase. The observed SD has a maximum at $t_j = 602$ s (SD = 0.0123; resolution $R_s = 0.083$). The SD of the estimates for the completely overlapped peaks (SD = 0.0003; $R_s = 0$; $t_j = 600$ s) is less than for the strongly overlapped ones (e.g., SD = 0.0114; $R_s = 0.091$; $t_j = 602.2$).

This is because no distinction is made between the target and unknown chromatographic peaks at $t_j = 600$ which have the same shape and position; the two fused peaks appear as one peak with twice the area.

Curve b in Fig. 4 shows the average of the square root of the error variance P_k of the adaptive Kalman filter. Curve b gives good estimates for the actual SD (curve a) if the peaks are sufficiently separated. Although curve b has a close similarity in shape to the actual SD, it underestimates the SD if the peaks are overlapped ($R_s < 0.82$; $t_j < 620$). We should note that the error variance P_k of the adaptive Kalman filter is a random variable that depends on the actual values for the measured responses, whereas the P_k calculated using the regular Kalman filter depends only on the a priori model information [16]. This is why curve b is noisy. The square root of the error variance of the adaptive filter obtained from filtering a single simulated data file is much noisier than curve b (not shown). Curve c in Fig. 4 represents the SD calculated from FUMI. FUMI, like the P_k for the regular Kalman filter, depends only on the a priori model information, and therefore curve c is smooth.

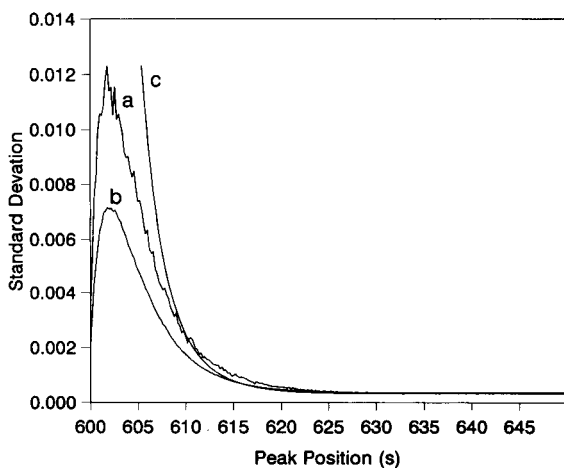


Fig. 4. Dependence of precision on peak overlap. Abscissa as in Fig. 3. (a) SD of the filter estimates for 500 simulations. (b) square-root of the error variance $P_k^{1/2}$ of the adaptive Kalman filter averaged over 500 simulations. (c) SD predicted from FUMI.

TABLE 1

Relationship between the observed mean and SD and the information FUMI

| t_j | Bias (%) ^a | SD (%) ^b | | R_s |
|-------|-----------------------|---------------------|-------------------|-------|
| | | Repl. ^c | FUMI ^d | |
| 600.0 | 100 | 0.033 | 19.9 | 0 |
| 602.0 | 47.9 | 1.2 | 6.66 | 0.083 |
| 606.0 | 9.78 | 0.62 | 1.06 | 0.25 |
| 607.8 | 5.06 | 0.41 | 0.54 | 0.32 |
| 610.0 | 2.42 | 0.26 | 0.26 | 0.41 |
| 613.0 | 1.01 | 0.14 | 0.12 | 0.54 |
| 615.8 | 0.50 | 0.091 | 0.072 | 0.65 |
| 624.2 | 0.10 | 0.042 | 0.036 | 0.99 |
| 628.0 | 0.051 | 0.036 | 0.034 | 1.14 |
| 635.0 | 0.0078 | 0.035 | 0.034 | 1.42 |
| 637.4 | 0.0042 | 0.036 | 0.034 | 1.51 |

^a Bias (%) is calculated as [(observed mean – true value)/(true value)] \times 100. The true value of the concentration is 1. ^b SD denotes the relative standard deviation. ^c SD calculated from replicate simulations. ^d Theoretical SD calculated from FUMI.

As the target peak moves from $t_j = 600$ s towards less overlap, the SD calculated from FUMI decreases. On the other hand, as the target peak moves from $t_j = 650$ s toward the unknown peak at $t_j = 600$ s, the peak becomes sharper (decrease in width σ_j ; see Eqn. 3) and the SD also decreases. Hence the SD must have a minimum value between 600 and 650 s; in this case, FUMI takes a maximum at $t_j = 632.2$ s and $R_s = 1.31$. The minimum in the theoretical SD is not clear in curve c in Fig. 4, because the change in the SD is small in this overlap-free region.

Table 1 lists the relationship between the bias, the SD and the resolution R_s , which is the most commonly used means of expressing the degree of peak overlap in chromatography, for a 1:1 peak area ratio. For example, if up to a 5% bias is acceptable in an analysis, peaks with an R_s as small as 0.3 can be analyzed by the adaptive Kalman filter. The SD in this analysis is 0.4%. If the required accuracy corresponds to a bias of less than 0.05%, then an R_s of 1.1 is the minimum permissible separation, with an SD of 0.036%. Baseline separation ($R_s = 1.5$) gives an excellent bias (0.0042%) and SD (0.036%). Table 1 also shows that the SD derived from FUMI gives good estimates for the actual SD.

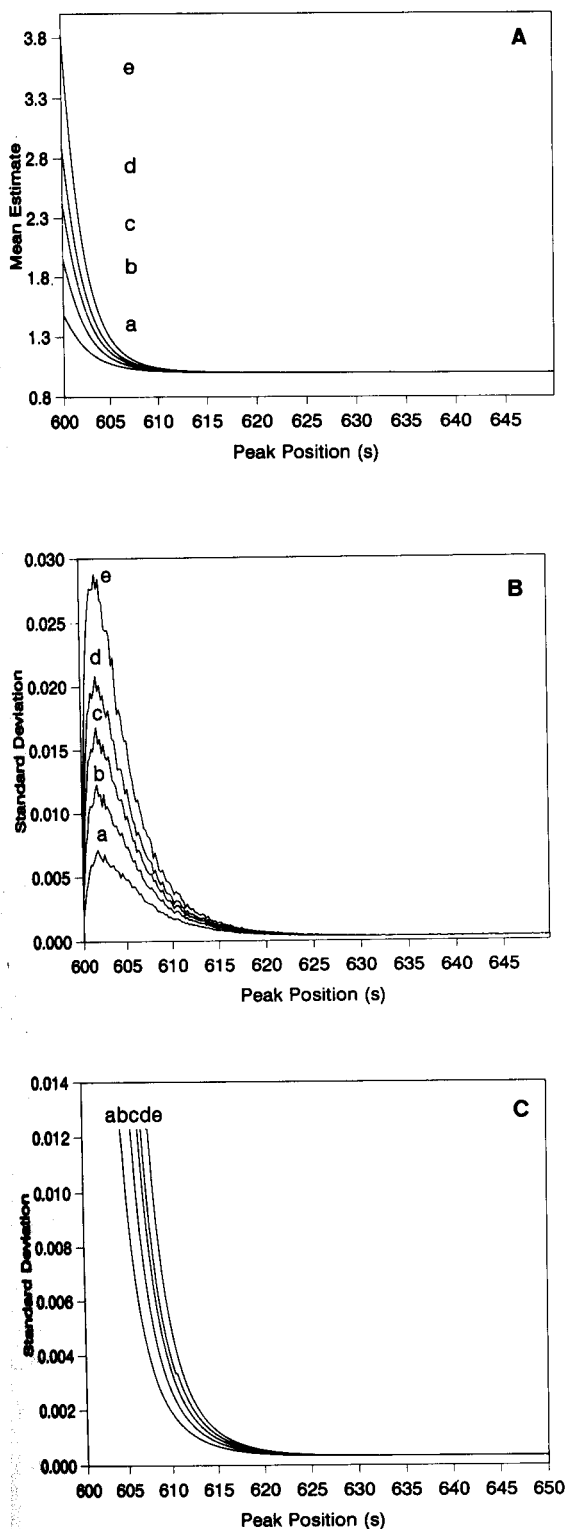


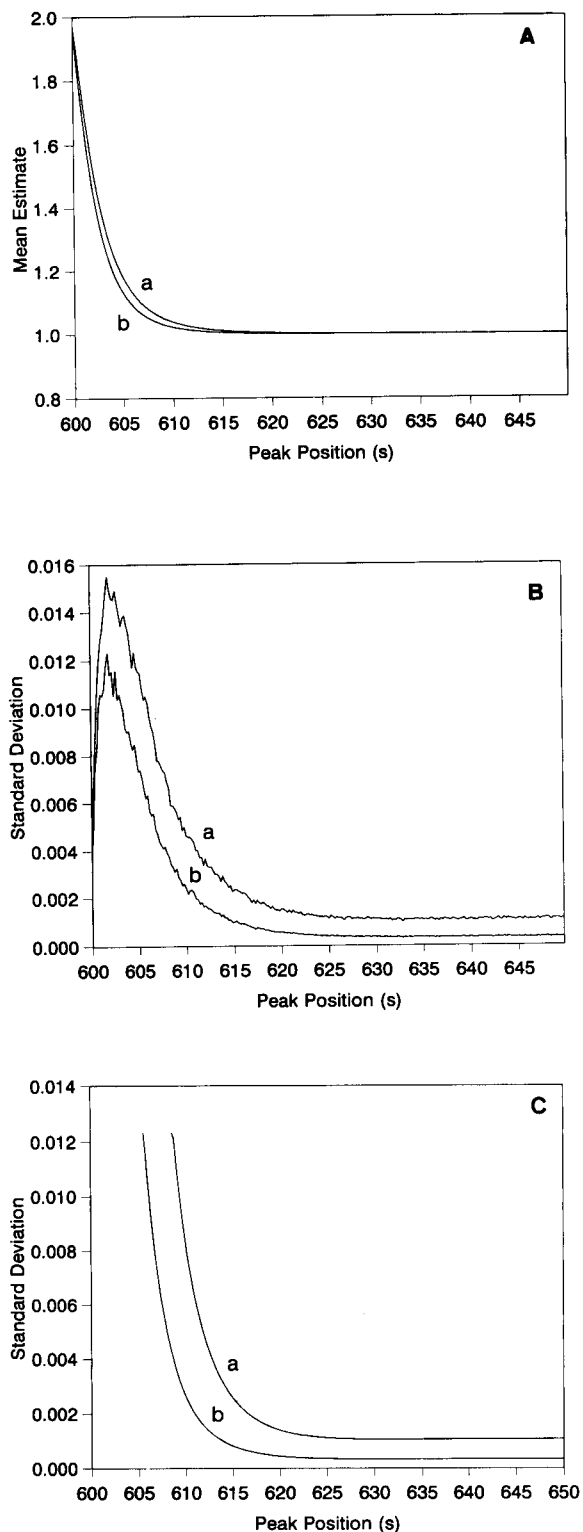
Figure 5 shows the effect of changing the peak area of the unknown peak on the accuracy and precision of the adaptive Kalman filter. As expected, if the peaks are sufficiently separated, the effects of the different areas are negligible. However, the size effect becomes more important when the peaks are overlapped. The observed mean (A), observed SD (B) and theoretical SD from FUMI (C) show similar behavior as a function of the peak area of the unknown peak as well as the peak overlap. The influence of the area ratio on the maximum of FUMI has been examined in detail previously [1].

Figure 6 shows the effect of white noise on the accuracy and precision of the filter estimates. The presence of white noise, which inevitably exists in chromatograms, affects the precision over the whole range of possible peak positions for the known peak. Thus, the precision (curves in Figs. 6B and C) is shifted by the noise level. On the other hand, the noise effect (for zero mean, white noise) on the accuracy is appreciable only when the peaks are strongly overlapped. Results analogous to those given in Table 1 can be deduced from the results shown in Figs. 5 and 6 for different noise levels and for peak area ratios other than 1:1.

DISCUSSION

Both accuracy and precision are important considerations in evaluating an analytical technique and determining the overall reliability of the method [2]. In general, the accuracy of an analysis is severely affected by a large degree of peak overlap. In this event, even results with acceptable precision may not be very reliable, owing to poor accuracy. As the peaks become more resolved but are broadened, the SD of the

Fig. 5. Effect of peak area and overlap on accuracy and precision. Abscissa as in Fig. 3. (A) Average; (B) observed SD; (C) SD calculated from FUMI. The unknown peak is fixed at $t_j = 600$ s, but the area is changed as (a) 5000, (b) 10000, (c) 15000, (d) 20000 and (e) 30000. The area of the known peak is fixed at $A_j = 10000$.



results more accurately reflects the reliability of the analysis, as the bias under these conditions is not significantly different from zero. This affirms that evaluation of both the accuracy and precision is necessary to characterize an analytical method completely.

In this study, however, the accuracy and precision observed are not entirely independent. They show similar trends with respect to peak overlap and peak area ratio in chromatography. However, the precision is the only factor which reflects the noise level of an analytical system, if the peaks are completely separated (see Fig. 6). Further, the reduced reliability of the analysis resulting from peak broadening at later elution times is not represented by the accuracy. As long as the peaks are not severely overlapped (at t_j from 605 to 650 s), results with high precision are also very accurate. However, improved accuracy does not always result in improved precision (see Fig. 6).

The error variance P_k is a good criterion for the evaluation of the adaptive Kalman filter (see Fig. 4 and refs. 7 and 8). The error $P_k^{1/2}$ provides a reasonable estimate of the SD of the concentration estimate obtained from a single experiment, even without any knowledge about the shape and position of an unmodeled peak. However, the SD represented by $P_k^{1/2}$ is a random variable (different from experiment to experiment) and the variation of $P_k^{1/2}$ with changes in peak overlap and white noise is noisy even with multiple simulations (see curve c in Fig. 4).

On the other hand, the information FUMI provides the theoretical SD and the resulting response as a function of peak overlap is smooth (see curve a in Fig. 4). However, FUMI and the corresponding SD cannot be calculated without a knowledge of the shape and position of the unknown peak. If this information is available, FUMI or the standard deviation derived from FUMI may be a better criterion than the SD from P_k for expressing the reliability of the results (see Fig. 4). In the situation used in this

Fig. 6. Effect of white noise and overlap on accuracy and precision. (A) Average; (B) observed SD; (C) SD from FUMI. The noise level \bar{a} is (a) 5 or (b) 0.5.

paper (a tolerated interference level of 0.5% of the target peak maximum), the SD values around $R_s = 0.4$ are well approximated by FUMI, e.g., the observed bias is 2.4% and the observed SD is 0.26%; the theoretical SD from FUMI is 0.26% (see Table 1).

Consequently, in practice, the combination of both FUMI and $P_k^{1/2}$ for the adaptive Kalman filter may be useful for evaluating the reliability of the latter. Situations often arise where a peak which interferes with a target peak is unknown and strong overlap hinders the estimation of the shape and position of the unknown peak. In these situations, FUMI cannot be calculated and the optimization of precision and efficiency [3,22–25] is no longer feasible. However, if the adaptive Kalman filter is used to provide an estimate for the peak shape of the unknown interferent, then FUMI can be calculated.

In previous studies of the optimization of liquid chromatographic analyses [3], the information loss $\delta\phi_j$ was calculated using an approximation based on truncation after the first term in a Taylor series expansion about the center of the peak. This calculation yields an optimum resolution R_s , corresponding to the maximum information, of 0.96. In contrast, the maximum information obtained in this study was obtained at a resolution of 1.31. The reason for this discrepancy is due to the fact that the use of the Taylor series approximation gives a steeper change in FUMI as the maximum FUMI is approached, compared with the calculation based on the actual Gaussian response used in this paper. Note that these values for the optimum R_s result from the use of the 0.5% tolerated interference level; if a different interference level is chosen, different optimum R_s values will be obtained.

It should be possible to relate the measurement variance, r_k , estimated for the adaptive Kalman filter (Eqn. 4) to the tolerated interference level in the analysis. Here, an interference level of 0.5% of the peak maximum of the target peak was used. This corresponds to a signal amplitude of approximately three times the standard deviation of the noise. For the conventional one-dimensional Kalman filter, this determines the point at which the filter is “shut off”. In the case

of the adaptive filter, the filter is “shut off” in a more gradual fashion, as the measured residuals rise above the predetermined noise level (W_c). If the relationship between the preset interference level and the r_k value estimated from Eqn. 4 can be determined, it should be possible to obtain an estimate for FUMI which should accurately represent the actual precision of the analysis as a function of peak overlap. This relationship will be examined more thoroughly in a future study.

The analytical limitations of the adaptive Kalman filter and the reliability of the estimates obtained from the filter have been systematically examined. In addition, the use of the information measure, FUMI, for evaluating the reliability of adaptive filter fits has been studied. Note that although simulated Gaussian peaks were used in this study, the general conclusions from this work should be applicable to any experimentally observed chromatographic peak shape. The information FUMI can also be determined for any peak shape. The results from the simulations reported here should be useful for guiding the proper use of the adaptive Kalman filter in analytical chemistry.

The authors thank Dr. Matsuda of the National Institute of Hygienic Sciences, Japan, for useful suggestions. They also acknowledge the support of the National Science Foundation (Grant CHE-8921315) for this research.

REFERENCES

- 1 R. Matsuda, Y. Hayashi, T. Suzuki and Y. Saito, *Chromatographia*, 32 (1991) 233.
- 2 D.L. Massart, B.G.M. Vandeginste, S.N. Deming, Y. Michotte and L. Kaufman, *Chemometrics: a Textbook*, Elsevier, Amsterdam, 1988.
- 3 Y. Hayashi and R. Matsuda, *Chemometr. Intell. Lab. Syst.*, (1992) in press.
- 4 L.R. Snyder, *J. Chromatogr. Sci.*, 10 (1972) 200.
- 5 J.P. Foley, *J. Chromatogr.*, 384 (1987) 301.
- 6 N. Dyson, *Chromatographic Integration Methods*, Royal Society of Chemistry, Cambridge, 1990, pp. 50–55.
- 7 A. Westerberg, *Anal. Chem.* 41 (1969) 1770.
- 8 R.E. Kalman, *J. Basic Eng.* 82 (1960) 34.
- 9 Y. Hayashi, T. Shibazaki, R. Matsuda and M. Uchiyama, *J. Chromatogr.*, 407 (1987) 59.

- 10 S.C. Rutan and S.D. Brown, *Anal. Chim. Acta*, 167 (1985) 39.
- 11 H.R. Wilk and S.D. Brown, *Anal. Chim. Acta*, 225 (1989) 37.
- 12 S.D. Brown, *Anal. Chim. Acta*, 181 (1986) 1.
- 13 S.C. Rutan, *Chemometr. Intell. Lab. Syst.*, 6 (1989) 191.
- 14 S.C. Rutan, *J. Chemometr.*, 4 (1990) 103.
- 15 S.C. Rutan, *Anal. Chem.*, 63 (1991) 1103A.
- 16 S.C. Rutan and S.D. Brown, *Anal. Chim. Acta*, 160 (1984) 99.
- 17 D.D. Gerow and S.C. Rutan, *Anal. Chim. Acta*, 184 (1986) 53.
- 18 S.C. Rutan and P.W. Carr, *Anal. Chim. Acta*, 215 (1988) 131.

- 19 Y. Hayashi, T. Shibasaki, R. Matsuda and M. Uchiyama, *Anal. Chim. Acta*, 222 (1987) 187.
- 20 Y. Hayashi, S. Yoshioka and Y. Tadeka, *Anal. Chim. Acta*, 212 (1988) 81.
- 21 Y. Hayashi, *Anal. Sci.*, 6 (1990) 15.
- 22 Y. Hayashi, R. Matsuda and A. Nakamura, *Chromatographia*, 30 (1990) 85.
- 23 Y. Hayashi and R. Matsuda, *Chromatographia*, 30 (1990) 171.
- 24 Y. Hayashi and R. Matsuda, *Chromatographia*, 31 (1991) 367.
- 25 Y. Hayashi and R. Matsuda, *Chromatographia*, 31 (1991) 374.

Deconvolution in one-dimensional chromatography by heuristic evolving latent projections of whole profiles retention time shifted by simplex optimization of cross-correlation between target peaks

Markku D. Hämmäläinen

Department of Chemistry, Swedish University of Agricultural Sciences, S-750 07 Uppsala (Sweden)

Yi-zeng Liang ¹ and Olav M. Kvalheim

Department of Chemistry, University of Bergen, N-5007 Bergen (Norway)

Roger Andersson

Department of Food Science, Swedish University of Agricultural Sciences, S-750 07 Uppsala (Sweden)

(Received 4th June, 1992; revised manuscript received 10th August 1992)

Abstract

A new approach to the detection and resolution of co-eluting components is developed for one-dimensional chromatographic analysis. In essence, the method consists of two steps. First, chromatograms from different runs are made comparable by using a simplex technique for adjusting the retention-time shifts so as to optimize the cross-correlation between selected target peaks in the chromatograms. Second, the heuristic evolving latent projections (HELP) method is used to detect and resolve co-eluting peaks in the resulting two-way data array. The new method represents a hybrid between conventional one-way and two-way resolution methods by which a collection of one-way chromatograms on samples with the same chemical components can be treated with chemometrics procedures developed for instruments with multi-wavelength detection. This permits the determination of the number of chemical components under a peak and subsequent resolution and quantification of the chemical components. Hence the hybrid method bridges the gap between traditional and coupled chromatography. The method provides the concentration pattern of each of the chemical components in different samples. In this respect, the approach makes traditional one-way chromatography an important supplement to coupled chromatography for solving problems of, e.g., peak homogeneity, in a series of samples with similar chemical components.

Keywords: Gas chromatography; Optimization methods; Cross-correlation; Deconvolution; Heuristic evolving latent projections; Simplex optimization

Correspondence to: O.M. Kvalheim, Department of Chemistry, University of Bergen, N-5007 Bergen (Norway).

¹ On leave from Department of Chemistry and Chemical Engineering, Hunan University, Changsha (China)

Despite the benefits of multi-wavelength detection [1], detectors giving one signal per retention time (e.g. gas chromatography with flame

ionization detection) are still the most common in chromatographic analysis. In complex one-dimensional chromatograms, detection of minor peaks co-eluting with major peaks and subsequent resolution and integration [2,3] for quantification are difficult and time-consuming tasks. Previous approaches for the deconvolution of overlapping peaks have mainly involved the inspection of different orders of derivatives of a single chromatogram at a time [4,5]. Although differentiation provides chromatograms with increased resolution, there are several drawbacks of such a procedure, the most serious probably being the deterioration of the signal-to-noise ratio (S/N), which decreases by a factor of ca. 2 on increasing the derivative order by one. In order to retain the S/N , smoothing has been proposed as an intermediate step, but this procedure introduces additional assumptions [6].

In many situations, series of samples with closely similar compositions are subjected to chromatographic analysis. Such sample sets are common, e.g., in process and quality control of pharmaceutical and petrochemical products. Further, in the development of manufacturing processes, design of the process variables is often coupled to single detection chromatographic analysis of the product stream. Deconvolution and integration of the chromatographic profiles and subsequent modelling of the connection between process variables and product stream can provide crucial information about the influence of process conditions on, for instance, purity or overall composition of the product.

In current implementations of the above strategy, deconvolution and peak integration are carried out for each chromatogram separately. The main reasons for this choice are tradition and the difficulty of handling several chromatographic profiles jointly because of problems imposed by retention time shifts and different backgrounds from one chromatogram to another. However, in a recent study [7], it was shown that by simplex optimization of the cross-correlation between selected peaks in a set of samples mixed from standards, retention time shifted chromatographic profiles were obtained that were amenable to joint analysis by means of latent-

variable projection methods [8–10]. In other words, the pretreatment succeeded in making the chromatographic profiles comparable.

With the whole adjusted chromatographic profiles available in digital form for series of similar samples, new possibilities arise for deconvolution in one-way chromatography. Thus, the chromatographic profiles can be subjected to a local rank examination as developed for coupled chromatography in the heuristic evolving latent projections (HELP) method [11–13]. With this development, partially overlapping and even hidden peaks can be detected in chromatograms obtained with single detection instruments. Assuming that some chromatographic selectivity exists for the co-eluting chemical components, overlapping peaks can subsequently be resolved and integrated.

The aim of this work was to assess the potential for deconvolution in one-way chromatography by simplex optimization of the cross-correlation between chromatographic profiles and two-way analysis as developed in the HELP method on the resulting retention time shifted profiles. Mixtures of known standards were analysed, which provides an interpretation of the loading vectors as carrying the information about the relative concentrations of each chemical component from one sample to another.

THEORY

Assumptions

There are two basic assumptions in the method: chromatograms must be analysed as digital profiles, as any integration procedure destroys the information about number of species under a peak (“local chemical rank”), and the chromatograms from different runs must be comparable in the sense that the signal acquired at a specific retention time must point to the same chemical component and thus that the peak shape is approximately the same for a particular chemical component from sample to sample. These assumptions suggest that one must be able to adjust chromatograms along the retention time direction to make up a consistent data matrix for

the subsequent detection and resolution procedure. An implicit assumption of the approach is that one compares a series of chromatograms obtained from similar samples. In order for “hidden” minor peaks to be detectable in the local rank analysis, the corresponding chemical species must possess some variation in their concentrations from run to run relative to the chemical species responsible for the major overlapping peaks. An assumption necessary for quantification, but not for detection, is that the chemical species are partly resolved. For the determination of the relative amounts of the chemical species in a particular sample, one must assume equal response on the detector for all species analysed. This precondition is not necessary for relative quantification of the same species in different samples as long as an internal standard is available.

An outline will now be given of how to obtain a matrix of comparable chromatographic profiles, before continuing with a description and interpretation of the necessary features for implementing the HELP method for component detection and resolution in one-way chromatography.

Retention time shifting of chromatographic profiles

As mentioned above, an important assumption for unique detection and subsequent resolution of co-eluting species is that the chromatographic digital profiles are comparable. This actually represents the most serious obstacle to the use of digital profiles in traditional one-way chromatography. Recently, Anderson and Hämäläinen [7] proposed a solution to this problem. In their procedure, the chromatograms are initially baseline-adjusted and normalized to an internal standard. The method then works as follows: a few distinct peaks in one of the chromatograms are selected as targets to be used for retention time adjustment of all the chromatographic profiles; the other chromatographic profiles are sequentially and independently adjusted until maximum correlation is obtained with the target peaks.

The optimization in the second step is performed by simplex [14]. The cross-correlation between the data points describing the target peaks

and the sample peaks is estimated separately for the selected peaks. The mean value of the correlation coefficients is used as the response in the simplex method. Further details can be obtained elsewhere [7].

Cross-correlation and local chemical rank

After adjustment for retention time shifts, the chromatograms are collected in a data matrix X . For ease of comparison with the HELP resolution procedure developed for multi-detection chromatography, each column is chosen to represent the digital chromatographic profile of one sample, and, consequently, each row the detected chromatographic concentration of the different samples at a specific retention time point. Hence retention time defines the vertical direction and the different samples the horizontal direction in the matrix X .

The transposed matrix, X' , appears similar to the common calibration matrix for estimating concentrations from spectral profiles [15]. There is, however, a distinct difference. A particular chemical species can provide widely spaced signals in the spectral direction so that neighbourhood is neither sufficient nor necessary for suggesting a single chemical source. For chromatographic profiles the situation is different. During elution, peaks arise and disappear in a continuous manner. Thus, signals at neighbouring retention time points tend to correlate, a correlation of 1.0 across a peak being indicative of a single chemical species under that peak in all chromatograms [16]. Similarly, widely spaced signals must originate from different chemical species. This observation suggests that correlation analysis of local chromatographic regions can be used to trace hidden or partly resolved peaks. However, the local correlation analysis must take into consideration that data are contaminated by noise. For this reason, a local rank analysis is performed where the significance of the correlations between signals at neighbouring retention time points is assessed by comparison with the random correlation in regions with no signals above baseline, i.e., the so-called zero-component regions [11,12].

Peak detection by local correlation analysis

The objective is now to determine the number of co-eluting chemical species (local chemical rank) under a peak or overlapping band of peaks. This task is executed by local rank analysis as illustrated in Fig. 1. Starting from the first retention point, a window of size two is moved across the matrix in the chromatographic direction. For each window, the two eigenvalues are calculated and their logarithm is plotted as a function of retention time. This procedure generates a rank map [13], showing the local rank in every retention time window. This is indicated in Fig. 2, which also shows the detection limit for eluting chemical components. The detection limit is calculated from the value of first eigenvalue in a zero-component region using an approximate *F*-test [11]. The local rank analysis is repeated with window sizes of 3, 4, etc., until the window size exceeds the highest local rank by one. This procedure, called the evolving-size moving window (ESMW) [13], is a necessary extension of the fixed-size moving window (FSMW) procedure introduced by Keller and Massart [17] in order to achieve optimum resolution power.

From the rank map, the elution time intervals can be determined for every peak. Thus, in addition to detection of the number of chemical species under a peak, the rank map provides the information about the first and last retention time of every eluting species.

Peak resolution

After detection of hidden or partially resolved peaks, the next step is the resolution of the chemical species into their corresponding pure peaks. This is basically a two-step procedure. First, the unresolved regions of the chromatograms are decomposed into principal components scores and loadings [8–10]:

$$X = TP' + E \quad (1)$$

Each retention time interval with unresolved peaks is decomposed separately and independently (local analysis) by means of Eqn. 1. The matrices *T* and *P* contain principal components scores and loadings, respectively, *P* being an orthonormal matrix (the prime implies transposition). The number of principal components used in Eqn. 1 is equal to the number of chemical species detected under the unresolved peak. The residual matrix *E* accounts for noise.

Second, a target rotation [8] is performed to obtain the chromatographic elution profile and the "sample" profile of each chemical species. The rotation matrix *R* is estimated by utilizing selective (one-component) retention time regions in combination with the so-called "zero-concentration region" (no signal above the noise limit) for each chemical species [11,13]. Thus,

$$X = TRR^{-1}P' + E \quad (2)$$

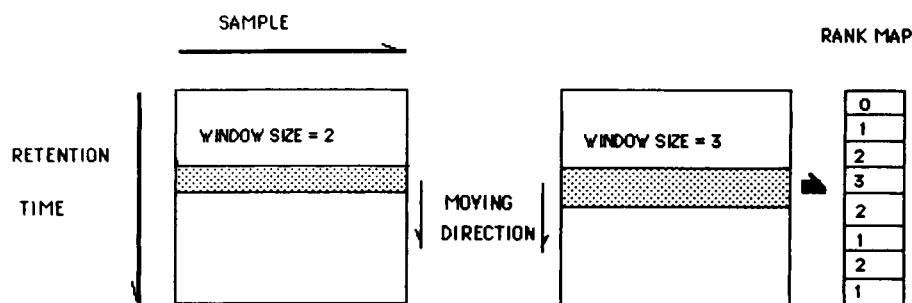


Fig. 1. Illustration showing the evolving-size moving window (ESMW) technique for window sizes of 2 and 3. Starting with a window size of 2, the local rank is calculated over the whole retention time interval. The procedure is repeated with the window size increased by one until the size exceeds the largest local "chemical" rank by one. This procedure provides a rank map with the best possible resolution of the concentration windows for the chemical components.

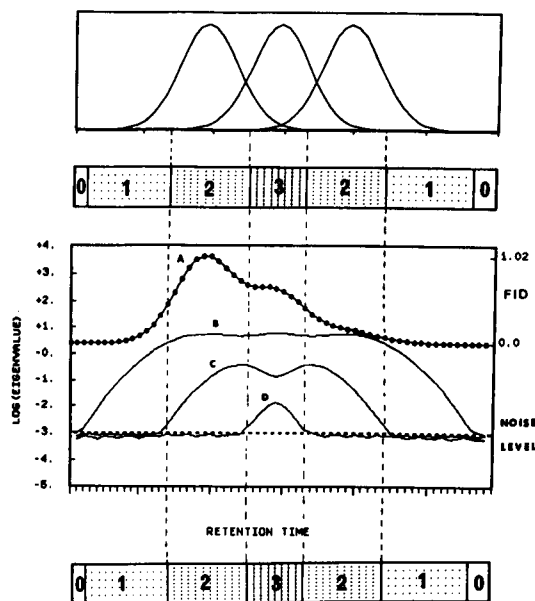


Fig. 2. Illustration showing how the rank map results from comparison of the eigenvalues of the moving window with the eigenvalue of the zero-component region. The chromatographic concentration profiles of the pure chemical components are shown at the top with the corresponding rank map underneath. At the bottom is shown the unresolved chromatographic profile (A) together with the three eigenvalue profiles (B, C, D) of the moving retention time window and the estimated detection limit (noise level). The logarithms of the eigenvalues are plotted in order to be able to compare eigenvalues differing in size by several orders of magnitude.

The chromatographic elution profiles $\{c_p\}$ and the sample profiles $\{s_p\}$ for the resolved species is now given by [11,13]

$$C = TR \quad (3a)$$

$$S' = R^{-1}P' \quad (3b)$$

In Eqns. 3a and b, the chromatographic elution profiles and sample profiles are collected in the matrices C and S , respectively.

Hence the deconvoluted peak can be expressed as

$$X_r = CS' \quad (4)$$

where the subscript r implies a reconstructed chromatogram. Each row (sample profile) in S' is standardized to unit length.

With completely hidden peaks, the above rotation procedure for unique resolution does not

apply. This means that one has to resort to classical methods for curve fitting in the resolution step. However, the crucial information about the number of chemical species at every retention time point is available, making curve-fitting procedures much more reliable than in the traditional cases where this information is absent.

Interpretation and quantification

Equation 4 is formally similar to the result obtained by using HELP to resolve two-way chromatograms obtained by analysing a single sample with a multi-detection instrument. In both one-way chromatography on a series of samples and two-way chromatography on a single sample, a column in the matrix C contains the chromatographic elution profile for a single pure chemical component. However, there is a crucial difference between the one-way and two-way cases in the interpretation of the matrix S .

For a two-way chromatogram obtained on multi-detector instruments, each row in S represents the relative absorptivities for a pure chemical component. Assuming the same total absorptivities for each chemical component, and remembering that the rows in S' are standardized to unit length, integration of the chromatographic elution profiles for the resolved components provides estimates of the detected amount I_p of each chemical species:

$$I_p = \sum c_{ip} \quad p = 1, 2, \dots, A \quad (5)$$

The summation i goes over the retention time interval with signal above the detection limit (zero-component eigenvalue) for chemical component p . In the presence of an internal standard r (and assuming the same total absorptivity for all the chemical components), absolute quantification can then be achieved by calculating the ratios $\{I_p/I_r; p = 1, 2, \dots, A\}$ (I_r is the integrated elution profile for the internal standard). If no internal standard is available, only relative concentrations can be obtained.

On the other hand, for several one-way chromatograms treated jointly the standardized matrix S contains information about amount injected and the relative amount of the chemical

components in different samples. For internal referenced samples this means that the sample direction can provide quantitative estimates of the relative concentrations of the eluting chemical component from one sample to another. The proof is as follows. For an internal standard r the absolute amount detected in all chromatogram is given by the product $I_r s'_r$. As I_r is constant for all chromatograms, the sample profile s'_r for the internal standard r contains the information about the relative amount injected for the samples (assuming a linear range for the detector). The relative amounts injected for samples $j + 1$ compared with j are given by the ratio $s_{r,j+1}/s_{rj}$. Correcting for different amounts injected, we then obtain "internal standardized sample profiles" for the other chemical components as the ratios

$$s_{pj}^r = s_{pj}/s_{rj} \quad j = 1, 2, \dots, N; p = 1, 2, \dots, A \quad (6)$$

Irrespective of whether the response at the detector is quantitative or not, or the same for the internal standard and the other chemical components, it follows from Eqn. 6 that the ratio $s_{p,j+1}^r/s_{pj}^r$ quantitates the amount of species p in sample $j + 1$ compared with sample j . Hence, the internal standardized sample profile s_p^r provides the relative concentrations of the chemical component p in the N samples. This observation means that the sample profiles can provide quantitative estimates of relative concentrations with no requirement for a quantitative detector as long as one remains within the linear range for the detector. This interpretation will also be approximately true for non-referenced chromatograms as long as the amount injected is approximately equal for different samples.

Quantification of a species p within a single chromatogram is obtained as the product of I_p/I_r and s_{pj}/s_{rj} , assuming the same response for the chemical component p and the internal standard r .

One-way versus two-way chromatography

Comparison of the above interpretation with the corresponding interpretation of a resolved two-way chromatogram of a single sample [10]

shows that while the matrix C has the same meaning in both cases, the matrix S has a very different meaning in one-way and two-way chromatography. For a two-way chromatogram obtained on multi-detector instruments, S represents the relative spectral absorptivities for the pure chemical components, whereas for several one-way chromatograms treated jointly the matrix S contains the relative amounts of the pure chemical components in the different samples. As the latter information has been shown to be quantitative in the presence of an internal standard, irrespective of component variations in response at the detector, one-way chromatography compares favourably with two-way chromatography in situations where series of samples composed of the same chemical species are analysed, at least as long as estimation of concentrations is the goal of the analysis. If component spectra are needed for the purpose of component identification, two-way chromatography is needed, but only in the identification stage of an investigation as long as series of samples composed of similar chemical components are analysed.

EXPERIMENTAL

Sample set

The sample set used in this work was mixed from three standards of xylose, arabinose and rhamnose. A four-level orthogonal design was used in the mixing of the standards in order to be able to distinguish random variation in detected impurities from systematic (designed) variation in the different isomers of the three sugar standards. Designed mixtures further simplify the evaluation of the results from the deconvolution procedure. Table 1 shows the amounts of xylose and arabinose in the mixed sample; rhamnose has been omitted as it is not further discussed in this paper.

The samples were analysed on a Packard Model 427 gas chromatograph equipped with a flame ionization detector and a CP-SIL 88 capillary column (9 m × 0.22 mm i.d.) with helium as the carrier gas at a linear flow-rate of 150 cm min⁻¹ (splitting ratio 1:20). Detailed conditions

TABLE 1

Design matrix used in the mixing of standards

| Standard No. | Xylose | Arabinose |
|--------------|--------|-----------|
| 1 | +1 | +1 |
| 2 | -1 | +1 |
| 3 | +1 | -1 |
| 4 | -1 | -1 |
| 5 | 0 | 0 |
| 6 | 0 | 0 |
| 7 | +3 | 0 |
| 8 | 0 | +3 |
| 9 | 0 | 0 |

| | Amount (mg) | | | |
|-----------|-------------|------|-----|----|
| | -1 | 0 | +1 | +3 |
| Xylose | 1 | 4.75 | 8.5 | 16 |
| Arabinose | 1 | 4.75 | 8.5 | 16 |

are given elsewhere [18]. Nelson 2600 chromatography software was used for collecting digital chromatographic elution profiles. In this work, only the digital profiles in the retention time interval from ca. 4 min 50 s to 6 min 30 s were used (Fig. 3). In this way, only peaks belonging to xylose and arabinose are included, providing two and three correlated peaks, respectively, of anomeric isomers of five- and six-membered rings in the chromatograms. Figure 3 shows the raw chromatographic profiles for the nine analysed samples before any baseline and retention time correction.

Baseline and retention time correction

Retention adjustment and baseline correction were performed by means of ChromPro software [7]. The simplex optimized cross-correlation used for retention time adjustment was performed using peaks 1 and 5 (Fig. 3) as targets. Thereafter, the digital profiles were normalized by dividing the intensity at each retention time point with the integrated intensity of an internal standard. The adjusted and normalized chromatograms are shown in Fig. 4.

Deconvolution of profiles

The digital chromatographic profiles were subjected to local rank analysis using window sizes of

2 and 3 in the HELP method. The profiles were pretreated in regions with large intensities in order to correct for the effect of increased noise with increased signal, i.e. heteroscedasticity [12,19]. After rank determination the profiles were resolved and integrated as described in the theory section.

RESULTS AND DISCUSSION

Detection of unresolved components by zero- and second-derivative chromatography

The baseline- and retention time-adjusted chromatograms were first inspected visually for unresolved chemical components. From the adjusted chromatograms (Fig. 4) incomplete resolution is obvious between peaks 3 (xylose) and 4

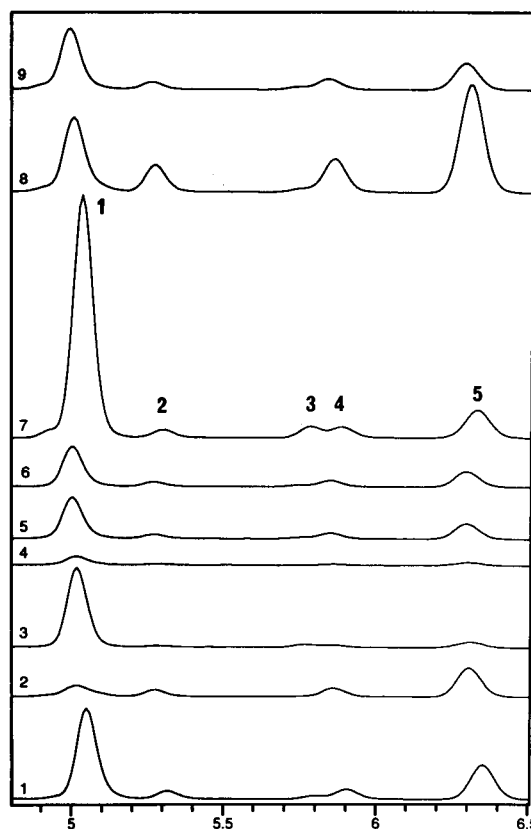


Fig. 3. Raw chromatographic profiles for the nine mixtures in Table 1. Retention time scattering is observed for the five peaks.

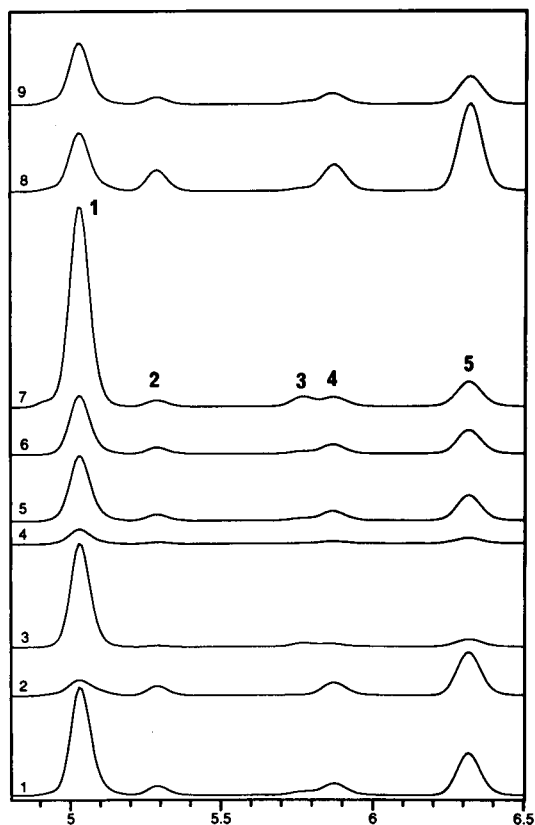


Fig. 4. Same profiles as in Fig. 3 after baseline and retention time adjustment and normalization towards an internal standard.

(arabinose). Further, a shoulder is observed at the left side of peak 1 (xylose) in samples 7 and 9. In samples 8 and 2, tailing is observed at the end of peak 1.

Figure 5a shows peak 1 in sample 2. The shape of the peak shows an unresolved chemical component at the beginning of the peak, and either a tailing or an unresolved component at the end of the peak. Inspection of the second-derivative chromatographic profile (Fig. 5b) of peak 1 in sample 2 does not add anything to this conjecture. For the other samples, visual inspection of zero- and second-derivative profiles of peak 1 is even less conclusive with respect to the presence and number of unresolved chemical components.

Estimation of lower limit of detection

The zero-component regions, i.e., regions where no chemical component elutes, were detected by local rank analysis by using a moving retention time window as described in the theory section. A window size of 2 was chosen as this choice provides the most accurate determination of the zero-component retention time intervals. The result of the local rank analysis is shown in Fig. 6. Three zero-component regions were detected. Local principal component analysis of

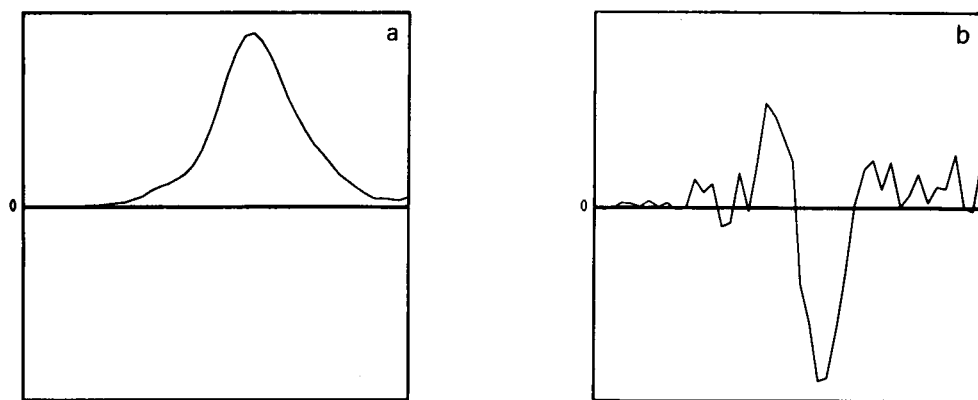


Fig. 5. (a) Zero- and (b) second-derivative chromatographic profiles of peak 1 in mixture 2 (Table 1).

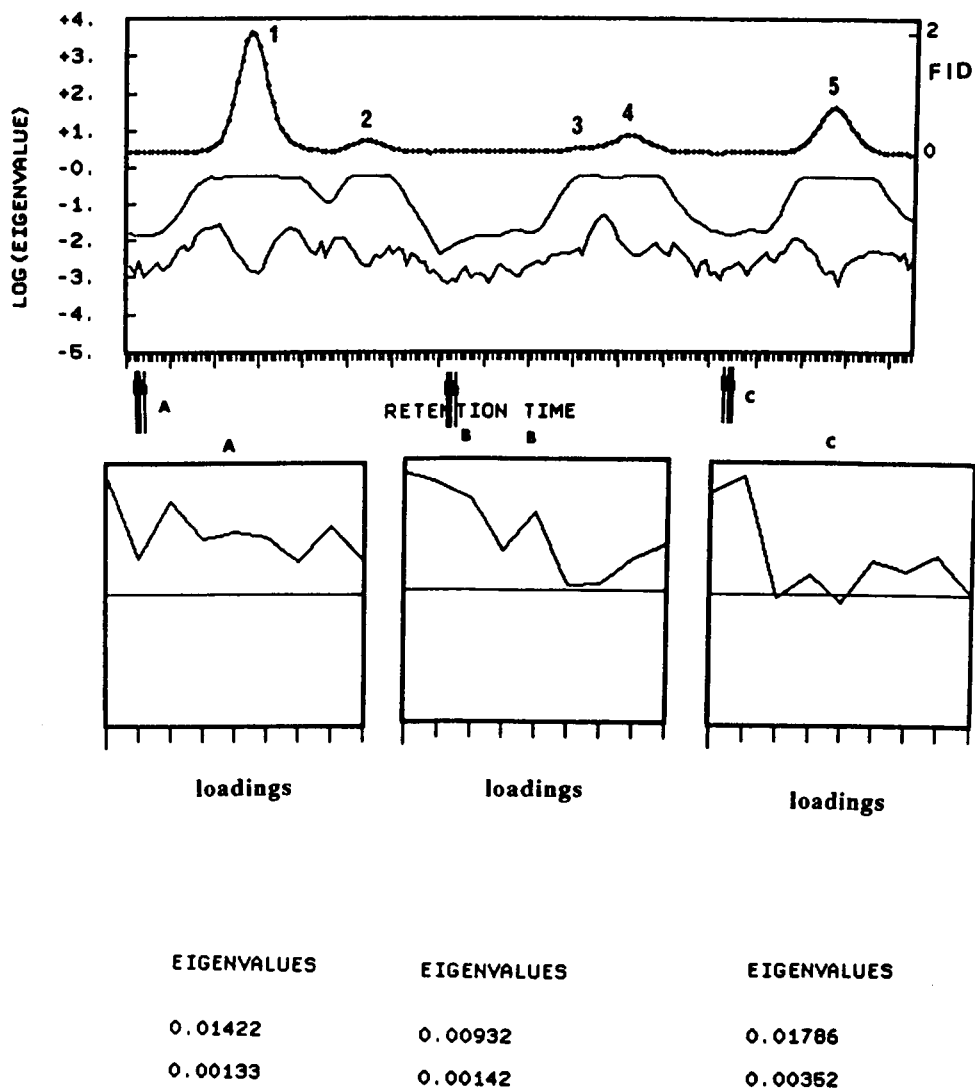


Fig. 6. Estimation of detection limit by use of the zero-component regions. The regions are located by use of a moving retention time window of size 2 to assess local chemical rank (top). Regions where both the eigenvalues are small are indicative of zero chemical rank. Local principal component analysis of the three located regions gave the eigenvalues and loading patterns for the major principal component as shown at the bottom.

the three regions gave the results for the first eigenvalue and the corresponding loadings as shown in the bottom part of Fig. 6. The eigenvalues calculated for the major principal component are of approximately the same size for all the three zero-component regions, i.e., 0.014, 0.010 and 0.018, respectively. Further, the loadings, showing the fluctuations in the noise level between samples, differ from region to region, sug-

gesting random noise and thus that the eigenvalues for the zero-component regions are representative of the noise level in the whole retention time interval examined in this investigation. Therefore, we choose for the estimation of the detection limit for chemical components the largest eigenvalue obtained for the three zero-component region. An *F*-test was used as described [11] to calculate the detection limit for

window size 2, 3, etc. Eigenvalues above this threshold are indicative of chemical components, i.e., the local chemical rank being equal to the number of eigenvalues above the threshold.

Detection of selective regions

Selective (one-component) regions are chromatographic regions where the local chemical rank, and thus the number of chemical components above the detection limit, is one. As discussed in the theory section, such regions are crucial for the unique resolution of unresolved peaks in the chromatograms. In order to achieve

the best possible resolution for the detection of one-component regions, a window size of 2 is used for the local rank analysis. Window size 2 is enough for local chemical rank one because the second eigenvalue (by definition of chromatographic selective regions) should be smaller than the detection limit. Figure 7 (top) shows five regions in the rank map with local chemical rank equal to one. This deduction is supported by the observation that the loadings (Fig. 7) for the major principal component follow the pattern of the designed concentration (Table 1). Hence, the loadings obtained for the selective regions 1 and

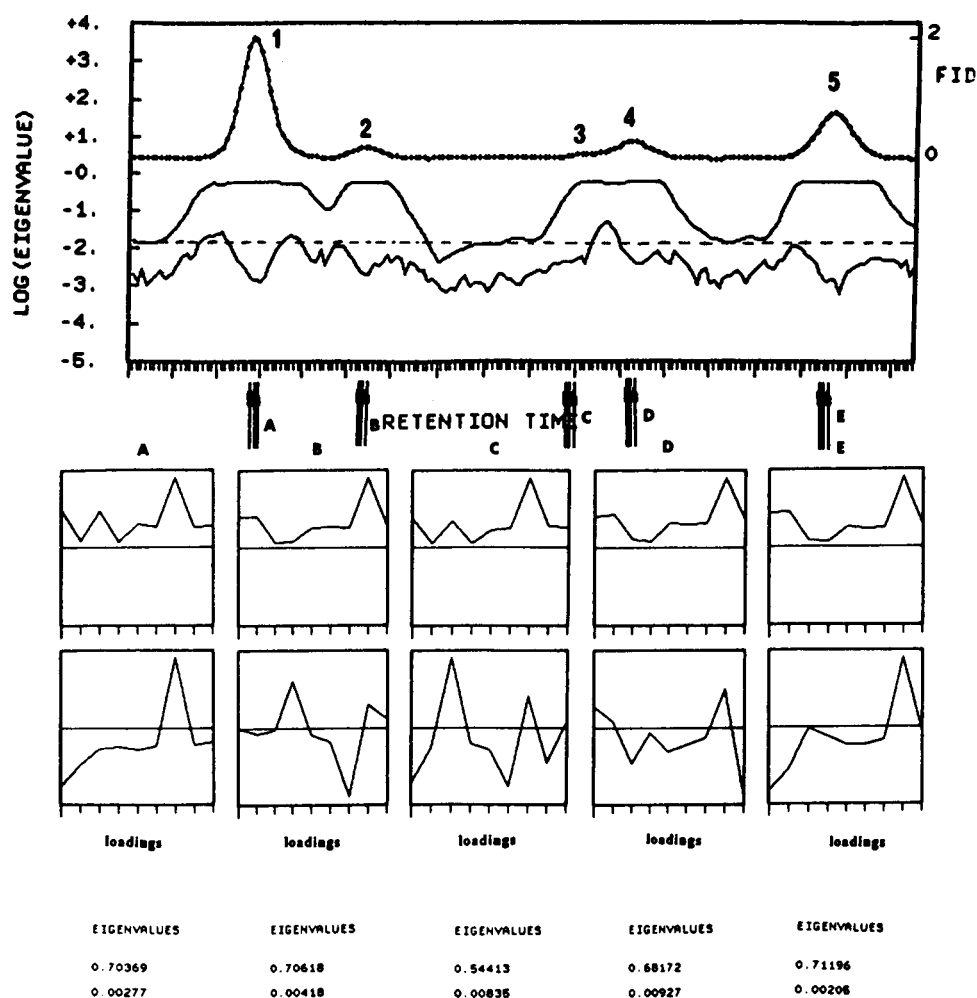


Fig. 7. Selective (one-component) regions detected in the local rank analysis. A retention time window size of 2 was used to provide the best possible resolution power. The eigenvalues and loading patterns for the two eigenvalues are shown.

3 are mutually congruent and follow the pattern of the mixed concentrations for xylose in Table 1, while regions 2, 4 and 5 are congruent and follow the mixing pattern of arabinose. Hence, the loading patterns confirm the presence of a single chemical component. Further, as the second eigenvalue for the suspected one-component regions is always smaller than the detection limit and as the loadings (Fig. 7) for the second principal component show no systematic pattern, we conclude that the five regions are really one-component regions.

Evolving size moving window

Local rank analysis reveals three regions where the second eigenvalue exceeds the eigenvalue of the zero-component regions. In this case, the number of chemical components is at least two, but it may even be three or more. In order to find the exact chemical rank in these regions, the window size is increased by one and a new local rank analysis run. The result is shown in Fig. 8. In the regions with at least two chemical components, the third eigenvalue is always below the zero-component threshold, confirming that the number of chemical components really is two in these regions. Should the local rank analysis reveal regions with three co-eluting chemical com-

ponents, one would have increased the window size to four and repeat the analysis. This procedure guarantees at the same time the best possible resolution and that no component above detection limit passes undetected in the rank analysis.

Deconvolution and quantification

The local rank analysis has revealed two minor chemical components co-eluting with xylose (peak 1). Local principal component analysis of the two regions where the small components are dominating the major xylose peak, i.e., at the beginning of peak 1 for the first and at the end of peak 1 for the second, shows that the loading pattern of the first principal component in both local regions (Fig. 9) differs strongly from the mixing patterns in the design matrix (Table 1). Further, there is no mutual similarity between the loading pattern of the principal component for the two regions with co-elution under peak 1. These observations strongly suggest that the two minor species are impurities from the derivation steps in the work-up of the standards. As both impurities are completely overlapped by the major component, one cannot resolve the peak uniquely by using the procedure developed in the HELP method [11] or any other currently existing resolution procedure.

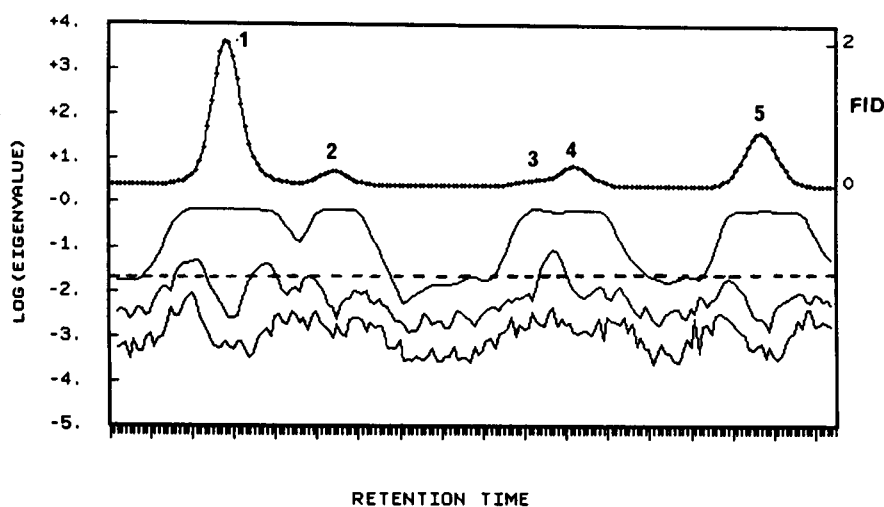


Fig. 8. Logarithms of the eigenvalues and the average chromatographic profile plotted as a function of retention time. A window size of three was used for the calculation. The largest eigenvalue from the zero-component region has been drawn to aid in the visual detection procedure.

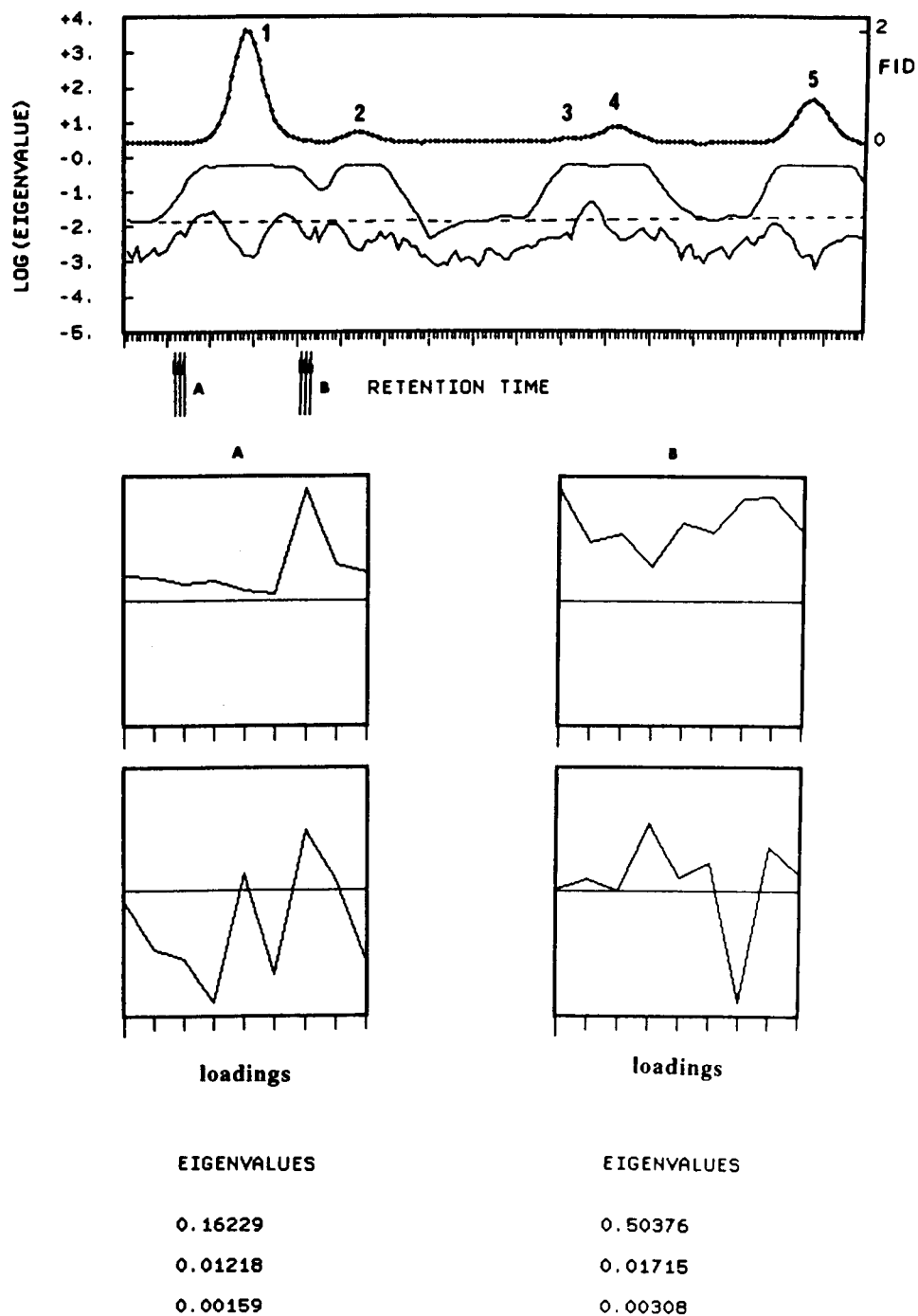


Fig. 9. Unresolved regions detected in the local rank analysis. A retention time window size of 3 was used for the calculation of the eigenvalues and loading patterns in the regions at the beginning and at the end of peak 1. In these local regions the minor chemical components dominate over the xylose isomer.

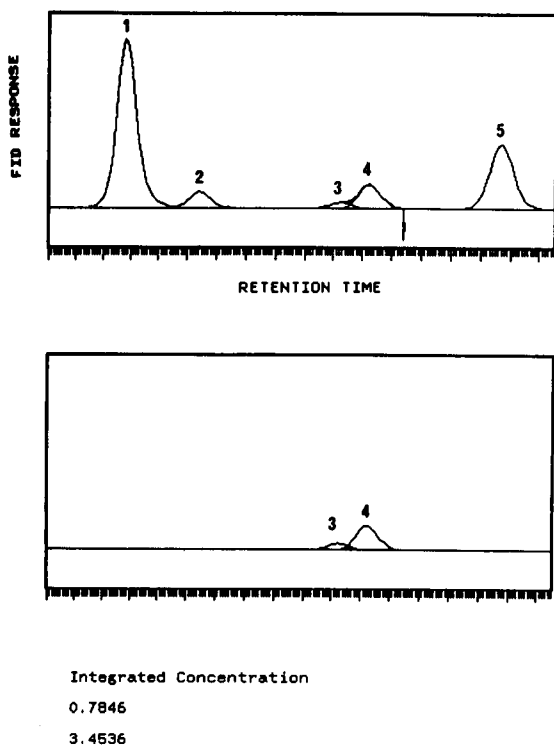


Fig. 10. Resolved concentration profiles for the overlapping peaks 3 (xylose) and 4 (arabinose) in mixture 7.

The overlapping peaks 3 and 4, however, both possess selective chromatographic regions, meaning that unique resolution and quantification are possible as described in the theory section. Figure 10 contains the resolved peaks 3 and 4 for sample

TABLE 2

Estimated amounts of the isomers under peaks 3 (xylose) and 4 (arabinose)

| Standard No. | Amount (mg) | |
|--------------|-------------|-----------|
| | Xylose | Arabinose |
| 1 | 1.31 | 4.70 |
| 2 | 0.20 | 5.00 |
| 3 | 1.19 | 1.13 |
| 4 | 0.17 | 0.94 |
| 5 | 0.78 | 3.45 |
| 6 | 0.83 | 3.37 |
| 7 | 3.15 | 3.71 |
| 8 | 0.93 | 10.00 |
| 9 | 0.89 | 4.04 |

5. The integrated amounts for all samples are given in Table 2. Comparison of the results in Table 2 with the mixed amounts in Table 1 (column 1 corresponds to peak 3, xylose, and column 2 to peak 4, arabinose) shows excellent agreement for the relative amounts. For instance, the ratio between sample 7 and samples 2 and 4 in xylose is close to 16, the exact ratio between the +3 and -1 level in the design (see Table 1). For arabinose, the agreement is excellent except for the -1 level, which shows higher amounts than expected. Note that the two resolved peaks correspond to isomers of xylose and arabinose representing only ca. 1% of the total amount of the two standards. Further, only the relative amounts between samples can be compared as the absolute amount of each isomer depends on the equilibria between the different isomers. This is exactly the information contained in the loadings S obtained for the selective regions of peaks 3 and 4. Figure 7 shows that the patterns of the loadings for the selective part of peaks 3 and 4 follow the mixing pattern in Table 1 for the two standards.

Conclusions

The traditional way of handling one-way chromatograms is to resolve and integrate the chromatograms one by one. The integrated peaks are then retention time shifted and series of similar samples can be collected in a data matrix and analysed jointly by chemometrics techniques. The major drawback of this procedure is that all information about local chemical rank is lost.

In this work, it has been shown that with proper methods for retention time adjustment and baseline adjustment [7], it is possible to determine in a series of one-way chromatograms the number of chemical components eluting in any local retention time region. For this task, an evolving-size moving window procedure is used [13]. This represents a natural extension of the fixed-size moving window method developed by Keller and Massart [17], but with enhanced resolution power. Further, unique resolution and quantification are possible if at least two consecutive retention time points are selective for co-eluting chemical components [11].

The use of whole retention time adjusted chromatographic profiles in combination with procedures developed in the HELP method opens up new possibilities for one-way chromatography, e.g., testing of peak purity in a series of samples. Chromatographic systems with a single flame ionization detector provide more quantitative results than the multi-detector diode-array systems.

Yi-zeng Liang is grateful for a postdoctoral fellowship from the Royal Norwegian Council for Scientific and Industrial Research (NTNF).

REFERENCES

- 1 N. Ostojic, *Anal. Chem.*, 46 (1974) 1653.
- 2 A.N. Papas and T.P. Tougas, *Anal. Chem.*, 62 (1990) 234.
- 3 J.P. Foley, *J. Chromatogr.*, 384 (1987) 301.
- 4 A.F. Fell, H. Scott, R. Gill and A.C. Moffat, *J. Chromatogr.*, 273 (1983) 3.
- 5 A.F. Fell, H. Scott, R. Gill and A.C. Moffat, *J. Chromatogr.*, 282 (1983) 123.
- 6 T.C. O'Haver and T. Begley, *Anal. Chem.*, 53 (1981) 1876.
- 7 R. Andersson and M.D. Hämäläinen, *Anal. Chem.*, submitted for publication.
- 8 E.R. Malinowski and D.G. Howery, *Factor Analysis in Chemistry*, Wiley, New York, 1980.
- 9 S. Wold, K. Esbensen and P. Geladi, *Chemometr. Intell. Lab. Syst.*, 2 (1987) 37.
- 10 O.M. Kvalheim, *Chemometr. Intell. Lab. Syst.*, 4 (1988) 11.
- 11 O.M. Kvalheim and Y.-z. Liang, *Anal. Chem.*, 64 (1992) 936.
- 12 Y.-z. Liang, O.M. Kvalheim, H.R. Keller, D.L. Massart, P. Kiechle and F. Erni, *Anal. Chem.*, 64 (1992) 946.
- 13 Y.-z. Liang, O.M. Kvalheim, A. Rahmani and R.G. Brerton, *J. Chemometr.*, in press.
- 14 E. Morgan and K. Burton, *Chemometr. Intell. Lab. Syst.*, 8 (1990) 97.
- 15 H. Martens and T. Næs, *Multivariate Calibration*, Wiley, Chichester, 1989.
- 16 J.M. Halket, *J. Chromatogr.*, 175 (1979) 229.
- 17 H.R. Keller and D.L. Massart, *Anal. Chim. Acta*, 246 (1991) 279.
- 18 M.D. Hämäläinen, O. Theander, E. Nordkvist and I.E. Ternrud, *Carbohydr. Res.*, 207 (1990) 167.
- 19 H.R. Keller, D.L. Massart, Y.-z. Liang and O.M. Kvalheim, *Anal. Chim. Acta*, 263 (1992) 29.

Assessment of environmental water with fuzzy cluster analysis and fuzzy recognition

Guo Nan Chen

Department of Chemistry, Fuzhou University, Fujian (China)

(Received 4th April 1992; revised manuscript received 23rd July 1992)

Abstract

On the basis of describing the basic principles of fuzzy cluster analysis and fuzzy recognition, the procedure of fuzzy cluster analysis and fuzzy recognition for assessment of environmental water was simulated on a computer. The computer program was written in BASIC and implemented on an Apple II computer. A set of data for environmental water samples was used to test the mathematical models and computer program. The results were basically in agreement with the experimental assessment.

Keywords: Pattern recognition; Cluster analysis; Fuzzy cluster analysis; Fuzzy recognition; Waters

Both pattern recognition and cluster analysis are multivariate analytical methods, their applications in analytical chemistry constituting the important branch of chemometrics [1–4]. The important aims of analytical chemical research are the collection, treatment and assessment of data. Modern analytical chemistry techniques provide the possibility of obtaining large amounts of information for several phenomena at the same time. For example, advanced automation in clinical chemistry enables one to determine an important number of biochemical parameters in blood and urine samples within a few hours. Chromatographic techniques permit the identification and determination of large numbers of compounds in only one run. For each sample analysed, a set of results is obtained. As groups of similar samples will have similar patterns, they can be used to identify groups of similar objects or they can be used to characterize a group of similar objects in

order to enable one to classify a new object in the group to which it belongs. However, the difficult problem is how to use so much information correctly. The use of cluster analysis and pattern recognition is indispensable in the treatment of information in an optimum way.

The purpose of this work was to evaluate the quality of environmental water by cluster analysis and pattern recognition. From the analysis of samples of environmental water, a large amount of information is obtained that can be used to evaluate the quality of environmental water. In addition to collecting the information on the samples, it is also the responsibility of the analytical chemist to use the information to make a correct assessment of the quality of the environmental water. As there are several sources of uncertainty in the data from the environmental units, including inaccurate measurements, random occurrences and vague descriptions, the assessment of quality of environmental units can be reasonably uncertain. Traditional cluster analysis and pattern recognition do not seem to be very suitable for treating this problem. Fuzzy clustering and

Correspondence to: Guo Nan Chen, Chemistry Department, La Trobe University, Bundoora, Victoria, 3083 (Australia) (present address).

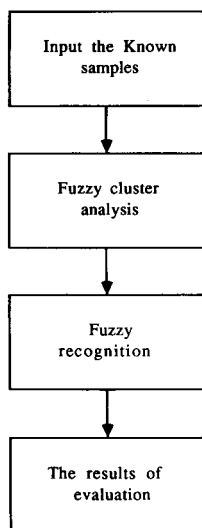


Fig. 1. Procedure for evaluation of environmental water.

recognition techniques have significant advantages over conventional methods, and have been used in geology, biology and medicine [4–7]. In this paper, fuzzy clustering and recognition techniques are recommended for the assessment of environmental water. On the basis of describing the basic principles of fuzzy cluster analysis and fuzzy pattern recognition, a computer program adapted to an Apple II computer was written in BASIC. A typical application to the assessment of environmental water is described.

BASIC PRINCIPLES

As far as the assessment of environmental water is concerned, the classification of the environmental units is the most important step. On the basis of dividing the environmental units into different groups, the recognition techniques are then used to evaluate these groups. The whole procedure is set out in Fig. 1. The basic principles of fuzzy cluster analysis and fuzzy recognition are described below. The symbols used are defined at the end of the paper.

Principle of fuzzy cluster analysis

Cluster analysis is a statistical method for the classification according to the qualitative and

quantitative characteristics of the objects to be analysed. In the view of set theory, a cluster is considered as a number of similar things gathered together. Then, the primary objective of the clustering technique would be to classify a given set of items by assigning them to a reasonably small number of homogeneous clusters. The term homogeneous in this context means that all items in the same cluster are similar to each other and are not similar to items in other clusters. Homogeneous also implies that members within each cluster are sufficiently alike to justify ignoring the individual differences between them. The key problem in clustering is to build up a suitable fuzzy relation to model the similitude between any two items [8,9].

According to fuzzy set theory, if X is an arbitrary set, a relation is a subset of the cartesian product $X \times X$, which can be denoted as

$$R: X \times X$$

where R can be represented as a fuzzy relation matrix, the elements of which are referred to r_{ij} , $i, j = 1, 2, \dots, n$. Here r_{ij} should be possessed of:

- (i) reflexivity: $r_{ij} = 1$
- (ii) symmetry: $r_{ij} = r_{ji} \quad 0 \leq r_{ij} \leq 1$
- (iii) transitivity: $R \cdot R \leq R$.

The fuzzy relation between these three properties is called the fuzzy equivalence relation. There are fuzzy equivalence relations among the elements of the same cluster, and vice versa.

Where the result of $R \cdot R$ is also defined as a matrix, referred to S , its elements S_{ij} are calculated by the following expression:

$$S_{ij} = \bigvee_{k=1}^n (r_{ik} \wedge r_{jk})$$

where \wedge and \bigvee mean if I and J are real numbers,

$$I \wedge J = \min(I, J)$$

$$I \bigvee J = \max(I, J)$$

The concept behind transitivity is that the shorter the chain, the stronger is the relation. In particular, the strength of the link between two elements must be greater than or equal to the

strength of any indirect chain [10]. Before proceeding with fuzzy cluster analysis, a fuzzy similarity relation, which is normally reflexive and

symmetric but not transitive, must be developed. However, the fuzzy cluster analysis is performed on the basis of fuzzy equivalence relation, so the

TABLE 1

Some mathematical models for developing fuzzy similar relations

(1) Euclidean distance:

$$r_{ij} = \sqrt{\frac{1}{n} \sum_{k=1}^n (X_{ik} - X_{jk})^2}$$

(3) Correlation coefficient

$$r_{ij} = \frac{\sum_{k=1}^m (X_{ik} - \bar{X}_i) \cdot (X_{jk} - \bar{X}_j)}{\sqrt{\sum_{k=1}^m (X_{ik} - \bar{X}_i)^2} \cdot \sqrt{\sum_{k=1}^m (X_{jk} - \bar{X}_j)^2}}$$

where

$$\bar{X}_i = \frac{1}{m} \sum_{k=1}^m X_{ik}; \quad \bar{X}_j = \frac{1}{m} \sum_{k=1}^m X_{jk}$$

(4) Exponent similarity coefficient

$$r_{ij} = \frac{1}{m} \sum_{k=1}^m \exp \left[-\frac{3}{4} \frac{(X_{ik} - X_{jk})^2}{S_k^2} \right]$$

where S_k is a proper positive number

(6) Arithmetic mean minimum:

$$r_{ij} = \frac{\sum_{k=1}^m \text{Min}(X_{ik}, X_{jk})}{\frac{1}{2} \sum_{k=1}^m (X_{ik} + X_{jk})}$$

(8) Absolute value exponent:

$$r_{ij} = \exp \left(-\sum_{k=1}^m |X_{ik} - X_{jk}| \right)$$

(10) Cosine:

$$r_{ij} = \frac{\sum_{k=1}^m X_{ik} - X_{jk}}{\sqrt{\left(\sum_{k=1}^m X_{ik}^2 \right) \left(\sum_{k=1}^m X_{jk}^2 \right)}}$$

(2) Scalar product:

$$r_{ij} = \begin{cases} 1 & (i=j) \\ \frac{1}{M} \sum_{k=1}^n X_{ik} \cdot X_{jk} & (i \neq j) \end{cases}$$

where M is a proper positive number

(5) Maximin:

$$r_{ij} = \frac{\sum_{k=1}^m \text{Min}(X_{ik}, X_{jk})}{\sum_{k=1}^m \text{Max}(X_{ik}, X_{jk})}$$

(7) Geometric mean minimum:

$$r_{ij} = \frac{\sum_{k=1}^m \text{Min}(X_{ik}, X_{jk})}{\sum_{k=1}^m \sqrt{X_{ik} \cdot X_{jk}}}$$

(9) Absolute value reciprocal:

$$r_{ij} = \begin{cases} 1 & (i=j) \\ \frac{M}{\sum_{k=1}^m |X_{ik} - X_{jk}|} & (i \neq j) \end{cases}$$

where M is properly selected to let $0 \leq r_{ij} \leq 1$

(11) Absolute value subtraction:

$$r_{ij} = \begin{cases} 1 & (i=j) \\ 1 - C \sum_{k=1}^m |X_{ik} - X_{jk}| & (i \neq j) \end{cases}$$

fuzzy similarity relation must be transferred to the fuzzy equivalence relation before fuzzy cluster analysis can be carried out.

The general procedures of cluster analysis are described as follows [11]:

(i) Develop a similarity relation matrix R of the environmental units. The similarity relation is a fuzzy relation, which is based on the physical or geometical meaning. There are many methods for developing the similarity relation and an appropriate method can be selected for a specific situation. In the present paper, eleven methods for developing fuzzy similarity relations are examined and are shown in Table 1

(ii) Transfer the similar relation matrix to the fuzzy equivalence relation matrix. The method for transformation is to obtain the square of R , i.e. $R \cdot R = R^2$, and $R^2 \cdot R^2 = R^4, \dots$, until $R^{(2^t)} \leq R^{[2(t-1)]}$, $R^{[2(t-1)]}$ becomes the fuzzy equivalence relation.

(iii) Perform cluster analysis with the fuzzy equivalence relation. All the elements of the $R^{[2(t-1)]}$ are arranged in order from largest to smallest, and a λ level set is then obtained ($0 \leq \lambda \leq 1$). The fuzzy equivalence matrix is transferred to a normal logical matrix by the λ level set, i.e.,

$$R_\lambda = \begin{cases} 1 & r_{ij} \geq \lambda \\ 0 & r_{ij} < \lambda \end{cases}$$

In fuzzy set theory, the clusters are changed by selecting different λ levels, a different approach to that followed in ordinary set theory. When λ is from 1 to 0, the cluster then becomes rough gradually, so a dynamic cluster graph can be obtained by selecting a different λ level.

Principle of fuzzy recognition

There are two approaches to performing pattern recognition for environmental units: one is singular recognition and the other is group recognition. These two techniques are described below.

In the first technique, the singular recognition of an environmental unit proceeds on the basis of the membership rule [12]. In set theory, the whole objects studied are called a universe of discourse, U , each object is called the element x and A is a subset of U . One usually indicates that the ele-

ment x of U is a member of A using the symbol \in :

$$x \in A$$

The membership relation between x and A can be described by a function $A(x)$, whose value indicates whether x is a member of A :

$$A(x) = \begin{cases} 1 & \text{if } x \in A \\ 0 & \text{if } x \notin A \end{cases}$$

In order to determine the function, a mapping F from U into $\{0, 1\}$ should be developed:

$$F : U \rightarrow \{0, 1\}$$

where mapping F is called the membership function of the subset A . The membership function only takes the values 0 or 1 in classical set theory, but the membership function may take any value in the interval $[0, 1]$ in fuzzy set theory. Thus mapping F will be

$$F : U \rightarrow [0, 1]$$

The membership function can be estimated from statistical data [9,10]. As far as environmental quality is concerned, each pollution level can be seen as a fuzzy subset A in the universe of discourse U made by all environmental units, and each pollution index, x , is a fuzzy variable in universe of discourse U . It has been verified that the possibility distribution of pollution level induced by x on the universe of discourse U can be described by the following membership function [9,13]:

$$A(x) = \exp \left[- \left(\frac{x - a}{b} \right)^2 \right]$$

i.e., the membership value of the j th environmental factor X_j for the i th pollution level A_i is

$$A_{ij}(x_j) = \exp \left[- \left(\frac{x_j - a_{ij}}{b_{ij}} \right)^2 \right]$$

where the parameters a_{ij} and b_{ij} can be calculated by the following equations:

$$a_{ij} = \frac{1}{n} \sum_{k=1}^n x_{ijk}$$

$$b_{ij} = \sqrt{\frac{1}{n-1} \sum_{n=1}^n (x_{ijk} - a_{ij})^2}$$

where i is the pollution level, j the environmental factor, n the number of the j th environmental

factor for the i th pollution level, k the k th environmental units in the i th pollution level and x_{ijk} the index of the j th environmental factor of the k th environmental unit in the i th pollution level.

For example, assume that an environmental unit involves four factors, with indices X_1 , X_2 , X_3 and X_4 . These indices are respectively substituted into the membership function of different environmental levels, and the membership values $A_{ij}(x_j)$ are then obtained. Let

$$L_i = \min A_{ij}(x_j) \\ (i = 1, 2, 3, \dots, n); 1 \leq j \leq 4$$

If

$$L_{i_0} = \text{Max } S_i \quad 1 \leq i \leq n$$

then this unit belongs to the i_0 th level.

The second technique is group recognition, which is performed using the nearest prototype decision rule [12]. Assume that A is the membership function of a factor for a certain level, which is a Gaussian distribution with parameters (a_1, b_1) , and B is a membership function of a group, which is also a Gaussian distribution with parameters (a_2, b_2) . Thus, the closing degree of A and B is referred to as

$$(A, B) = \left\{ 1 + \exp \left[- \left(\frac{a_1 - a_2}{b_1 - b_2} \right)^2 \right] \right\} / 2$$

The closing degree between B and factor A_{ij} of each level is calculated, and recognition can then be carried out by the nearest prototype decision rule.

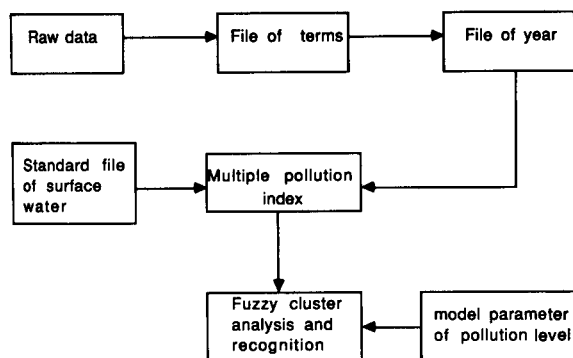


Fig. 2. File system.

TABLE 2

Pollution indices

| Element | Factor | | |
|---------|-------------------|--------------------|------------------------|
| | Organic pollution | Metallic pollution | non-metallic pollution |
| 1 | 0.686 | 0.157 | 0.534 |
| 2 | 0.632 | 0.130 | 0.399 |
| 3 | 0.663 | 0.675 | 0.412 |
| 4 | 0.548 | 0.137 | 0.417 |
| 5 | 0.518 | 0.116 | 0.429 |
| 6 | 2.314 | 0.158 | 0.443 |
| 7 | 0.513 | 0.124 | 0.411 |
| 8 | 0.508 | 0.167 | 0.437 |
| 9 | 0.439 | 0.144 | 0.442 |
| 10 | 0.464 | 0.224 | 0.444 |
| 11 | 0.496 | 0.141 | 0.431 |
| 12 | 0.488 | 0.139 | 0.489 |
| 13 | 1.043 | 0.135 | 0.644 |

The nearest prototype decision rule is defined as follows: assume that a group contains four factors, B_1 , B_2 , B_3 and B_4 . Their typical membership function is the same as A_{ij} . The closing degree between B and A_{ij} is easily calculated:

Let

$$L_i = \text{Min} \{ (A_{ij}, B) \} \\ i = 1, 2, 3, \dots, n; j = 1, 2, 3, 4; 1 \leq j \leq 4$$

If

$$L_{i_0} = \text{Max } S_i \quad 1 \leq i \leq n$$

then this group belongs to the i_0 th level. As usual, the singular recognition is used for the small cluster (less than three elements), and the group recognition is used for a large group (not less than three elements).

COMPUTER SIMULATION

The file system

The analysis of environmental water samples always provides a great deal of information, and this information cannot be used directly for cluster analysis and pattern recognition. It should be properly treated before it is used. Thus, the file system used in this work consisted not only of raw data but also a significant amount of indirect information. The file system is shown in Fig. 2, where all files are indirect information except the

raw data and standard file of surface water. The raw data file cannot be used as the known samples for cluster analysis, it must be transferred to the pollution index. The method of multiple pollution index is adopted in this work, which is described as follows:

$$P = \frac{1}{n} \sum_{i=1}^n p_i \quad P_i = C_i/T_i$$

where P is the multiple pollution index of the environmental water, n the number of pollution factors, p_i the pollution index of a certain pollution factor, C_i the measured concentration of a certain pollution factor and T_i the standard concentration of surface water of a certain pollution factor.

Computer program for fuzzy cluster analysis and fuzzy recognition

On the basis of the mathematical principles described above, a program for both fuzzy cluster

analysis and fuzzy recognition was written in BASIC and implemented on an Apple II computer. The program was designed to perform the fuzzy cluster analysis first and then to proceed immediately with the fuzzy recognition. A flow chart for this program is shown in Fig. 3. The flow chart is explained as follows.

M is the number of the environmental units and N is the number of the multiple pollution index which is involved in each unit. They are input by man-machine dialogue according to practical necessity.

The procedure for the cluster analysis is in two parts: first, to determine the degree of similarity among classified objects, and second, to select a suitable method for classification. There are several mathematical models that can be used for selection, and the result is usually dependent on the selected models. Therefore, the correct classification can only be obtained by selecting the correct model based on the environmental char-

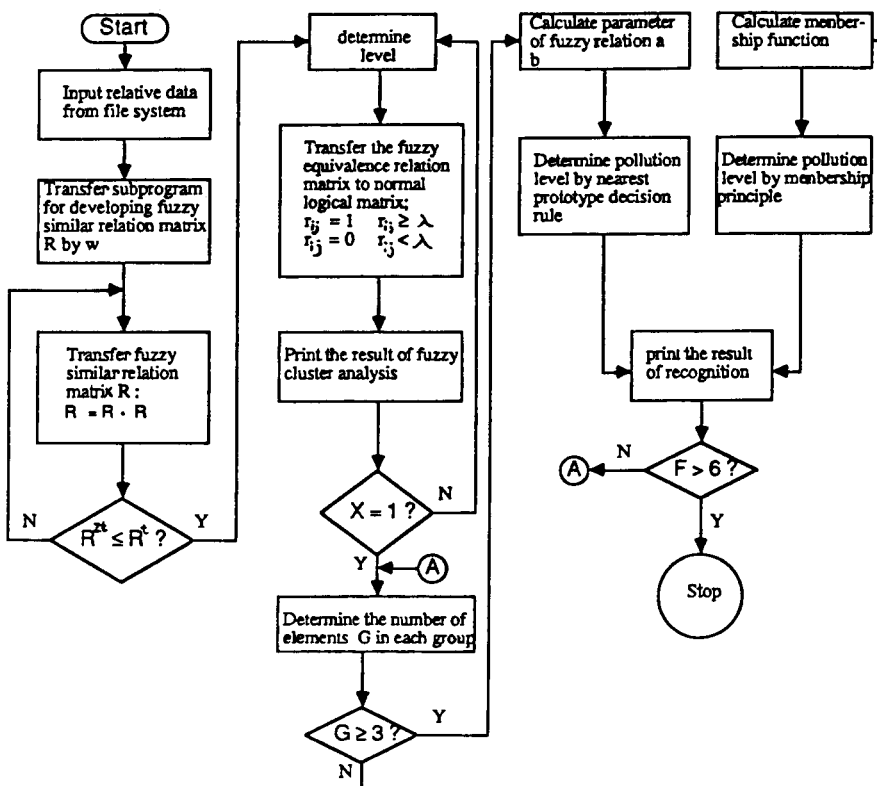


Fig. 3. Flow chart of program for fuzzy cluster analysis and recognition.

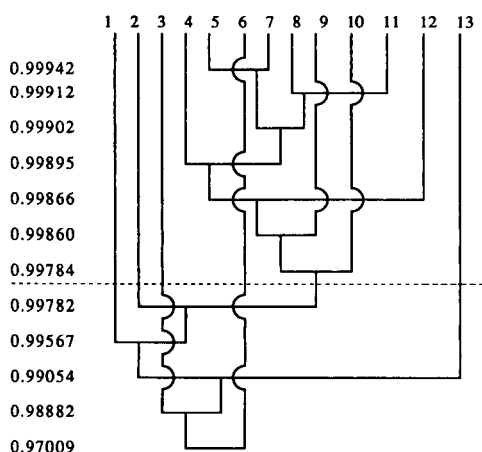


Fig. 4. Dynamic cluster graph.

acteristics. Eleven equations are recommended for the development of fuzzy similarity relations in this paper (see Table 1). W in the flow chart is used with a switching statement, which is input by man-machine dialogue. The user can select different W ($0 \leq W \leq 11$) to transfer a suitable sub-program for developing the fuzzy similarity relation matrix.

If the number of environmental units is < 3 the singular recognition is used, otherwise the group recognition is used. Such a combination of the singular recognition with the group recognition makes the program capable of tracing the results of dynamic cluster analysis.

F in the flow chart is a symbol to indicate the degree of tracing the dynamic cluster analysis by fuzzy recognition. Although F used in this in-

stance is ≥ 6 , users can select any number smaller than M depending on their own requirements.

APPLICATION TO ENVIRONMENTAL WATER

In order to test the mathematical model and computer program, a set of data from part of the Min River (China) was used for fuzzy cluster analysis and fuzzy recognition. The whole procedure and results are described below.

Fuzzy cluster analysis

The data set consisted of the accumulated results from six sampling events over a 12-month period. Thirteen sampling sites were involved in this part of Min River, each site involving at least three measurement points across the width of the river. At each measurement site, sixteen pollution factors were recorded. For these factors, oil, BOD₅, COD, phenol and benzene hexachloride were included in the organic pollutant factor, Cd, Pb, Cu, Hg and Cr were included in the metallic pollutant factor and As, CN⁻, dissolved oxygen (DO), NH₃-N, NO₃-N and NO₂-N were included in the non-metallic pollutant factor. The pollutant indices were calculated by the method of multiple pollution index, based on the standards for surface water in China. The pollution indices are presented in Table 2.

Although eleven models were examined in this paper, the results showed that the methods of absolute value reduction, absolute value index, absolute value reciprocal, exponent similarity co-

TABLE 3

Results of fuzzy cluster analysis

| Number of cluster | I | II | III | IV | V | VI |
|-------------------|---|----|-----|---------------------------|---|----|
| Element | 1 | 2 | 3 | 4, 5, 7, 8, 9, 10, 11, 12 | 6 | 13 |

TABLE 4

Division of pollution levels

| | Level | | | | |
|-------------------|------------|---------|---------|---------|---------|
| | Most heavy | Heavy | Middle | Light | Clean |
| Organic pollution | > 2.0 | 1.0–2.0 | 0.7–1.0 | 0.5–0.7 | < 0.5 |

TABLE 5
Indices for a typical sample

| Level | Factor | | |
|------------|-------------------|--------------------|------------------------|
| | Organic pollution | Metallic pollution | Non-metallic pollution |
| Most heavy | 2.314 | 0.675 | 0.644 |
| | 2.210 | 0.487 | 0.637 |
| Heavy | 2.100 | 0.300 | 0.631 |
| | 1.942 | 0.288 | 0.626 |
| Light | 1.493 | 0.241 | 0.571 |
| | 1.043 | 0.225 | 0.534 |
| Clean | 0.686 | 0.167 | 0.489 |
| | 0.663 | 0.158 | 0.444 |
| | 0.632 | 0.157 | 0.443 |
| | 0.548 | 0.144 | 0.442 |
| | 0.518 | 0.141 | 0.437 |
| | 0.513 | 0.139 | 0.431 |
| | 0.508 | 0.137 | 0.429 |
| | 0.496 | 0.135 | 0.417 |
| | 0.488 | 0.130 | 0.412 |
| | 0.464 | 0.124 | 0.411 |
| | 0.439 | 0.116 | 0.399 |

mental water, and it possesses evident level differences in the selected typical environmental units, the indices of organic pollutions are selected as a basis for dividing pollution levels. The results are given in Table 4.

On the basis of such a division, typical samples are given in Table 5. The model parameters of pollution level, a and b , are calculated and are given in Table 6.

The results of fuzzy recognition show that if $\lambda = 0.97009$, all thirteen units can be seen as a classification (see Fig. 4). As a result, the first conclusion can be drawn, i.e. this part of the Min River belong to the "light" level on the whole. If $\lambda = 0.99784$, the thirteen units can be divided into six groups, and the results of recognition are given in Table 7. From Table 7 the second con-

TABLE 6
Model parameters of pollution levels

| Level | Parameter | Factor | | |
|------------|-----------|-------------------|--------------------|------------------------|
| | | Organic pollution | Metallic pollution | Non-metallic pollution |
| Most heavy | a | 2.208 | 0.487 | 0.637 |
| | b | 0.107 | 0.188 | 0.007 |
| Heavy | a | 1.493 | 0.251 | 0.577 |
| | b | 0.450 | 0.033 | 0.046 |
| Light | a | 0.581 | 0.149 | 0.445 |
| | b | 0.077 | 0.012 | 0.020 |
| Clean | a | 0.472 | 0.126 | 0.410 |
| | b | 0.026 | 0.008 | 0.008 |

clusion can be drawn, i.e. most units belong to the "light" level and only some units belong to the "heavy" level.

LIST OF SYMBOLS

| | |
|------------------------------------|--|
| $R \cdot R$ | Max.-min. composition of R and R ; |
| $X \times X$ | Cartesian product of X and X ; |
| \vee | Maximum; |
| \wedge | Minimum; |
| $\text{Max}(I, J)$ or $I \vee J$ | Maximum of I and J ; |
| $\text{Min}(I, J)$ or $I \wedge J$ | Minimum of I and J ; |
| \in | Belongs to; |
| \notin | Does not belong to; |
| $A(x)$ | Membership function for the element x with respect to the fuzzy subset A ; |
| $F : U \rightarrow \{0, 1\}$ | Function F maps U into $\{0, 1\}$; |
| $F : U \rightarrow [0, 1]$ | Function F maps U into $[0, 1]$; |
| (A, B) | Closing degree of A and B . |

TABLE 7
Results of recognition of groups

| Group Level | I Heavy | II Light | III Most heavy | IV Light | V Heavy | VI Heavy |
|-------------|---------|----------|----------------|----------|---------|----------|
|-------------|---------|----------|----------------|----------|---------|----------|

REFERENCES

- 1 B.R. Kowalski, *Anal. Chem.*, 52 (1980) 112R.
- 2 I.E. Frank and B.R. Kowalski, *Anal. Chem.*, 54 (1982) 232R.
- 3 M.F. Delaney, *Anal. Chem.*, 56 (1984) 261R.
- 4 K.Y. Liu, *Fenxi Huaxue*, 13 (1985) 714.
- 5 X.S. Cao, *Huaxue Tongbao*, No. 12 (1985) 51.
- 6 H.D. Wang, *Assessment of Environmental Quality*, Education Publishing House, Beijing, 1981.
- 7 Z.X. He, *Fuzzy Mathematics and its Application*, Science Publishing House, Tianjin, 1985.
- 8 A. Kaufmann, *Introduction to the Theory of Fuzzy Subsets*, Vol. 1, Academic, New York, 1975.
- 9 D. Dubois and H. Prade, *Fuzzy Sets and Systems: Theory and Applications*, Academic, New York, 1980.
- 10 M. Smithson, *Fuzzy Set Analysis for Behavioral and Social Sciences*, Springer, New York, 1987.
- 11 A. Kandel, *Fuzzy Mathematical Techniques with Applications*, Addison-Wesley, Reading, MA, 1986.
- 12 J.C. Bezdek, *Pattern Recognition with Fuzzy Objective Function Algorithms*, Plenum, New York, 1981.
- 13 H.-J. Zimmermann, *Fuzzy Sets, Decision Making, and Expert Systems*, Kluwer, Boston, MA, 1987.

Diamond-like carbon coated microporous polycarbonate as a composite barrier for a glucose enzyme electrode

Séamus P.J. Higson and Pankaj M. Vadgama

Department of Medicine (Section of Clinical Biochemistry), University of Manchester, Hope Hospital, Eccles Old Road, Salford M6 8HD (UK)

(Received 23rd June 1992)

Abstract

Diamond-like carbon (DLC) coated microporous polycarbonate membranes were used as outer covering membranes in glucose enzyme electrodes. With optimised DLC deposition and the use of 0.01 μm microporous polycarbonate, biocompatibility has been seen to improve with only a loss of 6% response after 30 min exposure to whole blood, and a correlation to within 1 mM concentration with a standard laboratory method. In addition, control of the coating process allowed substrate diffusion-limiting properties to the bulk enzyme to be finely tuned permitting extensions in linearity ranges from 5 to > 80 mM glucose. Furthermore the higher biocompatibility coupled with the degree of permselectivity exhibited by DLC has enabled operation within whole blood without a second hydrogen peroxide selective barrier membrane. Permeability coefficients of glucose and O_2 determined for corresponding membranes by a classical diffusion chamber technique suggest that both the glucose/ O_2 permeability coefficient ratios and the absolute glucose permeability influenced the linearity range.

Keywords: Biosensors; Carbon electrodes; Glucose oxidase; Polycarbonate electrode coating

Enzyme electrodes permit simplified reagentless measurement of intermediary metabolites [1]. Optimization of such electrodes has involved both mediator chemistry and membrane technology [2]. Biocompatibility is an important issue in medical biosensors. The present work exploits the cumulative evidence that diamond-like carbon (DLC) has distinct advantages as a biocompatible surface. The present work has sought to exploit the recently demonstrated control over DLC deposition of various metallic, polymeric and inorganic surfaces [3–6], for coating neutron track etched polycarbonate membranes. DLC is a dense amorphous hydrocarbon polymer with properties that differ markedly from those of other hydrocarbon polymers, but in many ways resemble diamond

[7]. DLC has been shown to provide strong but flexible coatings, which are chemically highly inert and have electrical resistances [8], as well as exhibiting enhanced tissue biocompatibility [9]. Indeed cells have been shown to be capable of normal growth upon DLC *in vitro* [9,10]. DLC coated polycarbonate membranes therefore have been fabricated, for use as external membranes for use within a glucose enzyme electrode to provide membranes which may be substrate diffusion-limiting while exhibiting hitherto unseen levels of biocompatibility.

By modifications of the membrane permeability towards the reactants of the glucose oxidase catalysed enzyme reaction (glucose and O_2), and hopefully of other oxidoreductases, it was intended to again extend the electrode linearity to above the enzyme K_m and assay blood glucose over clinically useful concentration ranges [11]. A likely key parameter here would be the perme-

Correspondence to: S.P.J. Higson, Department of Medicine (Section of Clinical Biochemistry), University of Manchester, Hope Hospital, Eccles Old Road, Salford M6 8HD (UK).

ability of the coated membrane to organic microsolutes notably glucose as well as the permeability coefficient (P) ratios for glucose and O_2 . The latter would therefore be important in permitting high levels of O_2 diffusion relative to glucose to the enzyme layer and thereby avoiding O_2 limitation at the enzyme.

EXPERIMENTAL

Chemicals

Glucose oxidase from *Aspergillus niger* (75% protein, 150 000 U g⁻¹ solid), and bovine serum albumin (BSA) (fraction V), were obtained from Sigma (Poole). D-Glucose, disodium hydrogen-phosphate, sodium dihydrogen-phosphate, sodium benzoate and sodium chloride (AnalaR grade) were obtained from BDH (Poole). All chemicals were used without further purification. A buffer (pH 7.4) comprising 5.28×10^{-2} M Na_2HPO_4 , 1.3×10^{-2} M NaH_2PO_4 , 5.1×10^{-3} M NaCl, 6.24×10^{-3} M C_6H_5OONa was prepared in distilled water. This isotonic buffer was used for all enzyme preparations and diffusional studies.

DLC coating of polycarbonate membranes

The polycarbonate membranes were purchased from the Porectics Corporation (Livermore, CA) and the DLC coating procedure performed by Atom Tech (formerly Ion Tech, Teddington) as has been previously described [6]. The method involved a fast atom bombardment (FAB) cleaning process for 5 min in a neutral saddle field argon source followed by the coating of DLC in the same argon source with a hydrocarbon introduced to the beam as previously described [6]. Polycarbonate membranes of pore radii 0.01, 0.05 and 0.1 μm were coated with DLC using a range of deposition durations of notably 1 min, 3 min 30 s and 7 min. Control membranes without the DLC coating were similarly cleaned by subjection to 5 min FAB.

DLC coating times define total deposition times. Double-sided coated membranes therefore had a 50% coating duration for each surface. In this way, it was intended that single- and double-

sided coated membranes could be compared with regard to coating durations. The deposition rate of DLC was 0.45 μm per hour so 1 min, 3 min 30 s and 7 min coating correspond to thicknesses of 0.0075, 0.026 and 0.053 μm , respectively. These membranes had a quoted thickness of ca. 6 μm , so the maximum coating of DLC was less than 1% of the membrane thickness to which it was applied. It was therefore assumed to have a negligible effect on the thickness of the membranes used in the calculation of the P values.

Apparatus

An oxygen electrode assembly (Rank Brothers, Bottisham) as previously described [11], was utilized for glucose oxidase enzyme electrodes. The working electrode (anode) was polarized at +650 mV (vs. Ag/AgCl) for the oxidation of H_2O_2 . The cell comprised a central 2-mm diameter platinum disc working electrode with an outer pre-anodized 12-mm diameter, a 1-mm wide silver ring (Ag/AgCl) acting as a combined reference and counter electrode. The purpose-built voltage polarization source and potentiostat were constructed by the Chemistry Workshops, University of Newcastle, and an $x-t$ chart recorder (Lloyd Instruments, Fareham) was used to record the amperometric responses of the electrode assembly from the potentiostat current follower. A blood gas analyzer (Instrumentation Laboratory Model IL1802) was used in the Clinical Biochemistry laboratory (Hope Hospital) for the determination of pO_2 within buffer aliquots.

Fabrication of enzyme electrodes

A composite solution of glucose oxidase (GOD) (2560 U ml⁻¹) and BSA (0.1 g ml⁻¹) was prepared in buffer solution. 6 μl of GOD-BSA solution and 3 μl of glutaraldehyde (5%, v/v) were mixed rapidly and placed on a 1-cm² portion of 0.05- μm pore radii polycarbonate membrane. A 1-cm² portion of DLC coated polycarbonate membrane was then placed on top, and glass plates used to compress the enzyme and membrane laminate under finger pressure for approximately 5 min. The resulting crosslinked enzyme membrane laminate was placed over the

working electrode, prior to final electrode assembly with fixation by a rubber "O" ring.

Methodology – Determination of permeability coefficients

Solute mass transfer measurements across DLC coated polycarbonate membranes to assess their permeability were performed at $22 \pm 1^\circ\text{C}$ in a classical diaphragm diffusion cell apparatus comprising two chambers [12], as previously described. Both chambers were of 170 ml volume and were separated by two stainless-steel discs and two sealing rubber "O" rings clamped together to retain the membrane with a defined cross-sectional area available for mass transport (7.07 cm^2). The solute was rapidly injected into one chamber and mass transfer was determined by measuring solute concentrations in both chambers at periodic intervals. For the determination of $p\text{O}_2$ levels in each chamber, aliquots from a closed system were extracted by syringe and sealed within small glass vials to prevent mixing with the atmosphere, prior to $p\text{O}_2$ analysis. Oxygen within one chamber was consumed by placing cross-linked GOD–BSA films in excess, to create oxygen gradients across the membrane of interest. The $p\text{O}_2$ levels were determined by a blood gas analyser (Instrumentation Laboratory Model IL1802, Hope Hospital, Clinical Biochemistry laboratory). Aliquots analyzed for $p\text{O}_2$ levels from the chamber containing GOD–BSA confirmed that all oxygen was consumed. Permeability coefficients were calculated using the expression derived by Sun et al. [12].

Analysis of blood glucose concentrations

Whole blood samples previously tested for glucose (Hope Hospital, Clinical Biochemistry laboratory) were used for the evaluation of enzyme electrodes for whole blood analysis. Blood samples stored under refrigeration in tubes containing fluoride oxalate were used on the same day as the hospital analysis.

RESULTS AND DISCUSSION

Neutron track etched membranes have near-cylindrical channels formed by a well established

neutron beam track-etched method [13]. The relatively low thickness (ca. $6\ \mu\text{m}$) of these membranes has enabled minimisation of diffusional distances while facilitating a high degree of control over diffusional resistance due to the fine control possible of pore radius and pore density. By attempting to decrease the glucose/ O_2 P ratio for these membranes, enzyme electrodes were constructed that might become diffusion-controlled rather than reflecting intrinsic enzyme kinetics.

DLC-coated polycarbonate membranes were prepared in order to allow a further extension of linearity for glucose determination *in vitro* and also minimise biofouling of the sensor. A series of experiments was performed to determine the P values for O_2 and glucose across a spectrum of

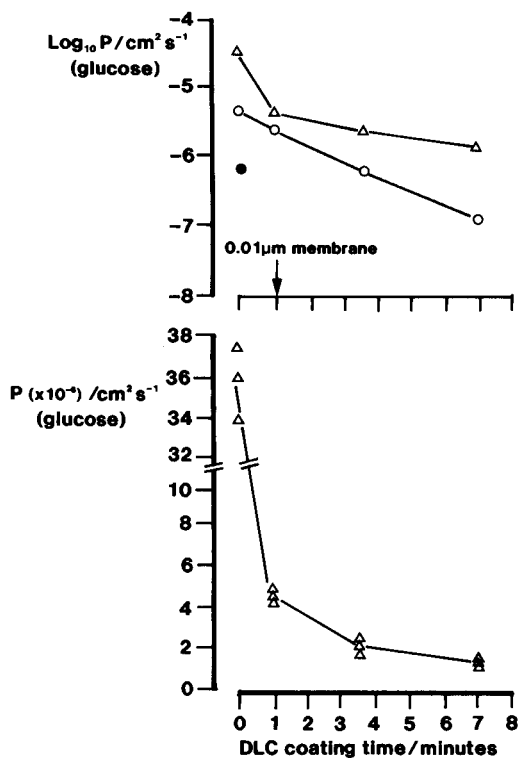


Fig. 1. (a) Relationship between permeability coefficients (P) for glucose across single-sided DLC-coated polycarbonate membranes. (b) Individual P values calculated for $0.1\text{-}\mu\text{m}$ pore radii DLC single-sided coated polycarbonate membranes. Polycarbonate membrane pore radii: ● 0.01 ; ○ 0.05 ; △ $0.1\ \mu\text{m}$.

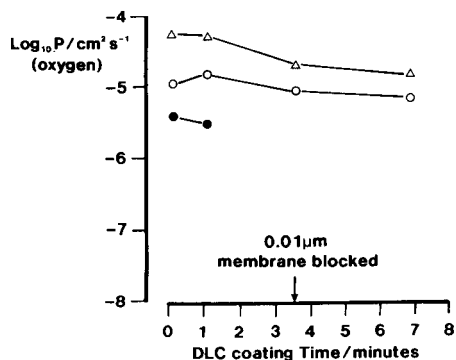


Fig. 2. Relationship between permeability coefficients (P) for oxygen across single-sided DLC-coated polycarbonate membranes. For definition of symbols see Fig. 1.

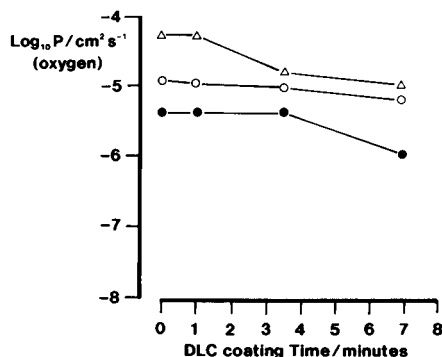


Fig. 4. Relationship between permeability coefficients (P) for oxygen across double-sided DLC-coated polycarbonate membranes. For definition of symbols see Fig. 1.

DLC single- and double-sided coated membranes, using a diffusion chamber apparatus. On each occasion, three membranes of each type were independently tested within the diffusion chamber, and a mean value for each P value calculated. For clarity only this value is shown in figures describing permeability coefficients trends.

Figures 1–4 show how the P values for glucose and O_2 are related to polycarbonate membranes of 0.01, 0.05 and 0.1 μm pore radii, with different durations of single- and double-sided DLC coating. Mean P values for glucose transport are shown in Fig. 1a, but Fig. 1b depicts individual, measured P values for glucose across 0.1- μm pore radii single DLC-coated membranes. This demonstrates that P values across three

membranes prepared by the same procedure may be attained to within a margin of 5%.

From Figs. 1–4, it can be seen that the P values for both glucose and O_2 decrease with decreasing pore radius. Furthermore Figs. 1 and 3 show that P values for glucose progressively diminish as the DLC coating thickness is increased, suggesting that the pore area steadily decreases. No previous technique used by us (such as organic solvent deposition) has allowed such “fine tuning” of membrane permeability at small pore radii. It should also be noted that Figs. 1 and 3, and Figs. 2 and 4 are similar, indicating that a similar application of DLC to a single surface or between both membrane surfaces has little influence on the diffusing species behaviour across the membrane.

The 0.01- μm pore radii polycarbonate membranes invariably become blocked to glucose transport when > 1 min coatings of DLC are applied. However, single-sided coated membranes become blocked at < 1 min DLC coating durations, whereas diffusion of glucose is permitted for double-sided coated membranes of 1 min DLC coating duration. This blocking difference is probably due to the build up of DLC at very small pores in single-sided coatings, whereas, the pore aperture is spared if this is distributed across two membrane surfaces. Of particular interest, however, is the finding that O_2 transport is much less affected by DLC application, and that when glucose is fully obstructed, O_2 trans-membrane

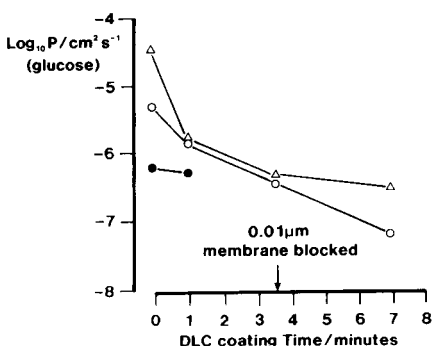


Fig. 3. Relationship between permeability coefficients (P) for glucose across double-sided DLC-coated polycarbonate membranes. For definition of symbols see Fig. 1.

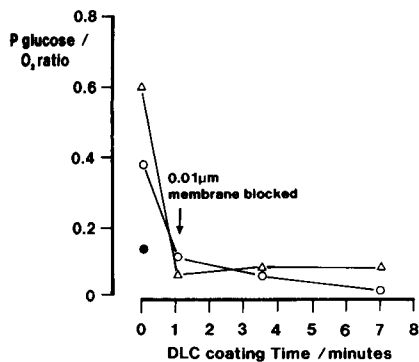


Fig. 5. Relationship between permeability coefficient ratio of glucose/O₂ and DLC coating time for single-sided DLC-coated polycarbonate membranes. For definition of symbols see Fig. 1.

passage is still maintained. Figures 5 and 6 describe how the glucose/O₂ ratios are affected by the DLC deposition as calculated using the data of Figs. 1-4. Again, the *P* ratio values are very similar for single- or double-sided DLC-coated membranes. The first application of DLC (1 min), results in the greatest reduction of the glucose/O₂ *P* ratios. Further coatings of DLC result in continued reduction in this ratio, although the effect is less prominent. The membranes showing the smallest glucose/O₂ *P* ratios are those for 0.05-µm pore radii membranes with 7 min DLC coating for both single- and double-sided coated membranes.

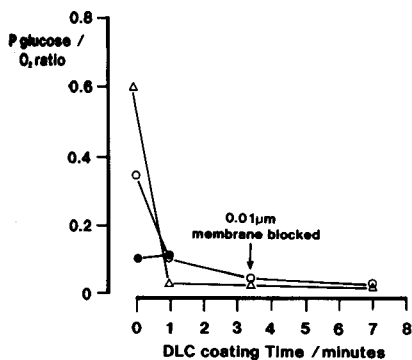


Fig. 6. Relationship between permeability coefficient ratio of glucose/O₂ and DLC coating time for double-sided DLC-coated polycarbonate membranes. For definition of symbols see Fig. 1.

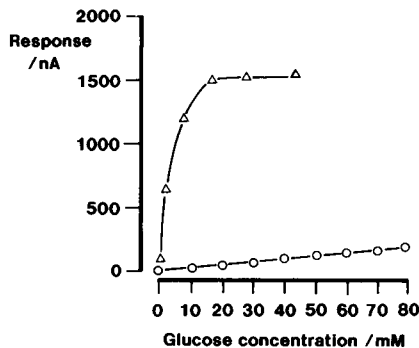


Fig. 7. Glucose electrode calibration using enzyme cross-linked between lower uncoated 0.05 µm pore radii polycarbonate membranes with outer 0.01-µm pore radii double-sided DLC-coated and uncoated control polycarbonate membranes. Δ Control, no DLC; ○ 1 min DLC. (○) Regression equation: Response/(nA) = -0.978 + 2.055 (glucose conc./mM). *x* intercept: 0.476 mM glucose; *y* intercept: -0.977 nA. Standard deviation *y* intercept: 0.378; standard error *y* intercept: ± 0.785; standard deviation slope: 0.004; standard error slope: ± 0.016; *r*²: 0.99.

Previously, we have predicted [11] that sensors utilizing membranes with the smallest glucose/O₂ *P* ratios would possess the largest linearity ranges. This is partially supported by Figs. 7-11, which show calibration graphs for enzyme electrodes, constructed with lower polycarbonate membranes of 0.05-µm pore radii and upper polycarbonate membranes of pore radii 0.01, 0.05 and 0.1 µm, respectively, with varied DLC depositions, in standard, buffered solutions of glucose.

However, Fig. 7 depicts the calibration of glucose oxidase enzyme electrodes with upper double-sided 0.01-µm pore radii membranes and the corresponding control. The linear range was found to extend to more than 80 mM glucose, well in excess of that attained with uncoated membranes. Calibrations for single-sided coated 0.01-µm pore radii membranes for the same coating time were not possible as these membranes were blocked to glucose transport.

Figures 8 and 9 depict calibration graphs for enzyme electrodes employing upper 0.05-µm pore radii membranes. The almost identical behaviour shown by enzyme electrodes utilizing single- and double-sided DLC-coated membranes confirms that for both types of membrane, the same coating times impart almost identical properties. In

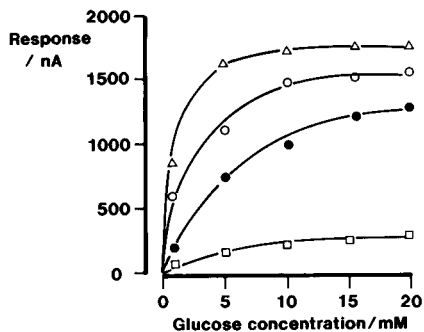


Fig. 8. Glucose electrode calibration using enzyme cross-linked between lower uncoated 0.05- μm pore radii polycarbonate membranes with outer 0.05- μm pore radii single-sided DLC-coated and uncoated control polycarbonate membranes. Δ Control, no DLC; \circ 1 min DLC; \bullet 3 min 30 s DLC; \square 7 min DLC.

addition, Figs. 8 and 9 both show that as the DLC coating time is increased, the enzyme electrode curvilinear range is progressively extended. However, the effect is relatively minor giving extensions between 10–15 mM glucose, as compared to > 80 mM as shown by the enzyme electrodes of Fig. 7. This is despite the rather similar glucose/ O_2 permeability ratios of Figs. 5 and 6. Similar findings are shown for 0.1 μm pore radii membrane-covered enzyme electrodes (Figs. 10 and 11). In addition, the calibration curves for single- (Fig. 10) and double- (Fig. 11) sided DLC-coated upper membrane-based enzyme

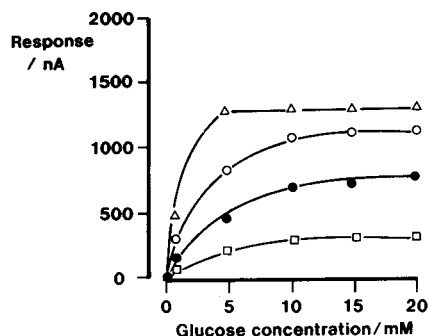


Fig. 9. Glucose electrode calibration using enzyme cross-linked between lower uncoated 0.05- μm pore radii polycarbonate membranes with upper 0.05- μm pore radii double-sided DLC-coated and uncoated control polycarbonate membranes. For definition of symbols see Fig. 8.

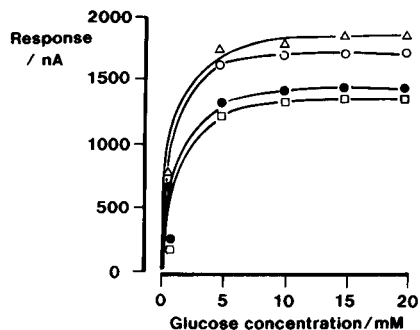


Fig. 10. Glucose electrode calibration using enzyme cross-linked between lower uncoated 0.05- μm pore radii polycarbonate membranes with outer 0.1- μm pore radii single-sided DLC-coated and uncoated control polycarbonate membranes. For definition of symbols see Fig. 8.

electrodes are similar, and longer durations of DLC coating result in extended linearity ranges.

It is therefore probable that in addition to the glucose/ O_2 P ratio, the absolute permeability is also important in determining linearity ranges.

One constraint in the commercialisation of existing sensors for whole blood measurements has been the intractable problem of signal drift as a result of biofouling [1]. Recently DLC has been the focus of interest as a possible coating for medical implants [9], and its biocompatibility compared to that of various alloys [14,15], high-density polyethylene and carbon fibre composites [16,17]. Indeed DLC was found to produce highly biocompatible films on which cells could grow

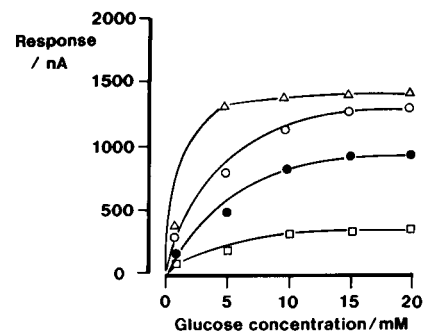


Fig. 11. Glucose electrode calibration using enzyme cross-linked between lower uncoated 0.05- μm pore radii polycarbonate membranes with outer 0.1- μm pore radii double-sided DLC-coated and uncoated control polycarbonate membranes. For definition of symbols see Fig. 8.

without eliciting an inflammatory response [9], and which provided strong but flexible coatings [9,10].

A series of experiments was therefore designed so that enzyme electrodes all with inner 0.05- μm pore radii uncoated polycarbonate membranes, and varying pore radii DLC-coated outer polycarbonate membranes (together with controls), were exposed to heparinised whole blood, and then rinsed with non-anticoagulated buffer solution. Responses to 5 mM glucose solutions, before and after blood exposure were recorded, and percentage losses of response determined.

Figures 12 and 13 describe the percentage loss of signal following 30 min exposure to stirred undiluted whole blood. The insert of Fig. 12 depicts a typical time course for such loss. Again

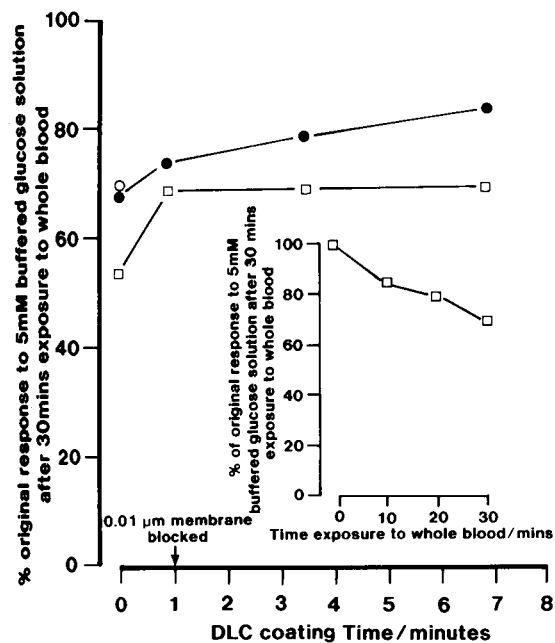


Fig. 12. Relationship between percent original response of enzyme electrodes with single-sided DLC-coated upper membranes and 0.05- μm pore radii uncoated lower polycarbonate membranes to 5 mM buffered glucose solutions, following 30 min exposure to whole blood. (Insert: relationship between percent original response of enzyme electrode with outer 0.1- μm pore radii with 1-min single-sided DLC-coated upper membranes and lower 0.05- μm uncoated polycarbonate membrane, with time exposure to whole blood/min.) Upper polycarbonate pore radii: ○ 0.01; ● 0.05; □ 0.1 μm . Arrow indicates point at which the 0.01- μm membrane is blocked.

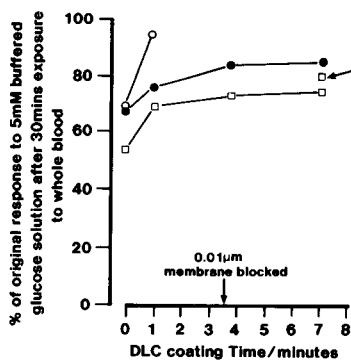


Fig. 13. Relationship between percent of original response of enzyme electrode with double-sided DLC-coated upper polycarbonate membranes and 0.05- μm pore radii uncoated lower polycarbonate membranes to 5 mM buffered glucose solutions, following 30 min exposure to whole blood. For definition of symbols see Fig. 12. Arrow indicates response after 1 h washing with buffer.

there are very few differences between single- or double-sided DLC-coated membranes. However, the resistance to biofouling appears to increase with greater deposition of DLC for all membranes. The greatest change is seen between uncoated membranes and the first deposition of DLC (1 min). Membrane pore radius also appears to be critical as smaller pore radii membranes always exhibit lower losses following blood exposure than enzyme electrodes with similar DLC coated membranes of larger pore radii. All control sensors with upper membranes without DLC coating showed no effect with extended washing regimes.

As before, only double-sided DLC-coated membranes of 0.01- μm pore radii could be tested for biofouling properties as single-sided DLC coated 0.01- μm pore radii membranes were all blocked to glucose. However, 0.01- μm pore radii polycarbonate membranes with 1 min deposition DLC double-sided coatings as the upper membrane of an enzyme laminate exhibited extreme resistance to biofouling, showing a loss of only 6% signal following 30 min exposure to whole blood.

Biofouling owing to the deposition of protein, lipids and cells may act as a diffusion barrier to the passage of microsolute to the enzyme layer. As the DLC presents a surface similar to dia-

mond possessing sp^3 hybridised C–C bonds in a tetrahedral structure on the surface, the structure probably presents a more inert surface [9]. This may help to decrease biofoulant adsorption onto a surface with DLC coatings and materials that had adhered onto the surface might be more easily dislodged with extended washing.

An enzyme laminate with an upper nominal pore radius of $0.1\ \mu\text{m}$ and 7 min double-sided DLC coating was exposed to blood, washed with distilled water, and buffer placed in the cell for continued washing for 1 h. The buffer was then replaced with a 5 mM glucose buffer and the response recorded. The final response was found to be 4% higher than previously noted, (Fig. 13), suggesting that some surface biofouling from the outer DLC-coated polycarbonate membrane may have been mechanically dislodged.

As linearity ranges for glucose determination over clinically useful ranges had been attained, and the effects of biofouling assessed following whole blood exposure, two sensors for comparison were constructed both with lower $0.05\ \mu\text{m}$ pore radii polycarbonate membranes; outer membranes were of $0.01\text{-}\mu\text{m}$ and $0.1\text{-}\mu\text{m}$ double-sided 1-min duration DLC-coated membranes. These two enzyme electrodes were calibrated following 30 min exposure to whole blood, and individual blood samples previously tested for glucose levels within the Clinical Biochemistry laboratory (Hope Hospital) were analysed. The correlations between the two electrodes and the Clinical Biochemistry laboratory results are shown in Fig. 14. The results for the $0.1\text{-}\mu\text{m}$ pore radii membranes show all results were consistently lower ($r^2 = 0.74$), than those of the Clinical Biochemistry laboratory probably due to a continuing and extended biofouling following every exposure to blood. By contrast, the $0.01\text{-}\mu\text{m}$ pore radii upper membrane glucose electrode yielded results which were in close agreement ($r^2 = 0.99$), with those of the Biochemistry laboratory.

This has two important consequences. Firstly, the $0.01\text{-}\mu\text{m}$ DLC-coated membranes allow reliable performance for glucose determination despite exposure to whole blood. Furthermore although no permselective membrane was used, the electrochemically active interferents in blood did

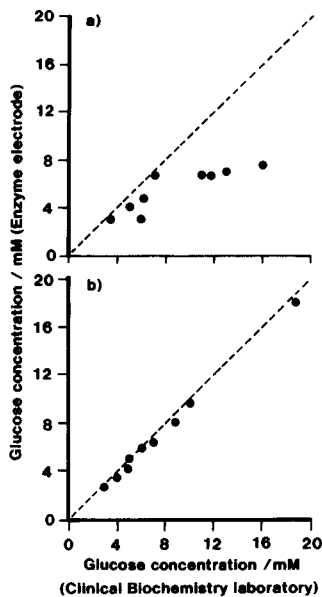


Fig. 14. Correlation between analysis of whole blood glucose concentrations, from Clinical Biochemistry laboratory analysis and enzyme electrode analysis. (a) Glucose enzyme electrode with upper $0.1\text{-}\mu\text{m}$ pore radii polycarbonate membrane with 1 min double-sided DLC-coating, and lower $0.05\text{-}\mu\text{m}$ uncoated pore radii membrane. $r^2 = 0.74$. (b) glucose enzyme electrode with upper $0.01\text{-}\mu\text{m}$ pore radii polycarbonate membrane with 1 min double-sided DLC-coating, and lower $0.05\text{-}\mu\text{m}$ uncoated pore radii membrane. $r^2 = 0.99$.

not influence the response. This suggests that the upper membrane though microporous is acting as a barrier to electrochemically active interferents.

Conclusions

A comprehensive series of DLC-coated microporous polycarbonate membranes have been assessed in terms of porosity, and the permeability coefficients calculated for glucose and oxygen using a classical diffusion chamber.

Glucose electrodes have been constructed utilising DLC-coated outer covering membranes, and their calibration curves assessed. Comparisons have been made between the permeability coefficient of glucose and O_2 , and their ratios related to linearity ranges attained using these membranes. Lower glucose/ O_2 P ratios were found to be associated with extension in linearity. Linearity ranges above 80 mM glucose were attained using $0.01\text{-}\mu\text{m}$, 1 min total duration, DLC dou-

ble-sided coated, polycarbonate membranes as outer covering membranes. This enzyme electrode utilized the membrane showing the greatest diffusional resistance to glucose, suggesting that both the glucose/O₂ *P* ratio and the absolute permeability for glucose are critical for linearising a glucose enzyme electrode. The same enzyme electrode exhibited a good resistance to biofouling, with losses in response of only 6% following repeated exposure to whole blood as well as showing a close correlation to glucose analysis using conventional clinical biochemistry techniques, despite the absence of an underlying selective membrane.

The authors thank the Science and Engineering Research Council and the Department of Trade and Industry for financial support for this work.

REFERENCES

- 1 P. Vadgama, *J. Membr. Sci.*, 50 (1990) 141.
- 2 A.P.F. Turner, I. Karube and G.S. Wilson, *Biosensors; Fundamentals and Applications*, Oxford University Press, Oxford, 1987.
- 3 C. Wild, P. Koidl and J. Wagner, in P. Koidl and P. Oelhafen (Eds.), *EMRS Symposia Proc.*, European Materials Research Society, Les Ulis, 17 (1987) 1374.
- 4 T. Taguchi, M. Morikawa, Y. Hiratsuk and K. Toyoda, in P. Koidl and P. Oelhafen (Eds.), *EMRS Symposia Proc.*, European Materials Research Society, Les Ulis, 17 (1987) 123.
- 5 M.J. Mirtich, in P. Koidl and P. Oelhafen (Eds.), *EMRS Symposia Proc.*, European Materials Research Society, Les Ulis, 17 (1987) 377.
- 6 J. Franks, *J. Vac. Sci.*, A71 (1989) 2307.
- 7 J.C. Angus, in P. Koidl and P. Oelhafen (Eds.), *EMRS Symposia Proc.*, European Materials Research Society, Les Ulis, 17 (1987) 179.
- 8 D.G. Thompson, *Proc. 30th Ann. Tech. Conf. SVC, Society of Vacuum Coaters*, Boston, MA, 1987, p. 135.
- 9 L.A. Thomson, F.C. Law, J. Franks and N. Rushton, *Biomaterials*, 12 (1991) 37.
- 10 A.C. Evans, J. Franks and P.J. Revell, *Med. Device Technol.*, May (1991) 26.
- 11 W.H. Mullen, S.J. Churchouse, F.H. Keedy and P. Vadgama, *Anal. Chim. Acta*, 183 (1986) 59.
- 12 Y. Sun, S. Furusaki, A. Yamauchi and K. Ichimura, *Biotechnol. Bioeng.*, 34 (1989) 55.
- 13 *Product Catalog*, Poretics Corporation, Livermore, CA, 1992.
- 14 T. Rae, *J. Bone Jt. Surg., Br. Vol.*, 57B (1975) 444.
- 15 T. Rae, *Biomaterials*, 7 (1986) 30.
- 16 T. Rae and N. Rushton, *Proceedings of the International Conference on Biological Biomedical Polymers*, The Biological Engineering Society and the Plastics and Rubber Institute, London, 1982, p. 23.
- 17 T. Rae, N. Thomson, L.A. Lardner and S.J. Martin, *J. Bone Jt. Surg., Br. Vol.*, 70B (1988) 724.

Chloride-selective electrodes based on mercury organic compounds as neutral carriers

Markus Rothmaier and Wilhelm Simon

Department of Organic Chemistry, Swiss Federal Institute of Technology (ETH), Universitätsstrasse 16, CH-8092 Zürich (Switzerland)

(Received 23rd July 1992)

Abstract

Mercury organic compounds incorporated in solvent polymeric membranes act as neutral carriers for chloride. In sharp contrast to classical anion exchangers, membranes containing $\{\mu\text{-}[4,5\text{-dimethyl-3,6-bis(octyloxy)-1,2-phenylene]bis(trifluoroacetato-O)}\}$ dimercury (ETH 9009) or tetrakis $\{\mu\text{-}(\text{dimethyl sulphoxide-O} : \text{O})\}$ bis $\{\mu\text{-}[\text{hexafluoropentanedionato}(2 -)\text{-O} : \text{O}']\}$ bis $\{\mu\text{-}[4,5\text{-dimethyl-3,6-bis(octyloxy)-1,2-phenylene]}\}$ tetramercury (ETH 9011) as anion carriers, tridodecylmethylammonium chloride as additive, bis(2-ethylhexyl) sebacate (DOS) as plasticizer and poly(vinyl chloride) as membrane matrix show a preference for chloride over bromide, thiocyanate, perchlorate, nitrate and salicylate. Ion-selective electrodes with such membranes displayed a Nernstian electrode function for chloride in the concentration range 10^{-5} –0.1 M. For the more concentrated NaCl solutions, the potential drift of the cell assembly was $< 1.5 \text{ mV h}^{-1}$ and the response time ($t_{90\%}$) was $< 10 \text{ s}$. In 0.01 M NaCl, e.m.f. repeatabilities were found to be ± 0.16 and $\pm 0.29 \text{ mV}$ for ISEs based on ETH 9009 and ETH 9011, respectively. ^{13}C NMR studies showed ETH 9011 to interact with chloride and thiocyanate, forming 4:1 complexes, but not with perchlorate and nitrate.

Keywords: Ion selective electrodes; Chloride; Mercury organic ionophores

In contrast to the great variety of cation complexes known in host–guest chemistry [1], only a few compounds that reversibly complex anions [2] have been used as ionophores in solvent polymeric membranes. The interactions between host and guest molecules can be divided into five types: (a) *Coulomb interactions*: classical anion exchangers [3], azamacrocycles with protonated [4] or quaternary nitrogen [5] and guanidine derivatives [6] behave according to this type; Koryta [7] gives 58 references for applications of anion-selective electrodes based on tetraalkylammonium salts; (b) *ligand exchange*: observed with metalloporphyrin complexes and cobester derivatives, which have been used in nitrite-selective

electrodes [8]; they induce completely different selectivity sequences as compared with the Hofmeister series [9] exhibited by classical anion exchangers; (c) *coextraction*: anions and cations are simultaneously extracted into the same heterotopic host molecule [10]; so far, no analytical application of such ionophores has been described; (d) *covalent bonding*: as an example, trifluoroacetophenones as neutral carriers form covalent bonds with carbonate [11]; the corresponding ion-selective electrode (ISE) membranes were shown to reject most relevant anions present in blood serum, except salicylate and benzoate, and response times and e.m.f. repeatabilities were satisfactory [12]; (e) *interactions between Lewis acids and bases*: representatives of Lewis acids are compounds containing B [13], Si [13], Sn [14] or Hg [15]; tin organic compounds (e.g., R_2SnX_2 and R_3SnX , with R = benzyl or alkyl and X = Cl

Correspondence to: W. Simon, Department of Organic Chemistry, Swiss Federal Institute of Technology (ETH), Universitätsstrasse 16, CH-8092 Zürich (Switzerland).

or OAc), whose tin centre on anion complexation changes from tetra- to pentahedral coordination, have been tested in membranes of anion-selective electrodes and optodes. ISEs based on bis(4-chlorobenzyl)tin dichloride and tri-*n*-octyltin chloride showed useful selectivities for hydrogenphosphate [16] and chloride [17], respectively, but were not suitable for practical purposes because of slow response and unstable potentials. In optode membranes, however, tin organic carriers were found to be adequate for chloride determinations in blood serum [18].

Up to now, in clinical analysis only electrodes and optodes with solvent polymeric membranes based on anion exchangers have been used [19], their selectivities on the whole following the Hofmeister series [9]. In the recent literature [20–25], cyclic and non-cyclic Lewis acids with two or more covalently bonded mercury atoms have been described which form reversible complexes with halides or basic solvents. With a view to determining relevant anions (Cl^- , HCO_3^- , CO_3^{2-} , HPO_4^{2-}) in biological fluids, this novel class of neutral carriers showing a different selectivity pattern was therefore studied. This paper reports on two mercury organic compounds (see Fig. 1), $\{\mu\text{-}[4,5\text{-dimethyl-}3,6\text{-bis}(\text{octyloxy})\text{-}1,2\text{-phenylene}]\}\text{bis}(\text{trifluoroacetato-}O)\text{dimercury}$ (ETH 9009) and tetrakis $\{\mu\text{-}(\text{dimethylsulphoxide-}$

$O : O)\text{-bis}\{\mu\text{-}[\text{hexafluoropentanedionato}(2-)\text{-}O : O']\}\text{-bis}\{\mu\text{-}[4,5\text{-dimethyl-}3,6\text{-bis}(\text{octyloxy})\text{-}1,2\text{-phenylene}]\}\text{tetramercury}$ (ETH 9011), acting as chloride carriers in solvent polymeric membranes.

EXPERIMENTAL

Reagents

Aqueous solutions were prepared with doubly quartz-distilled water and salts of the highest purity available. Tetrahydrofuran (THF), high-molecular-weight poly(vinyl chloride) (PVC), the additives tridodecylmethylammonium chloride (TDDMACl) and dimethyldioctadecylammonium bromide (DMDODABr) and the plasticizers dibutyl sebacate (DBS), bis(2-ethylhexyl) sebacate (DOS), 2-nitrophenyl octyl ether (o-NPOE), bis(1-butylpentyl)decane-1,10-diyl diglutarate (ETH 469), bis(1-butylpentyl) adipate (BBPA), tetraundecyl benzhydrol-3,3'-4,4'-tetracarboxylate (ETH 2112), tetraundecyl benzophenone-3,3'-4,4'-tetracarboxylate (ETH 2041), tris(2-ethylhexyl) trimellitate (TOTM) and tris(2-ethylhexyl) phosphate (TEHP) were used for membrane preparation and tridodecylmethylammonium nitrate (TDDMANO₃) for ¹³C NMR titrations, all Selectophore from Fluka (Buchs, Switzerland). Chloroalkanes 56C, 60C, 64C and 70C were obtained from Hüls (Marl, Germany). Chemicals for the syntheses were purchased from Fluka and CDCl₃ with tetramethylsilane (TMS) (99 + 1) from Ciba-Geigy (Basle).

NMR-monitored titrations

All ¹³C NMR spectra were recorded at 50.32 MHz on a Bruker ACF 200 SY 4.70-T 200 MHz Fourier transform NMR spectrometer (Bruker-Spectrospin, Fällanden, Switzerland). Tubes of 5 mm i.d. contained 100 mg (0.043 mmol) of ETH 9011 in 1 ml of CDCl₃ with TMS as internal standard. The recording conditions were spectral width 11.6 kHz, acquisition time 0.7045 s, data table size 16K of 24-bit words, r.f. pulse duration 2.50 μs, number of transients ca. 2000–2500, broad-band proton decoupling of generally 18 H and ambient temperature air cooling.

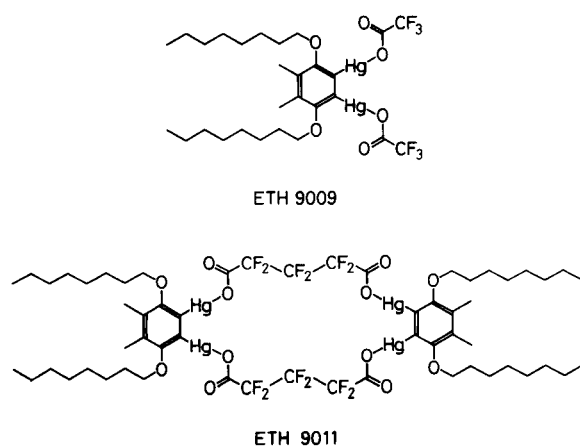


Fig. 1. Structure formulae of ionophores. ETH 9011 was prepared as 1:4 DMSO adduct (see Experimental).

Membranes

The solvent polymeric membranes were prepared according to [26]. For conditioning (overnight) and as internal filling solution of the electrodes, 0.01 M NaCl was used. To exchange Br⁻ for Cl⁻ and thus avoid e.m.f. instability due to the influence of bromide on the Ag/AgCl inner reference electrode, membranes containing DM-DODABr were conditioned in 0.01 M NaCl for several days before mounting them in electrode bodies.

E.m.f. measurements and evaluations

Potentiometric measurements were performed at 22 ± 1°C with the cell assembly Hg | Hg₂Cl₂ | KCl (satd.) ; 1 M LiOAc || sample || membrane || 0.01 M NaCl | AgCl | Ag. The calomel reference electrode corresponded to the free-flowing double-junction type [27]. The measuring equipment is described in [26]. For each solution, potentials were recorded for 60 min, the average of the final 10 min (*n* = 16) being taken for evaluations. All e.m.f. data were corrected for liquid-junction potentials. Single-ion activities were calculated according to the Debye–Hückel theory with equations and coefficients given elsewhere [28,29]. For salicylate (SalO⁻), the activity coefficients and equivalent ionic conductivity data of acetate were used.

Electrode response functions, selectivities

Electrode response functions were determined in 10⁻⁷–0.1 M aqueous NaCl of increasing concentration and the slopes calculated by linear regression in the range 10⁻⁵–0.1 M (*n* = 5). Selectivity coefficients were measured by the separate solution method (SSM) [30] in 0.1 M sodium salt solutions buffered at pH 7.4 ± 0.1 with 0.01 M tris(hydroxymethyl)aminomethane (Tris)–4.35 × 10⁻³ M sulphuric acid, starting with the less preferred anion. Between two solutions, the electrodes were rinsed with water and, with stirring, left standing in water for several minutes.

Repeatability

With membranes containing TDDMACl as additive, the repeatability of potentials was deter-

mined by measuring alternatively in 0.001 and 0.01 M NaCl for 5 min each. The mean e.m.f. value of the last 60 s (*n* = 20) was used for evaluation.

Response time

The electrode was placed in 100 ml of 0.001 M NaCl and the e.m.f. recorded till the potential drift was < 1 mV h⁻¹ (usually after 10 min). Then 10 ml of 0.1 M NaCl were quickly added with a syringe and the e.m.f. was measured for 5 min. The response time, *t*_{90%}, was determined according to [31].

Syntheses

2,3-Dimethyl-1,4-bis(octyloxy)benzene. A solution of 4.5 g (32.6 mmol) of 2,3-dimethylhydroquinone, 13.91 g (72.0 mmol) of 1-bromooctane and 23.46 g (72.0 mmol) of caesium carbonate in 400 ml of DMF was refluxed for 5 h [32]. After cooling, 100 ml of water were added and the solution was extracted twice with diethyl ether and washed with 10% NaOH solution. Evaporation of the solvent and purification of the residue by flash chromatography (250 g of silica gel 60) with hexane–ethyl acetate (9 + 1) and by bulb-to-bulb distillation (b.p. 140–145°C, 0.15 Torr) yielded a colourless liquid (6.84 g, 58%): IR (CHCl₃), 2855, 1467, 1255, 1107 cm⁻¹; ¹H NMR (200 MHz, CDCl₃), δ 0.87 (t, *J* = 6.5 Hz, 6H), 1.22–1.52 (m, 20H), 1.75 (m, *J* = 6.8 Hz, 4H), 2.15 (s, 6H), 3.88 (t, *J* = 6.6 Hz, 4H), 6.62 (s, 2H); MS, *m/z* (%) 362 (91, M⁺), 250 (21), 138 (100); analysis calculated for C₂₄H₄₂O₂ (362.60), C 79.50, H 11.68; found, C 79.24, H 11.92%.

{μ-[4,5-Dimethyl-3,6-bis(octyloxy)-1,2-phenylene]}bis(trifluoroacetato-O)dimercury (ETH 9009). ETH 9009 was prepared according to [15] but without removing the monosubstituted product by sublimation. Recrystallization of the product from hexane–CH₂Cl₂ yielded colourless needles (73%), m.p. 176–178°C: IR (KBr), 2850, 1662, 1421, 1351, 1204, 1082 cm⁻¹; ¹H NMR (200 MHz, CDCl₃), δ 0.88 ppm (t, *J* = 6.5 Hz, 6H), 1.25–1.55 (m, 20H), 1.79 (m, *J* = 6.8 Hz, 4H), 2.21 (s, 6H), 3.77 (t, *J* = 6.3 Hz, 4H); MS, *m/z* (%) 922 (2, M⁺ – CF₃), 810 (2), 598 (6), 486 (9), 374 (13), 360 (19), 250 (20), 202 (27), 138 (100); analysis calcu-

lated for $C_{28}H_{40}F_6Hg_2O_6$ (987.79), C 34.05, H 4.08; found, C 34.34, H 4.28%.

Oxo{ μ -[4,5-dimethyl-3,6-bis(octyloxy)-1,2-phenylene]}dimercury (ETH 9010). The compound, prepared from ETH 9009 according to [15], was a white powder (yield 95%), m.p. > 250°C: IR (KBr), 2856, 1466, 1353, 1204, 1083 cm^{-1} .

Tetrakis[μ -(dimethyl sulphoxide-*O*:*O*)]bis[μ -[hexafluoropentanedionato(2-)*O*:*O'*]]bis[μ -[4,5-dimethyl-3,6-bis(octyloxy)-1,2-phenylene]}tetramercury (ETH 9011, 1:4 DMSO adduct). ETH 9011 was obtained from ETH 9010 with dimethyl sulphoxide (DMSO) in analogy with [15]. Recrystallization from DMSO gave a white powder (yield 58%), m.p. 150°C: IR (KBr), 2858, 1699, 1350, 1165, 1012 cm^{-1} ; 1H NMR (200 MHz, $CDCl_3$), δ 0.88 ppm (t, $J = 6.4$ Hz, 24H), 1.20–1.52 (m, 80H), 1.76 (m, $J = 6.8$ Hz, 8H), 2.02 (s, 12H), 2.67 (s, 24H), 3.74 (t, $J = 6.5$ Hz, 8H); FAB-MS, m/z (%) 2339 (< 0.1, $M + Na^+$), 2123 (0.5), 2023 (0.5), 2004 (0.5, $M^+ - 4$ DMSO), 1778 (0.5), 1684 (1), 1563 (2), 360 (38), 247 (23), 177 (30), 163 (48), 138 (37), 69 (100).

Tridodecylmethylammonium perchlorate (TDDMAClO₄) and thiocyanate (TDDMASCN). The quaternary ammonium salts were prepared from TDDMACl by anion exchange according to [33]. TDDMAClO₄ (yield 77%), m.p. 106–107°C, hygroscopic. Analysis calculated for $C_{37}H_{78}ClNO_4$ (636.48), C 69.82, H 12.35, N 2.20, O, 10.05; found, C 70.02, H 12.57, N 2.18, O 10.19%. TDDMASCN (yield 73%), very hygroscopic. Analysis calculated for $C_{38}H_{78}N_2S$ (595.11), C 76.69, H 13.21, N 4.71; found, C 76.79, H, 13.41, N 4.60%.

RESULTS AND DISCUSSION

From ^{199}Hg NMR titrations and x-ray crystallography in previous work [15,20,21], the bidentate compound, dichloro-1,2-phenylenedimercury, was shown to form a 2:1 complex with tetraphenylphosphonium chloride. On the other hand, the corresponding multidentate macrocycle, tetrakis[μ -(1,2-dimethoxyethane-*O*:*O*, *O'*)]bis[μ -[hexafluoropentanedionato(2-)-*O*:*O'*]]bis[μ -(3,4,5,6-tetramethyl-1,2-phenylene)]tetramercury,

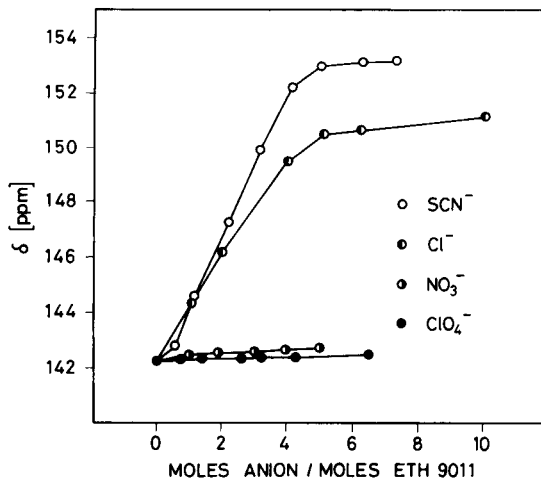


Fig. 2. ^{13}C chemical shift, δ (in $CDCl_3$), of the C atom adjacent to Hg in ETH 9011 as a function of TDDMA salt/ligand ratio. $\circ = SCN^-$; $\bullet = Cl^-$; $\bullet = NO_3^-$; $\bullet = ClO_4^-$.

gave a 1:4 and 1:2 complex with 1,2-dimethoxyethane and tetrahydrofuran, respectively [15].

With a view to using such complexes in solvent polymeric membrane electrodes for analytical purposes, the more lipophilic compounds, ETH 9009 and ETH 9011, were prepared (see Fig. 1). From ^{13}C NMR titrations with different tridodecylmethylammonium salts, observing the chemical shift of the carbon atom adjacent to mercury (see Fig. 2), it was found that the macrocycle, ETH 9011, forms 1:4 complexes with chloride and thiocyanate ($\Delta\delta \approx 7$ and 10 ppm, respectively), but does not interact appreciably with nitrate and perchlorate ($\Delta\delta < 1$ ppm).

For potentiometric studies, 2% (w/w) of ETH 9009 or ETH 9011 were incorporated in plasticized solvent polymeric PVC membranes. Regarding the amount of ionophore chosen, less than 2% (w/w) gave electrodes with no response, whereas larger amounts crystallized in the membrane phase after a few hours. Of the plasticizers tested, the most adequate proved to be DOS (for abbreviations, see Experimental). With other membrane solvents, no satisfactory results were obtained, e.g., poor electrode response functions (with TEHP), insufficient selectivity behaviour (with ETH 469, ETH 2112 or TOTM), sweating

membranes (with chloroalkanes or BBPA) or crystallization of the ionophores (with DBS, o-NPOE or ETH 2041). Selectivity measurements on DOS-PVC membrane electrodes in 0.1 M anion solutions by the separate solution method [30] revealed a significantly different sequence to that of classical anion exchangers (see Fig. 3, columns 2, 4 and 1). Especially noteworthy is the strongly reduced preference for the lipophilic anions, ClO_4^- and NO_3^- , and, to a lesser extent, for SCN^- , I^- , Br^- and even SalO^- . Surprisingly, the selectivity behaviour for ETH 9009 and ETH 9011 was similar in spite of their completely different complexing properties. With both ionophores, the slope of the chloride response functions in the range 10^{-5} –0.01 M NaCl was over-Nernstian (-65 to -75 mV) and at concentrations above 0.01 M NaCl, strong cation interference occurred. To avoid membranes becoming permselective for cations and to compensate for lipophilic anion sites originating from impurities in PVC [34], a lipophilic ammonium salt was added. With 1–3 mol% of TDDMACl (as referred to the ionophore), the slope of the re-

sponse functions was near-theoretical (cf., Fig. 4), with a detection limit of ca. 10^{-5} M Cl^- and only minor loss of Cl^- selectivity (cf., Fig. 3, columns 3 and 5). For membranes without additive, potential drifts were substantial and dependent on the anion measured (± 15 – 25 mV h^{-1} for hydrophilic and ± 3 – 10 mV h^{-1} for lipophilic anions). In contrast, with addition of 2.5 mol% TDDMACl, they decreased to < 1.5 and < 1 mV h^{-1} for electrodes based on ETH 9009 and ETH 9011, respectively. With higher ammonium salt concentrations, the electrode function, detection limit and response times (see below) were virtually the same, but the selectivity pattern gradually became that of a classical anion exchanger.

In Table 1, the selectivity coefficients obtained with ETH 9009 or ETH 9011 for some physiologically relevant anions are given together with the required $\log k_{\text{Cl}^-}^{\text{pot}}$ values taking into account a 1% error due to interfering anions (worst case) [35]. As can be seen, the experimental selectivities allow chloride to be determined in biological fluids even in the presence of salicylate.

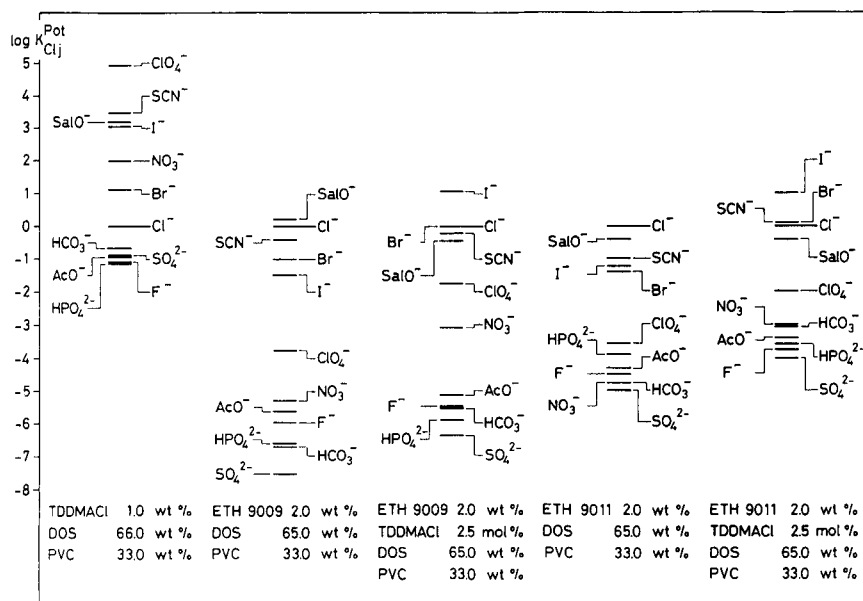


Fig. 3. Selectivity coefficients, $\log k_{\text{Cl}^-}^{\text{pot}}$, for membrane electrodes based on a classical anion exchanger (column 1) and on the mercury organic compounds ETH 9009 (columns 2 and 3) and ETH 9011 (columns 4 and 5). For details of measurements, see Experimental.

TABLE 1

95% normal concentration ranges and selectivity coefficients, $\log k_{Cl_j}^{pot}$, for interfering anions

| Anion | 95% normal concentration range (mmol l ⁻¹) ^a | Log $k_{Cl_j}^{pot}$ | | |
|--------------------------------|---|--------------------------|---------------------------|----------|
| | | Required ^b | Experimental ^c | |
| | | | ETH 9009 | ETH 9011 |
| Cl ⁻ | 95–110 | 0 | 0 | 0 |
| Br ⁻ | 0.009–0.17 | ≤ 0.7 | 0.0 | 0.1 |
| SCN ⁻ | 0.007–0.017 (0.15) ^d | ≤ 1.7 (0.8) ^d | -0.2 | 0.1 |
| SalO ⁻ | 2.2 ^e | ≤ -0.3 | -0.4 | -0.4 |
| HCO ₃ ⁻ | 21.3–26.5 | ≤ -1.4 | -5.5 | -3.0 |
| HPO ₄ ²⁻ | 0.26–0.89 | ≤ -1.2 | -5.9 | -3.6 |
| SO ₄ ²⁻ | 0.3–1.0 | ≤ -1.3 | -6.3 | -4.0 |

^a For whole blood, plasma and serum [35]. ^b Calculated for a minimum error of 1% due to interfering anion (worst case, 25°C) [35]. ^c Cf., Fig. 3, columns 3 and 5. ^d For non-smokers; values in parentheses for smokers. ^e Maximum therapeutical dosage (in plasma) [36].

For analytical applications, the response time of a sensor is an important factor. With ISEs based on anion carriers, $t_{90\%}$ values of seconds [8] to minutes [14] have been reported, depending on the anion measured and its concentration. For membrane electrodes containing ETH 9009 or ETH 9011, without ammonium salt, $t_{90\%} > 60$ s

was obtained, whereas with the addition of 2.5 mol% TDDMACl, this value was reduced to ca. 10 s (Fig. 5). The presence of > 5 mol% TDDMACl had no further influence on the response time, nor had the use of an ammonium salt (DMDODABr) with better phase-transfer catalytic properties.

When performing chloride analyses with ISEs in whole blood, plasma and serum, the standard deviation of the potential stability in the physiologically relevant concentration range must not exceed 0.19 mV (95% confidence limit) [35]. For membrane electrodes based on ETH 9009 or

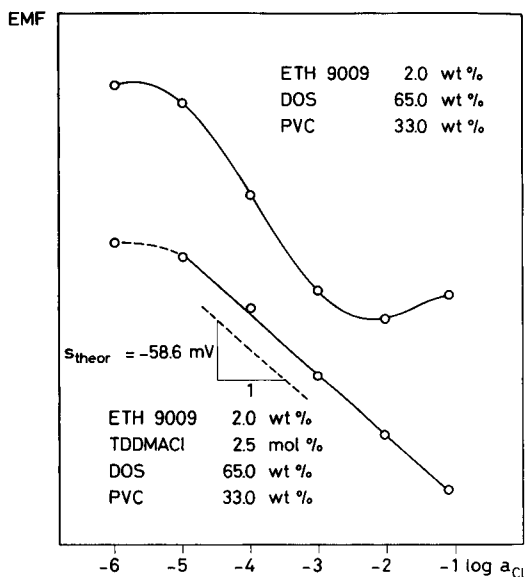


Fig. 4. Response functions of a cell assembly with membranes based on ETH 9009 (similar results for analogous membranes with ETH 9011). Slope for membrane electrode with addition of 2.5 mol% TDDMACl (as referred to ionophore), -57.6 ± 1.2 mV (S.D.); detection limit, $\log a_{Cl} \approx -5$ ($22 \pm 1^\circ\text{C}$).

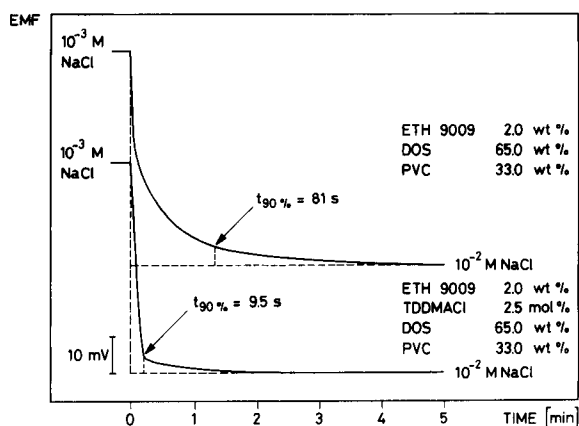


Fig. 5. Response time ($t_{90\%}$) determined for membrane electrodes based on ETH 9009 for a change in sample concentration from 0.001 to 0.01 M NaCl.

ETH 9011 with 2.5 mol% TDDMACl, the repeatability of the e.m.f. was determined by alternative measurements in 0.001 and 0.01 M aqueous NaCl. The corresponding standard deviations were 0.37 and 0.16 mV for ETH 9009 and 0.48 and 0.29 mV for ETH 9011 ($n = 10$). As expected, the potential stability is better at higher sample concentrations.

Further investigations on the use of these ISEs for chloride determinations in biological samples are planned.

The authors are grateful to Mr. H. Frohofer, University of Zürich, for microanalyses of the mercury compounds, and to Dr. D. Wegmann for helpful suggestions. Part of this work was supported by the Swiss National Science Foundation.

REFERENCES

- 1 F. Vögtle and E. Weber (Eds.), *Host-Guest Complex Chemistry/Macrocycles*, Springer, Berlin, 1985.
- 2 F.P. Schmidtchen, *Nachr. Chem. Tech. Lab.*, 36 (1988) 8.
- 3 D. Wegmann, H. Weiss, D. Ammann, W.E. Morf, E. Pretsch, K. Sugahara and W. Simon, *Mikrochim. Acta*, III (1984) 1.
- 4 H.E. Simmons and C.H. Park, *J. Am. Chem. Soc.*, 90 (1968) 2431.
- 5 F.P. Schmidtchen, *Chem. Ber.*, 114 (1981) 597.
- 6 B. Dietrich, D.L. Fyles, T.M. Fyles and J.M. Lehn, *Helv. Chim. Acta*, 62 (1979) 2763.
- 7 J. Koryta, *Anal. Chim. Acta*, 139 (1982) 1.
- 8 P. Schulthess, D. Ammann, B. Kräutler, C. Caderas, R. Stepánek and W. Simon, *Anal. Chem.*, 57 (1985) 1397.
- 9 F. Hofmeister, *Arch. Exp. Pathol. Pharmacol.*, 14 (1888) 247.
- 10 M.T. Reetz, C.M. Niemeyer and K. Harms, *Angew. Chem.*, 103 (1991) 1515, 1517.
- 11 M.E. Meyerhoff, E. Pretsch, D.H. Welti and W. Simon, *Anal. Chem.*, 59 (1987) 144.
- 12 B. Keller-Lehmann, *Dissertation*, ETH, Zürich, No. 9255, 1990.
- 13 H.E. Katz, *J. Am. Chem. Soc.*, 108 (1986) 7640.
- 14 U. Wuthier, H.V. Pham, R. Zünd, D. Welti, R.J.J. Funck, A. Bezegh, D. Ammann, E. Pretsch and W. Simon, *Anal. Chem.*, 56 (1984) 535.
- 15 F. Nadeau, M. Simard and J.D. Wuest, *Organometallics*, 9 (1990) 1311.
- 16 S.A. Glazier and M.A. Arnold, *Anal. Chem.*, 63 (1991) 754.
- 17 H.V. Pham, E. Pretsch, K. Fluri, A. Bezegh and W. Simon, *Helv. Chim. Acta*, 73 (1990) 1894.
- 18 S.S.S. Tan, P.C. Hauser, K. Wang, K. Fluri, K. Seiler, B. Rusterholz, G. Suter, M. Krüttli, U.E. Spichiger and W. Simon, *Anal. Chim. Acta*, 255 (1991) 35.
- 19 A. Lewenstam, *Anal. Proc.*, 28 (1991) 106.
- 20 J.D. Wuest and B. Zacharie, *Organometallics*, 4 (1985) 410.
- 21 A.L. Beauchamps, M.J. Olivier, J.D. Wuest and B. Zacharie, *J. Am. Chem. Soc.*, 108 (1986) 73.
- 22 A.L. Beauchamps, M.J. Olivier, J.D. Wuest and B. Zacharie, *Organometallics*, 6 (1987) 153.
- 23 V.B. Suhr, I.A. Tikhonova, A.I. Yanovsky, Y.T. Struchkov, P.V. Petrovskii, S.Y. Panov, G.G. Furin and M.E. Vol'pin, *J. Organomet. Chem.*, 418 (1991) C29.
- 24 X. Yang, C.B. Knobler and M.F. Hawthorne, *Angew. Chem.*, 103 (1991) 1519.
- 25 D.M. Pranis and M.E. Meyerhoff, *Anal. Chim. Acta*, 217 (1989) 123.
- 26 C. Behringer, B. Lehmann, J.-P. Haug, K. Seiler, W.E. Morf, K. Hartman and W. Simon, *Anal. Chim. Acta*, 233 (1990) 41.
- 27 R.E. Dohner, D. Wegmann, W.E. Morf and W. Simon, *Anal. Chem.*, 58 (1986) 2585.
- 28 P.C. Meier, D. Ammann, W.E. Morf and W. Simon, in J. Koryta (Ed.), *Medical and Biological Applications of Electrochemical Devices*, Wiley, New York, 1980, Chap. 2.
- 29 P.C. Meier, *Anal. Chim. Acta*, 136 (1982) 363.
- 30 G.G. Guilbault, R.A. Durst, M.S. Frant, H. Freiser, E.H. Hansen, T.S. Light, E. Pungor, G. Rechnitz, N.M. Rice, T.J. Rohm, W. Simon and J.D.R. Thomas, *Pure Appl. Chem.*, 48 (1976) 127.
- 31 E. Lindner, K. Tóth and E. Pungor, *Pure Appl. Chem.*, 58 (1986) 469.
- 32 B. Klieser, L. Rossa and F. Vögtle, *Kontakte (Darmstadt)*, No. 1 (1984) 3.
- 33 K. Hartman, S. Luterotti, H.F. Osswald, M. Oehme, P.C. Meier, D. Ammann and W. Simon, *Mikrochim. Acta*, II (1978) 235.
- 34 A. van den Berg, P.D. van der Wal, M. Skowronska-Ptasinska, E.J.R. Sudhölter, D.N. Reinhoudt and P. Bergveld, *Anal. Chem.*, 59 (1987) 2827.
- 35 U. Oesch, D. Ammann and W. Simon, *J. Chem. Soc., Faraday Trans. 1*, 82 (1986) 1179.
- 36 M. Steelman, C.H. Smith, A. Menon, B.T. Thach, R.E. Hillman and M. Landt, *Clin. Chem.*, 30 (1984) 562.

Development of a chemically modified electrode based on carbon paste and functionalized silica gel for preconcentration and voltammetric determination of mercury(II)

L.M. Aleixo, M. de Fátima B. Souza, O.E.S. Godinho, G. de Oliveira Neto and Y. Gushikem
Instituto de Química, Unicamp, C.P. 6154, 13081 Campinas, SP (Brazil)

José C. Moreira

Instituto de Química, Unesp, C.P. 174, 14800 Araraquara, SP (Brazil)

(Received 10th April 1992; revised manuscript received 3rd August 1992)

Abstract

A mercury-sensitive chemically modified electrode (CME) based on modified silica gel-containing carbon paste was developed. The functional group attached to the silica gel surface was 3-(2-thiobenzimidazolyl)propyl, which is able to complex mercury ions. This electrode was applied to the determination of mercury(II) ions in aqueous solution. The mercury was chemically preconcentrated on the CME prior to voltammetric determination by anodic stripping in the differential-pulse mode. A calibration graph covering the concentration range from 0.08 to 2 mg l⁻¹ was constructed. The precision for six determinations of 0.122 and 0.312 mg l⁻¹ Hg(II) was 3.2 and 2.9% (relative standard deviation), respectively. The detection limit for a 5-min preconcentration period was 0.013 mg l⁻¹. A study for foreign ions was also made.

Keywords: Voltammetry; Carbon paste electrodes; Chemically modified electrodes; Functionalized silica gel; Mercury; Preconcentration

Chemically modified electrodes (CMEs) have been developed in recent years for use in voltammetric measurements [1–8]. One interest is the use of these electrodes as chemical sensors for analytical determinations. Several materials have been employed as surface modifiers with the objective of preconcentrating the analyte at the electrode surface via a selective reaction with the surface modifier. The surface-bound analyte is then determined by a conventional voltammetric method [2–8].

The aim of this study was to develop a carbon paste CME for Hg(II) determination. Voltammetric approaches to mercury determination usually involve the use of solid graphite electrodes, including stripping analysis [9]. Gold electrodes are also used, in either a stationary or a flow system, for environmental samples [10–13]. The determination of Hg(II) with chemically modified solid electrodes has been reported [14–17]. The use of carbon paste electrodes with ligands incorporated in the carbon paste has also been attempted [18,19], with the purpose of improving the selectivity of the voltammetric determination.

In this work, functionalized silica gel was em-

Correspondence to: L.M. Aleixo, Instituto de Química, Unicamp, C.P. 6154, 13081 Campinas, SP (Brazil).

ployed as preconcentration agent in a carbon paste CME. Investigations on the preparation and uses of silica gel with organic functional groups covalently bonded on its surface for preconcentration of ions have been reported by others [20–23]. 2-Mercaptobenzimidazole, which has already been employed for the determination of Hg(II) [24], was chosen as the functionalization agent. It was incorporated in the silica gel surface by reaction with (3-chloropropyl)silica gel, resulting in the product 3-(2-thiobenzimidazolyl)propyl silica gel [25], which was employed as the electrode surface modifier.

This work involved the construction and voltammetric study of a chemically modified carbon paste electrode (CMCPE) with functionalized silica gel in presence of Hg(II) ions. One advantage of 2-mercaptobenzimidazole is the good selectivity that it presents as a complexing agent for Hg(II) ions [25]. The chemical selectivity of this functional group and the selectivity of voltammetry were combined for preconcentration and determination.

EXPERIMENTAL

Apparatus and reagents

Voltammetric measurements were made with a Metrohm E 506 Polarecord and a Metrohm E 505 stand. The voltammetric cell was a three-electrode system, consisting of the carbon paste electrode modified with functionalized silica gel as the working electrode, an Ag/AgCl, saturated KCl as the reference electrode and a platinum wire as the auxiliary electrode.

Reagents

The graphite used was UCP-1-200-U (Ultra Carbon), passed through a stainless-steel sieve of 250 mesh. The modified silica gel functionalized with 3-(2-thiobenzimidazolyl)propyl groups was prepared according to the literature [25].

Electrode construction

The CMCPEs were prepared with a mixture of graphite, 37% Nujol and silica gel functionalized with 3-(2-thiobenzimidazolyl)propyl in propor-

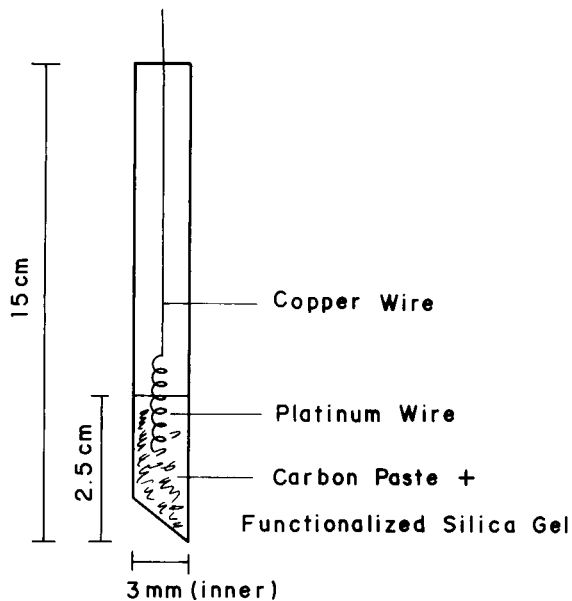


Fig. 1. Design of the working electrode.

tions of 5, 10 and 20%, respectively. After the mixture had been homogenized, it was used to fill a glass tube of i.d. 3 mm up to a height of 2.5 cm. The extremity of the tube was cut at an angle (Fig. 1).

Electrical contact was made with a platinum wire, with one end placed in the carbon paste of the tube and the other attached to the copper wire of the electric cable. The external surface of the electrode was smoothed on soft paper. A new surface can be produced by scraping out the old surface and replacing the carbon paste.

Electrode conditioning

An electrode with a fresh surface was preconditioned by immersing it in a stirred 1.5 mg l^{-1} mercury solution at pH 3.00, adjusted with HNO_3 , for 10 min with open circuit. The speed of stirring was 500 rpm. The differential-pulse voltammogram was recorded over the range -0.2 to $+0.6$ V in 0.01 M KNO_3 solution. In fact it was observed that this solution was also about 0.001 M in KCl owing to diffusion from the reference electrode. The surface of electrode was then cleaned for 3 min in 0.01 M KCN solution with open circuit. The cycle was repeated three more

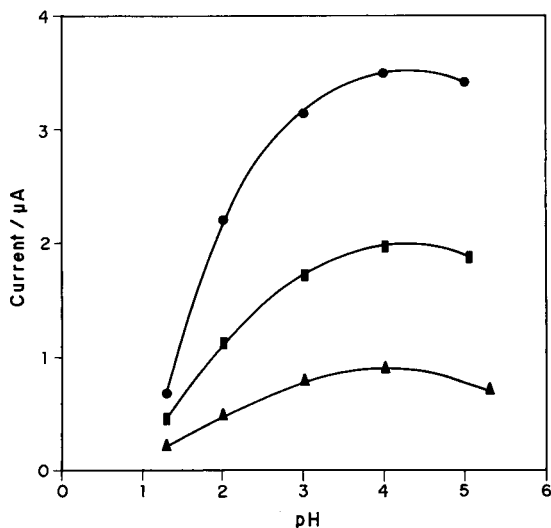
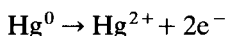


Fig. 3. Effect of the pH of the preconcentration solution of Hg(II) on the anodic peak current of Hg(II). Mode, differential-pulse voltammetry; preconcentration time, 5 min; $\Delta E = -50$ mV; scan rate, 8 mV s^{-1} . Hg(II) concentration; $\blacktriangle = 0.2$; $\blacksquare = 0.4$; $\bullet = 0.8 \text{ mg l}^{-1}$.

When the potential scan reaches the value of +288 mV, an anodic peak is produced owing to the oxidation of mercury:



The scan rate of 8 mV s^{-1} used in the differential-pulse mode showed no necessity for a fixed time at -0.2 V for the reduction of mercury and the scan started immediately after the connection of the electrodes.

Figure 3 shows the relationships between the measured current and pH at mercury concentrations of 0.2, 0.4 and 0.8 mg l^{-1} . The maximum current was obtained at pH 4.0, but it was observed that at pH 3.0 the method shows a better tolerance to interfering ions.

The effect of the paste composition for electrodes containing 5, 10 and 20% of functionalized silica is shown in Table 1. The results for a 0.4 mg l^{-1} mercury(II) solution indicated that the paste containing 10% of modified silica produced the highest current.

The cleaning solution was used 0.01 M KCN and was found to be very efficient. EDTA, KCl

TABLE 1

Effect of carbon paste composition on the peak current of mercury(II)

| Concentration of modified silica gel in carbon paste (%) | Current (μA) | R.S.D. (%) ($n = 6$) |
|--|---------------------------|------------------------|
| 5.0 | 1.20 | 4.6 |
| 10.0 | 1.72 | 3.6 |
| 20.0 | 1.36 | 4.0 |

and KSCN solutions were also tested, but were not efficient.

The influence of accumulation time in the preconcentration step for mercury concentrations of 0.08, 0.2 and 0.4 mg l^{-1} is shown in Fig. 4. The greatest increase in current occurred in the first 5 min and this time was chosen for the preconcentration step.

Figure 5 shows a calibration graph of current vs. mercury concentration in the range $0.08\text{--}2 \text{ mg l}^{-1}$ and Fig. 6 shows some voltammograms of points on this graph. The first four points on the curve ($0.08\text{--}0.6 \text{ mg l}^{-1}$) obey the straight-line equation

$$i = 4.10C - 0.073$$

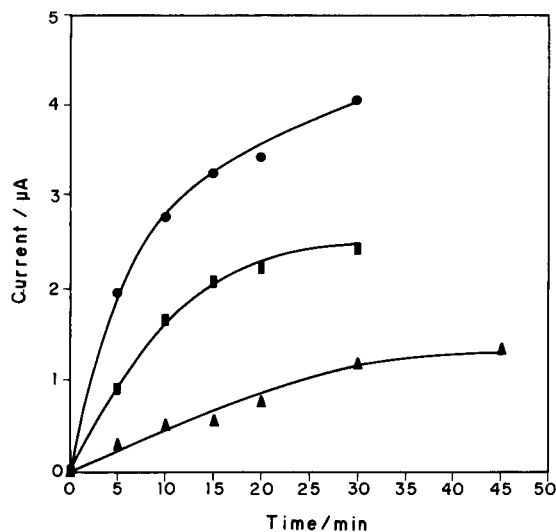


Fig. 4. Effect of the preconcentration time on the anodic peak current at various Hg(II) concentrations. Mode, differential-pulse voltammetry; $\Delta E = -50$ mV; scan rate, 8 mV s^{-1} . Hg(II) concentration: $\blacktriangle = 0.08$; $\blacksquare = 0.2$; $\bullet = 0.4 \text{ mg l}^{-1}$.

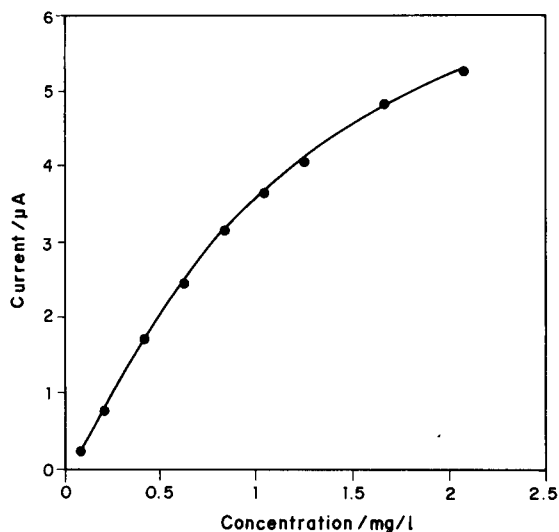


Fig. 5. Calibration graph of current versus mercury concentration. Mode, differential-pulse voltammetry; preconcentration time, 5 min; $\Delta E = -50$ mV; scan rate, 8 mV s^{-1} .

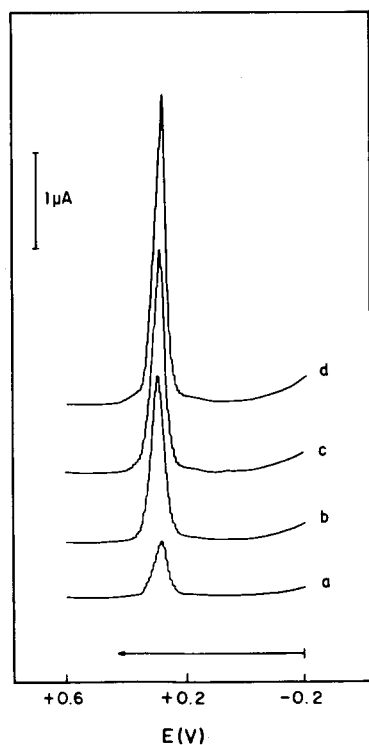


Fig. 6. Differential-pulse voltammograms for different Hg(II) concentrations after 5-min preconcentration: (a) 0.2; (b) 0.4; (c) 0.6; (d) 0.8 mg l^{-1} . $\Delta E = -50$ mV; scan rate, 8 mV s^{-1} .

TABLE 2

Study of the effect of interfering ions on the voltammetric signal of mercury(II)^a

| Metal ion (X) | $[X]/[\text{Hg}^{2+}]$ | Relative signal ^b |
|---------------|------------------------|------------------------------|
| Pb(II) | 100 | 0.97 |
| Zn(II) | 100 | 0.98 |
| Co(II) | 100 | 0.98 |
| Ni(II) | 100 | 0.99 |
| Cd(II) | 10 | 0.96 |
| | 100 | 1.02 |
| Cu(II) | 10 | 0.95 |
| | 100 | 1.03 |
| Ag(I) | 10 | 1.04 |
| | 100 | 1.37 |

^a $[\text{Hg}^{2+}] = 0.4 \text{ mg l}^{-1}$; accumulation time = 5 min; pH = 3.0.

^b The relative signal is the ratio of the peak current of Hg(II) in the presence to that in the absence of foreign ions.

with a correlation coefficient of 0.998, where i is the current in μA and C is the concentration of Hg(II) in mg l^{-1} . For points between 0.6 and 2 mg l^{-1} , the plot shows non-linear behaviour, which requires the use of a calibration graph in this concentration range. It was observed that the points in the non-linear range obey a logarithmic equation:

$$i = 1.02 \log C + 3.56$$

with a correlation coefficient of 0.999.

The precision obtained for six replicate determinations of each of 0.122 and 0.312 mg l^{-1} Hg(II) in the linear range of the calibration graph was 3.2 and 2.9% (relative standard deviation), respectively. The detection limit evaluated at a signal-to-noise ratio of 3 for 0.08 mg l^{-1} Hg(II) was $13 \mu\text{g l}^{-1}$.

The results of the study of the influence of foreign ions is presented in Table 2. Divalent ions showed virtually no interference in the concentration range studied. However, Ag(I) at a concentration ratio of 10:1 showed significant interference, as usually occurs in the voltammetric determination of mercury in presence of silver.

The results obtained in this study show that the CMCPE with functionalized silica gel has good potential for use in the voltammetric determination of mercury. The ligand used, 3-(2-thio-benzimidazolyl)propyl, has a good selectivity for

Hg(II) [25], which, in addition to the voltammetric selectivity, is an advantage for analytical purposes.

The authors are grateful to FAPESP, Fundação de Amparo à Pesquisa do Estado de São Paulo, for financial assistance.

REFERENCES

- 1 C. Urbaniczky and K. Lundström, *J. Electroanal. Chem.*, 176 (1984) 169.
- 2 R.P. Baldwin, J.K. Christensen and L. Kruger, *Anal. Chem.*, 58 (1986) 1790.
- 3 S.V. Prabhu and R.P. Baldwin, *Anal. Chem.*, 59 (1987) 1074.
- 4 J. Wang and T. Martinez, *Anal. Chim. Acta*, 207 (1988) 95.
- 5 L. Hernández, J.M. Melguizo, M.H. Blanco and P. Hernández, *Analyst*, 114 (1989) 397.
- 6 S. Tanaka and H. Yoshida, *Talanta*, 36 (1989) 1044.
- 7 S.A. Wring, J.P. Hart and B.J. Birch, *Analyst*, 116 (1991) 123.
- 8 K. Sugawara, S. Tanaka and M. Taga, *Analyst*, 116 (1991) 131.
- 9 J. Wang, *Stripping Analysis*, VCH, Dearfield Beach, FL, 1985.
- 10 M. Lev and H. Seiler, *Fresenius' Z. Anal. Chem.*, 321 (1985) 479.
- 11 G.J. Suoboda, J.P. Sottery and W.C. Anderson, *Anal. Chim. Acta*, 166 (1984) 297.
- 12 I. Gustavsson, *J. Electroanal. Chem.*, 214 (1986) 31.
- 13 F.S. Chagonda Lameck and J.S. Millership, *Analyst*, 113 (1988) 243.
- 14 M.D. Imisides, D.M.T. O'Riordan and G.G. Wallace, *Anal. Lett.*, 21 (1988) 1969.
- 15 M.D. Imisides and G.G. Wallace, *J. Electroanal. Chem.*, 246 (1988) 181.
- 16 J. Labuda and V. Plaskoň, *Anal. Chim. Acta*, 228 (1990) 259.
- 17 J. Lexa and K. Štulík, *Talanta*, 36 (1989) 843.
- 18 L. Ulrych and P. Rueggsegger, *Fresenius' Z. Anal. Chem.*, 277 (1975) 349.
- 19 I. Šuankara, K. Vytrás, C. Hua and M.R. Smyth, *Talanta*, 39 (1992) 391.
- 20 P. Suthivaiyakit and A. Kettrup, *Anal. Chim. Acta*, 169 (1985) 331.
- 21 M. Volkan, D.Y. Ataman and A.G. Howard, *Analyst*, 112 (1987) 1409.
- 22 K. Terada, K. Matsumoto and H. Kimura, *Anal. Chim. Acta*, 153 (1983) 237.
- 23 L.C. Sander and S.A. Wise, *CRC Crit. Rev. Anal. Chem.*, 4 (1987) 299.
- 24 A.A. Kovalenko, K.A. Uvarova, Yu.I. Usatenko and T.I. Zubstoka, *Zh. Anal. Khim.*, 32 (1977) 270.
- 25 J.C. Moreira, L.C. Pavan and Y. Gushikem, *Mikrochim. Acta*, III (1990) 107.

Potentiometric study of azide complexes of copper(II) in aqueous medium

J.F. de Andrade and O.M. Guimarães

Departamento de Química, FFCLRP-USP, Ribeirão Preto, 14040-901, SP (Brazil)

(Received 13th July 1992)

Abstract

The stepwise formation of copper(II)-azide complexes in aqueous sodium perchlorate medium was investigated at $25.0 \pm 0.1^\circ\text{C}$ and ionic strength 1.0 M. With the indirect potentiometric method employed, using a glass electrode and under the conditions studied, four mononuclear complexes were detected. No evidence of polynuclear species was found. The final analysis of the data, by solution of simultaneous equations (matrix method), led to the following overall formation constants: $\beta_1 = 2.44 \times 10^2 \text{ l mol}^{-1}$, $\beta_2 = 1.20 \times 10^4 \text{ l}^2 \text{ mol}^{-2}$, $\beta_3 = 1.45 \times 10^5 \text{ l}^3 \text{ mol}^{-3}$ and $\beta_4 = 3.18 \times 10^7 \text{ l}^4 \text{ mol}^{-4}$. The graphical method of Leden, with some refinements, was also utilized initially.

Keywords: Potentiometry; Azide complexes; Copper

A continuing, systematic investigation of azide complexes, with several metallic cations, has been made in order to obtain data on their coordination chemistry [1–5] and to develop analytical applications [6–8]. As part of these investigations, this paper reports a competitive and indirect potentiometric study of the copper(II)-azide system with the use of a glass electrode and pH measurements on solutions containing different copper(II) concentrations and azide-hydrazoic acid buffers. All measurements were made in aqueous medium at 25.0°C and ionic strength 1.0 M (sodium perchlorate).

The reaction in acidified medium between azide and copper(II) has previously been used spectrophotometrically to determine the metal [8–12] and the ligand [6,13] and to establish equilibrium constants [2,14–16]. In such equilibrium studies, principally the first stability constant was determined.

The formation constants of this system have been also studied by solubility [17,18], polarographic [19] and potentiometric [19,20] methods. Attempts to make potentiometric measurements with membrane ion-selective and solid-state electrodes in order to study the complex formation involving such species were unsuccessful. The low solubility of neutral species, $\text{Cu}(\text{N}_3)_2$, has been the main obstacle to other more complete potentiometric studies. However, a convenient, precise, indirect method, based on the change in the pH of an azide-hydrazoic acid buffer (after introduction of the metallic ion), was developed and has also been successfully applied to the similar cobalt(II)-azide [1], uranyl-azide [3], nickel(II)-azide [4] and iron(III)-azide [5] systems.

EXPERIMENTAL

Reagents and solutions

All reagents were chemically pure or of analytical-reagent grade. Sodium azide (Merck) was

Correspondence to: J.F. de Andrade, Departamento de Química, FFCLRP-USP, Ribeirão Preto, 14040-901, SP (Brazil).

prepared and analysed as described previously [8].

Sodium perchlorate (Merck) was used to prepare a solution of about 4.0 M. Standardization was performed by direct gravimetry [3,4].

A standard copper(II) perchlorate solution (0.356 M) was prepared containing excess of perchloric acid (both reagents from Merck) to prevent hydrolysis. Standardization was done by classical electrogravimetry. The free acid content in the metal stock standard solution was determined potentiometrically and by classical volumetric titration, utilizing standardized sodium hydroxide solution.

Apparatus and procedures

A Micronal B-375 digital potentiometer, adapted to a Metrohm EA-121 glass electrode and combined with an Ag/AgCl reference electrode (filled with 3.0 M sodium chloride solution), was used in all pH measurements. The condi-

tional pH data measured at 1.0 M ionic strength (with regard to hydrogen ion concentration instead of activity) require the use, for example, of a pH 2.000 standard solution to calibrate the apparatus (25.0°C). This standard medium was 0.99 M NaClO₄ with a free hydrogen concentration of 0.0100 M HClO₄. Before the calibration, the glass electrode was maintained in thermostated 1.0 M sodium perchlorate for at least 1 h. After the calibration, the electrode was checked against other standard solutions (pH 1.000, 3.000 and 4.000), yielding a rapid, exact and stable response.

In order to obtain still more confident measurements, the Nernstian response of the working electrode was determined by titration of a 0.009615 M acidic solution with NaOH (both standardized and at 1.0 M ionic strength). The experimental slope of the curve (measured potential vs. calculated pH) was inserted in the computer program, as a correction factor, to adjust

TABLE 1

Potentiometric results for the copper(II)–azide system at 25.0°C and ionic strength 1.0 M (NaClO₄)

| $C'_{N_3^-}$ (mM) | $[N_3^-]_1$ (mM) | pH ₁ | pH ₂ | pK _a | \bar{n} | $[N_3^-]_2^a$ (mM) | Log $[N_3^-]_2$ |
|----------------------|---------------------|-----------------|-----------------|-----------------|-----------|-----------------------|-----------------|
| 19.34 | 9.608 | 4.472 | 3.425 | 4.176 | 0.2924 | 1.879 | 0.274 |
| 29.97 | 15.44 | 4.513 | 3.370 | 4.202 | 0.3383 | 2.199 | 0.342 |
| 17.85 | 5.892 | 4.371 | 3.571 | 4.198 | 0.4284 | 2.923 | 0.465 |
| 29.97 | 15.44 | 4.513 | 3.572 | 4.202 | 0.5083 | 3.485 | 0.542 |
| 26.08 | 13.39 | 4.558 | 3.735 | 4.248 | 0.5846 | 4.025 | 0.605 |
| 29.97 | 15.44 | 4.513 | 3.674 | 4.202 | 0.6199 | 4.398 | 0.643 |
| 44.91 | 15.57 | 4.191 | 3.240 | 4.008 | 0.6954 | 4.732 | 0.675 |
| 52.16 | 14.72 | 4.142 | 3.146 | 4.000 | 0.7116 | 4.818 | 0.683 |
| 33.31 | 10.99 | 4.250 | 3.453 | 4.068 | 0.7235 | 5.201 | 0.716 |
| 29.97 | 15.44 | 4.513 | 3.773 | 4.202 | 0.7570 | 5.515 | 0.741 |
| 31.85 | 8.598 | 4.159 | 3.436 | 4.023 | 0.8521 | 5.909 | 0.771 |
| 59.92 | 16.59 | 4.090 | 3.190 | 4.008 | 0.9926 | 6.956 | 0.842 |
| 31.85 | 8.598 | 4.159 | 3.538 | 4.023 | 1.058 | 7.518 | 0.876 |
| 59.92 | 16.59 | 4.090 | 3.285 | 4.008 | 1.226 | 8.802 | 0.945 |
| 33.31 | 10.99 | 4.250 | 3.754 | 4.068 | 1.352 | 10.57 | 1.02 |
| 31.85 | 8.598 | 4.159 | 3.729 | 4.023 | 1.540 | 11.77 | 1.07 |
| 31.85 | 8.598 | 4.159 | 3.837 | 4.023 | 1.893 | 15.15 | 1.18 |
| 31.85 | 8.598 | 4.159 | 3.940 | 4.023 | 2.274 | 19.26 | 1.28 |
| 38.63 | 13.23 | 4.250 | 4.056 | 4.070 | 2.545 | 24.68 | 1.39 |
| 44.91 | 15.57 | 4.191 | 4.012 | 4.008 | 2.945 | 29.66 | 1.47 |
| 52.16 | 14.73 | 4.142 | 4.042 | 4.070 | 3.520 | 42.28 | 1.63 |
| 59.92 | 16.59 | 4.090 | 3.980 | 4.008 | 3.559 | 47.12 | 1.67 |

^a Represents the calculated free ligand final concentration, $[N_3^-]$, in conformity with the terminology and methodology previously reported and utilized [1,3–5].

measured pH values for non-Nernstian responses of the glass electrode. This procedure has been recommended for more accurated analytical results [21].

The calibrated electrode was then employed for pH measurements of the different azide buffer solutions at the same ionic strength. All experimental solutions were gently stirred during the measurements in a Metrohm EA-876 thermostated cell (25.0°C).

To 20.00 cm³ of a working azide solution of ionic strength 1.0 M, a small, known volume of 0.94 M perchloric acid was added (using a Metrohm EA-734-5 piston burette) to obtain an azide–hydrazoic acid buffer of conditional pH₁. Then, a known volume of standard 0.356 M copper(II) solution was added to this buffer and, immediately, a pH₂ was obtained due to equilibria readily attained. Successive metal additions to each sample are possible. Turbid or precipitated solutions were discarded.

The treatment of data with mass balances and all corrections for dilution by reagent additions were performed with a BASIC program for a PC-XT microcomputer. With this program, as described previously [22], the average ligand number (\bar{n}) and free ligand final concentration data can be determined from pH₁ and pH₂ values.

RESULTS AND DISCUSSION

General aspects

The adopted procedure is a competitive and indirect method based on the change in the conditional pH value of an azide–hydrazoic acid buffer on addition of a known concentration of copper(II). The measurement of the pH changes in a series of solutions with different concentrations leads to final values of the free ligand concentration and \bar{n} , as has already been fully discussed [1,3].

In this study, different series with distinct buffers and different metallic concentrations were examined. Table 1 gives some experimental and calculated results for the last series studied, in which the copper(II) concentrations were doubled compared with the others. As the same

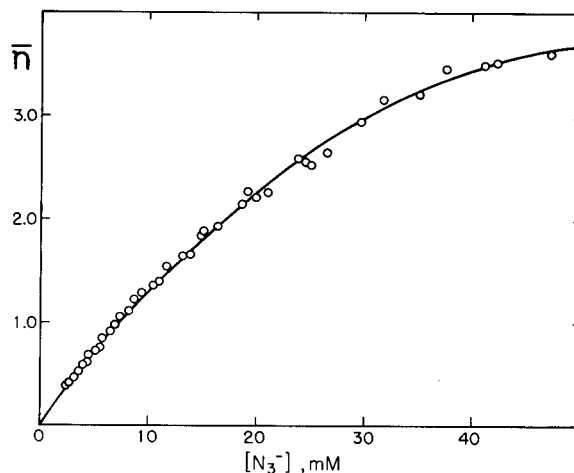


Fig. 1. Formation curve of the copper(II)–azide system under the studied conditions. The points represent experimental values and the curve represents \bar{n} calculated from the final formation constants.

experimental formation curve (\bar{n} vs. $[N_3^-]$) was obtained for different copper(II) concentrations, no significant polynuclear complexation is evident in the metal concentration range employed (2.12–70.0 mM).

It should be mentioned that the merit of this technique is the use of a conditional pK_a of the weak acid (HN_3) for each particular working solution, instead of an average value, in order to obtain more accurate \bar{n} data due to some factors described previously [1,3].

The best formation curve (normalized) was drawn from the experimental points via the mentioned BASIC program. The low initial \bar{n} values on the normalized curve (Fig. 1), as a function of the low free azide concentration, show that the early complexes are relatively weak. For free ligand concentrations higher than 50.0 mM, the curve reaches a constant value of \bar{n} (near 4), indicating a system with up to four successive complexes.

As Leden's function, $F_0(X)$, is more suitable than \bar{n} for the treatment of data in complicated systems (several stepwise complexes), the normalized (and calculated) values of \bar{n} were transformed into $F_0(X)$ values by the Fronaeus equation, using the normalized curve of \bar{n} vs. $\log[N_3^-]$ and a program for the mathematical integration.

TABLE 2

Matrix obtained with $F_0(X)$ and $[N_3^-]$ data from Table 1

| | | | |
|--|----------------------------------|----------------------------------|-----------------------------------|
| $2222.1 = 3.7514\beta_1$ | $+ 4.7003 \times 10^{-2}\beta_2$ | $+ 8.3937 \times 10^{-4}\beta_3$ | $+ 1.9528 \times 10^{-5}\beta_4$ |
| $41.906 = 4.7003 \times 10^{-2}\beta_1$ | $+ 8.3937 \times 10^{-4}\beta_2$ | $+ 1.9528 \times 10^{-5}\beta_3$ | $+ 5.5096 \times 10^{-7}\beta_4$ |
| $1.0865 = 8.3937 \times 10^{-4}\beta_1$ | $+ 1.9528 \times 10^{-5}\beta_2$ | $+ 5.5096 \times 10^{-7}\beta_3$ | $+ 1.7828 \times 10^{-8}\beta_4$ |
| $3.4188 \times 10^{-2} = 1.9528 \times 10^{-5}\beta_1$ | $+ 5.5096 \times 10^{-7}\beta_2$ | $+ 1.7828 \times 10^{-8}\beta_3$ | $+ 6.3545 \times 10^{-10}\beta_4$ |

This program also furnishes the subsidiary $F_1(X)$ values [1,3].

Calculation of equilibrium constants

The treatment of $F_0(X)$ data to find the constants was done by two different methods. The first was the classical Leden graphical method, extrapolating each subsidiary $F_n(X)$ function to zero ligand concentration. Some refinements were also introduced to improve the results from extrapolations, according to the technique of "multiple extrapolation" mentioned previously [5]. The graphical method is useful for providing a preliminary report of the formation constant values, for showing the number of different species present and for indicating the points with gross experimental error.

Four complex species were clearly detected within the ligand concentration range studied (up to 100 mM). In fact, plots of $F_1(X)$ and $F_2(X)$ values against $[N_3^-]$, to obtain the corresponding β_n overall formation constants, are non-linear. In contrast, $F_3(X)$ gives a straight line ($r^2 = 0.999$), indicating that this species (with three ligands) is really the penultimate one.

TABLE 3

Overall formation and equilibrium constants for the copper(II)-azide system at 25.0°C and ionic strength 1.0 M (NaClO₄)

| Leden's graphical method ^a | | Matrix method (4 × 4) ^b | |
|--|---------------------------------|--|---------------------------------|
| β_n (l ⁿ mol ⁻ⁿ) | K_n (l mol ⁻¹) | β_n (l ⁿ mol ⁻ⁿ) | K_n (l mol ⁻¹) |
| $\beta_1 = 241$ | $K_1 = 241$ | $\beta_1 = 244$ | $K_1 = 244$ |
| $\beta_2 = 1.03 \times 10^4$ | $K_2 = 42.7$ | $\beta_2 = 1.20 \times 10^4$ | $K_2 = 49.2$ |
| $\beta_3 = 2.17 \times 10^5$ | $K_3 = 21.1$ | $\beta_3 = 1.45 \times 10^5$ | $K_3 = 12.1$ |
| $\beta_4 = 2.90 \times 10^7$ | $K_4 = 134$ | $\beta_4 = 3.18 \times 10^7$ | $K_4 = 219$ |

^a With multiple extrapolation. ^b From levelled simultaneous equations.

The second treatment for obtaining the stability constants was an appropriate arrangement of $F_0(X)$ data in equations to be solved by matrix calculations. The main problem with this methodology (weighting factor) has been observed and studied as indicated previously [5]. From the data, matrix models including different equations were obtained and analysed by a computer program. The matrix containing four mononuclear complexes (Table 2) was unique in providing just positive values for all β_n , furnishing very reliable results.

Both methods gave similar values for the formation constants (see Table 3, where the corresponding equilibrium constants are shown).

Using the final β_n constants from each method, a comparison between calculated and experimental \bar{n} values was made by another computer program. A better fit was obtained by the matrix solution that exhibited a smaller average deviation than by the graphical preliminary treatment.

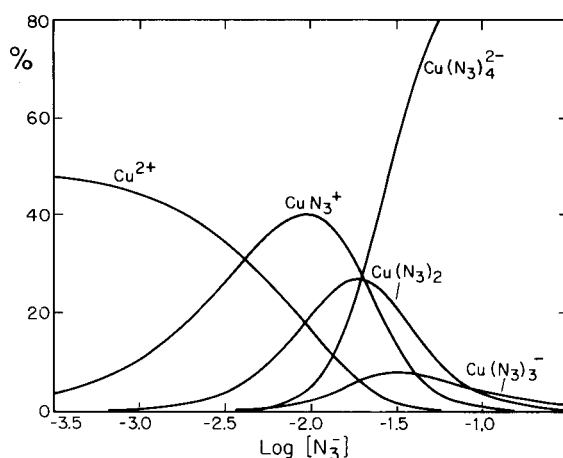


Fig. 2. Distribution diagram of various species present in the copper(II)-azide system.

TABLE 4

Values of stability constants obtained by different workers for the present system

| Method | Ionic strength (NaClO ₄) (M) | T (°C) | β_1 (l mol ⁻¹) | β_2 (l ² mol ⁻²) | β_3 (l ³ mol ⁻³) | β_4 (l ⁴ mol ⁻⁴) | Ref. |
|-------------------|---|-----------|----------------------------------|---|---|---|-----------|
| Spectrophotometry | 4.0 | 25 | – | 2.9×10^4 | 3.0×10^6 | – | 2 |
| Spectrophotometry | 0.1 | 20 | 280 | – | – | – | 14 |
| | 0.2 | 20 | 230 | – | – | – | 14 |
| Spectrophotometry | – | – | 270 | – | – | – | 15 |
| Spectrophotometry | 1.0 | 25 | 160 | – | – | – | 16 |
| Solubility | 0.2 → 0 | 25 | 720 ^a | 3.4×10^4 ^a | 1.7×10^6 ^a | 4.5×10^6 ^a | 17 |
| Solubility | 4.0 | 25 | 360 | 3.0×10^4 | 1.3×10^6 ^b | 6.6×10^7 | 18 |
| Polarography | 4.0 | 25 | – | – | 5.8×10^7 ^c | 6.5×10^7 | 19 |
| Potentiometry | 1.0 | 25 | 110 | – | – | – | 20 |
| | 3.0 | 25 | 5600 | – | – | – | 20 |
| Potentiometry | 1.0 | 25 | 240 | 1.2×10^4 | 1.5×10^5 | 3.2×10^7 | This work |

^a Thermodynamic values. ^b By interpolation. ^c Triazidocuprate(I).

Figure 1 shows the partial experimental data of \bar{n} vs. free ligand concentration. The curve was calculated from the final values of the stability constants obtained by the matrix method. There was no evidence of polynuclear or other complexes using the studied conditions, as no systematic deviations could be seen among the different experimental series of test solutions. The distribution diagram of the mononuclear complexes is shown in Fig. 2.

Table 4 gives a survey of several stability constants determined by a variety of methods, conditions and workers for the present system. A comparison between the present complete potentiometric results and all those reported previously (most of them partially) shows reasonable agreement among the β_n values.

The authors are grateful to the FAPESP and CNPq (Brazilian Foundations) for financial support and thank M.E.V. Suárez Iha for useful discussions.

REFERENCES

- 1 E.A. Neves, R. Tokoro and M.E.V. Suárez, *J. Chem. Res. (M)*, 11 (1979) 4401.
- 2 E.A. Neves, E. Oliveira and Z.L. Santos, *Talanta*, 27 (1980) 609.
- 3 G.O. Chierice and E.A. Neves, *Polyhedron*, 2 (1983) 31.
- 4 M.E.V. Suárez, E.A. Neves and R. Tokoro, *Can. J. Chem.*, 61 (1983) 1907.
- 5 E.A. Neves and J.F. Andrade, *Polyhedron*, 5 (1986) 717.
- 6 E.A. Neves, E. Oliveira and L. Sant'Agostino, *Anal. Chim. Acta*, 87 (1976) 243.
- 7 R. Luca, J.E. Bevilacqua, J.F. Andrade and E.A. Neves, *Anal. Lett.*, 20 (1987) 389.
- 8 E.A. Neves, J.F. Andrade and G.O. Chierice, *Anal. Chim. Acta*, 155 (1983) 269.
- 9 K. Kapitańczyk, Z. Kurzawa and Z. Prymiński, *Chem. Anal. (Warsaw)*, 6 (1961) 23.
- 10 F. Maggio and F.P. Cavasino, *Ann. Chim. (Rome)*, 51 (1961) 1392.
- 11 T. Kanie, *Bunseki Kagaku*, 7 (1958) 510; *Chem. Abstr.*, 54 (1960) 16260c.
- 12 E.A. Neves, J.F. Andrade and G.O. Chierice, *Anal. Lett.*, 18 (1985) 707.
- 13 M.P. Peters, PhD Thesis, University of São Paulo, 1980.
- 14 G. Saini and G. Ostacoli, *J. Inorg. Nucl. Chem.*, 8 (1958) 346.
- 15 H.K. El-Shamy and M.F. Nassar, *J. Inorg. Nucl. Chem.*, 16 (1960) 124.
- 16 L.M. Aleixo, Master Dissertation, University of Campinas, 1975.
- 17 P. Senise and E.A. Neves, *J. Inorg. Nucl. Chem.*, 33 (1971) 351.
- 18 E.A. Neves and P. Senise, *J. Inorg. Nucl. Chem.*, 34 (1972) 1915.
- 19 P. Senise and E.A. Neves, *J. Inorg. Nucl. Chem.*, 34 (1972) 1923.
- 20 F. Maggio, V. Romano and L. Pellerito, *Ann. Chim. (Rome)*, 57 (1967) 191.
- 21 E.A. Neves and T.V. Silva, in *Proc. Anais IV Simp. Bras. Eletroquím. Eletroanal.*, Dept. de Química da UFSCar e IFQSCar/USP, São Carlos, SP, Brazil, 1984, p. 63.
- 22 E.A. Neves, M.E.V. Suárez Iha and J.O.G. Pecchioni, in *Proc. Anais V Simp. Bras. Eletroquím. Eletroanal.*, IQ/USP, São Paulo, SP, Brazil, 1986, p. 793.

Optical sensing of glucose using phase-modulation fluorimetry

Joseph R. Lakowicz and Badri Maliwal

Department of Biological Chemistry, University of Maryland, School of Medicine, Baltimore, MD 21201 (USA)

(Received 1st April 1992; revised manuscript received 3rd August 1992)

Abstract

We describe a fluorescence assay of glucose based on fluorescence resonance energy transfer and phase-modulation measurements of the donor decay times. The assay is based on the decreased decay time of a donor fluorophore linked to Concanavalin A (ConA) upon binding of acceptor-labeled sugars. Displacement of the labeled sugars by glucose results in a decrease in energy transfer and an increase in the donor decay time. The assay was demonstrated with several donor–acceptor pairs, demonstrating the robustness and generality of this approach. A competitive glucose assay was demonstrated with both low-molecular-weight acceptors, and with acceptor-labeled dextran. Use of a polymeric acceptor would allow the glucose sensor to be placed behind a glucose-permeable barrier, as may be needed in clinical applications. The use of energy transfer allows the selection of excitation and emission wavelengths compatible with the desired light sources and optical properties of the samples. The use of fluorescence decay times rather than intensities, makes the measurements mostly independent of probe photobleaching, light losses in the optics, instrumental drifts, and mostly independent of scattering and/or absorption of the sample.

Keywords: Fluorimetry; Donor–acceptor pairs; Glucose

Measurements of blood glucose are performed routinely in clinical labs, doctor's offices and by diabetic individuals. Most measurements of glucose rely on chemical analysis of glucose by coupling its oxidation by glucose oxidase to colorimetric indicators [1–3]. Such methods require freshly drawn blood, which is not pleasant for the diabetic patients and precludes the use of this method as a feedback loop for an insulin pump. Consequently, the development of non-invasive optical sensing of glucose has been an active area of research. A variety of methods have been suggested for optical measurements of glucose. The proposed methods include measurement of

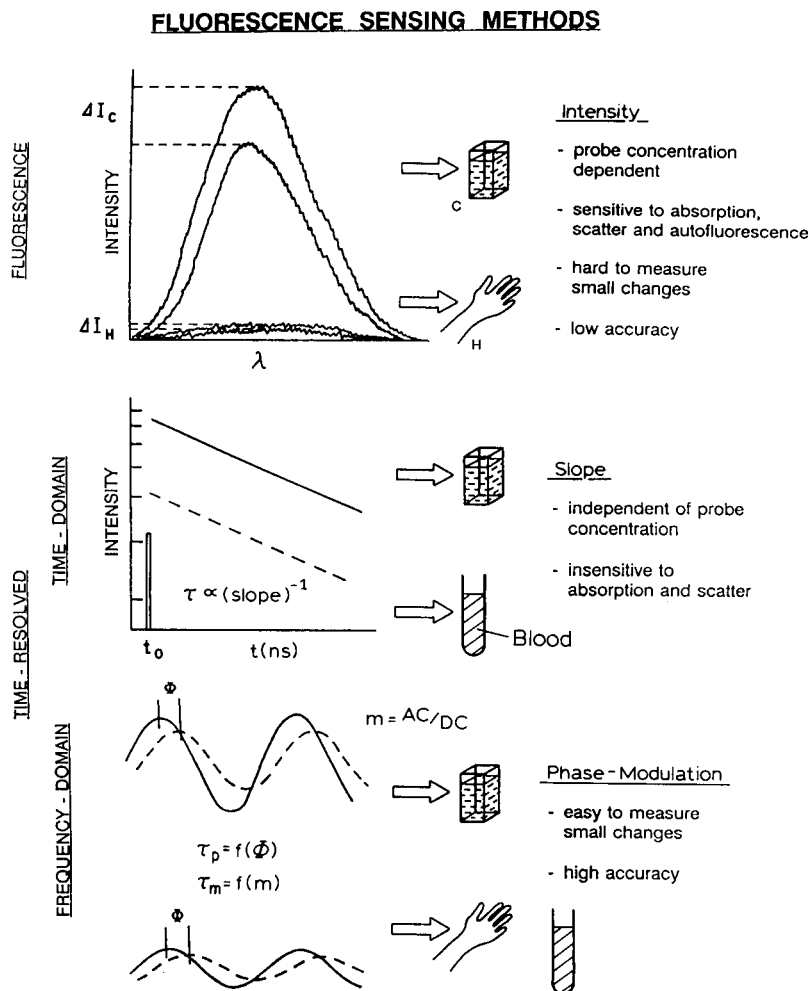
the oxygen consumption by glucose oxidase using an oxygen optrode [4,5] measurements of the changes in pH which accompany glucose oxidation [6,7], use of the intrinsic flavin fluorescence of glucose oxidase [8], and direct measurements of glucose by Fourier-transform infrared spectrometry (FT-IR) [9,10]. Others have proposed competitive displacement of fluorescently labeled Concanavalin A (ConA) from polymers by glucose [11,12]. The association between ConA and dextrans was followed by removal of fluorescein-labeled ConA from the region of observation by binding to surface-bound ConA [11], or by energy-transfer quenching of the fluorescein-labeled dextran by rhodamine-labeled ConA [12]. However, these glucose optrodes relied on measurements of the fluorescence intensity, which has proven unreliable due to drifts, probe bleaching or washout.

Correspondence to: J.R. Lakowicz, Center for Fluorescence Spectroscopy, Department of Biological Chemistry, University of Maryland, School of Medicine, 660 West Redwood Street, Baltimore, MD 21201 (USA).

Recent developments in fluorescence instrumentation [13-17] and increased understanding of the optical properties of tissues [18,19] caused us to reconsider the possibility of non-invasive measurements of glucose. Fluorescence lifetime measurements offer many advantages for sensing because the decay times can be mostly independent of the probe concentration, probe photobleaching or washout [20], and lifetime measurements can be performed in scattering media. In contrast, fluorescence assays based on intensity measurement are sensitive to conditions which alter the intensity and are thus difficult if not impossible in tissues or blood samples. Further-

more, advances in laser, detector and electronics technology make it practical to consider compact clinical instruments for lifetime-based sensing [21], even portable units as would be desirable for sensing of glucose. Such instruments will probably use the frequency-domain or phase-modulation method which is well suited for compact and inexpensive instrumentation.

The advantages of lifetime-based sensing are illustrated in Scheme 1. Intensity-based sensing depends on reliable measurements of the probe's intensity. While such measurements are easily performed in the laboratory using non-scattering solutions, intensity measurements are difficult in



Scheme 1. Comparison of intensity and lifetime sensing.

tissue, blood and in real-world situations. The observed intensity can be altered by numerous factors such as absorbance, scattering, light losses in the optics, and alignment, to name a few. It is generally difficult to measure the small changes in the probe's intensity in the presence of these undesired effects. To compensate for these artifacts, multi-wavelength ratiometric methods have been proposed for measurements of pH and calcium [22–24]. However, such measurements have not found widespread use in clinical sensing, and in any event, wavelength-ratiometric probes are not available for glucose.

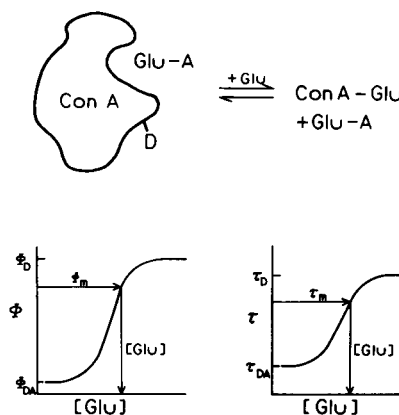
In contrast to intensity measurements, lifetime measurements depend on the signal during a short period of time, 1–20 ns, depending on the probe's lifetime. The decay time is obtained from the slope of the intensity decay following pulsed excitation (Scheme 1, middle). However, lifetime measurements based on the pulse method are presently too costly and complex for clinical applications.

Fluorescence lifetimes can also be conveniently measured by the phase-modulation method. In this technique, the sample is excited by light which is intensity-modulated at frequencies (f) ranging from 1 to 200 MHz. Frequencies above 200 MHz require more expensive microchannel plate photomultiplier tubes [15,16]. The lifetime can be determined by two independent measurements, these being the phase shift (θ) of the emission relative to the incident light and the modulation (m) of the emission. The values of θ and m can be related to apparent lifetimes by

$$\tan \theta = 2\pi f\tau_D \quad (1)$$

$$m = [1 + (2\pi f\tau_m)^2]^{-1/2} \quad (2)$$

At present, it is technically easy to obtain the intensity-modulated light using He–Ne lasers and external modulators [25], or even by the direct modulation of laser diodes [17,26]. In favorable cases, it is even possible to use an electroluminescent light source [27]. Measurement of the phase and modulation of the emission is performed using radio frequency (RF) methods which enhance the signal-to-noise ratio. Low-cost instru-



Scheme 2. Intuitive description of an energy-transfer glucose assay.

mentation seems easily possible at this time, and recent advances in integration of the components [28] promises to further reduce cost and increase reliability.

Based on these considerations, we developed a glucose assay based on the phase-modulation lifetime measurements. Additionally, we chose a transduction mechanism which is general and can be modified for future use with laser diodes or other desirable light sources. Our assay is based on fluorescence energy transfer [29,30] between a donor covalently linked to ConA and an acceptor linked to a sugar which binds to ConA (Scheme 2). Binding of the acceptor-labeled sugar to ConA is expected to decrease the decay time. Glucose in the sample will displace some of the labeled sugar, resulting in an increase in lifetime which can be measured by the phase and/or modulation of the donor emission. We note that phenomena of energy transfer is a through-space interaction which always occurs if spectral overlap is adequate. Hence, the excitation and emission wavelengths of an energy-transfer based assay can be adjusted as desired. Importantly, there is an increasing availability of red and/or near infrared (NIR) probes, some of which are conjugatable with proteins [31,32]. Since the skin is non-absorbing at wavelengths above 600 nm, it may be possible to perform lifetime measurements directly on tissues. While there may be some dispersion of the modulated light due to time-dependent light migration in the tissues, the

TABLE 1

Excitation and emission wavelengths for the various donors

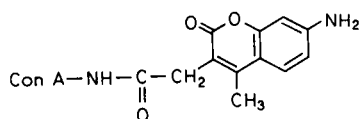
| Donor | Excitation wavelength (nm) | Emission filters (wavelengths, nm) ^a |
|--------------------------|----------------------------|---|
| AMCA-ConA | 356 or 360 | Corning 0-51/5-59; 435 (360–500) |
| Cascade Blue-ConA | 356 or 360 | Corning 0-51/5-59; 430 (360–500) |
| FITC-ConA | 300 or 442 | Corning 3-71/Schott 500 nm; 500 (496–506) |
| FITC-ConA (succinylated) | 442 | Corning 3-71/Schott 500 nm; 500 (496–506) |
| Texas Red-ConA | 570 or 576 | Schott 600 nm; 600 (595–608) |

^a The central wavelength of the filters is listed, along with the lower and upper wavelengths (in brackets) when the transmission is about 10% of the maximum transmission.

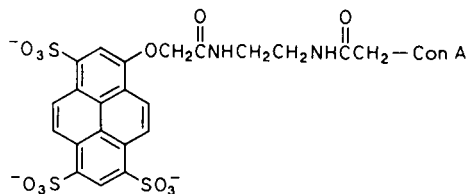
timescale of this phenomena is sub-nanosecond [18,19] and should have minimal effects on the measurement of nanosecond lifetimes. And finally, energy transfer can alter the decay times of the lanthanide chelates. These luminescent sub-

stances display long decay times [33–36], allow electronic suppression of the prompt autofluorescence and/or scatter from tissues, and could enable still simpler instrumentation for lifetime-based glucose assays.

Donors

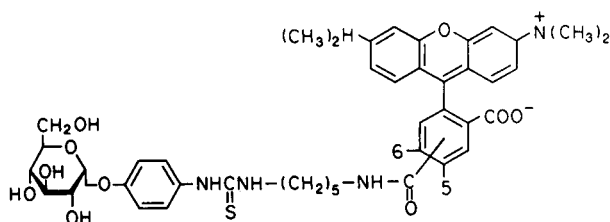


AMCA - Con A

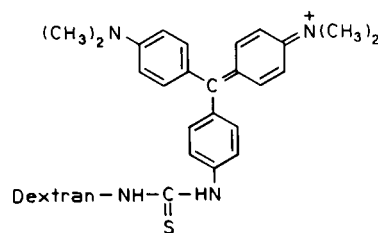


Cascade Blue - Con A

Acceptors



TRITC - Mannoside



Malachite Green - Dextran

Fig. 1. Fluorescence donors and acceptors for the glucose measurements.

MATERIALS AND METHODS

Amino dextran (MW = 10 000), eosin cadaverine, tetramethylrhodamine cadaverine (TRITC-cadaverine), Malachite Green isothiocyanate (MG-isothiocyanate), 7-amino-4-methyl-coumarin-ConA (AMCA-ConA), Cascade Blue-ConA, and Texas Red-ConA were purchased from Molecular Probes. Fluorescein ConA (FITC-ConA), its succinylated derivative and mannose pyranoside isothiocyanate were obtained from Sigma.

Preparation of eosin. Texas Red isothiocyanate-mannoside and MG-dextran

About 10 mg of amino dextran were dissolved in 500 μl of bicarbonate buffer, pH 9.0 and reacted with a 10-fold molar excess of MG-isothiocyanate (in 50 μl DMSO) for 4 h at room temperature. The labeled dextran was freed from excess fluorophore on a Sephadex G-50 column.

To prepare the mannoside-fluorophore conjugates, about 5 mg of eosin or Texas Red isothiocyanate (TRITC) cadaverine and 2- to 3-fold molar excess of isothiocyanate derivative of mannose pyranoside were initially dissolved in 50 μl of DMSO and made up to 500 μl with 0.2 M bicarbonate buffer, pH 9.0. The reaction was allowed to proceed for 2 h at room temperature. The mannoside-fluorophore conjugate was separated from the cadaverines by preparative silica gel thin-layer chromatography (TLC) using either ethanol (eosin derivative) or methanol (TRITC derivative). The mannoside-fluorophore conjugates showed significantly faster mobility than their cadaverine derivatives.

All fluorescence measurements were performed in 100 mM 4-morpholine propane sulphonic acid (MOPS), pH 7.0 at 20°C. In most of the experiment, the ConA concentration was 100 $\mu\text{g}/\text{ml}$, though some experiments were performed at 200 $\mu\text{g}/\text{ml}$ level. The excitation wavelengths and emission filters are given in Table 1.

Measurements of the phase-modulation and/or frequency responses were performed using the instrumentation described previously [14,15]. Analysis of the frequency-domain data in terms of a multi-exponential decay was accomplished as described previously [37,38].

RESULTS AND DISCUSSION

We examined the glucose energy-transfer assay using a number of donor-acceptor pairs (Fig. 1). Several ConA conjugates were tested as fluorescent donors. The fluorophores which were covalently attached to ConA were AMCA, Cascade Blue, FITC and Texas Red. The emission from these fluorophores covers approximately 400–700 nm. Among the acceptors were eosin, TRITC and MG, which were covalently linked to either a mannoside or amino dextran. Both eosin and TRITC cover 400–600 nm, while MG absorption extends to about 720 nm. The Förster distances range between 40 and 65 Å for these various donor-acceptor pairs. A Förster distance of 42 Å was calculated [29] for the AMCA-TRITC donor-acceptor pair using the usual assumptions of $\kappa^2 = 2/3$, and a refractive index of 1.33 and the quantum yield of 0.5 for AMCA quoted by Molecular Probes. The Förster distance of the other donor-acceptor pairs were not calculated explicitly but are known to be longer than 42 Å based on the greater extent of spectral overlap.

To illustrate the assay, we first describe the results using a coumarin donor covalently linked to ConA (AMCA-ConA) and a rhodamine acceptor linked to α -D-mannoside (TRITC-mannoside). The emission spectrum of AMCA-ConA and the absorption spectrum of TRITC-mannoside are shown in Fig. 2. While the spectral overlap does not seem strong, the high extinction coefficient of TRITC and quantum yield of the AMCA results in a characteristic Förster distance of about 42 Å.

Emission spectra of AMCA-ConA in the presence of the acceptor-labeled sugar are shown in Fig. 3 (top). As expected, the AMCA donor intensity decreases with increasing amounts of TRITC-mannoside. This effect was shown to be reversible by the addition of glucose (bottom). However, the data in Fig. 3 (bottom) illustrates the difficulties in using intensity-based measurements. Quenching of the AMCA-ConA was not completely reversed by even a large excess of glucose (250 mM, Fig. 3). The decreased intensity could be the result of inner filter effects due to absorbance of the acceptor. It is difficult to cor-

rect for such effects even in a laboratory setting, with ideal samples, and such corrections are not practical with optically turbid or dense samples.

Frequency-domain data for AMCA donor are shown in Fig. 4. The curves shift to higher frequency with increasing amounts of TRITC-mannoside (top), demonstrating a decrease in the AMCA decay time. This effect is progressively, reversed by addition of glucose (bottom). While the donor's intensity could not be completely restored by addition of glucose (Fig. 3, bottom), the original frequency-response was recovered at 250 mM glucose (Fig. 4, bottom). This demonstrates the insensitivity of lifetime-based sensing to changes in the total intensity of the donor.

The data in Fig. 4 represents research-type data which is adequate to resolve the multi-exponential law of the donor emission

$$I(t) = \sum \alpha_i e^{-t/\tau_i} \quad (3)$$

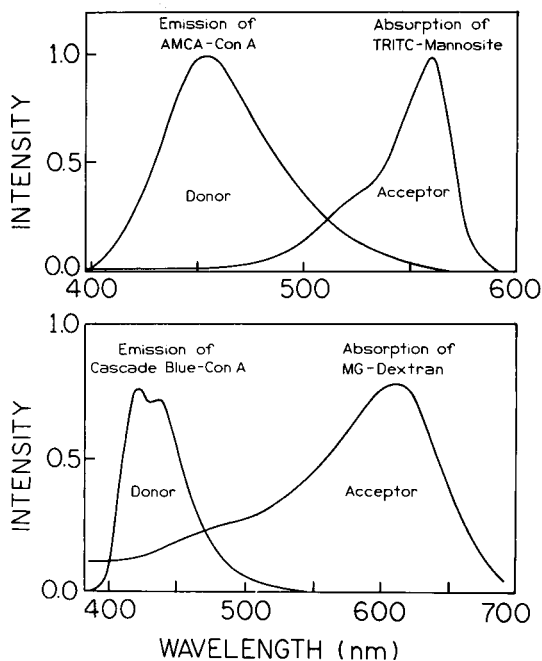


Fig. 2. Top: emission spectrum of the donor AMCA-ConA and the absorption spectrum of the acceptor TRITC-mannoside. Bottom: emission spectrum of the donor Cascade Blue-ConA and the acceptor Malachite Green-dextran. In our experiments, either donor displayed energy transfer to either acceptor.

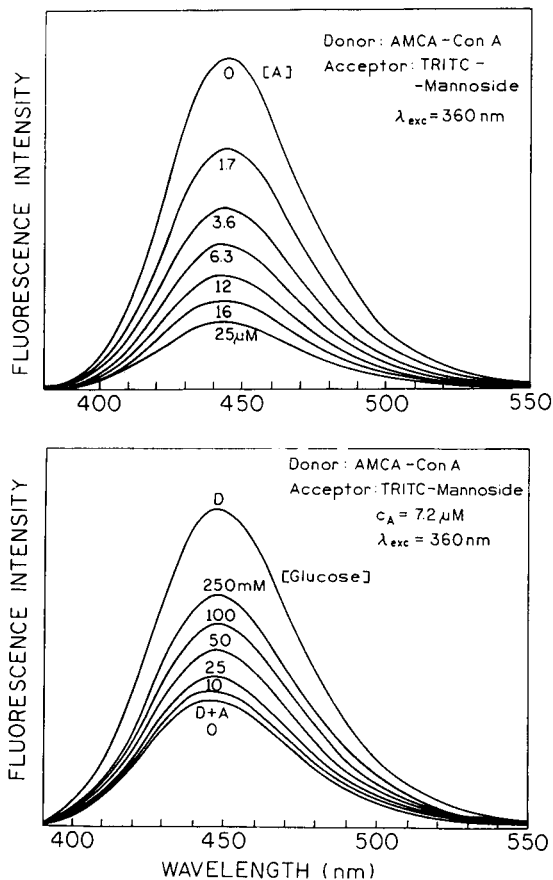


Fig. 3. Top: quenching of AMCA-ConA by binding of TRITC-mannoside. Bottom: displacement of TRITC-mannoside from AMCA-ConA by glucose.

where α_i are the amplitudes and τ_i the decay times [37,38]. The multi-frequency data could be used to determine α_i and τ_i , which could be used to determine the proportion of AMCA-ConA with and without bound TRITC-mannoside. However, such a multi-exponential analysis is not required for a glucose assay. Irrespective of the complexity of the intensity decay, there is a single phase and modulation value at each light modulation frequency. These phase and modulation values are frequency-dependent weighted averages of the decay times. For a glucose assay, one only requires a single phase or modulation measurement, although both values or data at several frequencies can be used to increase the precision and/or reliability of the measurements.

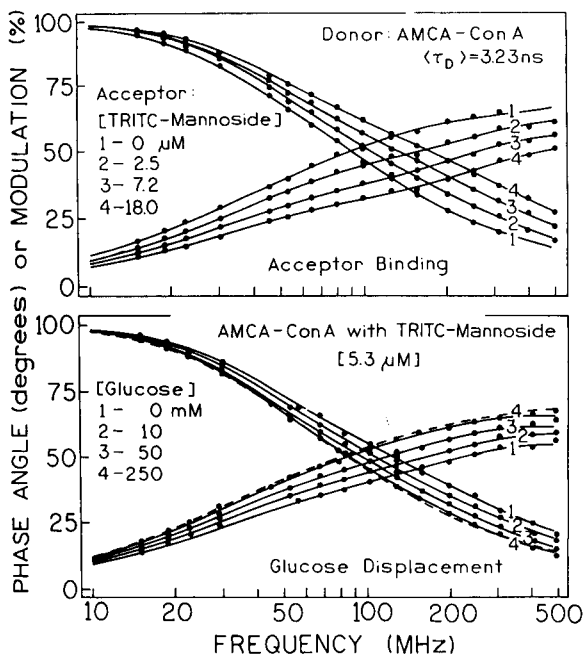


Fig. 4. Top: frequency-response of AMCA-ConA with increasing concentrations of TRITC-mannoside. Bottom: effect of glucose on the frequency-response of AMCA-ConA partially saturated with TRITC-mannoside. The dashed line shows the frequency response of AMCA-ConA in the absence of TRITC-mannoside.

Single-frequency phase and modulation glucose assays are shown in Fig. 5. The phase angle decreases (left) and the modulation increases (right) upon addition of TRITC-mannoside. Addition of glucose to the samples which are partially saturated with TRITC-mannoside results in complete reversal of the acceptor-induced changes in phase and modulation (Fig. 5, inserts). These data can also be present as the change in mean decay time (Fig. 6). The mean lifetimes were calculated from $\bar{\tau} = \sum f_i \tau_i$, where $f_i = (\alpha_i \tau_i) / (\sum \alpha_j \tau_j)$ are the fractional intensities and τ_i the decay times resulting from multi-exponential analysis of the frequency responses. One can expect the values of $\bar{\tau}$ to be more reliable than a single phase or modulation measurement, but of course, calculation of a meaningful value of $\bar{\tau}$ requires more experimental data at several frequencies.

Other donor-acceptor pairs

Less extensive studies were performed using other donor-acceptor pairs (Table 1). We tried the following donor-acceptor pairs: FITC-ConA to eosin mannose, FITC-ConA (succinylated) to eosin or TRITC-mannoside, Cascade Blue-

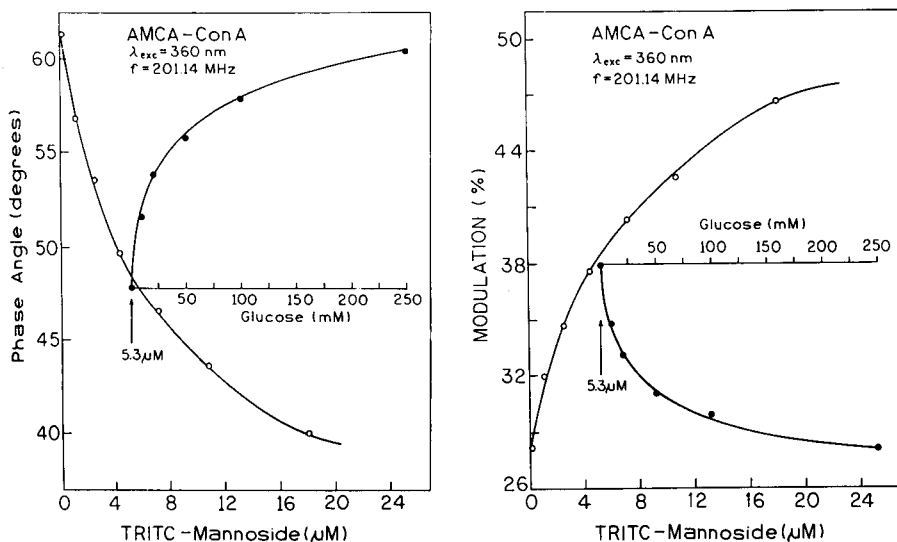


Fig. 5. Left: modulation assay of glucose sensing AMCA-ConA and TRITC-mannoside. Right: phase fluorescence assay of glucose-sensing AMCA-ConA and TRITC-mannoside. In both panels, the inserts show the reversal of energy-transfer quenching by added glucose.

ConA to eosin mannoside. In all cases we observed energy transfer from the donor-labeled ConA to acceptor-labeled sugar (results not shown). As an example, the emission spectra of Cascade Blue–ConA in the presence of several TRITC–mannoside concentrations is shown in Fig. 7. The binding of TRITC–mannoside to Cascade Blue–ConA results in significant quenching of donor fluorescence intensity (Fig. 7, top) which is partially reversed by glucose (not shown). The fact that this decrease in intensity is accompanied by a decrease in decay time is seen from the smaller phase angles of the Cascade Blue–ConA from 50 to 200 MHz (Fig. 7, bottom). This effect of TRITC–mannoside is partially reversed by 100 mM glucose.

These results demonstrate that the energy-transfer mechanism is general and will work with most donor–acceptor pairs. Importantly, this will allow use of long-wavelength donors and acceptors, which can be excited with red He–Ne or diode laser sources. Importantly, the skin is not strongly absorbing at these wavelengths, which suggests an opportunity for non-invasive glucose sensing. This possibility exists because lifetime measurements can be insensitive to the total intensity, and hence unaffected by the attenuation

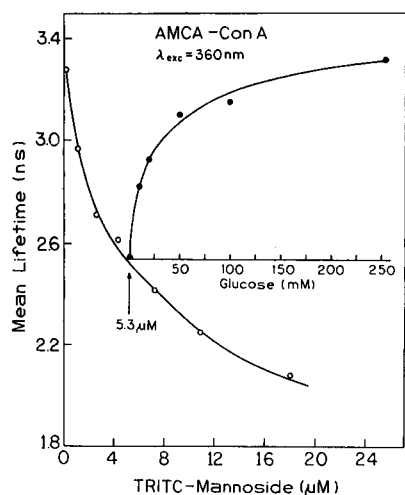


Fig. 6. Energy-transfer glucose assay as quantified by the mean donor decay time. $\bar{\tau}$ was calculated using $\bar{\tau} = \sum_i f_i \tau_i$, where $f_i = (\alpha_i \tau_i) / (\sum_j \alpha_j \tau_j)$ and τ_i are from the multi-exponential fit.

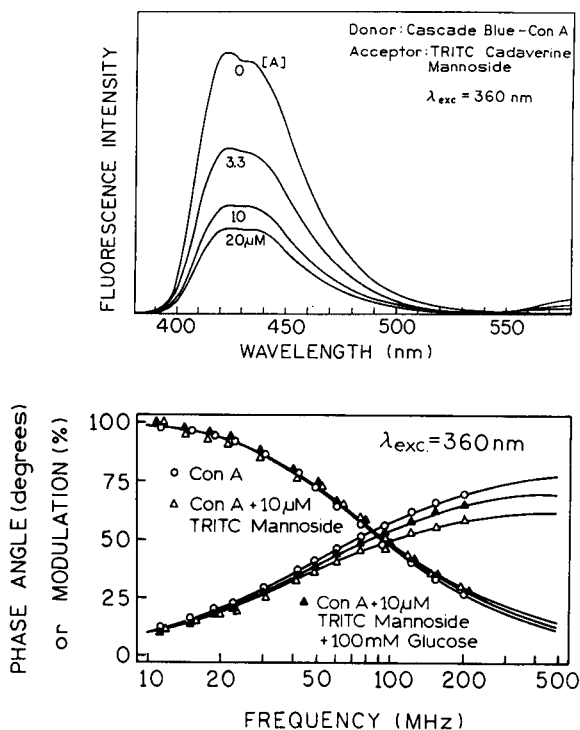


Fig. 7. Top: emission spectra of Cascade Blue–ConA, with increasing amounts of TRITC–mannoside acceptor. Bottom: frequency-response of Cascade Blue–ConA, with TRITC–mannoside, and with TRITC–mannoside and excess glucose.

resulting from light scatter and/or absorption by tissues. Additionally, the auto-fluorescence from tissues is weak for red/NIR excitation. And finally, the effects of tissue scattering are on the picosecond to sub-nanosecond timescale. Hence, transdermal lifetime measurements appear to be possible with long-wavelength donor–acceptor pairs.

Glucose assay with polymeric acceptor

In order to develop a practical glucose assay it may be desirable to prevent diffusion and/or dilution of the labeled acceptor from the ConA. This is evident from our use of acceptor-mannoside concentrations adequate to partially saturate the ConA. Under these conditions, one expects and finds competitive displacement of the acceptor by glucose. Hence, we questioned whether the glucose energy-transfer assay would work with a

polymeric acceptor which could be kept behind a glucose-permeable membrane.

The polymeric acceptor was 10000 MW dextran labeled with Malachite Green (Fig. 1). The donors were ConA labeled with either Cascade Blue or AMCA. In both cases, the donor emission was quenched in the presence of Malachite Green (MG)-dextran (Fig. 8), and the quenching was partially reversed by the addition of mannoside. We note that the quenching due to added acceptors can be due in part to acceptor absorption and/or inner filter effects. However, glucose and mannoside are non-absorbing at these wavelengths, and thus the sugar-induced reversal of quenching can be confidently assigned to displacement of the polymeric acceptor from the labeled ConA.

Frequency-response of AMCA-ConA and Cascade Blue-ConA are shown in Fig. 9. Addition of the polymeric acceptor results in decreased phase angles and increased modulation at frequencies above 50 MHz (Fig. 9). These changes are due to the decreased lifetime of the donors. Addition of mannoside results in reversal

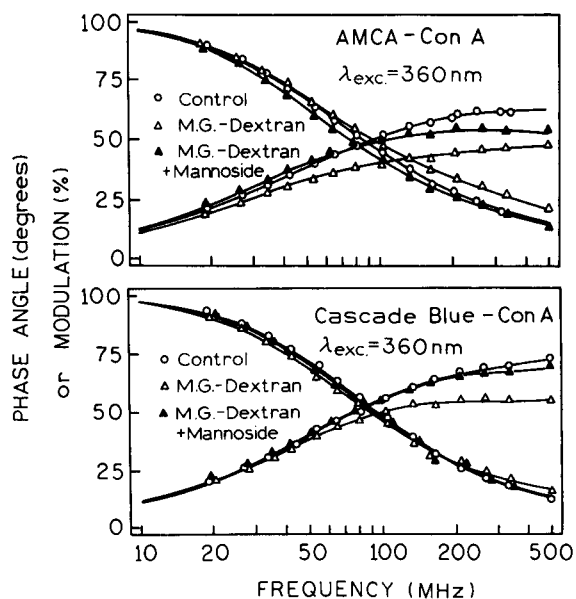


Fig. 9. Frequency-response of donor-labeled ConA, with Malachite Green-dextran and with added mannoside. Top: AMCA-ConA; bottom: Cascade Blue-ConA.

of these shifts, indicating displacement of the dextran from ConA.

A competitive glucose assay based on AMCA-ConA and MG-dextran is shown in Fig. 10. In this case, we use phase-angle measurements at a single frequency to quantitate mannoside binding. One notices that the acceptor-induced phase change is completely reversed by addition of the mannoside. Some preliminary measurements were also performed with Texas Red-ConA and MG-dextran system. Again, we observed quenching of donor intensity upon acceptor-dextran binding, which could be reversed with methylmannoside. The trend was also seen in phase angles (results not shown).

The results described above are not intended to define a definitive glucose energy-transfer assay. Such an assay requires more careful consideration of the clinical environment, patient needs and numerous other factors. However, the present results demonstrate that glucose assays can be performed by lifetime measurements or phase-modulation measurements at a single light-modulation frequency. Importantly, the energy transfer mechanism can be confidently ex-

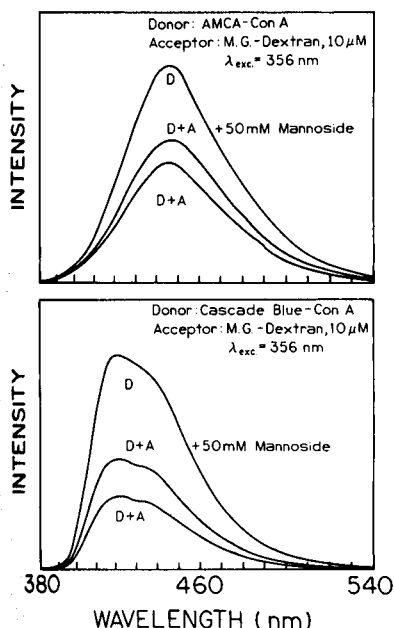


Fig. 8. Emission spectra of donor-labeled ConA in the presence of the polymeric acceptor Malachite Green-dextran. Top: AMCA-ConA; bottom: Cascade Blue-ConA.

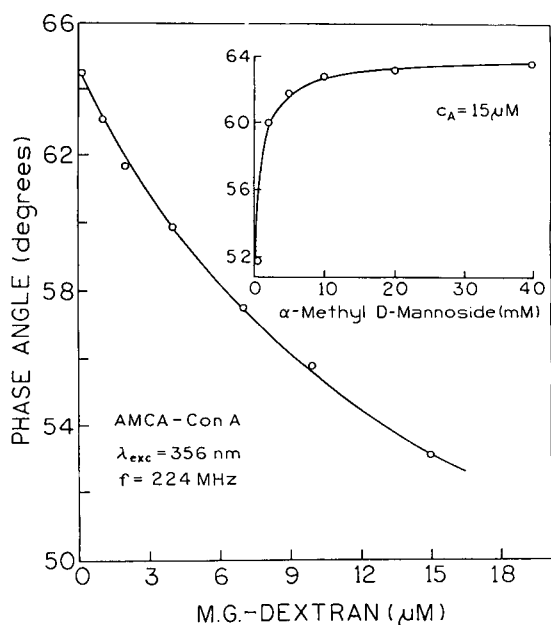


Fig. 10. Competitive displacement assay for mannoside using AMCA-ConA and Malachite Green-dextran.

pected to work at all wavelengths, so that an assay can be designed which takes advantage of currently available long-wavelength probes, laser and detectors.

This work was supported by grants from the National Science Foundation DIR-8710401, and the National Institutes of Health RR-04800, RR-07510 and RR-08119. The authors thank Dr. Wieslaw Wicz for assistance with preparation of the acceptor-labeled sugars.

- 1 D.R. Matthews, E. Bown, A. Watson, R.R. Holman, J. Steemson, S. Hughes and D. Scott, *Lancet*, 1 (1987) 778.
- 2 W. Clarke, D.J. Becker, D. Cox, J.V. Santiago, N.H. White, J. Betschart, K. Eckenrode, L.A. Levandoski, E.A. Prusinski, L.M. Simineiro, A.L. Snyder, A.M. Tideman and T. Yaeger, *Diabetes Res. Clin. Pract.*, 4 (1988) 209.
- 3 G.M. Schier, R.G. Moses, I.E.T. Can and S.C. Blair, *Diabetes Res. Clin. Pract.*, 4 (1988) 177.
- 4 M.C. Moreno-Bondi, O.S. Wolfbeis, M.J.P. Leiner and B.P.H. Schaffar, *Anal. Chem.*, 62 (1990) 2377.
- 5 W. Trettnak, M.J.P. Leiner and O.S. Wolfbeis, *Analyst*, 113 (1988) 1519.
- 6 W. Trettnak, M.J.P. Leiner and O.S. Wolfbeis, *Biosensors*, 4 (1988) 15.
- 7 M. Shichiri, R. Kawamori and Y. Yamasaki, *Methods Enzymol.*, 137 (1988) 326.
- 8 W. Trettnak and O.S. Wolfbeis, *Anal. Chim. Acta*, 221 (1989) 195.
- 9 B. Bauer and T.A. Floyd, *Anal. Chim. Acta*, 197 (1987) 295.
- 10 N. Kaiser, *J. Horm. Metab. Res. Suppl.*, 8 (1977) 30.
- 11 J.S. Schultz, S. Mansouri and I.J. Goldstein, *Diabetes Care*, 5 (1982) 245.
- 12 D. Meadows and J.S. Schultz, *Talanta*, 35 (1988) 145.
- 13 E. Gratton and M. Limkemann, *Biophys. J.*, 46 (1984) 479.
- 14 J.R. Lakowicz and B.P. Maliwal, *Biophys. Chem.*, 21 (1985) 61.
- 15 J.R. Lakowicz, G. Laczko and I. Gryczynski, *Rev. Sci. Instrum.*, 57 (1986) 2499.
- 16 G. Laczko, I. Gryczynski, Z. Gryczynski, W. Wicz, H. Malak and J.R. Lakowicz, *Rev. Sci. Instrum.*, 61 (1990) 2331.
- 17 K.W. Berndt, I. Gryczynski and J.R. Lakowicz, *Rev. Sci. Instrum.*, 61 (1990) 1816.
- 18 B. Chance, J.S. Leigh, H. Miyake, D.S. Smith, S. Nioka, R. Greenfield, M. Finander, K. Kaufmann, W. Levy, M. Young, P. Cohen, H. Yoshioka and R. Boretsky, *Natl. Acad. Sci. U.S.A.*, 85 (1988) 4971.
- 19 J.R. Lakowicz and K.W. Berndt, *Chem. Phys. Lett.*, 166 (1990) 246.
- 20 J.R. Lakowicz, H. Szmazinski and K.W. Berndt, *SPIE Proc.*, 1648 (1992) 150.
- 21 J.R. Lakowicz, M.L. Johnson, W.J. Lederer, H. Szmazinski, K. Nowaczyk and H. Malak, *Laser Focus World*, May (1992) 60.
- 22 R.Y. Tsien, *Methods Cell Biol.*, 30 (1989) 127.
- 23 *Molecular Probes Catalogue*, 1989–1991, pp. 86–89.
- 24 J.E. Whitaker, R.P. Haugland and F.G. Prendergast, *Anal. Biochem.*, 194 (1991) 330.
- 25 H. Szmazinski and J.R. Lakowicz, submitted for publication.
- 26 R.B. Thompson, J.K. Frisoli and J.R. Lakowicz, *Anal. Chem.*, (1992) in press.
- 27 K.W. Berndt and J.R. Lakowicz, *Anal. Biochem.*, 201 (1992) 319.
- 28 B.A. Feddersen, D.W. Piston and E. Gratton, *Rev. Sci. Instrum.*, 60 (1989) 2929.
- 29 L. Styer, *Ann. Rev. Biochem.*, 47 (1978) 819.
- 30 I.Z. Steinberg, *Ann. Rev. Biochem.*, 40 (1971) 83.
- 31 R.B. Mujumdar, L.A. Ernst, S.R. Mujumdar and A.S. Waggoner, *Cytometry*, 10 (1989) 11.
- 32 *Research Organics, Inc.*, Cleveland, OH 44125.
- 33 V. Balzani and R. Ballardini, *Photochem. Photobiol.*, 52 (1990) 409.
- 34 R.C. Holz, C.A. Chang and W. Horrocks, Jr., *Inorg. Chem.*, 30 (1991) 3270.
- 35 L. Prodi, M. Maestri, V. Balzani, J.-M. Lehn and C. Roth, *Chem. Phys. Lett.* 180 (1991) 45.
- 36 E.J. Soini, L.J. Pelliniemi, I.A. Hemmila, V.-M. Mukkala, J.J. Kankare and K. Frojzman, *J. Histochem. Cytochem.*, 36 (1988) 1449.
- 37 J.R. Lakowicz, G. Laczko, H. Cherek, E. Gratton and M. Limkemann, *Biophys. J.*, 46 (1984) 463.
- 38 E. Gratton, M. Limkemann, J.R. Lakowicz, B.P. Maliwal, H. Cherek and G. Laczko, *Biophys. J.*, 46 (1984) 479.

Fluorimetry of haemolysis of red blood cells by catalytic reaction of leaked haemoglobin: application to homogeneous fluorescence immunoassay

Yoshiro Tatsu, Soichiro Yamamura, Hitoshi Yamamoto and Susumu Yoshikawa

Government Industrial Research Institute, Osaka, Midorigaoka Ikeda, Osaka 563 (Japan)

(Received 4th June 1992; revised manuscript received 10th August 1992)

Abstract

A novel method was developed for the homogeneous fluorescence immunoassay using complement-mediated haemolysis of sheep red blood cells. Fluorescent substrates of peroxidase, 4-hydroxyphenylpropionic acid (HPPA) or fluorescein were catalysed by haemoglobins leaked from haemolysed red blood cells. Non-haemolysed cells showed no enzymatic activity and only haemoglobins released from the cells showed catalytic activity. The extent of hemolysis could therefore be measured without separating haemolysed and non-haemolysed cells. The immunological binding of antibodies with the antigens on the cell membrane activates the complement system and the cell is finally lysed. Homogeneous fluorescence immunoassay was performed by combining the complement-mediated haemolysis technique and the fluorimetry of haemolysis. The immunoassay was done for the immunoagents; complement and bovine serum albumin (BSA). The sensitivity was 0.051 CH50 unit ml⁻¹ for complement and < 1.0 µg ml⁻¹ of BSA.

Keywords: Fluorimetry; Immunoassay; Blood; Haemolysis; Red blood cells

Because the interactions of antibodies and antigens have attracted much interest owing to the high selectivity, many techniques for immunochemical analysis have been developed [1]. From a practical point of view, homogeneous measurement, i.e., which needs no separation of binding and non-binding immunoagent, would simplify the assay procedures. There have been several reported homogeneous methods, such as enzyme [2], fluorescent polarization [3], electrochemical [4] and liposome immunoassays [5]. The liposome immunoassay has been studied extensively since its introduction by Kinsky et al. [6]. The principle of the assay is based on the release of marker entrapped within the liposome by complement-mediated lysis. Complement is one of the defence

systems in the body and is activated by antigen-antibody complexes and makes the membrane attack complexes on lipid bilayers. The entrapped markers used include glucose [6], fluorescent dyes [7], spin labels [8], enzymes [9] and electroactive compounds [10]. In many reports, liposomes were artificially prepared from a lipid film and marker solution. Intact red blood cell membrane, as liposome, has also been reported [8,11], because the cell membrane is preferred owing to its stability, uniformity of size and availability.

Recently the homogeneous chemiluminescence immunoassay based on complement-mediated haemolysis using sheep red blood cells was reported [12]. Haemoglobin, which is encapsulated in the cell with high concentration, has a peroxidase-like activity that catalyses chemiluminescent reactions of luminol. In addition, non-haemolysed cells caused no chemiluminescence

Correspondence to: Y. Tatsu, Government Industrial Research Institute, Osaka, Midorigaoka, Ikeda, Osaka 563 (Japan).

and, therefore, the homogeneous measurement of haemolysis was possible. Further developments of this principle could be achieved by using other dyes or measuring methods. This paper describes homogeneous immunoassay using fluorescent substrates for peroxidase, fluorescein and HPPA, which can be measured with a conventional fluorimeter. The homogeneous assay for haemolysis was examined and applied to assays for complement and bovine serum albumin (BSA).

EXPERIMENTAL

Reagents and materials

Fluorescein from Merck and HPPA from Nacalai Tesque were used as received. Lyophilized guinea-pig complement was obtained from Handai-Biken and reconstituted as directed. Reconstituted complement solution was frozen at -70°C and the thawed solution was used within 1 day of thawing below 4°C to prevent loss of activity. The complement activity was at the ordinal level around 200 CH50 units ml^{-1} , as measured by Mayer's method [13]. Rabbit anti-bovine albumin antiserum from Seikagaku Kogyo (2.9 mg ml^{-1} of the antibody) was heated for 30 min at 56°C to remove any complement activity. Sheep red blood cells or haemolysin-sensitized cells (EA) were purchased from Ishizu Seiyaku. BSA was obtained from Sigma. All chemicals used were of analytical-reagent grade.

Assay procedures

The buffer used was veronal-buffered saline of pH 7.4 containing 0.1% gelatin (GVB) or GVB containing 0.5 mM CaCl_2 and 0.15 mM MgCl_2 (GVB^{2+}). Sheep red blood cells were washed several times with GVB^{2+} . The cells were suspended in GVB^{2+} at a concentration of 1×10^9 cells ml^{-1} .

The complement assay was performed as follows. EA (5×10^8 cells ml^{-1} , 0.4 ml) was mixed with the diluted complement (2.6 ml) and incubated at 37°C for 1 h. After the haemolytic reaction, 185 μl of the reaction mixture were diluted to 3.0 ml with GVB and kept at 4°C until the fluorescence was measured. The measurement

was done as soon as possible although no haemolysis by complement at 4°C was observed.

BSA assay was performed in the same way. BSA (0.8 ml) was mixed with 80-fold diluted anti-BSA (0.8 ml) and 240-fold diluted complement (1.0 ml) and incubated at 37°C for 1 h. EA (5×10^8 cells ml^{-1} , 0.4 ml) was then added and the mixture incubated again for 1 h. After the haemolytic reaction, 185 μl of the reaction mixture were diluted to 3.0 ml with GVB and kept at 4°C .

To 3.0 ml of red blood cell suspension in a 1-cm quartz cell, 50 μl each of H_2O_2 and the fluorescent substrate were added. The time course of the fluorescence intensity was recorded over 10 min, the excitation and fluorescence wavelengths being 315 and 415 nm, respectively, for HPPA and 490 and 520 nm, respectively, for fluorescein. All fluorescence measurements were performed at 25.0°C with Hitachi Model 850 spectrofluorimeter. In immunochemical measurements, 1.0 mM fluorescein and 10 mM H_2O_2 or 50 mM HPPA and 100 mM H_2O_2 were used.

RESULTS AND DISCUSSION

Fluorescein and its analogues are known as fluorescent substrates for peroxidase [14]. The substrates in the reduced form are oxidized by peroxidase and H_2O_2 and converted into the deprotonated form, which is generally highly fluorescent, such as fluorescein and rhodamine. HPPA and its analogues have also been studied as fluorescent substrates [15]. The coupling reaction of two hydroxyphenyl groups is catalysed by peroxidase and the resulting dimer is fluorescent. First the substrates were checked as probes for the homogeneous measurement of haemolysis. Figure 1 shows the time course of fluorescence intensity during the reaction of fluorescein and H_2O_2 with both haemolysed and non-haemolysed cell suspensions. Non-haemolysed cells caused no fluorescence increment but haemolysed cells showed a fluorescence increment. The background fluorescence after addition of the substrates is attributed to fluorescein as impurity in fluorescein. The fluorescence increment for

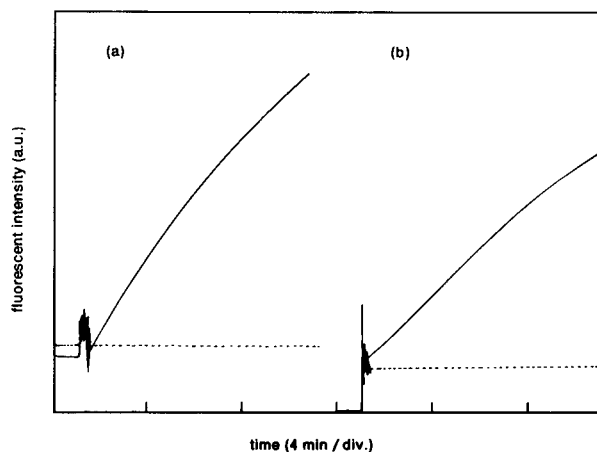


Fig. 1. Time course of fluorescence intensity during the reaction of the fluorescent substrates and red blood cells. To 3.0 ml of a sheep red blood cell suspension (1.25×10^4 cells), the fluorescent substrates were added; (a) 100 mM H_2O_2 and 50 mM HPPA; (b) 10 mM H_2O_2 and 1 mM fluorescein. The solid and dashed line are for a haemolysed and non-haemolysed cells, respectively.

haemolysed cells was also observed with HPPA and non-haemolysed cells caused no fluorescence increment. The difference between non-haemolysed and haemolysed cells revealed that the haemolysis can be homogeneously measured by fluorimetry. H_2O_2 permeates through the cell membrane [16] and reacts with haemoglobin, because the colour of the non-haemolysed cells changed from red to dark brown on adding H_2O_2 . The rates of permeation of the fluorescent substrates and the reaction products are, however, very low and the fluorescence increment could not be observed during the measuring period.

The reaction was then examined by varying the concentrations of the cells, H_2O_2 and the fluorescent substrates. Figure 2 shows the dependence of fluorescence increment on the number of cells in 3.0 ml of buffer. With non-haemolysed cells, there was no fluorescence increment. Haemolysed cells increased the fluorescence intensity but the maximum fluorescence increment was observed at around 2.5×10^4 cells. The decrease at high cell numbers is caused by shielding of the excitation or fluorescence radiation by the cell suspension because the apparent fluorescence intensity decreased with increasing cell

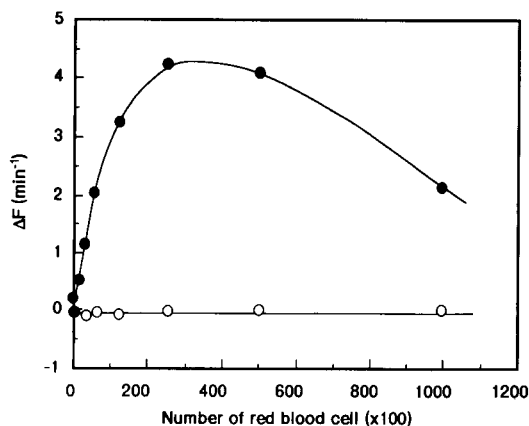


Fig. 2. Dependence of fluorescence increment on the number of cells. To 3.0 ml of a sheep red blood cell suspension, 50 μ l each of H_2O_2 (100 mM) and HPPA (100 mM) were added. The ordinate represents the initial rate of fluorescence (arbitrary units) increase. Closed and open circles are for haemolysed and non-haemolysed cells, respectively.

number. Subsequent experiments were done using 1.25×10^4 cells in 3.0 ml, where the shielding will be virtually negligible.

Figure 3 shows the dependence of fluorescence increment on the concentrations of HPPA and fluorescein. In both substrates, the fluore-

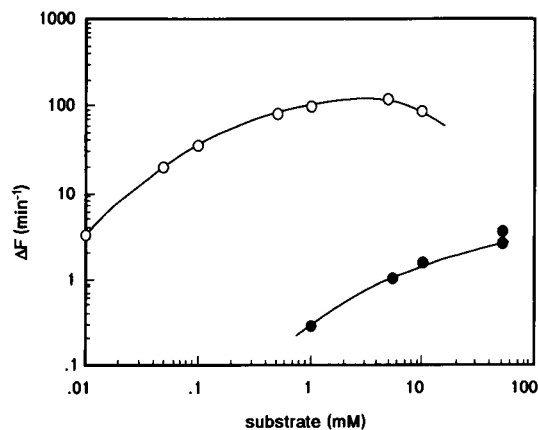


Fig. 3. Dependence of fluorescence increment on the concentration of the fluorescent substrate. To 3.0 ml of sheep red blood cell suspension (1.25×10^4 cells), 50 μ l each of H_2O_2 and the substrate were added. The ordinate represents the initial rate of fluorescence (arbitrary units) increase. Closed circles are for HPPA with 100 mM H_2O_2 and open circles for fluorescein with 10 mM H_2O_2 .

cence increment increased with increasing concentration. With fluorescein, the fluorescence increment peaked at 5 mM. Because the fluorescence of fluorescein is quenched at high concentrations [17], the appearance of the peak is attributed to the concentration quenching. Figure 4 shows the dependence of fluorescence increment on the concentration of H_2O_2 . Similarly to the fluorescent substrates, the fluorescence increment increased with increasing concentration of H_2O_2 . The sensitivity and detectability for fluorescein were superior to those for HPPA.

The kinetic assay for enzymatic activity is generally better than end-point assay [18]. Using high concentrations of substrates, the rate of reaction was too large to be measured by the chart recorder and the linear range in the time course was too small because of rapid saturation. With fluorescein, concentration quenching inhibits the assay at high concentration. The following experiment was therefore done using 1.0 mM fluorescein and 10 mM H_2O_2 or 50 mM HPPA and 100 mM H_2O_2 , where no saturation occurred during 10 min.

Under the conditions adopted, the degree of haemolysis was measured fluorimetrically as shown in Fig. 5. The haemolysed cell solution was

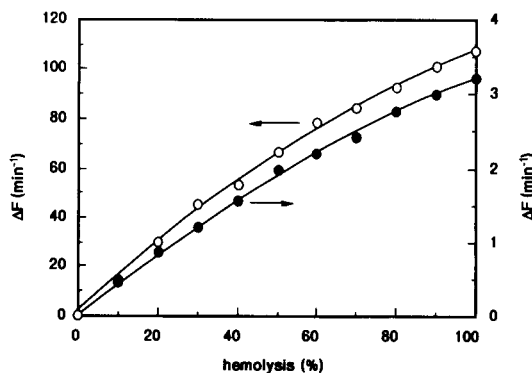


Fig. 5. Calibration graph of degree of haemolysis measured by the homogeneous method. To 3.0 ml of a sheep red blood suspension, 50 μ l each of H_2O_2 and the substrate were added. The ordinate represents the initial rate of fluorescence (arbitrary units) increase. Closed circles are for HPPA and open circles for fluorescein.

prepared by freezing and thawing of the cell suspension and then mixed with prescribed amount of non-haemolysed cells. The curves revealed that the degree of haemolysis could be measured homogeneously by fluorimetry. The sensitivity for fluorescein was also superior to that for HPPA. For measuring the haemolysis, however, the advantage will be small. At 50% haemolysis, the relative standard deviations for five replicate measurements were 4.1% for fluorescein and 2.0% for HPPA. The reproducibility with HPPA was slightly superior to that with fluorescein, but both fluorescent substrates are sufficient for the measurement of haemolysis.

Figure 6 shows the fluorescent response of EA to the diluted complement. As the complement is diluted, the fluorescence increased and saturated. EA responded up to 3600-fold diluted complement (0.051 CH50 unit ml^{-1}). The inset shows the relationship between this method and the heterogeneous method [13]. Good linearity was obtained with a correlation coefficient of 0.990. With HPPA, almost the same result was obtained with a response up to 2400-fold diluted complement with a correlation coefficient of 0.988.

In the assay of BSA, fluorescence measurement of haemolysis was combined with the complement fixation technique [19]. Figure 7 illustrates the principle of the assay of BSA. BSA in a

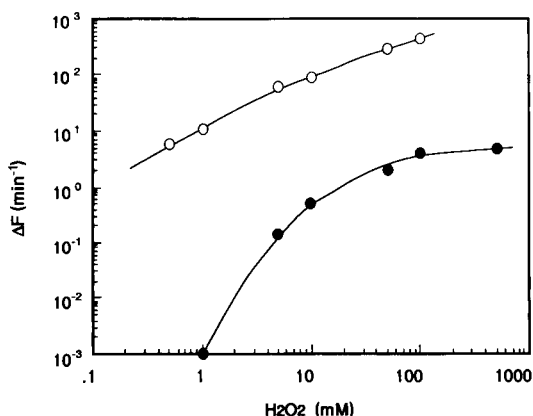


Fig. 4. Dependence of fluorescence increment on the concentration of H_2O_2 . To 3.0 ml of a sheep red blood cell suspension (1.25×10^4 cells), 50 μ l each of H_2O_2 and the substrate were added. The ordinate represents the initial rate of fluorescence (arbitrary units) increase. The concentrations of HPPA and fluorescein were 100 mM (closed circles) and 10 mM (open circles), respectively.

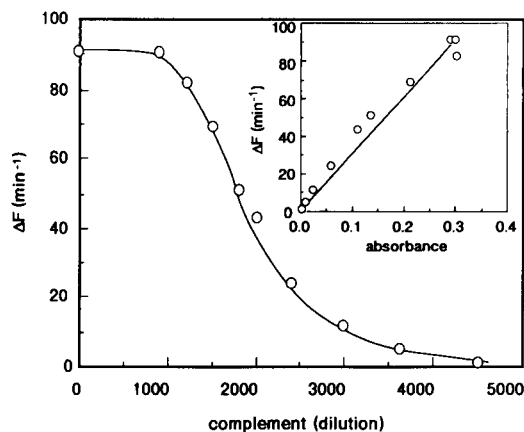


Fig. 6. Fluorescence response versus dilution factor of the complement using fluorescein as fluorescent substrate. The ordinate represents the initial rate of fluorescence (arbitrary units) increase. The inset is the correlation to the heterogeneous method. The abscissa is the absorbance of the centrifuged supernatant after the complement-mediated haemolysis.

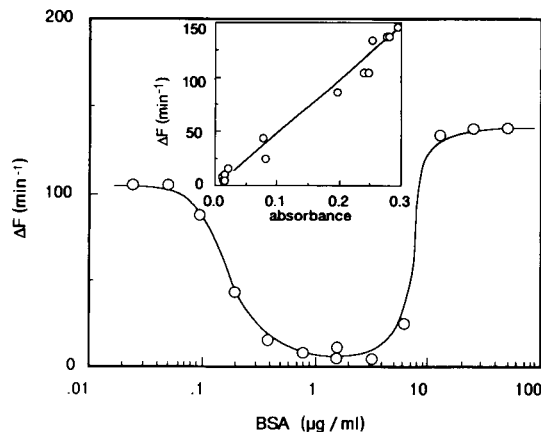


Fig. 8. Fluorescence response curve for BSA using fluorescein as fluorescent substrate. The ordinate represents the initial rate of fluorescence (arbitrary units) increase. The inset is the correlation to the heterogeneous method. The abscissa is the absorbance of the centrifuged supernatant after the complement-mediated haemolysis.

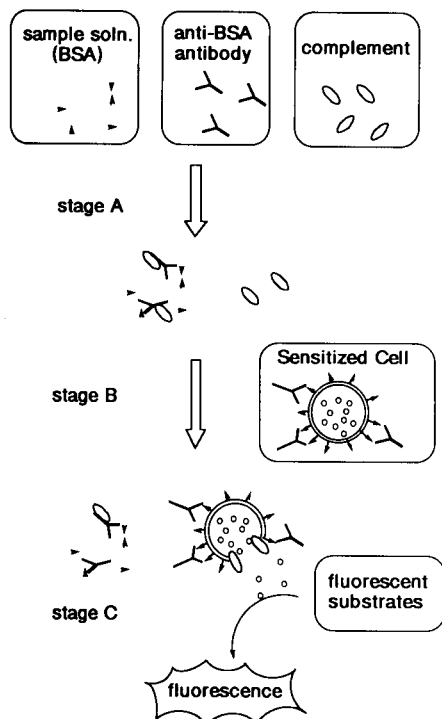


Fig. 7. Schematic representation of the principle of the assay for BSA. In the first stage, the sample solution containing BSA was mixed with anti-BSA antibody and the complement. In the next stage, the remaining complement was reacted with EA. Finally, the haemolysis was measured fluorimetrically by adding fluorescent substrates.

standard or sample solution was bound with anti-BSA and then the binding complex activated the complement, where the degree of activation was related to the binding complex formed. The remaining complement was measured by homogeneous haemolysis assay. Figure 8 shows the response to various amounts of BSA. The minimum fluorescence intensity was observed around $1.0 \mu\text{g ml}^{-1}$ BSA. At lower or higher concentrations of BSA, the fluorescence increment was reached up to saturation. The correlation against the heterogeneous method was 0.994. With HPPA, almost the same result was obtained, with the minimum at $1.0 \mu\text{g ml}^{-1}$ and a correlation coefficient of 0.995. Complement is activated by the antigen-bound antibodies where at least two IgG molecules are neighbours to each other. At higher concentrations of BSA, a smaller number of antibodies bind to one BSA molecule and the complement will be activated mainly by EA. At lower concentrations of BSA, a small number of the complex moieties will be formed and complement will be activated mainly by EA also. The optimum concentration for the inhibition of the fluorescence will therefore be observed.

Other types of homogeneous fluorescence immunoassay techniques have been developed, such as fluorescent polarization [3], fluorescent energy

transfer [20] and enzymatic fluorescence immunoassay [21]. In these methods, an immunoagent labeled with a fluorescent dye or enzyme was prepared for each analyte. Compared with these methods, the proposed method has the advantage of simplicity, because the conjugation of labels or enzymes is unnecessary and the equipment consists of a conventional incubator and fluorimeter.

REFERENCES

- 1 D.S. Hage, *Anal. Chem.*, 62 (1991) 206R.
- 2 K.E. Rubenstein, R.S. Scheider and E.F. Ullman, *Biochim. Biophys. Res. Commun.*, 47 (1972) 846; E.F. Ullman, J. Blackmore, R.K. Leute, W. Einted and A. Jaklitsch, *Clin. Chem.*, 21 (1975) 1011; D.J. Litman, T.M. Hanlon and E.F. Ullman, *Anal. Biochem.*, 106 (1980) 223; T.T. Ngo and H.M. Lenhoff, *FEBS Lett.*, 116 (1980) 285.
- 3 J.S. O'Neal and S.G. Schulman, *Anal. Chem.*, 56 (1984) 2888; C.J. Halfman, F.C.L. Wong and A. Schneider, *Anal. Chem.*, 56 (1984) 1648; P. Urios and N. Cittanova, *Anal. Biochem.*, 185 (1990) 308.
- 4 Y. Ikariyama, H. Kunoh and M. Aizawa, *Biochem. Biophys. Res. Commun.*, 128 (1985) 987.
- 5 D. Monroe, *J. Liposome Res.*, 1 (1990) 339; L. Locascio-Brown, A.L. Plant, V. Horvath and R.A. Durst, *Anal. Chem.*, 62 (1990) 2587; M. Flechtner, M. Wong, C. Bler-niarz and M.T. Shipchandler, *Anal. Biochem.*, 180 (1989) 140; T. Nakamura, S. Hoshino, N. Hazemoto, M. Haga, Y. Kato and Y. Suzuki, *Chem. Pharm. Bull.*, 37 (1989) 1629.
- 6 S.C. Kinsky, J.A. Haxby, D.A. Zopf, C.R. Alving and C.B. Kinsky, *Biochemistry*, 8 (1969) 4149.
- 7 M. Umeda, Y. Ishimori, K. Yoshikawa, M. Takada and T. Yasuda, *J. Immunol. Methods*, 95 (1986) 15.
- 8 G.K. Humphries and H.M. McConnell, *Proc. Natl. Acad. Sci. U.S.A.*, 71 (1974) 1691.
- 9 M. Haga, H. Itagaki, S. Sugawara and T. Okano, *Biochem. Biophys. Res. Commun.*, 95 (1980) 187.
- 10 K. Shiba, Y. Umezawa, T. Watanabe, S. Ogawa and S. Fujiwara, *Anal. Chem.*, 52 (1980) 1610.
- 11 P. D' Orazio and G.A. Rechnitz, *Anal. Chem.*, 49 (1977) 2083.
- 12 Y. Tatsu and S. Yoshikawa, *Chem. Lett.*, (1990) 1467; Y. Tatsu and S. Yoshikawa, *Anal. Chem.*, 62 (1990) 2103; Y. Tatsu, S. Yamamura and S. Yoshikawa, *Anal. Sci.*, 7 (1992) S903.
- 13 E.A. Kabat and M.M. Mayer, *Experimental Immunochem-istry*, Charles C Thomas, Springfield, IL, 1961, Chap. 4.
- 14 A.S. Keston and R. Brandt, *Anal. Biochem.*, 11 (1965) 1; M.J. Black and R. Brandt, *Anal. Biochem.*, 58 (1974) 246; R.P. Haugland, *Handbook of Fluorescent Probes and Re-search Chemicals*, Molecular Probes, Eugene, OR, 1989, p. 72.
- 15 G.G. Guilbault, P. Brignac, Jr., and M. Zimmer, *Anal. Chem.*, 40 (1968) 190; G.G. Guilbault, P. Brignac, Jr., and M. Juneau, *Anal. Chem.*, 40 (1968) 1256; K. Zaitzu and Y. Ohkura, *Anal. Biochem.*, 109 (1980) 109.
- 16 A.A. Frimer, A. Forman and D.C. Borg, *Isr. J. Chem.*, 23 (1983) 442.
- 17 I.L. Arbeloa, *J. Chem. Soc., Faraday Trans. 2*, 77 (1981) 1735.
- 18 T. Murach, in E. Ishikawa, T. Kawai and T. Murachi (Eds.), *Enzyme Immunoassay*, Igakushoin, Tokyo, 1982, Chap. 1–2.
- 19 E. Wasserman and L. Levine, *J. Immunol.*, 87 (1961) 290.
- 20 E.F. Ullman, M. Schwarzberg and K.E. Rubenstein, *J. Biol. Chem.*, 251 (1976) 4172; L.E. Morrison, *Anal. Biochem.*, 174 (1988) 101.
- 21 T.A. Kelly and G.D. Christian, *Talanta*, 29 (1982) 1109.

Different sample introduction systems for the simultaneous determination of As, Sb and Se by microwave-induced plasma atomic emission spectrometry

E. Bulska¹ and P. Tschöpel

Laboratorium für Reinstoffanalytik, Max-Planck-Institut für Metallforschung, Stuttgart, Postfach 12 26 52, W-4600 Dortmund 1 (Germany)

J.A.C. Broekaert

Universität Dortmund, Fachbereich Chemie, Postfach 50 05 00, W-4600 Dortmund 50 (Germany)

G. Tölg

Laboratorium für Reinstoffanalytik, Max-Planck Institut für Metallforschung, Stuttgart, Postfach 12 26 52, W-4600 Dortmund 1; and Institut für Spektrochemie und Angewandte Spektroskopie (ISAS), Postfach 10 13 52, W-4600 Dortmund 1 (Germany)

(Received 21st May 1992; revised manuscript received 27th July 1992)

Abstract

The determination of hydride-forming elements using different sample introduction procedures into microwave-induced plasmas (MIPs) has been studied. For the determination of As, Sb and Se analyte introduction was accomplished with a pneumatic concentric glass nebulizer, a graphite furnace, or with hydride generation followed by cold-trapping or hot-trapping in a graphite furnace. The detection limits obtained with different types of low power MIPs (toroidal, 1 or 3 filament MIPs) operated in a TM_{010} cavity according to Beenakker also were investigated. The construction of the flow system used for preconcentration and the effects of reagent concentration, gas flow rates as well as other experimental conditions were described in detail. Suitable conditions for multielement determination with MIP-atomic emission spectrometry (AES) were investigated. The trapping of the hydrides followed by their vaporization showed substantial advantages over the other introduction systems investigated, especially with respect to power of detection. Further, mutual interferences being a big problem in atomic absorption spectrometry are widely absent in MIP-AES. Under compromise operating conditions the detection limits for As, Sb and Se are 0.4; 0.35; 0.25 ng ml⁻¹ respectively, while the sample volume can be varied from 0.05 ml up to several millilitres.

Keywords: Atomic emission spectrometry; Antimony; Arsenic; Hydride generation; In situ trapping; Microwave-induced plasmas; Selenium

Correspondence to: P. Tschöpel, Laboratorium für Reinstoffanalytik, Max-Planck-Institut für Metallforschung, Stuttgart, Postfach 12 26 52, W-4600 Dortmund 1 (Germany).

¹ On leave from Department of Chemistry, University of Warsaw, 02-093 Warsaw (Poland).

Low-power Ar- or He-microwave-induced plasmas (MIPs) generated in the TM_{010} cylindrical resonant cavity have attractive features as

sources for analytical atomic spectrometry [1]. These systems are easy to construct, simple to operate and relatively inexpensive; they can easily be coupled with a variety of sample introduction devices [2,3].

The major disadvantage of MIPs as compared with other plasma discharges is their sampling capacity for solids and wet aerosols. Indeed, at low power the delivered energy is not sufficient to evaporate large amounts of solid or liquid [3]. Further, the stability of the plasma can be degraded when a relatively small amount of sample material is introduced [4].

The analysis of solutions by MIP-AES, necessitates either minimizing the amount of liquid entering the low power plasma by aerosol desolvation [5], or increasing the power applied to the discharge [6–8]. The optimization of a toroidal type of MIP with respect to the uptake of wet aerosols as generated by pneumatic nebulization has been described previously [9,10]. The detection limits obtained in the pneumatic nebulization of liquid samples are limited by the efficiency of the nebulizer, which is typically not better than a few percent. The most important application of MIPs is the analysis of gaseous samples. In contrast to pneumatic nebulization, the analysis of gases and sample vapors is characterized by a high sample transport efficiency (close to 100%) and an accordingly high sensitivity. As several elements have volatile hydrides, sample introduction in MIP-AES using hydride generation (HG) seems to be an effective approach [11]. The determination of As, Sb and Se by hydride generation followed by atomic absorption spectrometry (AAS) [12], inductively coupled plasma atomic emission spectrometry (ICP-AES) [13,14], or by MIP-AES are well known [15–21].

Compared with HG-AAS, HG combined with MIP-AES delivers a high linear dynamic range and simultaneous determination of the analytes is feasible. However, due to the fact that the plasma is easily affected or even extinguished by large amounts of H_2 , CO_2 , HCl or water aerosol, which are by-products in HG, only small portions of the sample solution may be added onto a $NaBH_4$ pellet to keep H_2 evolution low [16,17], or the hydrides have to be separated from the H_2 e.g. by

a chromatographic column [18,19], or by trapping e.g. with liquid nitrogen.

A direct, continuous introduction was described by Ng et al. [20], who operated the MIP at a relatively high power and gas flow rate and accordingly could sustain the MIP without removal of H_2 and other by-products. A more efficient continuous flow mode with a HG-MIP-AES system was recently described by Tao and Miyazaki [21], who had the evolved gaseous species pass through a hollow fiber membrane, by which H_2 and H_2O vapour could be removed, while the hydrides passed through and reached the plasma.

In the work described here the analytical performance of different systems for the introduction of As, Sb and Se into the MIP were evaluated. In the case of hydride generation AAS suffers from mutual interferences which most probably occur in the gas phase [22–26]. It can be expected that some of those interferences are eliminated in the MIP-AES.

For the direct introduction of wet aerosols the toroidal MIP (T-MIP) was used. One- and three-filament MIPs (1F-, 3F-MIP) were used for the introduction of gaseous samples as produced by: (i) graphite furnace evaporation of the solvent followed by vaporization of the analyte and transport into the plasma, (ii) HG using cold-trapping of the hydrides in a liquid N_2 cooled cell or, (iii) hot-trapping of the hydrides in a graphite furnace, both followed by evaporation and analyte transport into the plasma.

EXPERIMENTAL

Instruments

Spectrometer. A 0.5-m Ebert monochromator (Jarrell-Ash), with wavelength range of 200–450 nm, a grating with a constant 1/2242 mm, a width of 54 mm, a reciprocal linear dispersion of 0.8 nm mm^{-1} , slit widths of $30 \mu\text{m}$, an EMI 9781A photomultiplier, and a Beckman 610 000 potentiometric recorder, for signal acquisition using peak height measurements for calibration, were used.

Electrodeless discharge lamps for As (8 W), Sb

TABLE 1

Optimum working conditions for different types of MIPs obtained in a TM_{010} cavity (according to Beenakker)

| | MIP | | |
|--------------------------|----------|----|-----|
| | Toroidal | 1F | 3F |
| Forward power (W) | 120 | 50 | 90 |
| Reflected power (W) | 5–8 | 0 | 1–2 |
| Gas flow ($l\ h^{-1}$) | 24 | 20 | 30 |

(9 W) and Se (6 W) powered by an EDL Power Supply (Perkin-Elmer) were used for wavelength selection.

Cavity. A cylindrical TM_{010} cavity provided with an X–Y–Z translation table to optimize the position of the capillary in the cavity and to select the observation point was used for the T-MIP [9]. In the case of the 3F-MIP a chuck with three jaws was screwed into the central hole of the cavity. The quartz capillaries used were made of Suprasil (Heraeus Quarzschmelze, Hanau). For the T-MIP and 3F-MIP the capillaries had a diameter of 6.0 mm (o.d.) and 4.0 mm (i.d.) and for the case of 1F-MIP the diameters were 2.0 mm (o.d.) and 1.0 mm (i.d.). The optimum working conditions for the different MIPs are listed in Table 1.

Microwave generator. An EMS-Microtron EMS 6000 Mark III, operating at a frequency of 2.45 GHz with a maximal forward power of 200 W was used. The reflected power was adjusted to a minimum after ignition of the plasma.

Aerosol generation by pneumatic nebulization (PN). For this aim a concentric glass Meinhard

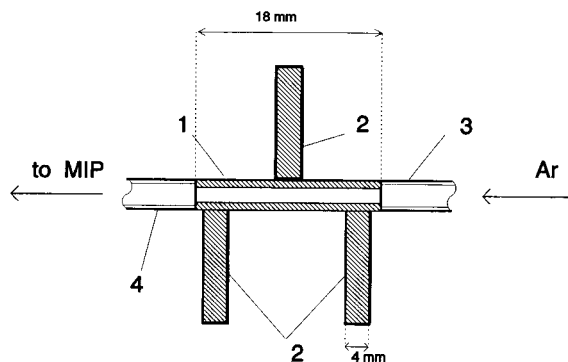


Fig. 1. Schematic diagram of the electrothermal vaporizer (part I and III of Fig. 3). (1) graphite tube (5.0 mm o.d., 2.8 mm i.d.); (2) graphite support rods (4 mm o.d.); (3) quartz capillary (5.0 mm o.d., 3.0 mm i.d.); (4) plasma capillary of Suprasil (6.0 mm o.d., 4.0 mm i.d.).

nebuliser was positioned in a spray chamber according to Scott [27] (material: glass; diameter: 22 mm; length: 50 mm).

Electrothermal evaporation system (GF). A modified CRA-63 electrothermal atomizer (Varian Techtron) was mounted on an X–Y–Z adjustment table (details in Ref. 28). The graphite tube was connected directly to the quartz capillary of the MIP (Fig. 1). Graphite tubes (5.0 mm o.d. and 2.8 mm i.d.; 18 mm long) were machined from RWO quality graphite (Ringsdorf GmbH, Bonn–Bad Godesberg), and were positioned between three supporting rods for more efficient heating and temperature distribution in the graphite tube. As power supply the CRA unit Model 61 (Varian Techtron, Mulgrave) was used.

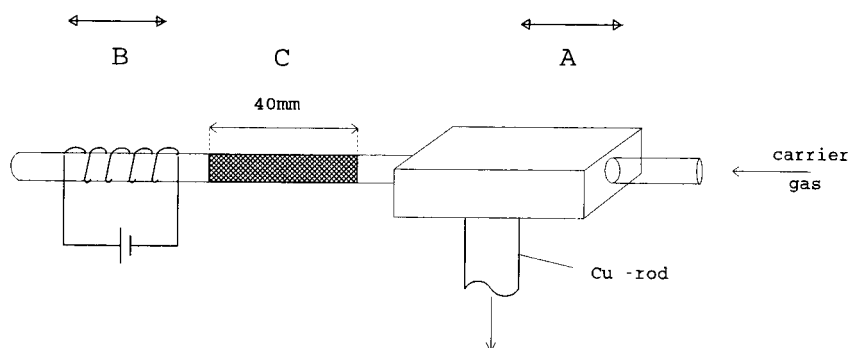


Fig. 2. Schematic diagram of the preconcentration system for cold-trapping. (A) movable cooling device (copper block, copper rod); (B) movable heating spiral; (C) preconcentration zone (quartz wool).

This equipment was used for the direct vaporization of the dry sample residue from the graphite furnace (GF) as well as for HG using hot-trapping of the hydrides in the graphite furnace (GFT).

Cold trapping unit (CT). A quartz tube (5 mm o.d., 3 mm i.d.) packed with quartz wool (40 mm length) was cooled down to retain the hydrides (Fig. 2). The cooling block consisted of a copper jacket with a 10 cm long bar, which was kept in liquid N_2 contained in a Dewar vessel (Fig. 3II). During the preconcentration step the copper block (A in Fig. 2) is moved over the trapping zone of the capillary containing the quartz wool so as to fix the hydrides (C in Fig. 2). During the vaporization step the cooling block is removed, the heating device (W coil; B in Fig. 2) pushed over the quartz wool and the CRA power supply heats the block to the desired temperature to release the collected hydrides.

Hydride generation unit (HG). A diagram of the flow hydride generator used is shown in Fig. 3. The sample and the $NaBH_4$ solution were fed continuously with a four-channel Gilson Miniplus 2 peristaltic pump. Solution flow rates of 2.0 ml min^{-1} were used. The sample (or the blank) flow was mixed with the $NaBH_4$ solution stream in a T-piece. The mixtures of liquid and gaseous reaction products were continuously pumped into a

gas–liquid separator. The latter was optimized so that the amount of water vapour introduced into the system was minimal and a smooth gas flow was produced. It was important to avoid the formation of large bubbles. The gaseous products were carried away by a continuous Ar flow (at a rate of 0.5 l h^{-1}) and the waste drained.

Reagents

The $NaBH_4$ solution was prepared by dissolving 0.5 g of $NaBH_4$ (Merck, Darmstadt) in 100 ml of NaOH (0.5%). The solution was filtered and stored in a refrigerator. As(III), Se(IV) and Sb(III) stock solutions were prepared from their Titrisol solutions (Merck, Darmstadt), each containing 2 g l^{-1} of the element. Aliquots were diluted with 3 mol l^{-1} HCl, to give standard solutions with concentrations of 0.4 ng ml^{-1} up to $1 \text{ } \mu\text{g ml}^{-1}$.

The gases Ar (plasma gas) and N_2 (shielding gas for the graphite furnace), both 99.99% pure, were used.

RESULTS AND DISCUSSION

Pneumatic nebulization (PN–MIP–AES)

For the determination of As, Sb and Se the use of a T–Ar–MIP in combination with a pneumatic nebulization was investigated. The analyte

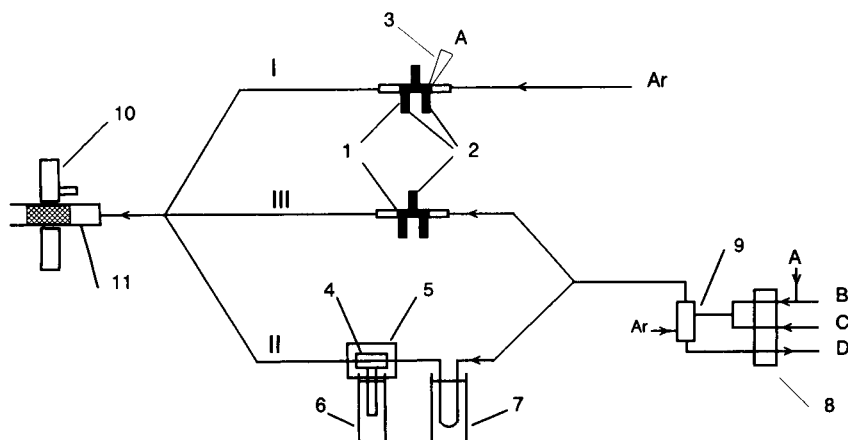


Fig. 3. Schematic diagram of sample introduction techniques for MIP. I and III: graphite furnace: (1) graphite furnace, (2) graphite electrodes, (3) micropipette tip. II: cold-trap: (4) copper block, (5) isolating box, (6) Dewar cooling-trap (N_2), (7) Dewar water-trap (dry ice–ethanol). (8) Peristaltic pump, (9) gas–liquid separator, (10) TM_{010} cavity, (11) Suprasil discharge tube. (A) sample, (B) carrier solution, (C) reductant solution, (D) waste.

TABLE 2

Measured relative sensitivities of various spectral lines

| Element | Wavelength (nm) | Electrodeless discharge lamp | T-MIP | 3F-MIP |
|---------|-----------------|------------------------------|-------|--------|
| As | 200.3 | 10 | – | – |
| | 228.8 | 100 | 100 | 100 |
| | 234.9 | 97 | 48 | 64 |
| | 278.0 | 95 | 56 | 80 |
| | 286.0 | 30 | 10 | 25 |
| Sb | 206.8 | 75 | – | – |
| | 217.6 | 38 | 65 | 40 |
| | 231.1 | 40 | 25 | 45 |
| | 252.8 | 100 | 100 | 100 |
| Se | 196.1 | 39 | 25 | 24 |
| | 203.99 | 100 | 100 | 100 |
| | 206.28 | 64 | 49 | 55 |
| | 207.48 | 78 | 7 | 10 |
| | 241.35 | 34 | – | – |

solution was fed to the pneumatic concentric glass nebulizer with an uptake rate of 0.40 ml min⁻¹ and the nebulizer gas flow was 24 l h⁻¹. A comparison of the sensitivity of different emission lines (Table 2) can be easily done when using pneumatic nebulization for a continuous introduction of the samples. It was shown that in MIP-AES as well as for EDL the most sensitive line for the elements investigated are: As I 228.8 nm, Sb I 252.8 nm and Sb I 203.99 nm.

The 3 σ detection limits for As, Sb, Se were 500, 250 and 540 ng ml⁻¹ respectively (Table 3) and thus higher than in ICP-AES (cf. Table 4) [29]. The relative standard deviations (R.S.D.,

TABLE 3

Comparison of the concentration detection limits for As, Sb and Se obtained with different sample introduction techniques^a

| Procedure | As (ng ml ⁻¹) | Sb (ng ml ⁻¹) | Se (ng ml ⁻¹) |
|---------------|---------------------------|---------------------------|---------------------------|
| PN-T-MIP | 500 (4.8) | 250 (4.0) | 540 (4.2) |
| GF-3F-MIP | 50 (1.8) | 20 (2.0) | 46 (1.5) |
| HG-CT-3F-MIP | 0.8 (6.7) | 0.4 (6.8) | 0.5 (7.2) |
| HG-GFT-3F-MIP | 0.4 (4.5) | 0.35 (4.8) | 0.25 (4.6) |

^a At 10 \times detection limit; data in parentheses are R.S.D. in %.

TABLE 4

Comparison of literature values for the detection limits (ng ml⁻¹) for As, Sb and Se in AAS, AES and MS

| Technique | Reference | As | Sb | Se |
|-----------|-----------|-------|-------|------|
| PN-ICP | [29] | 50 | 32 | 75 |
| PN-MIP | [9] | 300 | – | – |
| HG-ICP | [13] | 1.0 | 2.4 | 1.3 |
| HG-ICP | [14] | 1.0 | – | – |
| HG-ICP | [45] | 0.06 | 0.18 | – |
| HG-MIP | [21] | 0.32 | 6.1 | – |
| HG-GF-MIP | [44] | 0.12 | – | – |
| PN-ICP-MS | [46] | 0.14 | 0.019 | 1.5 |
| HG-ICP-MS | [46] | 0.017 | 0.031 | 0.17 |
| HG-AAS | [24] | 0.16 | 0.08 | 0.18 |

$n = 12$) of the signals in standard aqueous solution at analyte concentrations of ten times the detection limit ranged from 4.0 to 4.8% (Table 3). For MIP-AES the matrix effects and spectral interferences are higher than those in ICP-AES. In particular, the presence of alkali salts [9] can make the plasma unstable. A major drawback of the nebulization technique both in ICP- and MIP-AES is its poor sample introduction efficiency which influences the detection limits.

Graphite furnace evaporation (GF-MIP-AES)

As the introduction of gaseous samples and vapours seems to be the most efficient way of introducing analytes into the MIP electrothermal vaporization in connection with MIP was described extensively (for a review see Ref. 30). Just as in GF-AAS drying and vaporization are achieved in the electrothermal atomizer. Here, however, the sample vapour is then introduced into the MIP with the aid of a carrier gas and the excitation takes place in the plasma. A low power MIP operated in a Beenakker cavity has been successfully applied in combination with electrothermal vaporization from a graphite cup [31], from a graphite furnace [31–33], or from a tungsten wire loop [34].

A simple graphite furnace MIP system (section *Electrothermal evaporation system*) was used for the optimization of the parameters with the 1F and 3F-MIP (Table 1), as well as for the determination of the absolute detection limits for As, Sb and Se (Table 3). Sample aliquots were intro-

TABLE 5

Experimental conditions for the sample introduction techniques used ^a

| Step | Temperature (°C) | Time (s) | Ar flow (l h ⁻¹) |
|------------------------------|------------------|--------------|------------------------------|
| A | | | |
| 1 Evaporation (of 5 μ l) | 100 | 60 | 0.5 |
| 2 Plasma ignition | Ambient | – | 30 |
| 3 Atomization | Maximum | 2 | 30 |
| B | | | |
| 1 Pre-cooling | –120 | 60 | 0.5 |
| 2 Collection | –120 | ^b | 0.5 |
| 3 Plasma ignition | –120 | – | 30 |
| 4 Evaporation | 100 | 1–2 | 30 |
| C | | | |
| 1 Preheating | 400 | 10 | 0.5 |
| 2 Collection | 400 | ^b | 0.5 |
| 3 Plasma ignition | Ambient | – | 30 |
| 4 Evaporation | Maximum | 2 | 30 |

^a A = Electrothermal vaporization of aqueous solution (GF-MIP-AES); B = Hydride generation followed by cold-trapping (HG-CT-MIP-AES); C = hydride generation followed by GF preconcentration (HG-GFT-MIP-AES). ^b Collection time depends on the sample volume.

duced into a graphite furnace by micropipette. Injection volumes of up to 5 μ l could be introduced into the tube without spilling the solution out of the tube. The sample was dried, atomized and carried directly into the MIP with the plasma gas (Table 5). No special gas circulation system was necessary with the configuration used (Fig. 3I). Here each time after the evaporation of the solvent the plasma was re-ignited. The spectral background differs not only with the wavelength used but also within the heating period of the graphite furnace. Further, the background emission intensity strongly depends on the atomization temperature which in turn influences the atomization efficiency. Therefore compromise conditions should be used. For the As and Se determinations the most sensitive lines were used. For Sb the 252.8 nm line suffered from such a high background that the detection of the atomic signal was not possible. The background emission was not broad-band as it disappeared at about ± 0.1 nm beside the emission line. It is obvious that it is caused by volatilization of Si from the

quartz tube attached to the heated graphite tube. Indeed, the Si 252.851 nm line is only 0.003 nm away from the more sensitive Sb line [35]. Therefore, when the graphite furnace technique is used for the determination of Sb the 217.56 nm line should be used. The obtained detection limits and R.S.D. values for As, Sb and Se are given in Table 3.

Flow hydride generation (HG)

Elements with volatile hydrides such as As, Se and Sb can be determined by hydride generation, subsequent atomization of the hydride and measurement by AAS [22–26]. The HG technique is also an attractive method for introducing vapour species of some analyte into plasmas [13–21]. In the literature on MIP many problems associated with discharge instability due to an excess of generated hydrogen, entering the plasma, are reported. Preliminary experiments in this work also indicated that the introduction of hydrogen or of water vapour stemming from the hydride generation reaction, MIP discharge can be affected or even extinguished. Therefore, a suitable separation of the generated hydrides from H₂ has been developed.

The HG-MIP procedure includes several completely independent steps [36]: namely, hydride generation, transport of the gaseous mixture, trapping of the hydrides and their atomization. Hydride generation in a flow system results from acidifying the analyte solution followed by mixing it with a reductant solution in order to form volatile hydrides. The concentration of acid and reductant as well as the flow of the sample and the reductant are critical. Therefore these parameters were optimized, at first separately for each of the hydride forming elements. In a second step compromise conditions for multielement analyses were selected.

The data on the optimized conditions reported in the literature are very inconsistent [37–39]. It can be concluded that the exact operating conditions for HG depend on a number of experimental parameters and differ from one system to another. The relation between the working conditions and the analytical response for the three elements studied was investigated. The influence

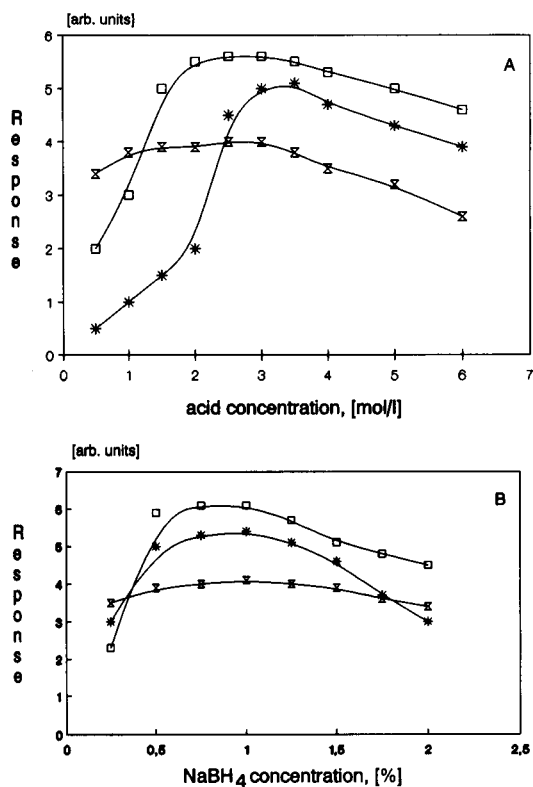


Fig. 4. Effect of (A) HCl (0.5% w/v NaBH₄), and (B) NaBH₄ (3 mol l⁻¹ HCl) concentration on the analyte response in HG-MIP-AES: (□) 50 ng of As, (⊗) 40 ng of Sb, and (*) 50 ng of Se. Sample volume: 50 μl; T-MIP; forward power: 120 W; argon flow: 24 l h⁻¹.

of HCl concentrations between 0.1 and 6 mol l⁻¹ in the case of a 0.5% (w/v) NaBH₄ solution is given in Fig. 4A. At 3 mol l⁻¹ HCl, the response for all elements was a maximum and this concentration was selected for further investigations. The NaBH₄ concentrations used in the literature vary between 0.3 and 10% (w/v), but they are reported to be optimum at 1 to 3% (w/v), or in the case of flow techniques even less. The effect of different concentrations of NaBH₄ on the response was investigated (Fig. 4B) and found to be optimum at 0.5–1% (w/v). Therefore, a concentration of 0.75% (w/v) NaBH₄ was used.

Additionally, an improvement in power of detection may be realized by collection and preconcentration of the hydrides prior to their introduction into the MIP. Also several interferences are

avoided by such a preconcentration and separation of the hydrides from gaseous by-products (H₂, H₂O vapour etc.). Experimentally, two preconcentration techniques, namely a cold-trapping and a hot-trapping in a graphite furnace and two types of plasma forms, namely the 1F- and 3F-MIPs in a TM₀₁₀ cavity were compared with respect to power of detection. The results show that the 3F-MIP permits lower detection limits in the case of hydride generation.

Preconcentration of the hydrides by cold-trapping (HG-CT-MIP-AES). For the preconcentration of the hydrides by cold trapping, the use of silanized Chromosorb W [40] was investigated, but soon was found not to be useful in connection with MIP-AES. Indeed, the volatile products released during the heating step caused severe interferences, disturbed the plasma and after several measurements led to troublesome devitrification of the inner wall of the plasma capillary. Therefore, it was decided to trap the hydrides on quartz wool. The reaction mixture from the gas-liquid separator was transported to the liquid nitrogen cold trap (Fig. 3II and the section *Cold trapping unit*). To make sure that water droplets and vapor do not reach the preconcentration section, a water trap was also included. It consisted of a U-shaped tube immersed in a dry ice-ethanol bath. Taking into account the melting and boiling points of the hydrides, a temperature of about -20°C was maintained in the water trap tube. After a throughput of about 25 samples the tube was blocked by ice and had to be replaced. A quartz tube (5 mm o.d., 3 mm i.d.) was used for the transport of the gas mixture to the trapping zone. Before starting the hydride evolution the tube was cooled with the copper block and after the trapping, the hydrides were vaporised (see the section *Cold trapping unit*).

The carrier gas flow (Ar), the temperature during trapping and evaporation of the hydrides, as well as the plasma gas flow (Ar) and the plasma forward power were optimized with respect to the power of detection (Tables 1 and 5). The applied temperature of the cooling block and the carrier gas flow during preconcentration appeared to be very critical for the efficiency of freezing of the hydrides. The preconcentration

temperature should be as low as possible to ensure a high trapping efficiency. A temperature of about -120°C could be achieved with the copper block (Fig. 3II), and this is lower than the melting points of three of the hydrides. However, it can be concluded from the relationship between the analyte response and the preconcentration temperature (Fig. 5A), that in the case of As a yield of 100% has not been obtained, which means that some losses of elements occurred during the preconcentration step. The preconcentration efficiency was also affected by the carrier gas flow which should be low (Fig. 5B). The general trends of the graphs for As, Sb and Se are similar and a

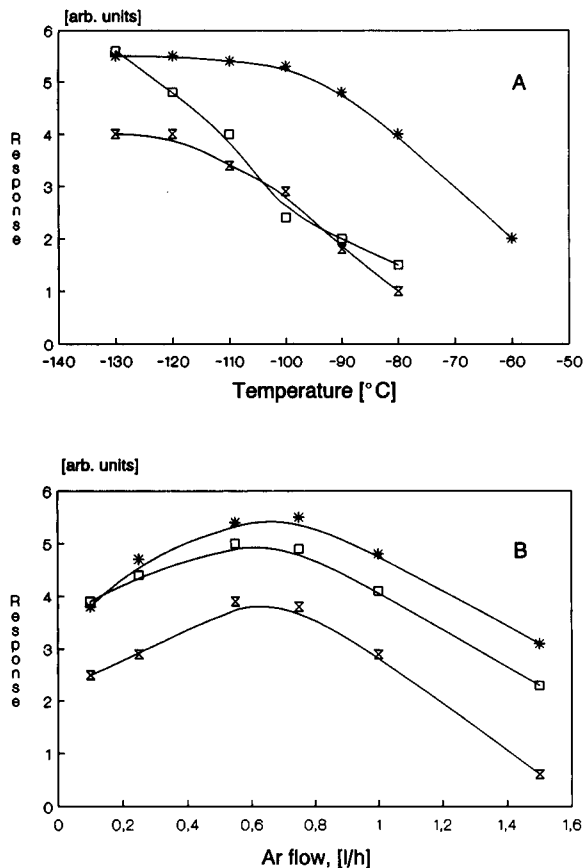


Fig. 5. Effect of (A) the cold trap temperature and (B) carrier gas flow during cold trapping on the analyte response in HG-CT-MIP-AES: (□) 20 ng of As, (X) 10 ng of Sb, and (*) 10 ng of Se. Sample volume: 100 μl . 3F-MIP; forward power 90 W; argon flow 30 l h^{-1} .

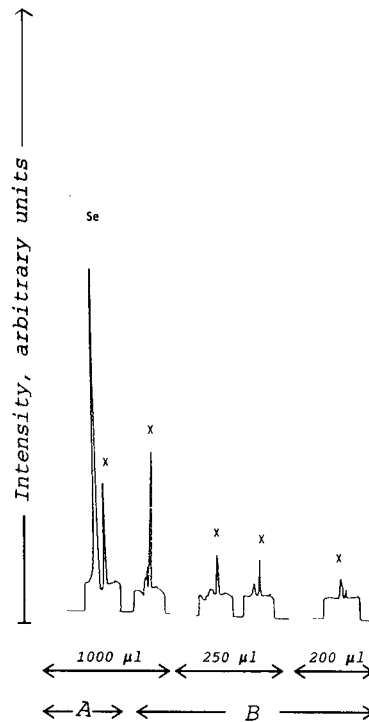


Fig. 6. Emission signal chart recordings at 203.9 nm of Se line in HG-CT-MIP-AES: 50 ng of Se in (A) 3 mol l^{-1} HCl and (B) blank (3 mol l^{-1} HCl). Signals: Se and X from evolved HCl molecule. 3F-MIP; forward power: 90 W; argon flow: 30 l h^{-1} .

flow rate of 0.5 l h^{-1} was selected. During the HG step the sample was pumped into the reagent flow and the plasma was switched off. After the preconcentration step the plasma was ignited, the cooling system was removed from the collection zone, the W-spiral was moved over the quartz wool and heated immediately to about 100°C . Under the optimized multielement conditions, detection limits of 0.8 ng for As, 0.4 ng for Sb and 0.5 ng for Se were found. The R.S.D. ranged from 6.5 to 7.2%. However, when the total sample volume exceeded 1 ml the plasma was disturbed and the reflected power increased during the measurements. In addition, tailing of the signal was observed. HCl can also be trapped at low temperatures and then is evaporated together with hydrides, and so causes severe interference. This was shown by the signal shape obtained under slow heating of the quartz wool. Indeed, a

double signal was obtained (Fig. 6). The first peak (X) was also obtained when only the blank ($3 \text{ mol l}^{-1} \text{ HCl}$) was introduced into the reaction vessel. Further, wet pH paper situated at the end of the capillary indicated the presence of the HCl. Therefore, the volumes used were limited to 1 ml. Although the procedure gives low detection limits, it is relatively complicated and required approximately 15 min per 1-ml sample.

Preconcentration of hydrides by hot-trapping in a graphite furnace (HG-GFT-MIP-AES). The hydrides of As, Sb and Se can also be trapped in a preheated graphite furnace. There have been several reports on the successful application of in-situ trapping in the preheated graphite furnace followed by AAS measurements [41–43]. Matusiewicz et al. [44] described an interface between the graphite furnace and the MIP which was based on the system described by Aziz et al. [32] and includes a special gas circulation system for continuous plasma operation. In the present study a simpler HG-GFT-MIP system has been used (see the section *Electrothermal evaporation system*, and Fig. 3III). As the 3F-Ar-MIP sustained in a TM_{010} cavity is easy to ignite reproducibly and needs no time to stabilize, a special gas circulation system was not required. The optimized conditions for multielement trapping and determination of As, Sb and Se as well as the interferences in both steps of the procedure have been investigated in detail.

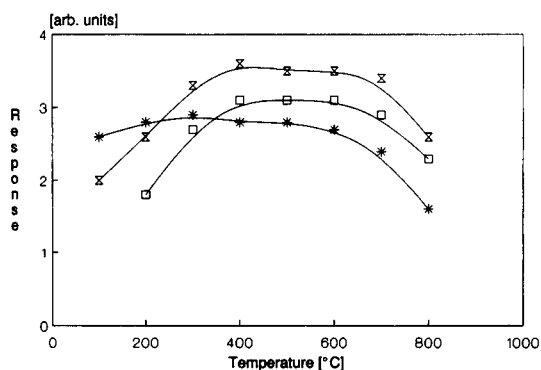


Fig. 7. Effect of deposition temperature on the analyte response in HG-GFT-MIP-AES: (□) 1 ng of As, (X) 5 ng of Sb, (*) 1 ng of Se. Sample volume: $50 \mu\text{l}$. 3F-MIP; forward power: 90 W; argon flow: 30 l h^{-1} .

The influence of the furnace temperature and the gas flow during the preconcentration on the response have been studied for the three elements separately. While the dependence of the signal on the carrier gas flow was similar to that in the cold-trap system, an Ar flow of 0.5 l h^{-1} in the preconcentration step should be optimum (Table 5). Further, a furnace temperature of 400°C was found to be suitable for simultaneous trapping of the investigated elements (Fig. 7). The period of time required for sweeping the hydrides into the graphite tube is dependent on the injected sample volume as well as on the pump speed and varied from 10 s for 0.1 ml to about 3 min for 5 ml. The signals for As, Sb and Se were not influenced by the sample volume introduced by the peristaltic pump, however, a decrease in the precision with increase in the sample volume was observed.

Absolute detection limits of 0.4, 0.35 and 0.25 ng for As, Sb and Sb respectively were obtained. For a sample volume of 1 ml the concentration detection limits were 0.4, 0.35 and 0.25 ng ml^{-1} . The detection limit values for GF-MIP-AES and HG-GFT-MIP-AES are of the same order of magnitude with respect to the absolute amount of analyte, while the concentration detection limits, because of the preconcentration from a larger volume, are much lower. With GF-MIP, the sample volume was restricted to $5 \mu\text{l}$ by which for As, Sb and Se the concentration detection limits were much higher.

The substantial advantage of the HG-GFT-MIP over the HG-CT-MIP techniques is that the sample volume can be varied from 0.05 ml up to several ml and thus better concentration detection limits can be achieved. The data in Table 2 also show an enhancement in precision.

Interferences. As known from AAS measurements, the hydride generation technique suffers from mutual interferences. They have been shown to occur in the gas phase during the atomization [22–24]. Therefore, for both preconcentration methods (HG-CT and HG-GFT) the influence of several hydride-forming elements (As, Bi, Pb, Sb, Se, Sn, and Te and Pb) on the analyte response for As, Sb and Se was investigated. In all cases interferences were negligible at interferent

concentrations of up to a 100-fold wt. excess with respect to the analytes. This is much lower than in HG–AAS, where in some cases interferences were observed even in the equal concentration of analyte and interferent [22,23]. Therefore, in addition to the multielement capabilities, the mutual interferences of HG–AAS can be easily eliminated by applying MIP-AES.

Conclusions

For the determination of the hydride-forming elements by MIP-AES, the hydride generation technique in many aspects is superior to the direct nebulization of the sample solution. The detection limits are considerably improved (Table 5). Moreover, the separation of the analyte from the matrix avoids many of the interferences. However attempts to apply hydride generation as the direct sample introduction technique into the low-power MIP failed due to interfering gaseous by-products which disturb the plasma stability. Therefore the hydrides have to be separated by trapping before entering the plasma.

MIP-AES coupled with hydride generation using trapping of the analytes in the graphite furnace was found to be a powerful analytical technique. Simultaneous multielement determination under the optimal experimental conditions for As, Sb and Se is possible due to the multielement capabilities of all single steps (hydride generation, in-situ trapping in the graphite furnace and determination by MIP-AES).

With respect to the ease of operation and the precision, HG–GFT–MIP-AES was superior to HG–CT–MIP-AES. Of all the techniques investigated, the lowest detection limits obtained for 1 ml of sample are: 0.4 ng ml⁻¹ for As, 0.35 ng ml⁻¹ for Sb and 0.25 ng ml⁻¹ for Se respectively.

E. Bulska thanks the Max-Planck Gesellschaft (München) for the grant of a research fellowship.

REFERENCES

- 1 J.A.C. Broekaert, *Anal. Chim. Acta.*, 196 (1978) 1.
- 2 S.R. Goode and K.W. Baughman, *Appl. Spectrosc.*, 38 (1984) 755.
- 3 J.P. Matousek, B.J. Orr, and M. Selby, *Prog. Anal. At. Spectrosc.*, 7 (1984) 275.
- 4 A.T. Zander and G.M. Hieftje, *Appl. Spectrosc.*, 35 (1981) 357.
- 5 K.G. Michlewicz and J.W. Carnahan, *Anal. Chem.*, 58 (1986) 3122.
- 6 D.L. Haas and J.A. Caruso, *Anal. Chem.*, 56 (1984) 2014.
- 7 J.J. Urh and J.W. Carnahan, *Appl. Spectrosc.*, 40 (1986) 877.
- 8 J.M. Gehlhausen and J.W. Carnahan, *Anal. Chem.*, 61 (1989) 674.
- 9 D. Kollotzek, P. Tschöpel and G. Tölg, *Spectrochim. Acta*, 39B (1984) 625.
- 10 Gy. Heltai, J.A.C. Broekaert, F. Leis and G. Tölg, *Spectrochim. Acta*, 45B (1990) 301.
- 11 T. Nakahara, *Prog. Anal. At. Spectrosc.*, 6 (1983) 163.
- 12 E.M. Donaldson, *Talanta*, 37 (1990) 955.
- 13 G.S. Pyen and R.F. Browner, *Appl. Spectrosc.*, 42 (1988) 508.
- 14 J.D. Hwang, H.P. Huxley, J.P. Diomiguardi and W.J. Vaughn, *Appl. Spectrosc.*, 44 (1990) 491.
- 15 F.E. Lichte and R.K. Skogerboe, *Anal. Chem.*, 44 (1972) 1480.
- 16 N.W. Barnett, L.S. Chen and G.F. Kirkbright, *Spectrochim. Acta*, 39B (1984) 1141.
- 17 N.W. Barnett, *Spectrochim. Acta*, 42B (1987) 859.
- 18 K.J. Mulligan, M.H. Hahn, J.A. Caruso and F.L. Fricke, *Anal. Chem.*, 51 (1979) 1935.
- 19 W.B. Robbins, J.A. Caruso and F.L. Fricke, *Analyst*, 104 (1979) 35.
- 20 K.C. Ng, X.X. Xu and M.J. Brechmann, *Spectrosc. Lett.*, 22 (1989) 1251.
- 21 H. Tao and A. Miyazaki, *Anal. Sciences*, 7 (1991) 55.
- 22 A. Hulanicki, E. Bulska and M. Walcerz, *Fresenius' Z. Anal. Chem.*, 332 (1988) 176.
- 23 E. Bulska, M. Walcerz and A. Hulanicki, submitted to *J. Anal. At. Spectrom.*
- 24 K. Dittrich and R. Mandry, *Analyst*, 111 (1986) 269.
- 25 J. Dedina and I. Rubeska, *Spectrochim. Acta*, 35B (1980) 119.
- 26 B. Welz and M. Melcher, *Analyst*, 108 (1983) 213.
- 27 R.H. Scott, V.A. Fassel, R.N. Kniseley and D.E. Nixon, *Anal. Chem.*, 46 (1974) 75.
- 28 G. Volland, P. Tschöpel and G. Tölg, *Spectrochim. Acta*, 36B (1981) 901.
- 29 A. Montaser and D.W. Golightly, *Inductively Coupled Plasmas in Analytical Atomic Spectrometry*, Verlag Chemie, Weinheim, 1987.
- 30 H. Matusiewicz, *Spectrochim. Acta Rev.*, 13 (1990) 47.
- 31 M. Zereghzi, K.J. Mulligan and J.A. Caruso, *Anal. Chim. Acta*, 154 (1983) 219.
- 32 A. Aziz, J.A.C. Broekaert and F. Leis, *Spectrochim. Acta*, 37B (1982) 381.
- 33 Gy. Heltai, J.A.C. Broekaert, P. Burba, F. Leis, P. Tschöpel and G. Tölg, *Spectrochim. Acta*, 45B (1990) 857.
- 34 U. Richts, J.A.C. Broekaert, P. Tschöpel and G. Tölg, *Talanta*, 38 (1991) 863.

- 35 A.N. Zaidel, V.K. Prokof'ev, S.M. Raiskii, V.A. Slavnyi and E.Ya. Schreider, *Tables of Spectral Lines*, IFI-Plenum, New York, 1970.
- 36 Narsito, J. Agterdenbos and S.J. Santosa, *Anal. Chim. Acta.*, 237 (1990) 189.
- 37 B.T. Sturman, *Appl. Spectrosc.*, 39 (1985) 48.
- 38 L.S. Cutter, G.A. Cutter and M.L.C. San Diego-McGlone, *Anal. Chem.*, 63 (1991) 1138.
- 39 B. Welz and M. Schubert-Jacobs, *J. Anal. At. Spectrosc.*, 1 (1986) 23
- 40 J. Piwonka, G. Kaiser and G. Tölg, *Fresenius' Z. Anal. Chem.*, 321 (1985) 225.
- 41 R.E. Sturgeon, S.N. Willie and S.S. Berman, *Anal. Chem.*, 57 (1985) 2311.
- 42 S.N. Willie, R.E. Sturgeon and S.S. Berman, *Anal. Chem.*, 58 (1986) 1140.
- 43 M.M. Chaudhry, A.M. Ure, B.G. Cooksey, D. Littlejohn and D.J. Halls, *Anal. Proc.*, 28 (1991) 44.
- 44 H. Matusiewicz, R.E. Sturgeon and S.S. Berman, *Spectrochim. Acta*, 45B (1990) 209.
- 45 H. Tao, A. Miyazaki and K. Bansho, *Anal. Sci.*, 6 (1990) 195.
- 46 D.T. Heitkemper and J.A. Caruso, *Appl. Spectrosc.*, 44 (1990) 228.

Internal viscosity of sodium dodecyl sulfate micelles as a function of the chain length of *n*-alcohol modifiers

Diane A. Piasecki and Mary J. Wirth

Department of Chemistry and Biochemistry, University of Delaware, Newark, DE 19716 (USA)

(Received 22nd June 1992; revised manuscript received 17th August 1992)

Abstract

The rotational diffusion behavior of tetracene was used to probe the internal viscosity of sodium dodecyl sulfate micelles in the presence of several *n*-alcohols (C_3 – C_8). Fluorescence anisotropy of tetracene was measured using frequency-domain spectroscopy. Several solutions were studied which contained approximately the same number of alcohol molecules per micelle. The results indicate that, while the addition of alcohol allows tetracene to reorient faster within the micelle, the chain length of the alcohol has little effect on the reorientation behavior. These findings have important ramifications regarding the choice of a mobile phase modifier in micellar liquid chromatography.

Keywords: Fluorimetry; Liquid chromatography; *n*-Alcohols; Frequency-domain spectrometry; Micellar liquid chromatography; Mobile phase modifiers; Sodium dodecyl sulphate

The unique structure of micelles has led to their use in a number of applications. Because of their hydrophobic interiors, they can solubilize organic compounds and are therefore useful in industrial applications such as emulsion polymerization [1,2] and detergency [3]. Micelles are used in analytical spectroscopy to enhance fluorescence [4], thermal lensing [5] and room-temperature phosphorescence [6].

Much of the literature reported on micelles includes the effect of alcohols on the properties of micellar solutions [7–10]. These micellar systems are vital in tertiary-oil recovery [11], as it has been established that the addition of larger amounts of short-chain alcohols (C_4 – C_5) promotes microemulsion formation [12,13]. However, these studies concentrate on the effect of alcohol on properties such as the critical micelle concen-

tration, micellar aggregation number, or the hydrophobic radius. Several techniques have been used to sense the viscosity of the micelle interior, but results from these studies do not agree [14–19].

Armstrong and Henry [20] were the first to use micellar mobile phases in liquid chromatography. The unique selectivity provided by micellar mobile phases occurs as a result of solute interactions with hydrophobic and electrostatic sites; therefore, solute interactions with micelles remains a question of fundamental interest. In addition, low operation costs and reduced toxicity makes the use of micellar mobile phases much more attractive than the conventional organic solvents used for modifying the mobile phase [21]. However, a reduction in chromatographic efficiency was observed and attributed to slow mass transfer between the mobile phase and the surfactant-modified stationary phase [22]. It has been established that the addition of small amounts of short-chain alcohols such as ethanol or propanol

Correspondence to: M.J. Wirth, Department of Chemistry and Biochemistry, University of Delaware, Newark, DE 19716 (USA).

improves the efficiency of micellar liquid chromatography to values obtained when using traditional hydroorganic phases [23–25].

The effect of adding *n*-propanol to a micellar solution has been shown spectroscopically to lower the internal viscosity of the sodium dodecyl sulfate (SDS) micelle [26]. The amount by which the viscosity is lowered is consistent with the amount by which the chromatographic efficiency is improved for a hydrophobic solute [24]. For a hydrophobic solute, the efficiency in micellar liquid chromatography is limited by the direct mass transfer of the solute from the micelle to the stationary phase [27,28], thus explaining why the micellar internal viscosity corresponds to chromatographic efficiency. While *n*-propanol is often the choice of mobile phase modifier in micellar liquid chromatography, Borgerding et al. [29] have suggested the use of a longer-chain *n*-alcohol, such as *n*-pentanol, to achieve higher chromatographic efficiencies.

The purpose of this work is to investigate how the chain length of the *n*-alcohol modifier affects the viscosity of the interior of an SDS micelle. Frequency-domain fluorescence depolarization measurements are used to determine the rotational diffusion behavior of a very hydrophobic solute, tetracene, in an SDS micelle in the presence of several *n*-alcohols (C₃–C₈), where the number of alcohols per micelle was constant. Two sets of experiments were performed, one with small enough alcohol concentrations to minimally perturb the micelles, and the other with the larger alcohol concentration typically used in chromatography.

THEORY

The fluorescence anisotropy, $r(t)$, in isotropic media is defined as

$$r(t) = \frac{I_{\parallel} - I_{\perp}}{I_{\parallel} + 2I_{\perp}} \quad (1)$$

where I_{\parallel} and I_{\perp} are the time-dependent intensities of light emitted with polarization parallel (I_{\parallel})

and perpendicular (I_{\perp}) to the excitation polarization. Also, $r(t)$ is the orientational correlation function of the emission transition moment.

The rotational diffusion coefficient, D , is related to the decay constant, τ_r , of the angular correlation function.

$$\tau_r = \frac{1}{6D} \quad (2)$$

These parameters are, in turn, related to the viscosity, η , by the following equation

$$\tau_r = \frac{\eta V}{kT} f_{\text{stick}} C \quad (3)$$

where V is the hydrodynamic volume of the solute and kT is the thermal energy. The solute geometry determines the value of f_{stick} [30]. The value of C is a function of the stick or slip boundary conditions.

Chuang and Eisinger [31] have derived the relationship between the parameters of the fluorescence anisotropy decay and the components of the diffusion tensor. For a planar symmetric solute, such as tetracene, the expression simplifies to a double exponential decay, where D is the average of the components of the diffusion tensor:

$$r(t) = 0.3(\beta + \alpha) \exp[-(6D + 2\Delta)t] + 0.3(\beta - \alpha) \exp[-(6D - 2\Delta)t] \quad (4)$$

$$D = \frac{D_x + D_y + D_z}{3} \quad (5)$$

Delta measures the asymmetry of the diffusion tensor:

$$\Delta = (D_x^2 + D_y^2 + D_z^2 - D_x D_y - D_x D_z - D_y D_z)^{1/2} \quad (6)$$

α and β are defined as follows, where the solute is excited along the y -axis and the emission is at an angle θ with respect to the y -axis.

$$\alpha = \frac{(D - D_y \cos^2 \theta - D_z \sin^2 \theta)}{\Delta} \quad (7)$$

$$\beta = \cos^2 \theta - 1/3 \quad (8)$$

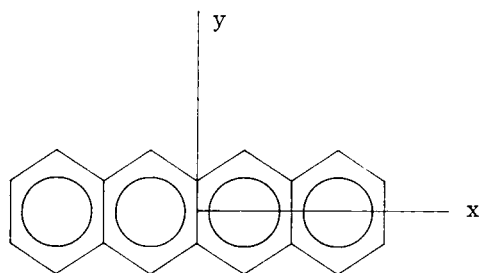


Fig. 1. Structure of tetracene and hydrodynamic dimensions. Dimensions (Å): $14.2 \times 7.4 \times 3.0$.

The experimental results are fit to the following double exponential decay which corresponds to the parameters of Eqn. 4:

$$r(t) = r(0) [F \exp(-t/\tau_1) + (1 - F) \exp(-t/\tau_2)] \quad (9)$$

The experimental determination of τ_1 , τ_2 , $r(0)$ and F allows for the calculation of the compo-

nents of the diffusion tensor, D_x , D_y and D_z . These experimentally determined values of D_x , D_y and D_z serve as diagnostics for hydrodynamic behavior and thus allow one to relate the rotational diffusion coefficient to the viscosity through Eqn. 3 [26,32].

EXPERIMENTAL

Sodium dodecyl sulfate (SDS) (98%) was obtained from Aldrich and was used without further purification. Previous studies had shown no difference in behavior for SDS purified by either a chromatographic procedure or by recrystallization [33]. Therefore, SDS was not purified. Tetracene (2,3-benzanthracene) was also obtained from Aldrich and used as received. The structure of tetracene and its hydrodynamic dimensions are

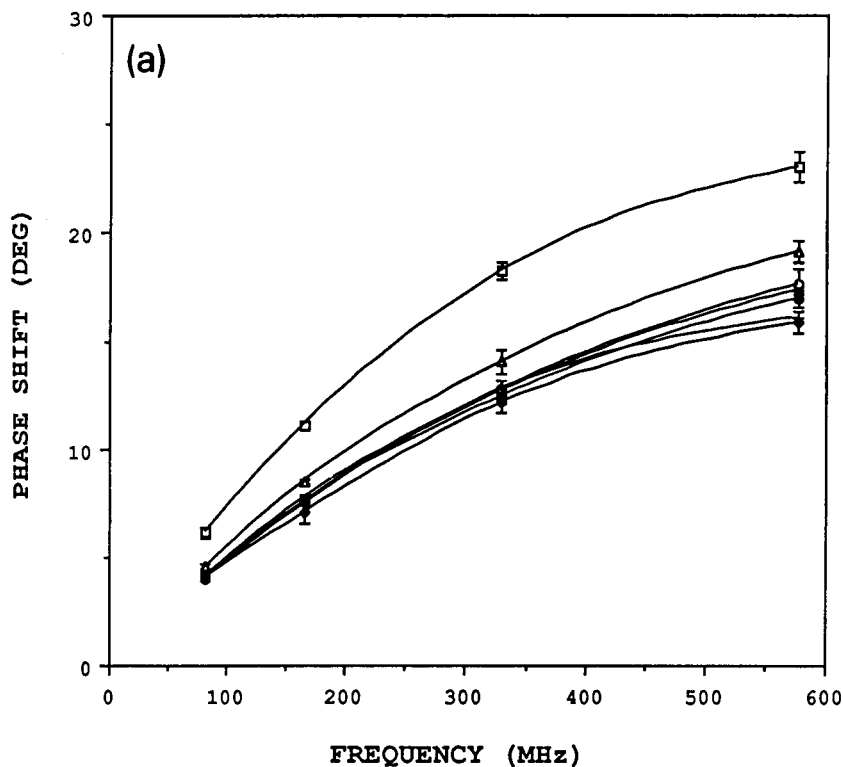


Fig. 2. Raw frequency-domain fluorescence anisotropy data for alcohol-SDS solutions containing approximately 14 ± 2 alcohol molecules per micelle. (a) Differential phase data; (b) amplitude ratio data. (\square) No alcohol; (+) propanol; (Δ) butanol; (\times) pentanol; (\circ) hexanol; (\bullet) heptanol; (\blacklozenge) octanol.

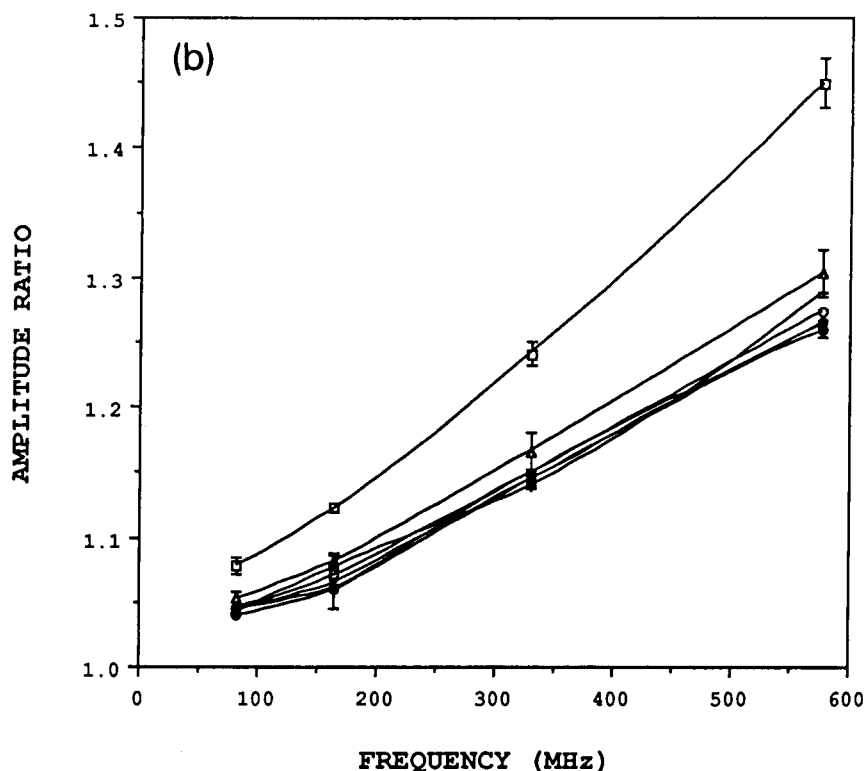


Fig. 2 (continued).

shown in Fig. 1. *n*-Propanol and *n*-butanol were purchased from Fisher Scientific. *n*-Pentanol, *n*-hexanol, *n*-heptanol and *n*-octanol were obtained from Aldrich. The purity of all alcohols is at least 98%, and each was subsequently purified by passage through a silica-based trifunctionally bonded C_{18} column. Water was purified by passage through Cole-Parmer Ion-X-Changer Research and Adsorber Cartridges. These remove most organic compounds and ion minerals, producing water equivalent to triply distilled water. The water was further purified by passage through a trifunctionally bonded C_{18} column.

A saturated solution of tetracene in *n*-propanol was prepared and used as the stock solution. The concentration of tetracene in the alcohol-SDS solutions was $0.6 \mu\text{M}$. The solutions were prepared by adding the appropriate amount of the tetracene stock solution to a volumetric flask and evaporating off the solvent with N_2 gas. The concentration of tetracene was sufficiently

low to avoid the presence of more than one tetracene molecule per micelle [26]. A known amount of alcohol and SDS was added to the volumetric and then diluted with ultrapure water to give a composition of $0.6 \mu\text{M}$ tetracene, $n\%$ ROH, and 0.1 M SDS, where n was varied. All solutions were deoxygenated and experiments were conducted with the sample under N_2 . The temperatures of the solutions were controlled to $25.0 \pm 0.5^\circ\text{C}$. The solutions were flowed during the experiments to avoid photo-decomposition.

The sample was excited with 10 mW of the 476-nm line of an argon ion laser. The beam was passed through a Glan-Thompson prism to provide vertically polarized light. The beam was sent through a Pockels cell which electronically controlled the polarization with an extinction greater than 500:1. The emission wavelength was detected at 516 nm using a monochromator having a 2-nm bandwidth. The spectroscopic equipment used in this work was identical to that used in

previous experiments [26,32] where the 1st, 2nd, 4th and 7th harmonics of the 82-MHz mode beat frequency of a mode-locked Ar⁺ ion laser were used as the modulation frequencies for the frequency-domain measurements. The differential phase shifts, $\Delta\phi_{\parallel} - \Delta\phi_{\perp}$ and demodulation ratios, a_{\parallel}/a_{\perp} comprise $r(t)$ and were measured for each frequency [34,35]. Data were analyzed as previously described [26].

RESULTS AND DISCUSSION

The raw frequency-domain data for solutions containing low alcohol concentrations are shown graphically in Fig. 2. Figure 2a and b shows the phase shifts and amplitude ratios as a function of frequency for the tetracene–0.1 M SDS solution containing approximately 14 ± 2 alcohol molecules per micelle. The phase shifts and amplitude ratios exhibit the normal behavior in all cases, increasing as a function of frequency. As alcohol is added to the micellar solutions, the phase shifts and amplitude ratios decrease by a significant amount. This suggests that tetracene reorients faster, assuming that factors such as the transi-

tion symmetry and solvent disorder remain constant. The raw data also show, more importantly, that the fluorescence anisotropy behavior of tetracene does not depend on which *n*-alcohol is used, that is, there is apparently no dependence upon the chain length of the alcohol.

The data in Fig. 2a and b were analyzed by fitting the phase shifts and amplitude ratios into the double exponential decay of Eqn. 9. The results are presented in Table 1. Since no trend was observed for $r(0)$, the raw data were analyzed with $r(0) = 0.32$, the consensus value. (The value for $r(0)$ is less than 0.4 because the emission band at 516 nm has a lower symmetry than the emission band at 476 nm [36].) Also, since τ_{r1} and F are correlated, F was fixed to 0.90 in order to observe the trend seen in τ_{r1} . When fit to Eqn. 9, it was found that tetracene reorients in an SDS micelle in 0.21 ± 0.01 ns. For the C₃–C₈ alcohols, τ_{r1} was found to be 0.119 ± 0.009 ns. The analyzed data substantiates the finding from the raw data that reorientation of tetracene is independent of the chain length of the *n*-alcohol.

The concentration of alcohol present in the micellar solutions discussed above was intentionally kept low so as to perturb minimally the

TABLE 1

Anisotropy decay parameters of tetracene in SDS micelles in the presence of (a) 14 alcohols per micelle and (b) 50 alcohols per micelle^a

[$r(0) = 0.32$ and $F = 0.90$]

| ROH | %ROH | R_a ^b | τ_{r1} (ns) | τ_{r2} (ns) | χ^2 |
|------------|------|--------------------|-------------------|------------------|----------|
| (a) | | | | | |
| No alcohol | 0 | 0 | 0.21 ± 0.01 | 0.8 ± 0.2 | 3.0 |
| Propanol | 0.5 | 15.9 | 0.11 ± 0.01 | 0.7 ± 0.2 | 3.1 |
| Butanol | 0.34 | 16 | 0.135 ± 0.005 | 0.7 ± 0.2 | 1.1 |
| Pentanol | 0.3 | 12.8 | 0.12 ± 0.01 | 0.7 ± 0.1 | 1.4 |
| Hexanol | 0.31 | 11.2 | 0.12 ± 0.01 | 0.6 ± 0.2 | 1.2 |
| Heptanol | 0.34 | 13.0 | 0.12 ± 0.01 | 0.5 ± 0.2 | 3.1 |
| Octanol | 0.38 | 14.8 | 0.11 ± 0.01 | 0.9 ± 0.2 | 3.0 |
| (b) | | | | | |
| No alcohol | 0 | 0 | 0.21 ± 0.01 | 0.8 ± 0.2 | 3.0 |
| Propanol | 3.1 | 45.7 | 0.098 ± 0.005 | 0.7 ± 0.1 | 1.3 |
| Butanol | 2.11 | 47.7 | 0.09 ± 0.01 | 0.6 ± 0.2 | 1.4 |
| Pentanol | 1.3 | 53.9 | 0.093 ± 0.006 | 0.7 ± 0.2 | 1.3 |
| Hexanol | 1.98 | 56.4 | 0.087 ± 0.009 | 0.5 ± 0.2 | 1.4 |

^a SDS solutions with heptanol and octanol could not be studied because the amount of alcohol required exceeded the solubility limit. ^b R_a refers to the number of alcohols per micelle, calculated from Terabe's [49] partition coefficients and literature values for c.m.c., N_s and r , listed in Table 2.

TABLE 2

Diffusion coefficients of tetracene in SDS micelles as a function of chain length

| ROH | %ROH | R_a^a | D_x/D | D_y/D | D_z/D | D (GHz) |
|----------------------|------|---------|-----------------|-----------------|-----------------|-----------|
| No alcohol | 0 | 0 | 2.15 | 0.18 | 0.68 | 0.511 |
| Propanol | 0.5 | 15.9 | 2.43 | -0.028 | 0.60 | 0.872 |
| Butanol | 0.34 | 16 | 2.33 | 0.042 | 0.62 | 0.731 |
| Pentanol | 0.3 | 12.8 | 2.41 | -0.014 | 0.60 | 0.839 |
| Hexanol | 0.31 | 11.2 | 2.32 | 0.053 | 0.63 | 0.827 |
| Heptanol | 0.34 | 13.0 | 2.25 | 0.104 | 0.65 | 0.882 |
| Octanol | 0.38 | 14.8 | 2.5 | -0.079 | 0.58 | 0.870 |
| Any alcohol | | | 2.34 ± 0.12 | 0.04 ± 0.09 | 0.62 ± 0.03 | |
| No alcohol | 0 | 0 | 2.15 | 0.18 | 0.68 | 0.511 |
| Propanol | 3.1 | 45.7 | 2.46 | -0.051 | 0.59 | 0.969 |
| Butanol | 2.11 | 47.7 | 2.39 | 0.004 | 0.61 | 1.045 |
| Pentanol | 1.3 | 53.9 | 2.45 | -0.044 | 0.59 | 1.024 |
| Hexanol | 1.98 | 56.4 | 2.37 | 0.02 | 0.62 | 1.125 |
| Any alcohol | | | 2.36 ± 0.13 | 0.02 ± 0.09 | 0.62 ± 0.04 | |
| Octanol ^b | | | 2.36 | 0.12 | 0.51 | 1.0 |

^a R_a refers to the number of alcohols per micelle, calculated from Terabe's [49] partition coefficients and literature values for c.m.c., N_s and r , listed in Table 3. ^b Data for tetracene in *n*-octanol at 34°C, taken from Ref. 32.

TABLE 3

Reported values for critical micelle concentration (c.m.c.), in mmol l^{-1} , aggregation number (N_s) and radius of an SDS micelle, in Å, in the presence and absence of *n*-alcohol

| ROH | %ROH | c.m.c. | N_s | r | Reference |
|------------|------|--------|-------|------|-----------|
| No alcohol | - | 8.01 | - | - | 37 |
| | - | 8.6 | - | - | 38 |
| | - | 8.0 | - | - | 39 |
| | - | 8.2 | - | - | 39 |
| | - | 8.25 | - | - | 40 |
| | - | - | - | 27 | 41 |
| | - | 8.2 | 62 | 25 | 42,43 |
| | - | 8.2 | - | 25 | 21 |
| | - | 8.0 | 67 | - | 44 |
| | - | 8.1 | 62 | - | 29 |
| | - | - | 70 | 18.1 | 46 |
| | - | - | 70 | 18.1 | 46 |
| | - | - | 68 | 18.0 | 48 |
| | - | - | 65 | - | 45 |
| Propanol | 0.75 | 6.4 | - | - | 39 |
| | 0.75 | 5.9 | - | - | 39 |
| | 0.75 | 7.4 | - | - | 29 |
| | 3.74 | 5.8 | - | - | 39 |
| | 3.74 | 5.6 | - | - | 39 |
| | 4.0 | - | 51.4 | 18.1 | 46 |

TABLE 3 (continued)

| ROH | %ROH | c.m.c. | N_s | r | Reference |
|----------|----------|--------|-------|------|-----------|
| Butanol | 0.4 | 6.96 | – | – | 37 |
| | 0.9 | 5.4 | – | – | 29 |
| | 0.92 | 6.0 | – | – | 39 |
| | 0.92 | 6.1 | – | – | 39 |
| | 1.0 | – | 63.2 | 18.2 | 46 |
| | 1.0 | – | 50 | 16.9 | 48 |
| | 1.0 | – | 64 | 18.1 | 48 |
| | 1.07 | 5.32 | – | – | 37 |
| | 1.83 | 5.0 | – | – | 39 |
| | 1.83 | 5.0 | – | – | 39 |
| | 1.87 | 4.18 | – | – | 37 |
| | 2.75 | 2.8 | – | – | 39 |
| | 2.75 | 3.0 | – | – | 39 |
| | Pentanol | 0.2 | – | 68.6 | 18.2 |
| 0.22 | | 5.1 | – | – | 39 |
| 0.22 | | 5.6 | – | – | 39 |
| 0.34 | | 5.70 | – | – | 37 |
| 0.54 | | 3.9 | – | – | 39 |
| 0.54 | | 4.0 | – | – | 39 |
| 0.70 | | 4.17 | – | – | 37 |
| 0.80 | | – | 62.0 | 18.3 | 46 |
| 1.0 | | 3.0 | 54 | – | 29 |
| 1.0 | | – | 49 | 18.1 | 46 |
| 1.08 | | 3.0 | – | – | 39 |
| 1.08 | | 3.1 | – | – | 39 |
| 1.4 | | – | 61.2 | 18.9 | 46 |
| 1.5 | | 5.0 | – | – | 38 |
| 2.0 | | – | 33.3 | 17.3 | 46 |
| 2.0 | | – | 57.2 | 19.0 | 46 |
| 2.0 | | – | 57.2 | 19.0 | 47 |
| 2.2 | – | 35 | – | 45 | |
| Hexanol | 0.25 | 2.9 | – | – | 39 |
| | 0.25 | 3.0 | – | – | 39 |
| | 0.38 | 1.1 | – | – | 39 |
| | 0.38 | 1.4 | – | – | 39 |
| | 0.30 | 5.9 | 49 | – | 44 |
| | 0.40 | 4.7 | – | – | 38 |
| | 0.40 | – | 49.4 | 17.7 | 46 |
| | 0.50 | 5.4 | 47 | – | 44 |
| | 0.60 | – | 46.5 | 18.1 | 46 |
| | 0.80 | 4.9 | 39 | – | 44 |
| | 0.80 | – | 42.4 | 18.2 | 46 |
| | 1.0 | – | 38.5 | 18.3 | 46 |
| Heptanol | 0.38 | 5.8 | 53 | – | 44 |
| | 0.40 | – | 52.7 | 18.9 | 46 |
| | 0.45 | – | 85 | 20.6 | 48 |
| | 0.6 | 5.3 | 43 | – | 44 |
| | 0.6 | – | 42.6 | 18.5 | 46 |
| Octanol | 0.16 | – | 80 | 19.4 | 48 |
| | 0.20 | 6.5 | 64 | – | 44 |
| | 0.20 | – | 64.3 | 19.2 | 46 |
| | 0.40 | 5.7 | 59 | – | 44 |
| | 0.40 | – | 58.7 | 20.0 | 46 |

integrity of the micelle. As a result, changes in the critical micelle concentration, aggregation number and micellar radius have a negligible effect on the calculated number of alcohols per micelle. These alcohol concentrations, however, are much lower than those used in micellar liquid chromatography, e.g., 3–5% *n*-propanol is typical. An additional set of experiments was conducted in which the concentration of alcohol was raised to values comparable to those found in micellar liquid chromatography. In this set of experiments the concentration of *n*-propanol was chosen to be 3%, and the concentrations of the longer-chain alcohols were calculated to maintain the same number of alcohols per micelle for each solution. To control the number of alcohols per micelle at these higher concentrations requires knowledge of how the critical micelle concentra-

tion, the micelle radius and the aggregation number change with alcohol concentration. Details of the calculations for determining the amount of alcohol required to maintain a constant number of alcohols per micelle are presented in the Appendix.

Frequency-domain fluorescence anisotropy data for micellar solutions containing 50 ± 5 alcohols per micelle, calculated as described in the Appendix, are presented in Fig. 3. Micellar solutions of heptanol and octanol could not be studied due to the fact that the amount of alcohol required exceeded the solubility limit. Analysis of the data of Fig. 3 recovers the time-domain parameters summarized in Table 1b. The solutions behave very similarly to one another, regardless of alcohol chain length. Thus, the results for both low alcohol concentrations and for the high con-

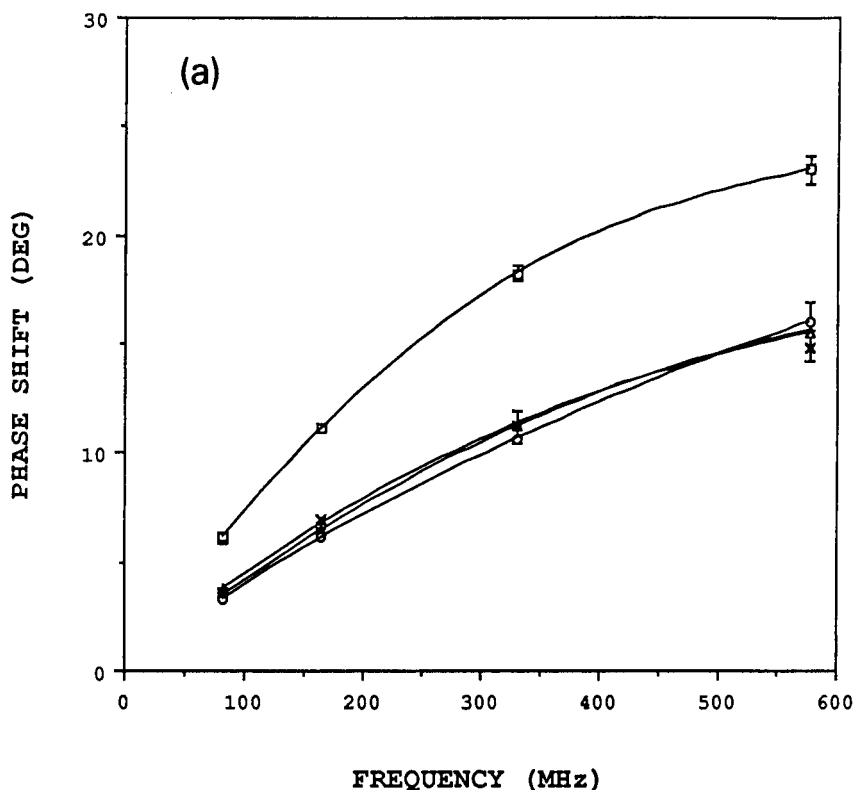


Fig. 3. Raw frequency-domain fluorescence anisotropy data for alcohol-SDS solutions containing approximately 51 ± 5 alcohol molecules per micelle. (a) Differential phase data; (b) amplitude ratio data. (□) No alcohol; (+) propanol; (Δ) butanol; (×) pentanol; (○) hexanol; the solubility limit was exceeded for heptanol and octanol at these alcohol concentrations and so no data was obtained.

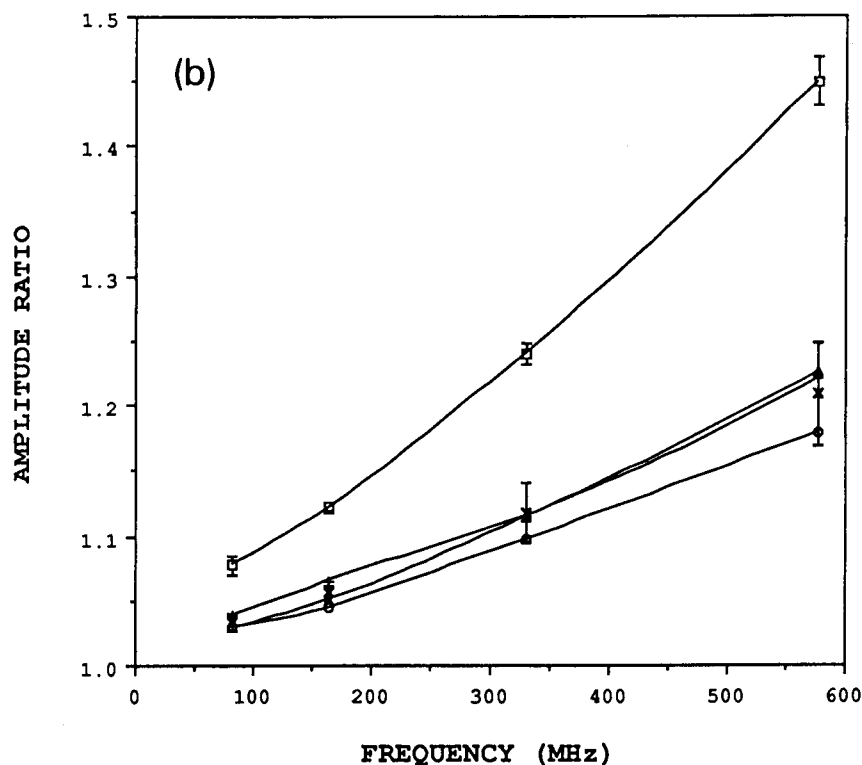


Fig. 3 (continued)

centrations used in chromatography reveal that alcohol chain length does not appreciably affect the reorientation of tetracene.

The reorientation time of a probe molecule can be used to calculate the viscosity of its environment through Eqn. 3 only if the rotational diffusion is hydrodynamic. For example, if the long-chain alcohols caused the interiors of the SDS micelles to become more structurally ordered, the rotational diffusion would deviate from hydrodynamic behavior and give reorientation time constants that were not representative of the viscosity. The advantage of using the anisotropy decay of tetracene to probe micellar viscosity is that it provides an internal check on hydrodynamic behavior [32]. This internal check was shown to be accomplished by examining the components of the diffusion tensor, D_x , D_y and D_z . The double-exponential decay parameters in parts a and b of Table 1 were used to calculate the components of the diffusion tensor for tetracene in each ROH–SDS solution according to Eqns. 4

and 9. These values are listed in Table 2. The average values of D_x/D , D_y/D and D_z/D for all cases are comparable to those found for the standard octanol system (listed at the bottom of Table 2), differing by no more than 0.13; thus, the rotational diffusion is hydrodynamic. The reorientation times are thus directly related to internal viscosity; therefore, it can be concluded that the internal viscosity of the SDS micelle is unaffected by the chain length of the alcohol modifier at both low concentrations and chromatographic concentrations.

The results have ramifications in choosing alcohols for micellar liquid chromatography: smaller amounts of longer-chain alcohols can be used to speed up the dynamics of the micelle interior with minimal perturbation of the aqueous solution.

This work was supported by the National Science Foundation under grant CHE-9113544.

APPENDIX

The results of several studies [21,29,37–48] are compiled in Table 3. These show that the addition of alcohol can drastically affect the critical micelle concentration, surfactant aggregation number and micelle radius. The experimentally determined values for these parameters are thus essential in calculating the correct amount of alcohol required to obtain the desired number of alcohols per micelle.

The amount of alcohol required to maintain a constant number of alcohols per micelle for a series of *n*-alcohols was calculated from the derived ratio of the moles of alcohol present in the micelle, $mol_{a,mic}$, to the moles of micelles present in the solution, mol_{mic} .

$$\frac{mol_{a,mic}}{mol_{mic}} = R_a \quad (10)$$

R_a is the total number of alcohols in the average micelle, which was fixed in the experiments.

The number of moles of micelles present in the solution was calculated from known values, as shown in the equation below:

$$mol_{mic} = \frac{(C_{SDS} - c.m.c.)V_t}{N_s} \quad (11)$$

where C_{SDS} = concentration of SDS, c.m.c. = critical micelle concentration, V_t = total volume of solution, and N_s = SDS aggregation number (See Table 3).

Substitution of Eqn. 11 into Eqn. 10 yielded the value of $mol_{a,mic}$.

Equation 12 describes the total number of moles of alcohol, mol_t , present in the solution.

$$mol_t = mol_{a,mic} + mol_{a,aq} \quad (12)$$

This quantity mol_t was used to calculate the amount of alcohol to be added to the SDS solution to give the desired value of R_a . In this equation, $mol_{a,aq}$ is the moles of alcohol present in the aqueous solution.

Since the above equation contains two unknowns, the partition coefficient, K , which is a function of the concentration of alcohol in the micelle and the concentration of alcohol in the

aqueous phase [49], was used to eliminate one of the variables.

$$K = \frac{mol_{a,mic}/V_{mic}}{mol_{a,aq}/V_{aq}} \quad (13)$$

where V_{mic} is the volume of micelles in the solution and was calculated using the equation below, r is the radius of the micelle (see Table 3) and N is Avogadro's number.

$$V_{mic} = \frac{4}{3}\pi r^3 mol_{mic} N \quad (14)$$

where V_{aq} is the volume of the aqueous solution and was calculated by subtracting the volume of micelles from the total volume of solution:

$$V_{aq} = V_t - V_{mic} \quad (15)$$

Substitution of Eqns. 13–15 into Eqn. 12 yields the solution for the total moles of alcohol present in the micelle.

$$mol_t = mol_{a,mic} \left(1 + \frac{V_{aq}}{KV_{mic}} \right) \quad (16)$$

The volume of alcohol, V_a , to be added to the SDS solution was finally calculated from the total moles of alcohol present in the solution and the molecular weights, MW_a , and the densities, d_a , of the alcohols.

$$V_a = mol_t \left(\frac{MW_a}{d_a} \right) \quad (17)$$

REFERENCES

- 1 A. Cahn and J.L. Lynn, Jr., Kirk-Othmer Encyclopedia of Chemical Technology, Vol. 2, Wiley, New York, 3rd edn., 1983, p. 332.
- 2 M.E.L. McBain and E. Hutchinson, Solubilization and Related Phenomena, Academic Press, New York, 1955.
- 3 F.W. Goodhart and A.N. Martin, J. Pharm. Sci., 51 (1962) 50.
- 4 K. Nithipatikom and L.B. McGown, Anal. Chem., 60 (1988) 1043.
- 5 C.D. Tran and T.A. Van Fleet, Anal. Chem., 60 (1988) 2478.
- 6 L.J. Cline Love, M.L. Grayeski, J. Noroshi and R. Weinberger, Anal. Chim. Acta, 170 (1985) 3.
- 7 L. Magid, in K.L. Mittal (Ed.), Solution Chemistry of Surfactants, Plenum Press, New York, 1975, pp. 427–453.

- 8 M. Almgren and S. Swarup, in K.L. Mittal and B. Lindman (Eds.), *Surfactants in Solutions*, Plenum Press, New York, 1984, pp. 613–625.
- 9 L.G. Ionescu, L.S. Romanesco and F. Nome, in K.L. Mittal and B. Lindman (Eds.), *Surfactants in Solutions*, Plenum Press, New York, 1984, pp. 789–803.
- 10 D. Attwood, V. Mosquera and V. Perez-Villar, *J. Colloid Interface Sci.* 127 (1989) 532.
- 11 S. Yiv and R. Zana, *J. Colloid Interface Sci.* 65 (1978) 286.
- 12 A. Berthod, I. Girard and C. Gonnet, *Anal. Chem.*, 58 (1986) 1362.
- 13 P.G. DeGennes and C. Taupin, *J. Phys. Chem.*, 86 (1982) 2294.
- 14 H.A. Zachariasse, *Chem. Phys. Lett.*, 57 (1978) 429.
- 15 S. Miyagishi, T. Asakawa and M. Nishida, *J. Colloid Interface Sci.*, 115 (1987) 199.
- 16 N.J. Turro, M. Aikawa and A. Yekta, *J. Am. Chem. Soc.*, 101 (1979) 772.
- 17 J. Emert, C. Behrens and M. Goldenberg, *J. Am. Chem. Soc.*, 101 (1979) 771.
- 18 N.J. Turro and T. Okubo, *J. Am. Chem. Soc.*, 103 (1981) 7224.
- 19 W.D. Turley and H.W. Offen, *J. Phys. Chem.*, 89 (1985) 2933.
- 20 D.W. Armstrong and S.J. Henry, *J. Liq. Chromatogr.*, 3 (1980) 657.
- 21 A. Berthod, I. Girard and C. Gonnet, *Anal. Chem.*, 58 (1986) 1356.
- 22 D.W. Armstrong, T.J. Ward and A. Berthod, *Anal. Chem.*, 58 (1986) 579.
- 23 J.G. Dorsey, M.T. DeEchegaray and J.S. Landy, *Anal. Chem.*, 55 (1983) 924.
- 24 P. Yarmchuk, R. Weinberger, R.F. Hirsch and L.J. Cline Love, *J. Chromatogr.*, 283 (1984) 47.
- 25 M.F. Borgerding, W.L. Hinze, L.D. Stafford, G.W. Fulp and W.C. Hamlin, *Anal. Chem.*, 61 (1989) 1353.
- 26 M.J. Wirth, S.-H. Chou and D.A. Piasecki, *Anal. Chem.*, 63 (1991) 146.
- 27 M.F. Borgerding, F.H. Quina, W.L. Hinze, J. Bowermaster and H.M. McNair, *Anal. Chem.*, 60 (1988) 2520.
- 28 F.P. Tomasella and L.J. Cline Love, *Anal. Chem.*, 62 (1990) 1315.
- 29 M.F. Borgerding, R.L. Williams, W.L. Hinze and F.H. Quina, *J. Liq. Chromatogr.*, 12 (1989) 1367.
- 30 F. Perrin, *J. Phys. Radium*, 7 (1936) 1.
- 31 T.J. Chuang and K.B. Eisenthal, *J. Chem. Phys.*, 57 (1972) 5094.
- 32 M.J. Wirth, S.-H. Chou, *J. Phys. Chem.*, 95 (1991) 1786.
- 33 M.J. Rosen, *J. Colloid Interface Sci.*, 79 (1981) 587.
- 34 U.K.A. Klein and H.-P. Haar, *Chem. Phys. Lett.*, 58 (1978) 531.
- 35 J.R. Lakowicz, H. Cherek, B.P. Maliwal and E. Gratton, *Biochemistry*, 24 (1985) 376.
- 36 J.J. Dekkers, G.Ph. Hoorweg, C. Maclean and N.H. Velthorst, *Chem. Phys.*, 5 (1974) 393.
- 37 K. Hayase and S. Hayano, *Bull. Chem. Soc. Jpn.*, 50 (1977) 83.
- 38 H.N. Singh and S. Swarup, *Bull. Chem. Soc. Jpn.*, 51 (1978) 1534.
- 39 A.K. Jain and R.P.B. Singh, *J. Colloid Interface Sci.*, 81 (1981) 536.
- 40 S. Kaneshina, H. Kamaya and I. Ueda, *J. Colloid Interface Sci.*, 81 (1981) 589.
- 41 S. Candau, E. Hirsch and R. Zana, *J. Colloid Interface Sci.*, 88 (1982) 428.
- 42 A. Berthod and J. Georges, *Nouv. J. Chim.*, 9 (1985) 101.
- 43 A. Berthod, I. Girard and C. Gonnet, *Anal. Chem.*, 58 (1986) 1362.
- 44 A. Malliaris, *J. Photochem. Photobiol. A*, 40 (1987) 79.
- 45 P. Llanos, J. Lang, C. Strazielle and R. Zana, *J. Phys. Chem.*, 86 (1982) 1019.
- 46 M. Almgren and S. Swarup, *J. Colloid Interface Sci.*, 91 (1983) 256.
- 47 M. Almgren and S. Swarup, *J. Phys. Chem.*, 86 (1982) 4212.
- 48 S. Reekmans, H. Luo, M. Van der Auweraer and F.C. DeSchryver, *Langmuir*, 6 (1990) 628.
- 49 S. Terabe, H. Tanaka, K. Otsuka and T. Ando, *J. Chromatogr. Sci.*, 27 (1989) 653.

PUBLICATION SCHEDULE FOR 1993

| | S'92 | O'92 | N'92 | D'92 | J | F | M | A | M |
|------------------------------|----------------|----------------|----------------|----------------|----------------|---------------------------|----------------|----------------|----------------|
| Analytica Chimica Acta | 267/1 267/2 | 268/1 268/2 | 269/1 269/2 | 270/1 270/2 | 271/1 271/2 | 272/1 272/2 273/1-2 | 274/1 274/2 | 275/1 275/2 | 276/1 276/2 |
| Vibrational Spectroscopy | | 4/1 | | | 4/2 | | | | |

INFORMATION FOR AUTHORS

Manuscripts. The language of the journal is English. English linguistic improvement is provided as part of the normal editorial processing. Authors should submit three copies of the manuscript in clear double-spaced typing on one side of the paper only. *Vibrational Spectroscopy* also accepts papers in English only.

Abstract. All papers and reviews begin with an Abstract (50-250 words) which should comprise a factual account of the contents of the paper, with emphasis on new information.

Figures. Figures should be prepared in black waterproof drawing ink on drawing or tracing paper of the same size as that on which the manuscript is typed. One original (or sharp glossy print) and two photostat (or other) copies are required. Attention should be given to line thickness, lettering (which should be kept to a minimum) and spacing on axes of graphs, to ensure suitability for reduction in size on printing. Axes of a graph should be clearly labelled, along the axes, outside the graph itself. All figures should be numbered with Arabic numerals, and require descriptive legends which should be typed on a separate sheet of paper. Simple straight-line graphs are not acceptable, because they can readily be described in the text by means of an equation or a sentence. Claims of linearity should be supported by regression data that include slope, intercept, standard deviations of the slope and intercept, standard error and the number of data points; correlation coefficients are optional. Photographs should be glossy prints and be as rich in contrast as possible; colour photographs cannot be accepted. Line diagrams are generally preferred to photographs of equipment.

Computer outputs for reproduction as figures must be good quality on blank paper, and should preferably be submitted as glossy prints.

Nomenclature, abbreviations and symbols. In general, the recommendations of the International Union of Pure and Applied Chemistry (IUPAC) should be followed, and attention should be given to the recommendations of the Analytical Chemistry Division in the journal *Pure and Applied Chemistry* (see also *IUPAC Compendium of Analytical Nomenclature, Definitive Rules, 1987*).

References. The references should be collected at the end of the paper, numbered in the order of their appearance in the text (not alphabetically) and typed on a separate sheet.

Reprints. Fifty reprints will be supplied free of charge. Additional reprints (minimum 100) can be ordered. An order form containing price quotations will be sent to the authors together with the proofs of their article.

Papers dealing with vibrational spectroscopy should be sent to: Dr J.G. Grasselli, 150 Greentree Road, Chagrin Falls, OH 44022, U.S.A. Telefax: (+1-216) 2473360 (Americas, Canada, Australia and New Zealand) or Dr J.H. van der Maas, Department of Analytical Molecule Spectrometry, Faculty of Chemistry, University of Utrecht, P.O. Box 80083, 3508 TB Utrecht, The Netherlands. Telefax: (+31-30) 518219 (all other countries).

© 1993, ELSEVIER SCIENCE PUBLISHERS B.V. All rights reserved.

0003-2670/93/\$06.00

No part of this publication may be reproduced, stored in a retrieval system or transmitted in any form or by any means, electronic, mechanical, photocopying, recording or otherwise, without the prior written permission of the publisher, Elsevier Science Publishers B.V., Copyright and Permissions Dept., P.O. Box 521, 1000 AM Amsterdam, The Netherlands.

Upon acceptance of an article by the journal, the author(s) will be asked to transfer copyright of the article to the publisher. The transfer will ensure the widest possible dissemination of information.

Special regulations for readers in the U.S.A.—This journal has been registered with the Copyright Clearance Center, Inc. Consent is given for copying of articles for personal or internal use, or for the personal use of specific clients. This consent is given on the condition that the copier pays through the Center the per-copy fee for copying beyond that permitted by Sections 107 or 108 of the U.S. Copyright Law. The per-copy fee is stated in the code-line at the bottom of the first page of each article. The appropriate fee, together with a copy of the first page of the article, should be forwarded to the Copyright Clearance Center, Inc., 27 Congress Street, Salem, MA 01970, U.S.A. If no code-line appears, broad consent to copy has not been given and permission to copy must be obtained directly from the author(s). All articles published prior to 1980 may be copied for a per-copy fee of US \$2.25, also payable through the Center. This consent does not extend to other kinds of copying, such as for general distribution, resale, advertising and promotion purposes, or for creating new collective works. Special written permission must be obtained from the publisher for such copying.

No responsibility is assumed by the publisher for any injury and/or damage to persons or property as a matter of products liability, negligence or otherwise, or from any use or operation of any methods, products, instructions or ideas contained in the material herein.

Although all advertising material is expected to conform to ethical (medical) standards, inclusion in this publication does not constitute a guarantee or endorsement of the quality or value of such product or of the claims made of it by its manufacturer.

This issue is printed on acid-free paper.

PRINTED IN THE NETHERLANDS

Analytical Voltammetry

edited by **M.R. Smyth** and **J.G. Vos**, School of Chemical Sciences, Dublin City University, Dublin, Ireland

Series editor: **G. Svehla**, University College, Cork, Ireland

The aim of this volume is to review the state-of-the-art in analytical voltammetry with regard to theory and instrumentation, and show how these relate to the analysis of inorganic, organometallic, organic and biological molecules. Modern voltammetric techniques have practical applications in biological, pharmaceutical and environmental chemistry. The growing importance of voltammetry in the development of modified electrodes and biological electrodes and chemical and biological sensors is also highlighted.

Contents:

1. Theory of Analytical Voltammetry

(J.F. Cassidy). Introduction to analytical voltammetry. Classical techniques. Modern techniques. Electroanalysis in flowing streams. Microelectrodes, microelectrode arrays and hydrodynamically modulated rotating disc electrochemistry. Mathematical, coulostatic and reflectance methods applied to voltammetry. Conclusions. **2. Instrumentation** (J.N. Barisci, P.J. Riley, G.G. Wallace). Introduction. The electrochemical cell. The working electrode. The reference electrode. The auxiliary electrode. Electronics. **3. Analytical Voltammetry of Biological Molecules** (J.M. Séquaris). In vivo voltammetry in neurochemistry. Electrochemical immunoassay. Voltammetric analysis of biological macromolecules: proteins and nucleic acids.

4. Analytical Voltammetry in Pharmacy

(P.M. Bersier, J. Bercier). Introduction. Polarographic and voltammetric techniques applied to drug analysis. Practical applications of polarography, voltammetry and hybrid techniques in drug analysis. **5. Analytical Voltammetry in**

Environmental Science. I. Inorganic Species

(J.M. Fernandez, P.J. Hayes, M.R. Smyth). Introduction. General aspects of trace analysis. Polarography and voltammetric methods. Trace metals. Application of polarographic and voltammetric methods to trace metal analysis.

6. Analytical Voltammetry in Environmental Science. II. Organic and Organometallic Species

(P.M. Bersier, J. Bersier). Introduction. Use of advanced polarographic, voltammetric and hybrid techniques for the determination of organometallic and organic pollutants. Polarographic and voltammetric determination of organometallic and organic pollutants in air. Polarographic and voltammetric determination of organometallic and organic pollutants in aqueous environment. Determination of organic pollutants in soils. Determination of organometallic and organic pollutants in foodstuffs- and biological matrices.

7. Theory and Analytical Applications of Modified Electrodes

(R.J. Forster, J.G. Vos). Introduction. Preparation of modified electrode surfaces. Characterisation of modified electrodes. Theoretical aspects of mediation processes at modified electrodes. Analytical applications of modified electrodes. Conclusion. **8. Amperometric Biosensors** (J. Rodriguez Flores, E. Lorenzo).

Introduction. Principles of biosensors. Fundamentals of amperometric biosensors. Classification. Applications. **Subject Index.**

1992 xxvi + 578 pages

Price: US \$ 283.00 / Dfl. 495.00

Subscription price: US \$ 254.00 / Dfl. 445.00

ISBN 0-444-88938-8



Elsevier Science Publishers

P.O. Box 211, 1000 AE Amsterdam, The Netherlands

P.O. Box 882, Madison Square Station, New York, NY 10159, USA